MCR-73-97
NAS9-12182

$\mathcal{CR}$-134155

Volume III

Cryogenic Test

October 1973

Final Report
Acquisition/
Expulsion System
for Earth Orbital
Propulsion System
Study

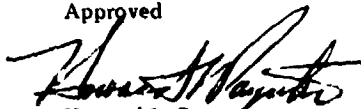***MARTIN MARIETTA***

FINAL REPORT
ACQUISITION/EXPULSION
SYSTEM FOR EARTH
ORBITAL PROPULSION
SYSTEM STUDY

Approved

Howard L. Paynter
Program Manager

G. Robert Page
Technical Director
Cryogenic Systems Phase

Prepared for

National Aeronautics and Space Administration
Lyndon B. Johnson Space Center
Houston, Texas

Prepared by

MARTIN MARIETTA CORPORATION
DENVER DIVISION
Denver, Colorado 80201

FOREWORD
_____

This document is submitted to the National Aeronautics and Space
Administration, Johnson Space Center by Martin Marietta Corporation
Denver Division, as part of the final report for Contract NAS9--
12182, *Acquisition/Expulsion System for Earth Orbital Propulsion
System Study.* The final report consists of five volumes as follows:

Volume I   - Summary Report;

Volume II   - Cryogenic Design;

Volume III - Cryogenic Test;

Volume IV   - Flight Test Article;

Volume V   - Earth Storable Design.

This work was administered under the technical direction of Mr.
Larry Rhodes, NASA-JSC Technical Monitor. Mr. Howard L. Paynter,
Chief of the Thermodynamics and Fluid Mechanics Section, Propul-
sion Department, was the Martin Marietta Program Manager.

The following Martin Marietta personnel made significant contri-
bution to the Phase A Cryogenic Test effort:

A. J. Villars, Jr., S. P. White,
P. E. Uney, W. L. Karlin, T. R.
Stumpf   Bench Model Analysis and Test

E. R. Wilson, D. E. Gilmore,
T. R. Barksdale   Bench Model Design and Test

J. S. Marino, A. T. Pecarich,
D. J. Brown, J. E. Littlefield   Subscale LH_2 DSL Model Design
                                  and Test

CONTENTS

Table
_____

SUMMARY

A ground test program was conducted to verify several of the design methods and techniques that were used in designing cryogenic acquisition/expulsion systems. The ground test program utilized bench models and subscale models to successfully verify the DSL designs presented in Chapters III, IV, and V of Volume II.

A total of 15 bench models were tested in both the low-g environment, provided by the KC-135 aircraft, and under plus and minus 1-g environments, using Martin Marietta's engineering laboratories. Both cryogens and ambient fluids were used during tests. Some of the ambient fluids used were methanol, Freon, and pentane. The cryogen test fluids were LN_2, LO_2, and LH_2.

The testing of a 63.5-cm (25-in.) diameter DSL subscale model was particularly significant. Under these tests, the operational characteristics of the DSL concept were verified using LH_2 and LN_2. Demonstration of the gas-free liquid expulsion characteristics was accomplished by expelling LH_2 under -1 g using both GH_2 and GHe pressurization. Loading of the acquisition/expulsion device was successfully accomplished using LH_2 and LN_2. The liquid-free vapor venting performance of the model was limited because of the thermal stratification under the -1 g test conditions.

The cryogenic systems phase of the contract benefitted from two Martin Marietta IR&D programs. Under one program a large screen liner, 178-cm (70-in.) dia was successfully designed and fabricated. Inspection techniques were developed and verified through ground testing. A second IR&D program demonstrated that a cryogenic DSL feedline can be fabricated using existing methods. The performance characteristics of this 5-m (16-ft) long test model are being evaluated using LN_2 as the test fluid. Both of these IR&D programs are being continued during 1973.

I. INTRODUCTION

One of the primary objectives of the cryogenic system phase of
the program was to verify the cryogenic system designs with sub-
scale ground tests. Test results from previous programs (Ref I-1
thru I-4) had verified the capillary propellant acquisition/ex-
pulsion designs; however, the test fluids had been limited to non-
cryogens. For cryogenic systems, high-temperature and low-temp-
erature effects are significant design considerations. Therefore,
the approach that was adapted for the Phase A effort included a
strong emphasis on testing with cryogens. This volume presents
the experimental program conducted to verify the passive acqui-
sition/expulsion designs for subcritical cryogenic storage during
low-g.

The program followed the schedule illustrated in Fig. I-1. Dur-
ing the 18 months of testing, data were acquired that supported
the selection and verification of the cryogenic designs presented
in Volume II. The information collected during the ground tests
discussed in Chapter II was categorized into three areas that
influence th acquisition/expulsion system design: (1) fluid
mechanics; (2) heat transfer and thermodynamics; and (3) structures.
Most of these tests were designed to provide data with regard to
the specific performance and design features of the passive cryo-
genic capillary systems. In addition to the normal 1-g condition,
test environments included low-g, which was provided by a KC-135
aircraft flying the Keplerian trajectory. A total of 15 tests
was conducted using different models and noncryogenic test liquids.

The successful modeling of the individual performance character-
istics and design features, as investigated and verified under
the ground tests, does not completely guarantee operational suc-
cess of the DSL system. Therefore, comprehensive testing of the
passive design itself was considered to be an important part of
the experimental program. A representative subscale model of the
DSL tank designs, as presented in Volume II, was successfully de-
signed, fabricated, and tested. The program included simulation
of certain performance characteristics, such as: tank filling;
-1g gas-free liquid expulsion; pressurization; and -1g vapor vent-
ing, using liquid hydrogen as the test liquid. In addition, boil-
off tests were conducted using LN_2 and LH_2 as the test liquid.
Details on the design, fabrication, and testing of the subscale
model are presented in Chapter III.

FROGRAM SCHEDULE

Design Development
Task I - Analysis
 Cryogenic System
 Earth Storable System
Task II - Design
 Cryogenic System
 Earth Storable System
Task III - Testing
 Cryogenic System
 Earth Storable System
Task IV - Development Planning
 Cryogenic System
 Earth Storable System
Flight Test Article
Task V - Program Plan - Atlas F
Task VI - Program Plan TIII/Centaur
Task VII - CVS Model (Design & Fab)
Design Development Documentation
 Cryogenic System
 Design Requirements
 Program Design Review
 Test Plan
 Earth Storable System
 Design Requirements
 Program Design Review
 Test Plan
Monthly Progress Report
Oral Review
Final Report (Draft)
 Volume I - Summary Report
 Volume II - Cryogenic Design
 Volume III - Cryogenic Test
 Volume IV - Flight Test Article
 Volume V - Earth Storable Design

1971 · 1972 · 1973
A S O N D J F M A M J J A S O N D J F M A M J J A S O N D
1 2 3 4 5 6 7 8 9 10 11 12 13 14 15 16 17 18 19 20 21 22 23 24 25 26 27 28 29

Figure I-1 Program Schedule

Two Martin Marietta-funded (IRAD) programs were conducted concurrently with Task III and complimented the contractual test program. These two programs are part of our continuous research and development in capillary system technology and low-g fluid behavior and passive management. Under one program, entitled *Capillary Screen Fabrication Technology*, fabrication and manufacturing methods are being improved for fine-mesh screen devices. During 1972, different screen forming and joining methods were compared. The preferred techniques were used for the 178-cm (70-in.) dia DSL screen tank designed and fabricated under the IRAD task. This DSL system is nearly identical to the dedicated OMS (LO$_2$) design shown in Chapter IV of Volume II. Details of this IRAD program are presented in Chapter IV of this volume.

Under a second IRAD program, *Low-g Fluid Behavior and Control*, application of the DSL concept for use in cryogenic feedlines is under investigation. A 3.66-m (12-ft) long feedline containing a single screen liner was designed and fabricated during 1972. A test program was initiated in early 1973 to demonstrate the capability of the passive liner to: (1) maintain a gas-free liquid core under static conditions; and (2) provide gas-free liquid under flow conditions. The test liquid is LN$_2$. The design, fabrication, and preliminary testing of this DSL model are presented in Chapter V.

Conclusions and recommendations based on results of the experimental verification program phase are presented separately in Chapter VI.

GROUND TEST PROGRAM

The ground test program objective was to generate the experimental data needed to support the design of the selected cryogenic propellant acquisition/expulsion system. Consequently, tests were directed at providing insight into the basic problems associated with surface tension devices. The program was designed to obtain both qualitative and quantitative data to verify established principles and analytical models, and to correlate empirical test data.

The program objectives were accomplished by a number of low-g aircraft and 1-g bench tests. A total of 14 tests were conducted to provide information in such areas as screen wicking, screen flow losses, structural capability, and bubble point variation with temperature. Both cryogenic and noncryogenic experiments were conducted to provide empirical and analytical correlations and to verify existing design techniques for successful design of surface tension systems.

A.   AIRCRAFT TESTS

Airborne low-g testing was accomplished using the KC-135 aircraft test bed operated at Wright-Patterson AFB, Ohio. The Keplerian trajectory flown by the aircraft to provide a low-g test period of 32 sec is shown in Fig. II-1. An average of 15 to 20 trajectories can be flown during the normal 2 1/2-hr flight. Both tiedown and free-float tests are possible. Accelerometers are used to provide g-level data and tiedown rings are provided throughout the fuselage to secure the test equipment. For this test program, only tiedown tests were conducted because the models were of plexiglas and were considered too fragile for a free-float environment. Following checkout at Martin Marietta, the test articles were delivered to NASA-MSC where proper operation was again verified before installation in the KC-135 aircraft. Low-g tests were supervised by NASA-MSC personnel.

1.   Low-g Subscale Acquisition/Expulsion Model Outflow Tests

a. Test Objectives - The objective of these tests was to demonstrate the dual-screen-liner (DSL) passive acquisition/expulsion concept under low-g conditions. Two subscale models were flown to qualitatively verify gas-free liquid expulsion on demand during the low-g eplerian maneuvers of a KC-135 aircraft. Each test period was approximately 30 seconds. The plexiglas models, Backup Demonstration Device (BUDD) and Transparent Expulsion Demonstration Device (TEDD), are surface tension devices that use fine mesh screens to stabilize the liquid/gas interface and provide a controlled liquid region capable of gas-free liquid expulsion on demand. The expulsion performance for both models using methanol was recorded and documented on film.

II-1

Mach = 0.47
n = 0 g

—·— Flight Path = 1 g
— — — Flight Path > 1 g
——— Flight Path = 0 g

Mach = 0.74
n = 0 g
Angle = 50 deg

Mach = 0.74
n = 0 g
Angle = 50 deg

32 sec

Transition
Zones

Mach < 0.82
n = <2.5 g

Mach = 0.87
n = 2.5 g
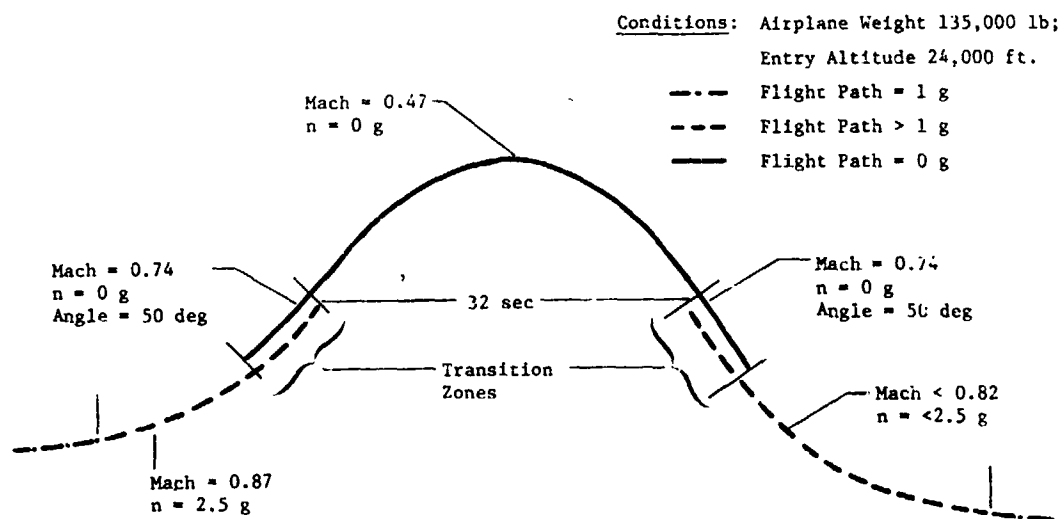
Fig. II-1 Keplerian Trajectory for KC-135 Aircraft

b. *Test Article Description* - The test articles were stainless
steel cylindrical DSL devices mounted in a cylindrical plexi-
glass tank with flat ends. The DSL acquisition/expulsion device
consisted of two concentric cylinders made of 325x2300 mesh Dutch
twill screen and support material. The area between these cylin-
ders forms a gas-free liquid annulus from which liquid is expelled.
The inner cylinder forms the bulk region and the gap between the
outer cylinder, and the plexiglass tank forms the vapor annulus,
which is representative of the liquid-free controlled volume
the cryogenic design. The communication screen between the vapor
annulus and bulk liquid region was 250x1370 mesh Dutch twill
screen. This screen allows the bulk region to be pressurized dur-
ing outflow.

The BUDD subscale model is pictured in Fig. II-2 and II-3. The
stainless steel DSL barrel section is shown enclosed in the plexi-
glass cylinder. The screen liner subassembly is sealed at the
end plates with aerospace sealant to assure that the system is
free of intercompartmental leakage. The view in Fig. II-2 is from
the bottom of the model and shows the radial channels (at the top
of the model) that lead from the liquid annulus to the liquid
drain port. It also shows the steel sheeting used to support the
325x2300 mesh Dutch twill metal cloth that forms the liquid annu-
lus. The 250x1370 mesh communication screen is shown in Fig. II-3.
Three distinct controlled regions--vapor annulus, liquid annulus,
and central bulk region--are visible in both photographs.

II-2

Fig. II-3 BUDD Plexiglass DSL Model Showing
Communication Screen

Fig. II-2 BUDD Plexiglas DSL Model

Details of the BUDD model are shown in Fig. II-4. Various ports in the different regions of the tank are shown, in addition to the liquid drain port. Four additional ports are shown, two in the vapor annulus, one in the liquid annulus, and one in the bulk region. These ports allow the model to be filled and drained and the pressure to be monitored, as well as pressurization and outflow flexibility. The BUDD model was ground-tested in the -1 g configuration before the low-g aircraft tests. Liquid expulsions were gas-free.

The TEDD model was a refined version of the BUDD acquisition/expulsion device. Components of the TEDD are shown in Fig. II-5 through II-7. Figures II-5 and II-6 show the stainless steel screen liner at various stages of fabrication. Figure II-5 shows the cylinders of perforated plate attached to the stainless steel end rings and the 250x1370 Dutch twill communication screen. The completed assembly covered with 325x2300 Dutch twill screen is shown in Fig. II-6. The plexiglass cylinder and end sections are shown in Fig. II-7. Figure II-8 is a detailed drawing of the TEDD.

Sealing the end plates of the screen device was accomplished by two O-rings (inner and outer) instead of by the sealant used for the BUDD model. This allows easy disassembly and replacement of the plexiglass tank, which tends to craze after being exposed to methanol. Minus 1-g expulsion tests on the TEDD model were successfully completed, using methanol, before delivery to NASA-MSC for the low-g testing.

c. Test Apparatus and Procedure - The test configuration and procedure were basically the same for testing of both models. The expulsion liquid was methanol and the pressurant gas was GN_2. The model was positioned in the support test fixture with the accompanying instrumentation that included an accelerometer for recording g-level and a pressure gage for monitoring system pressure. Pressurization gas was introduced in the outer annulus and liquid methanol was expelled through the outflow line positioned at the top of the model.

Generally, expulsion was initiated at the beginning of each low-g period following the pull-up acceleration of 2.5 g. Expulsions were demonstrated both with liquid in the vapor annulus and with the vapor annulus depleted. Outflow was monitored for gas-free liquid expulsion and documented on 16-mm color film.

d. Results - Despite some bulk liquid sloshing, gas-free liquid outflows were observed with only minor exceptions. During BUDD model testing, some bubbles were observed for a brief period during flow initiation. This gas ingestion occurred because of several screen pore enlargements created during fabrication and assembly of the model. These enlargements did not provide interface stability during high-g loading, but caused some gas ingestion during these periods. During low-g, the pores were stable.

II-4

O-RING (2-169) 2 PLCS

385x2300 DUTCH TWILL SCREEN WRAPPED AROUND EXPANDED/ROLLED STEEL SHEETS.

D" TO BE SLIP FIT WITH -03

8 (SQUARE)

-09
SECTION A-A

Fig. II-4 BUDD Zero-g Expulsion Model Detail Design

II-5 and II-6

5 6 7 8 9 10

Fig. II-5 TEDD Model Liner Device
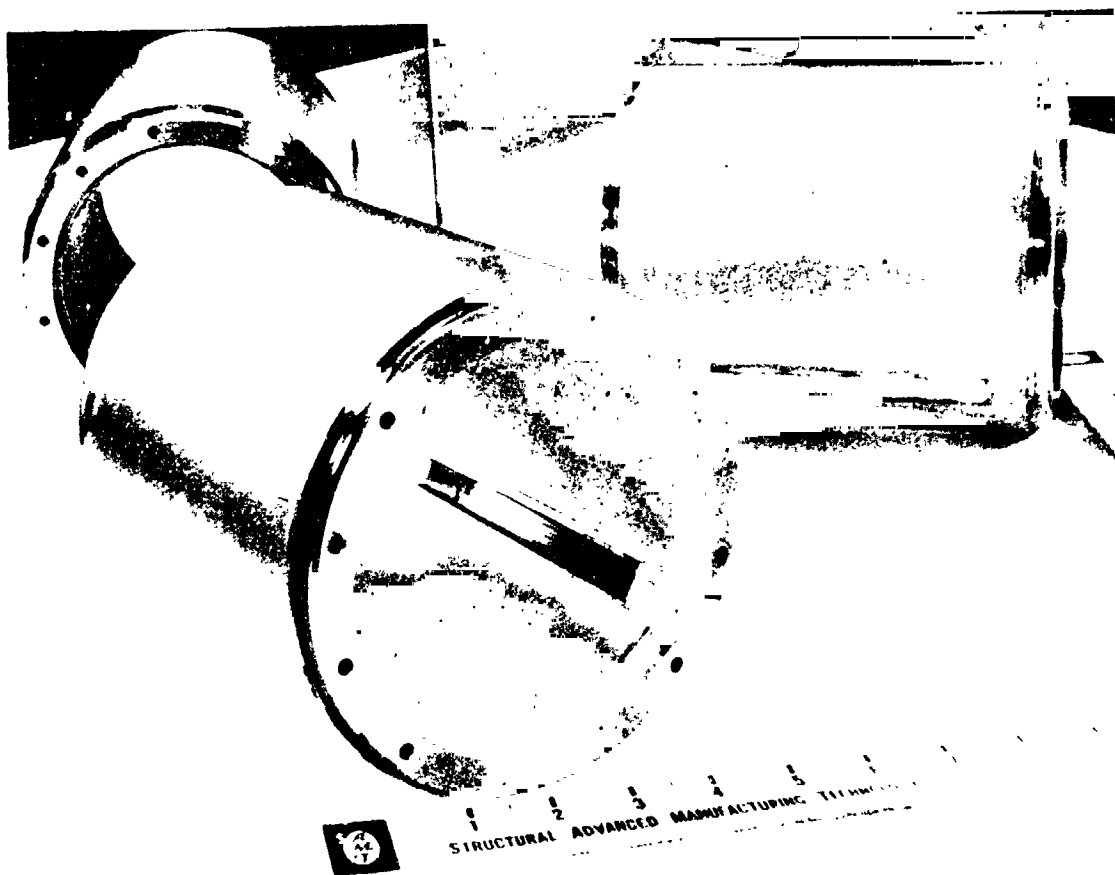
Fig. II-6   TEDD Model Completed Screen Liner Assembly
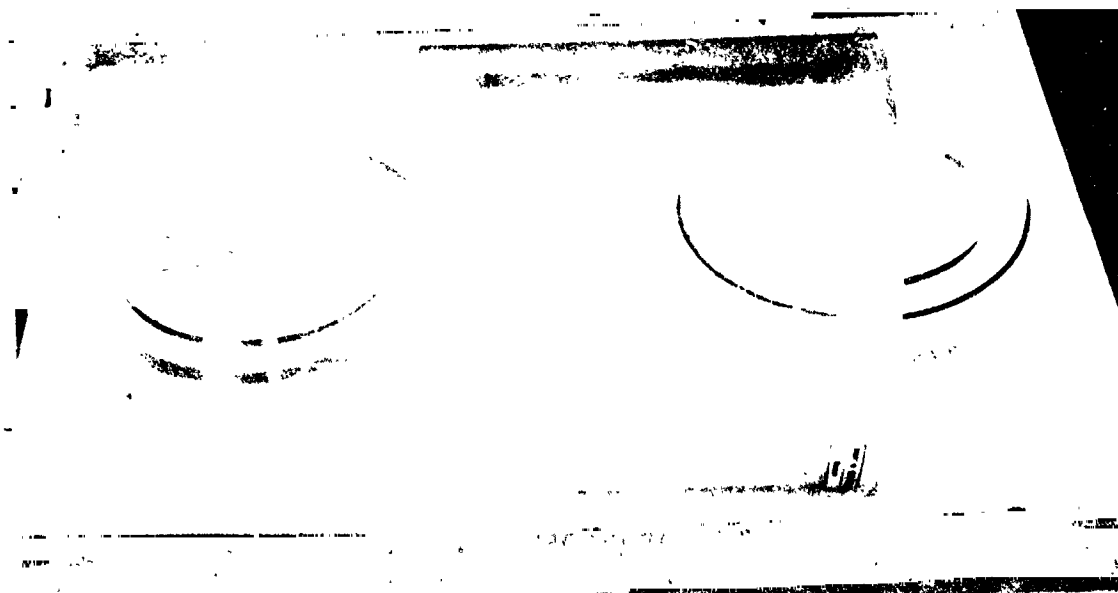
Fig. II-7   TEDD Plexiglass Assembly

II-8

SECTION B-B
-O6

FOLDOUT FRAME

DRILL Nº18 (.1695)
THRU, 8 PLCS
45° SPACING

C   C

4⅛ R

B

7½⁺
NOM ID

SEE DETAIL "X", SHEET 2

9.0 DIA
7.5 DIA (REF)
MEDIUM FIT WITH -08
2¹¹⁄₁₆   3⅝

NOM.
8.0 DIA

⁵⁄₃₂ TYP

TURN ID UNTIL TRUE
1.0 ONLY (TYP. BOTH ENDS)

DRILL ²⁷⁄₆₄ THRU
TAP ¼ NPT

DRILL ²¹⁄₃₂ THRU
TAP ⅛ NPT, 2 PLCS
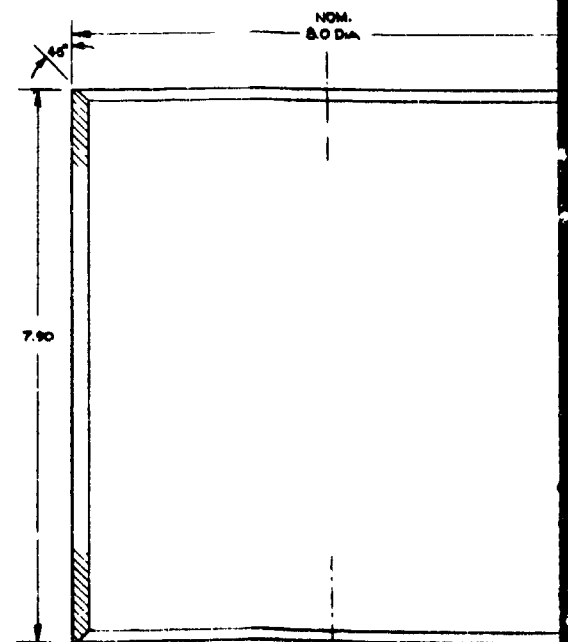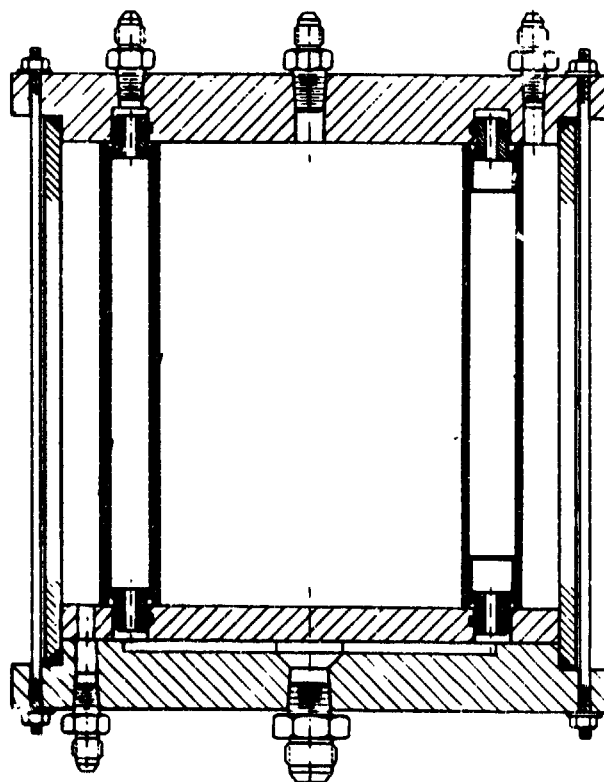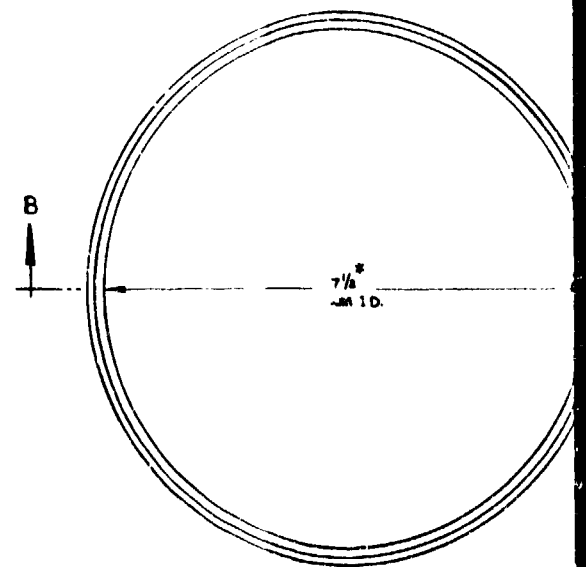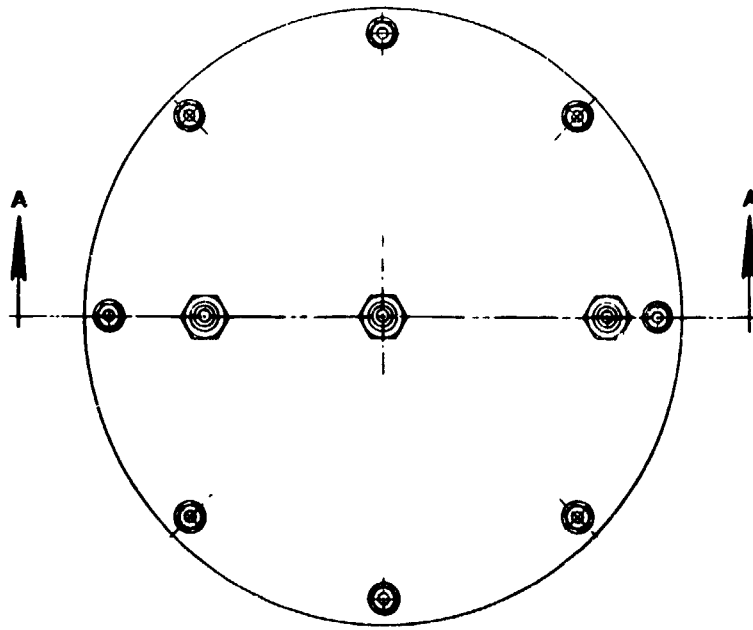
SECTION C-C
-10

SECTION B-B
-06
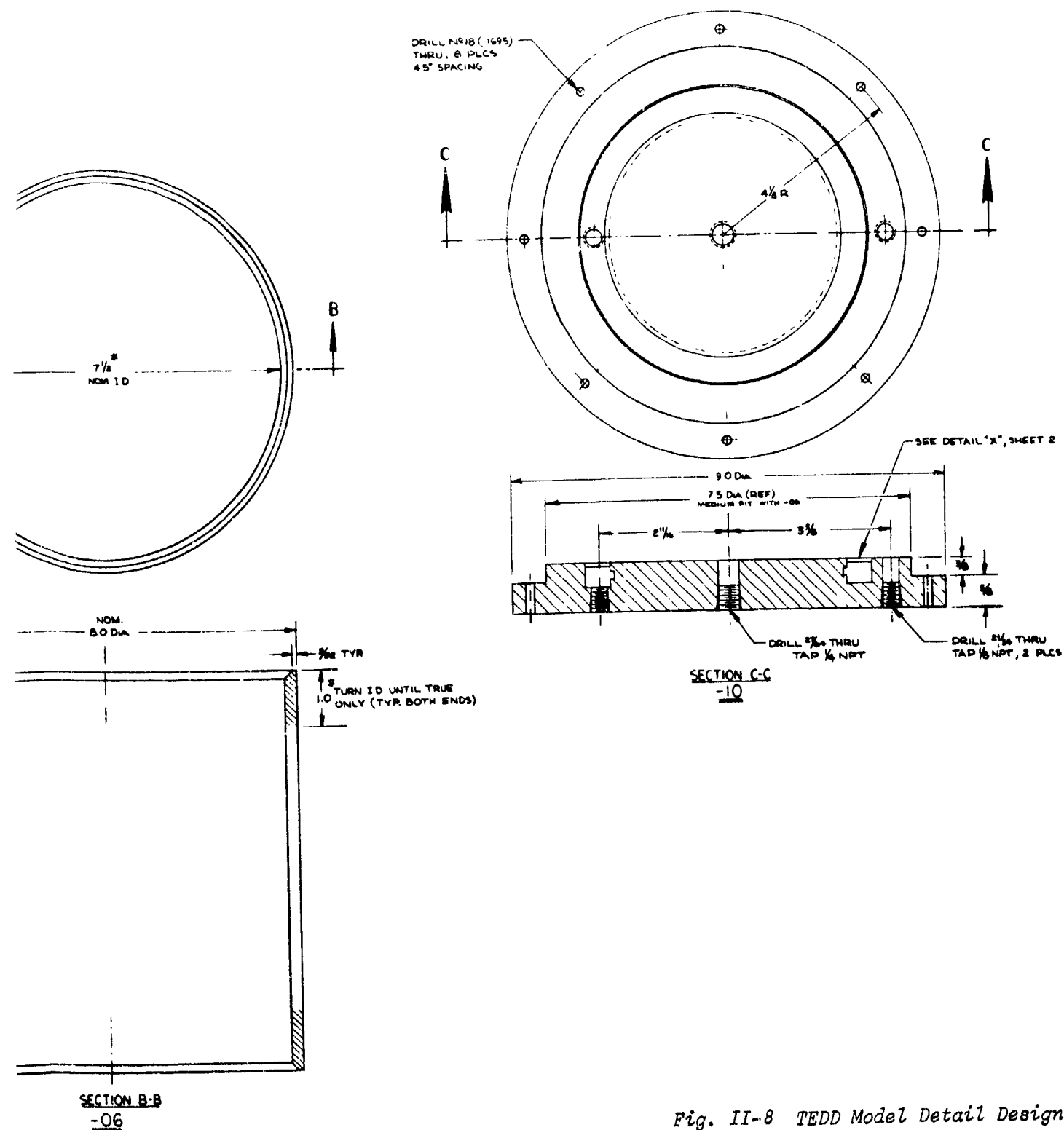
Fig. II-8   TEDD Model Detail Design

II-9 and II-10

FOLDOUT FRAME

With the TEDD model, methanol expulsions were completely gas-free
during all of the g-levels encountered. Figure II-9 shows the TEDD
during a period of low-g outflow. Low-g conditions are shown by the
liquid/vapor interface in the outer annulus of the model. Gas-free
liquid expulsion was verified by the absence of vapor in the drain
port and line located at the top center of the device. This was re-
presentative of the system's performance throughout low-g testing.
It should be pointed out that although the environment in the pic-
ture is very close to zero-g, the nominal acceleration level during
the entire series of tests was on the order of +0.1 g. This tended
to settle the liquid in the bottom of the model during the majority
of low-g expulsions.

*Fig. II-9 Low-g Expulsion of TEDD Model during
           KC-135 Flight*

e. *Conclusions* - Although the g-level for this test series aver-
aged approximately +0.1 g, periods of very low g-level ($\simeq 0$) were
noted during several expulsion tests (see Fig. II-9) with no detri-
mental effects on system operation. These test results indicate
that low-g environments do not adversely affect the expulsion capa-
bility of the DSL acquisition/expulsion device.

2   Bubble Collapse Tests

a. *Test Objectives* - A detailed discussion of the mechanics and analysis of collapsing bubbles in a controlled liquid volume was presented in Vol II, Chap B. The analytical predictions were primarily based on empirical correlations obtained from experimental work by Hewitt and Parker (Ref II-1) and Florschuetz and Chao (Ref II-2). The difficulty with these tests was that most of the data were obtained in a 1-g environment, resulting in bubbles of relatively small diameter. In the low-g test data available, test times were so short that the initial bubble motion was never completely arrested prior to initiation of bubble collapse.

In order to substantiate the analytical predictions made during this program, bubble collapse data for longer test periods at low-g that would produce larger bubbles were needed. The objective of these tests was to provide those data by a series of tests aboard the KC-135 aircraft.

b. *Test Apparatus and Procedure* - Two series of tests were originally planned using Freon-11 and LN_2. However, the LN_2 test apparatus was not compatible with KC-135 safety regulations and, consequently, LN_2 testing was not performed.

A schematic of the Freon-11 test apparatus is shown in Fig. II-10. The instrumentation consisted of a movie camera, pressure gage, and stop watch in the camera field of view. The bubble generator was a small resistor mounted on a swinging arm, connected to a variable power supply. A similar heater was used to control the vapor pressure in the Freon-11 reservoir. The fill reservoir served the dual function of providing liquid to the test vessel and supplying pressurant for collapsing bubbles during test. The vapor pressure in the reservoir was, therefore, maintained at 1.4 to 6.9 N/cm^2 (2 to 10 psi) above that in the test vessel.

Figures II-11(a) and II-11(b) are photographs of the test article. These pictures show the clear glass barrel and front plate sections, the 5-W, 50-Ω resistor, and the pressurization and fill lines. Note the swing arm mechanism for removing the bubble generator from the area of bubble formation when a bubble of suitable size was formed. Figure II-11(b) shows the camera view during 16-mm film exposure. The entire experimental apparatus is shown in Fig. II-12.
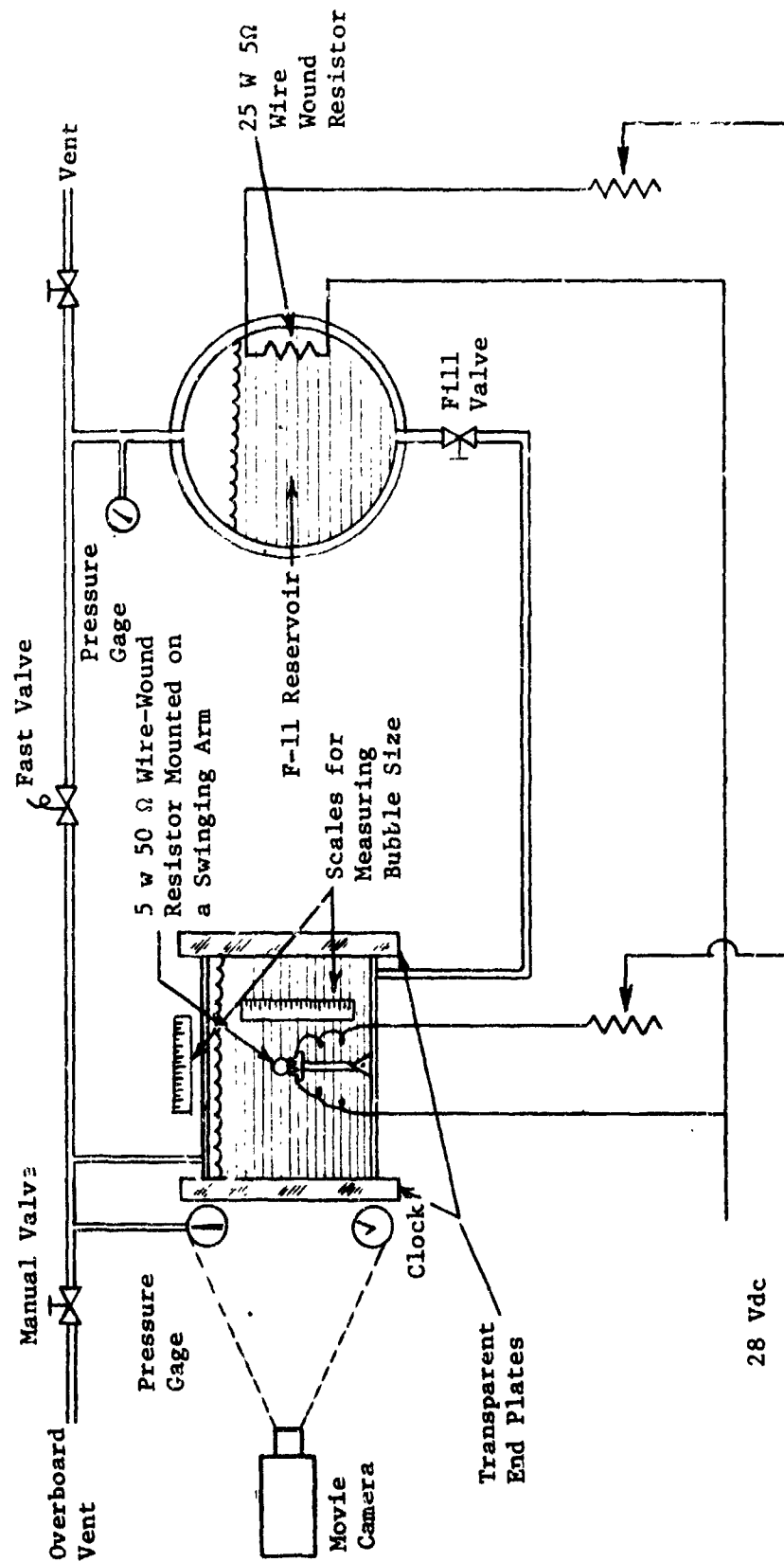
Fig. II-10 Bubble Collapse Test Schematic
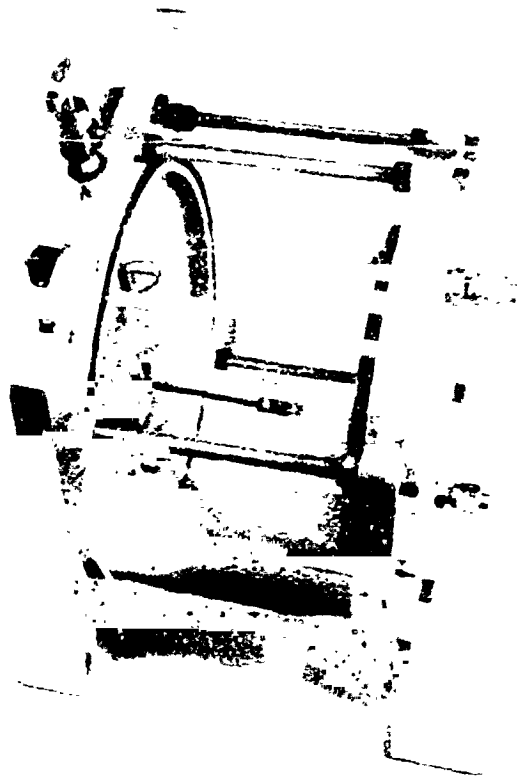
(a) Top View
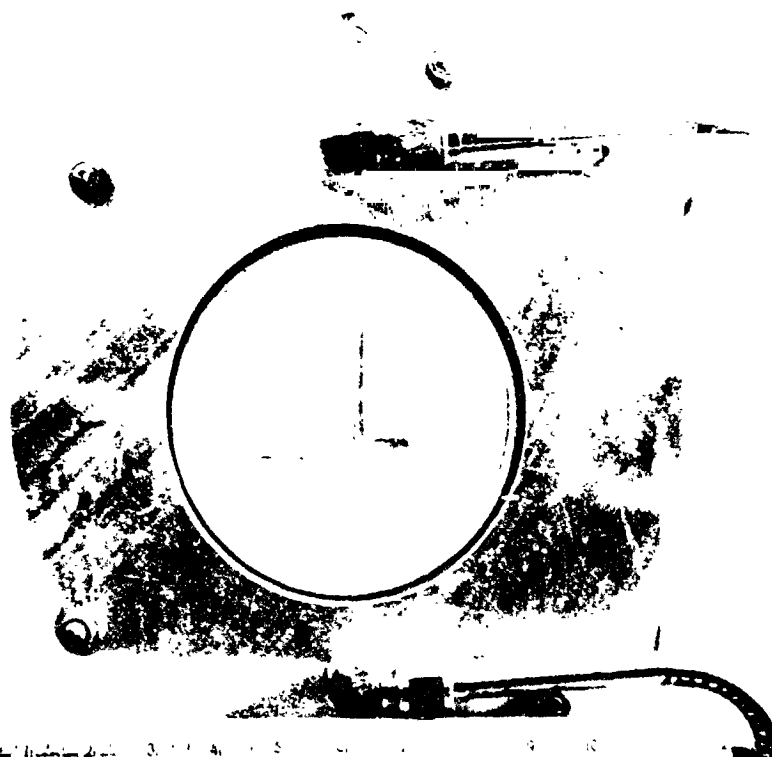
(b) Front View

Fig. II-11 Photographs of Bubble Collapse Test Device
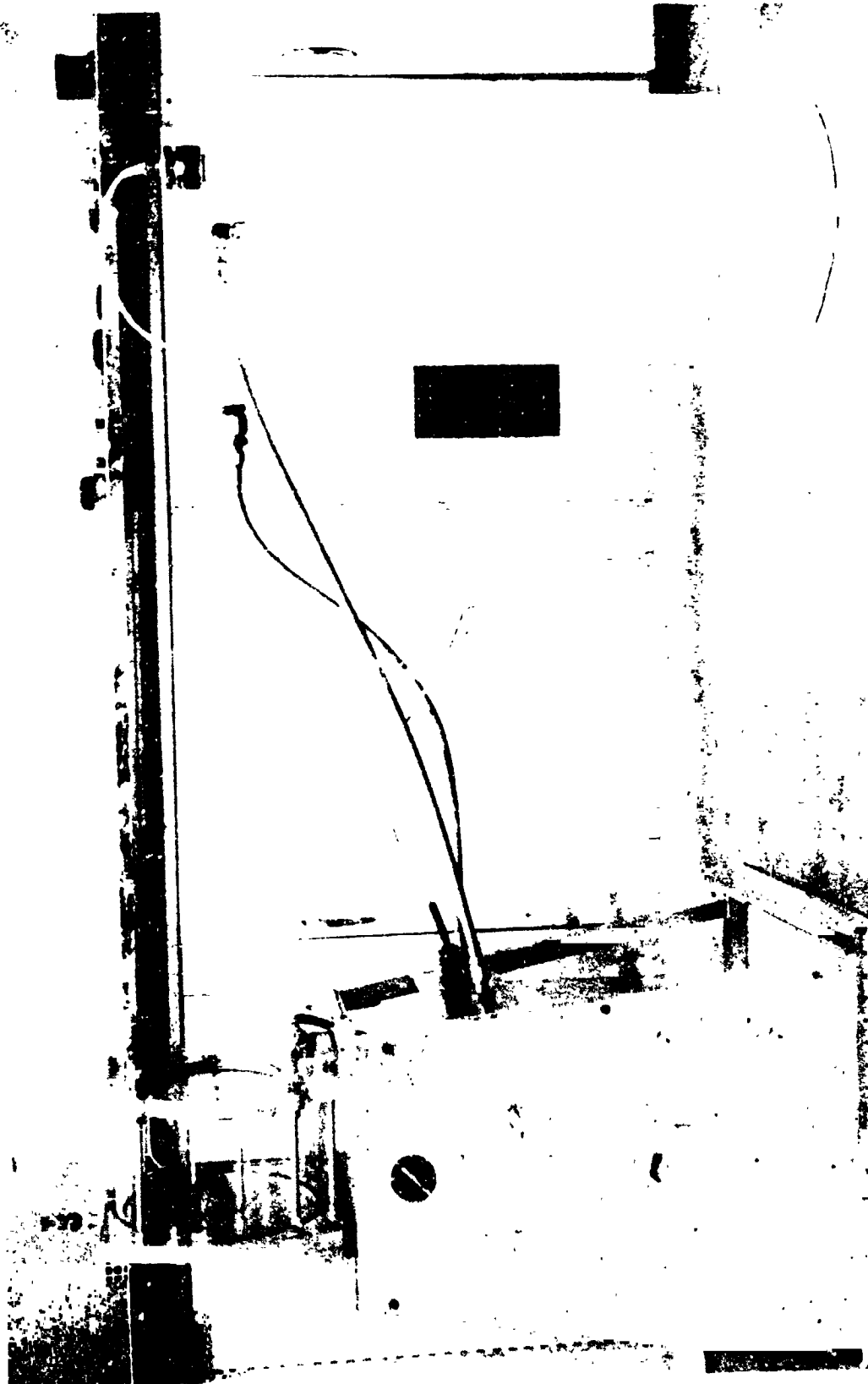
Fig. II-12 Complete Bubble Collapse Test Apparatus

Prior to testing, the liquid in both containers was boiled using electric heaters and vented overboard to eliminate dissolved non-condensible gas. Prior to each test (with fast-opening valves closed), the heaters and vent valves were adjusted for the desired ΔP between the reservoir and test vessel. The liquid in the test was topped off at this time. The ullage was kept very small to minimize liquid motion during the transition maneuvers. After the near zero-g period started, the bubble generator, which was positioned near the center of the test vessel, was allowed to continue heating until a bubble of suitable size was formed. The power was then switched off and the movable arm was rotated to remove the resistor from the vicinity of the bubble. After sufficient time passed to allow any disturbance resulting from this action to dissipate, the fast-opening valve was opened, pressurizing the test vessel to approximately the level of the reservoir and initiating bubble collapse. A stop watch recorded the time required to collapse the bubble. The entire test was documented on film.

c. *Results* – Figure II-13 shows the bubble collapse test apparatus during KC-135 tests with Freon-11. Also shown is the pressure gage indicating initial pressure and ΔP (NPSH). Note the bubble being formed at the heating element, while other bubbles formed earlier rise in the low-g environment. Two lights indicate pressurization and time from pressurization by an on/off oscillation every 0.2 sec. Bubbles are distorted from a spherical shape because of the higher-g environments than expected (average acceleration during low-g portions of the test was approximately +0.1 g) and the resulting convective and buoyant effects.

Fig. II-13   Sample Bubble Collapse Test Results

Several problems plagued the tests, making correlation of the data difficult. In addition to the problems mentioned previously, high acceleration levels caused the bubbles to disappear before complete collapse. Due to improper liquid level, pressurization during some tests severely disturbed and engulfed the collapsing bubbles, making accurate determination of collapse times impossible. Also exact pressure level and ΔP determination were difficult due to visual obstruction of the pressure gage at the higher pressure readings. However, several tests provided reliable data for analysis.

Figure II-14 shows test data plotted with theoretical collapse times predicted by the following equation,

$$\gamma = 1 - 2\varepsilon \sqrt{\tau_H} \qquad\qquad\qquad [\text{II-1}]$$

where $\gamma = r/r_o$, nondimensional radius;

$$\tau_H = \frac{4}{\pi} Ja^2 \frac{\alpha t}{r_o^2}, \text{ nondimensional time;}$$

$$Ja \text{ (Jacob Number)} = \frac{\rho_\ell C_{p_i} \Delta T}{\rho_v \lambda}$$

α = thermal diffusivity of liquid

t = time

r = bubble radius

r_o = bubble radius at time $t = 0$

$\Delta T = T_{sat} - T_\ell$

λ = latent heat of evaporation

$\varepsilon = 1 + \rho_v/\rho_\ell (2Ja - 1)$

ρ_v = vapor density

ρ_ℓ = liquid density
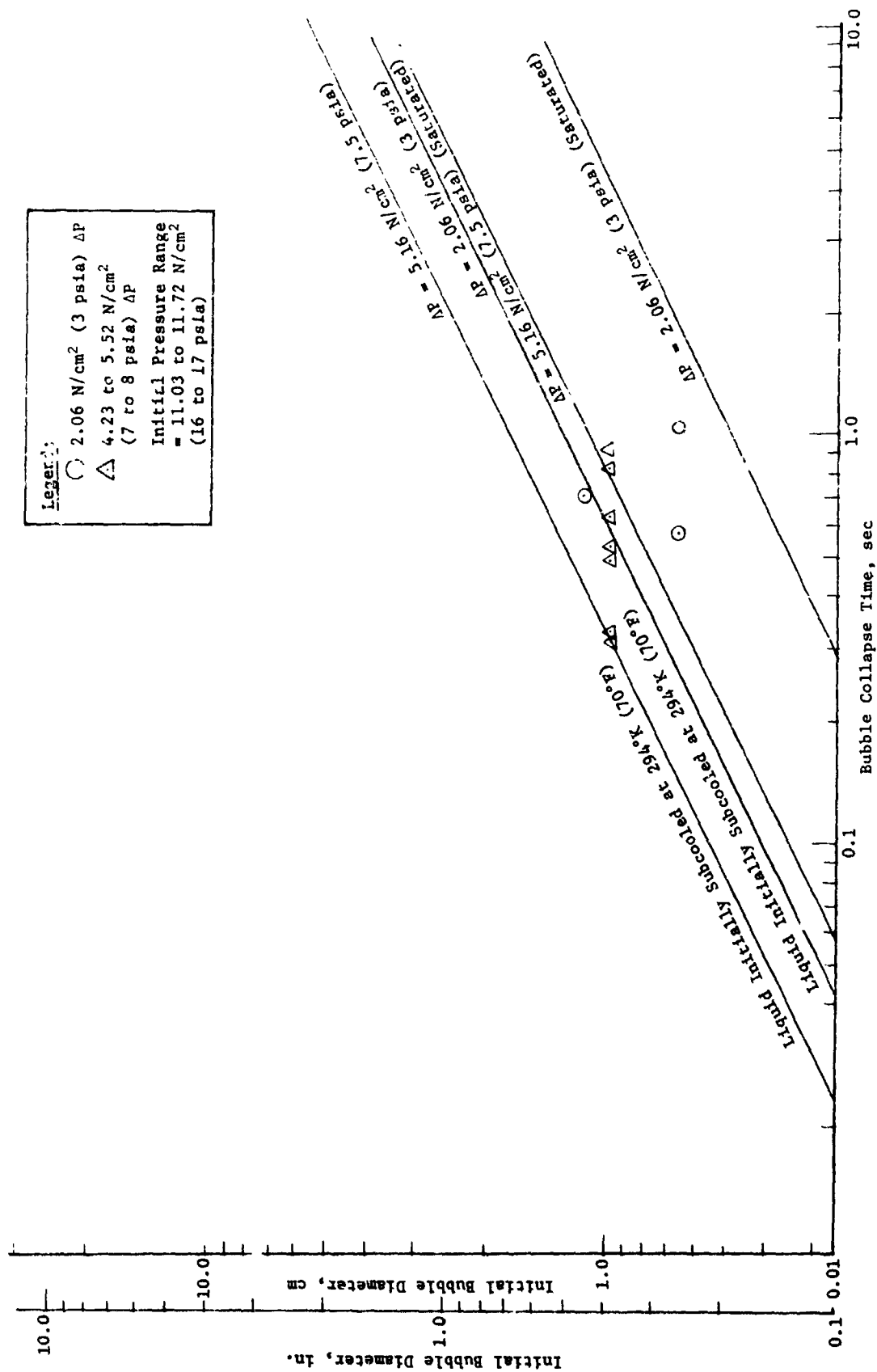
Fig. II-14 Freon-11 Bubble Collapse Data Correlation

Bubble collapse times were calculated as a function of initial bubble diameter for pressure differentials of 2.06 N/cm^2 (3 psia) and 5.16 N/cm^2 (7.5 psia). Two sets of curves are shown for (1) initially saturated liquid at 299.8°K (80°F) and (2) liquid sub-cooled at 294°K (70°F). The latter value was selected because it corresponded to ambient temperature in the KC-135 aircraft. Exact liquid temperature was not recorded, but was between the initial saturated condition and the 294°K (70°F) temperature. The analytical curves shown should, therefore, bracket liquid temperatures experienced during testing.

The experimental data show good agreement with analytical results. Test results for the two ΔP values are generally bounded by corresponding theoretical values indicating that liquid temperature did vary between the stated limits. Although the test data correlated with the collapse times predicted by Eq [II-1], additional data is needed, with a larger range of bubble diameters, to substantiate the analytical model.

Experimental collapse times range from 0.32 to 0.94 sec for an initial bubble diameter of 0.94 cm (0.37 in.) and NPSH of 5.16 N/cm^2 (7.5 psia) depending on initial Freon-11 temperature. Collapse times for a ΔP of 2.06 N/cm^2 (3 psia) do not vary significantly from larger ΔP times due to smaller initial bubble diameter.

d. *Conclusions* – Limited test results using Freon-11 liquid verify analytical predictions for the bubble diameters and NPSH values considered. However, additional data are required for a wider range of bubble diameters for substantial experimental-analytical correlation.

3. Capillary Pumping Test

a. *Test Objectives* – In a cryogenic propellant/acquisition system, continuous evaporation at the screen surface due to tank heat leak tends to dry out the screen device. During periods of pressurization and venting, elevated evaporation rates may cause some portion of the screen retention device to dry out completely. For successful system operation, dryout must be minimized or, preferably, prevented altogether. For screen barriers not in contact with liquid, this requires resupply of liquid by screen wicking, or some other means, at a rate sufficient to rewet the screen in a reasonably short period of time. Previous work that evaluated wicking through Dutch-twill screen and parallel plates, concluded that some sort of channel would be required to provide sufficient liquid to these areas. Performance data are needed to establish the optimum geometry and spacing of the wicking channels.

A preliminary evaluation of wicking channels was made in Ref II-2. Selected channel geometries, including square, circular, triangular, open-finger (equilateral triangle), semicircular, rectangular, and annular were optimized and compared on the basis of estimated wicking capacity for the same system weight. Results indicated that the semicircular and open-finger configurations would deliver the greatest flows for a given wicking system weight.

Because the open-finger channel geometry is the least likely to trap vapor or gas bubbles and, thereby, inhibit uniform wetting of the liquid retention barrier, it appeared to be the preferred design. The tests discussed here were proposed to obtain comparative data on the wicking of methanol through the selected channel geometries in a zero-g environment. Data consisted of film documentation during the zero-g portion of the KC-135 Keplerian traject ries.

b. *Test Apparatus and Procedure* - The five test channels (shown in Fig. II-15) are attached to the top of the test article along with two scales for measuring wicking distance. The test channels were constructed of plexiglass, as was the methanol container. The channels were 45.7-cm (18-in.) long with approximately equal wicking areas. This area corresponds t the geometric cross sectional area of the channel, with the exce on of the open-finger design. The circular channel was slightly smaller because that was the size of plexiglass tubing available. The channels were designed to wick their entire length within a 20-sec period in a 0.02-g environment.

Figure II-16 shows the test articles mounted in the plexiglass container. The holes visible at the top of each channel were for purging gas from the channels as the liquid wicked up. The scales for measuring the wicking distance are also shown. Notice also the slosh baffle, made of perforated plate, mounted just above the entrance to the channels.

The test procedure for the KC-135 tiedown tests was straightforward. With the test article filled with methanol to a level just above the slosh baffle, the relative rise of methanol in each channel was noted during periods of low-g. The tests were documented on 16-mm color film.

II-20

Fig. II-15 Wicking Channels Used in Capillary Pumping Test
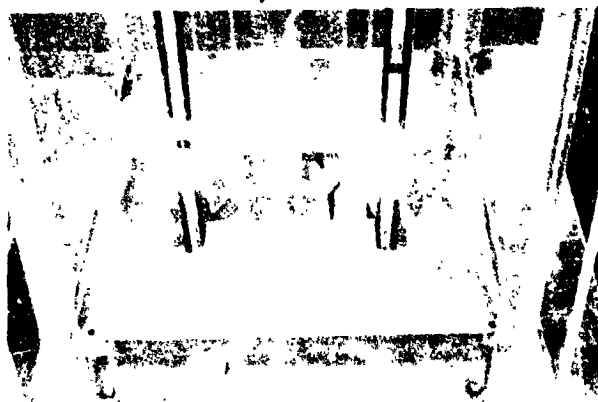
Fig. II-16 Capillary Pumping Test Apparatus

II-21

c. Results - The channels were designed to wick in a 0.02-g envi-
ronment. However, the test acceleration environment was generally
much higher; on the order of +0.1 g. Consequently, wicking dis-
tances were much less than expected, and the basis for comparison of
the test channels was greatly diminished. This is evident from the
film analysis. As a result of these high g-levels and the tran-
sients associated with the Keplerian maneuvers, the single slosh
baffle installed was inadequate and significant liquid slosh oc-
curred. The slosh effects during the majority of the tests pre-
cluded any comparison of relative wicking heights. Even in the few
tests where differences in wicking height could be discerned, slosh
effects were still present.

Figure II-17(a) shows representative results of the capillary pump-
ing tests. Note the severe distortion of the liquid surface, caused
by slosh, which tended to force liquid into selected channels. Fig-
ure II-17(b) shows significantly less slosh, although it was still
observable during film analysis. The different wicking heights are
obvious in this photograph. Test results are listed in Table II-1.

Table II-1 Selected Capillary Pumping Test Results

Triangle	Open-Finger	Circle	Square	SemiCircle
1	2	3	--	--
2	1	2	--	--
2	1	1	1	3
2	1	1	1	3
Note: The highest liquid rise for each of the four tests shown is signified by a 1, with decreasing height signified by 2 and 3.				

Although a definite pattern is not established, the open-finger
channel appears to wick higher than the other specimens tested.
However, the inconsistent data denote that slosh is still signifi-
cant and an attempt to draw any conclusions would be highly specu-
lative.

d. Conclusions - Test results were inconclusive and further testing
is required for positive identification of the best wicking geome-
try. Significant test results were hampered by problems encountered
during testing. Higher acceleration environments were encountered
than the tests were originally designed for. Resulting slosh ef-
fects made determination of relative wicking distances extremely
difficult. However, based on the limited test results obtained, the
open-finger channel design appeared to wick higher than the other
specimens tested.

II-22

(a) Severe Slosh

(b) Reduced Slosh

Fig. II-17 Capillary Pumping Test Results

B.   BENCH TESTS

The bench test program consisted of a series of cryogenic and non-cryogenic tests conducted at Martin Marietta, Denver division test facilities. A total of 11 tests were run to support the passive acquisition/expulsion device design.

1.   Bubble Point Verification of Multiple Screen Layers

a. Test Objectives - Certain capillary system designs may require a higher pressure retention capability than is presently available with a single layer of fine mesh screen. Although other materials are available with higher pressure retention capabilities, the advantages of fine mesh screen in areas such as ease of fabrication and weight make it a desirable choice in the construction of a capillary acquisition/expulsion device. To meet increased pressure retention capability requirements, additional screen layers must be considered. The lack of test data to verify the bubble point capabilities of multilayered screen configurations was the justification for this bench test.

The objective of this test series was to establish the bubble point capability of multiple screen layers in methanol and liquid nitrogen. Several different screens were tested to verify or establish the conditions under which the pressure retention capability of double and triple layers of screen can be considered additive. This involved testing multiple layers with zero spacing as well as separated by coarse mesh screen, perforated plate, and with gaps provided by 0.32-cm (1/8-in.) Teflon washers. Only the finest mesh Dutch twill stainless steel screens were of interest. These included 200x1400, 250x1370, and 325x2300 mesh screens.

b. Test Apparatus and Procedure - The basic test article consisted of a cylindrical stainless steel reservoir with a removable cap that allowed the test specimen to be changed. A schematic of the test apparatus is shown in Fig. II-18. Two stainless steel lines enter the pressurization chamber--the inlet or pressurization line and the vent line for chamber pressure sensing and relief. The test article is attached to a coverplate and mounted inside a glass dewar, which is sealed at the top by a silicone rubber gasket. Two additional lines are attached to the coverplate for filling the dewar with test fluid and venting the dewar to prevent pressure buildup. A linear scale is shown for measuring the height of liquid above the screen surface. This height was generally small, but, nevertheless, was compensated for in the determination of actual screen differential pressures.

To Pressure Differential Gage (Low Side)

Fill Line

Pressurization Line

Dewar Vent Line

To System Pressure Gage

To Pressure Differential Gage (High Side)

Scale

Glass Dewar

Screens

Temperature Sensor

Test Section
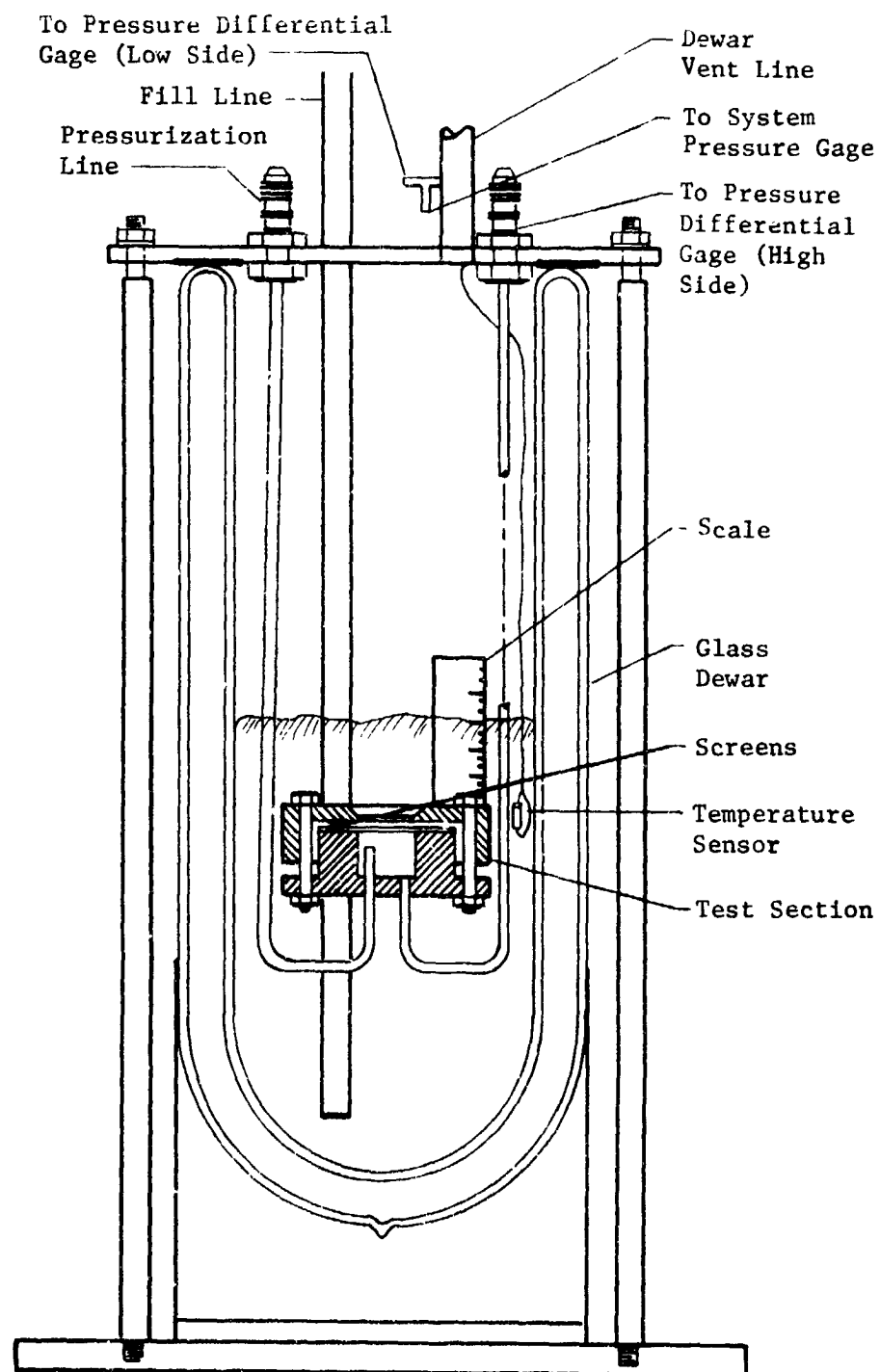
Fig. II-18 Bubble Point Test Apparatus

Instrumentation included a 0 to 152.4-cm (0 to 60-in.) water mano-
meter for measuring the pressure differential across the screen. A
pressure gage was also available for monitoring dewar pressure dur-
ing liquid nitrogen testing. Liquid temperature was determined by
a temperature sensor located just below the surface of the test
fluid.

Figure II-19 shows the test configuration for methanol tests. The
test article and coverplate are shown mounted in the glass dewar
with the pressurization and vent lines clearly visible. The water
manometer can be seen in the background with pressurization and
pressure-sensing flex lines also shown. Dewar fill and vent lines
protrude through the coverplate, but have little functional value
for ambient tests. Of the four valves visible, only three were used
for pressurization, venting, and differential pressure sensing.

The basic test procedure was the same for both methanol and LN_2
tests. With the screen mounted in the test article the dewar was
filled with test liquid to a level that provided a thin layer of
fluid over the screen sample. Some gas flow through the pressurant
line was desirable so no liquid would fall into the pressurization
region. The dewar vent line was fully open during all tests so the
dewar held an essentially ambient pressure. Liquid temperature and
depth (above the screen surface) were recorded. At this time, gas
was slowly added through the pressurization line, increasing the
pressure under the screen. At the moment of first bubble break-
through the manometer reading was recorded as the specimen bubble
point. The reservoir was then vented, decreasing the pressure dif-
ferential to approximately 2.54 cm (1 in.) water gage above that re-
quired to support the liquid head over the screen. This ensured
complete rewetting of the screen pores for subsequent tests. Gener-
ally, three data points were taken for each test configuration.

Three different screen specimens were tested in the single, double,
and triple screen configurations. Geometry considerations were
taken into account by investigating the effect of spacing between
the screen layers. The test matrix (Table II-2) summarizes the dif-
ferent tests that were run using both helium and nitrogen pressur-
ant. Multiple screens were tested with zero spacing distance as
well as 0.32-cm (1/8-in.) and 0.64-cm (1/4-in.) gaps between the
screens. This was achieved by inserting appropriately sized Teflon
washers. The effect of coarse mesh screen and perforated plate as
spacers was also investigated for 200x1400 mesh Dutch twill screen.

II-26
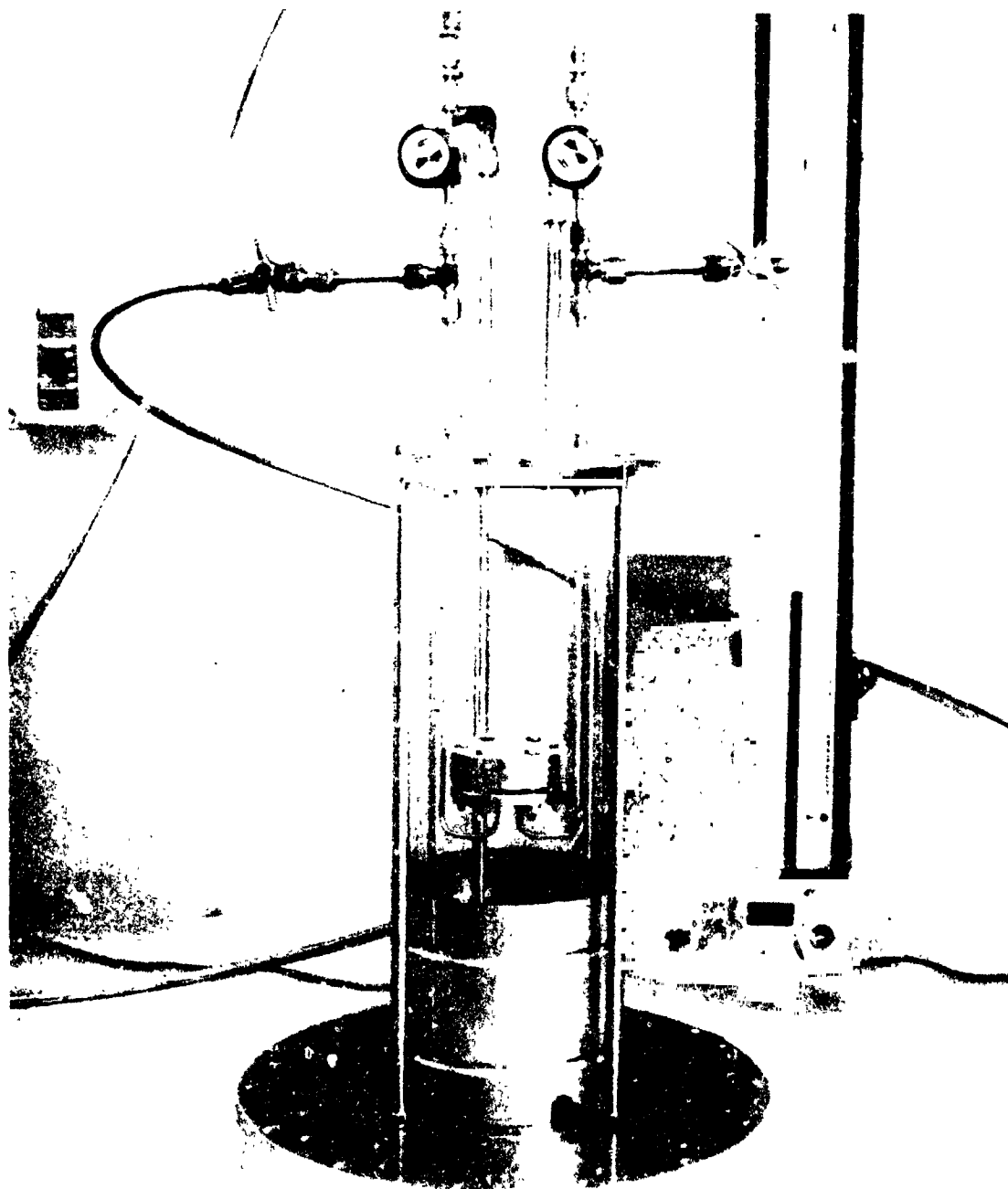
Fig. II-19   Bubble Point Test Article

[illegible]

Liquid	Spacing	Number of Screen Layers								
		200x1400			250x1370			325x2300		
		1	2	3	1	2	3	1	2	3
Methanol	0	X	X	X	X	X	X	X	X	X
Methanol	0.32 cm (1/8 in.)		X	X		X	X		X	X
Methanol	0.64 cm (1/4 in.)		X	X		X	X		X	X
Methanol	100x100 screen		X							
Methanol	Perforated Plate		X							
LN_2	0	X			X			X		
LN_2	0.32 cm (1/8 in.)		X	X		X	X		X	X
LN_2	0.64 cm (1/4 in.)		X	X		X	X		X	X

c. *Results* - Layering test results are summarized in Fig. II-20 and II-21 for methanol and LN_2 respectively. The nondimensionalized bubble point is defined as $\Delta P_{ms}/\Delta P_{ss}$, where ms is multiple screen and ss is single screen. This parameter is plotted for two and three layers of screen for the various geometries considered. The data show that spacing must be provided between screens before any improvement in bubble point can be expected. In no case did a zero spacing configuration improve the bubble point over that of a single screen. Screens with spacing provided an approximate additive pressure retention capability for two and three layered configurations. Inconsistencies in the data are attributed to the difficulty in maintaining the lower screens in a wetted condition. This is especially true of LN_2 data, which was generally erratic compared to methanol results.

Generally, the smaller gap, 0.32 cm, was slightly more reliable than the 0.64-cm spacing for yielding an additive effect. The larger gap appeared more likely to dry out prematurely. Although the horizontal test configuration assured wetting of the upper screen, the gas pressurant tended to hold all the liquid above the top screen while the lower screens remained dry. Because the pressure retention capability of dry screen is nearly zero, the effective bubble point in this situation is only that of the upper screen. Therefore, special care was required to assure that all screens were wetted before pressurizing.
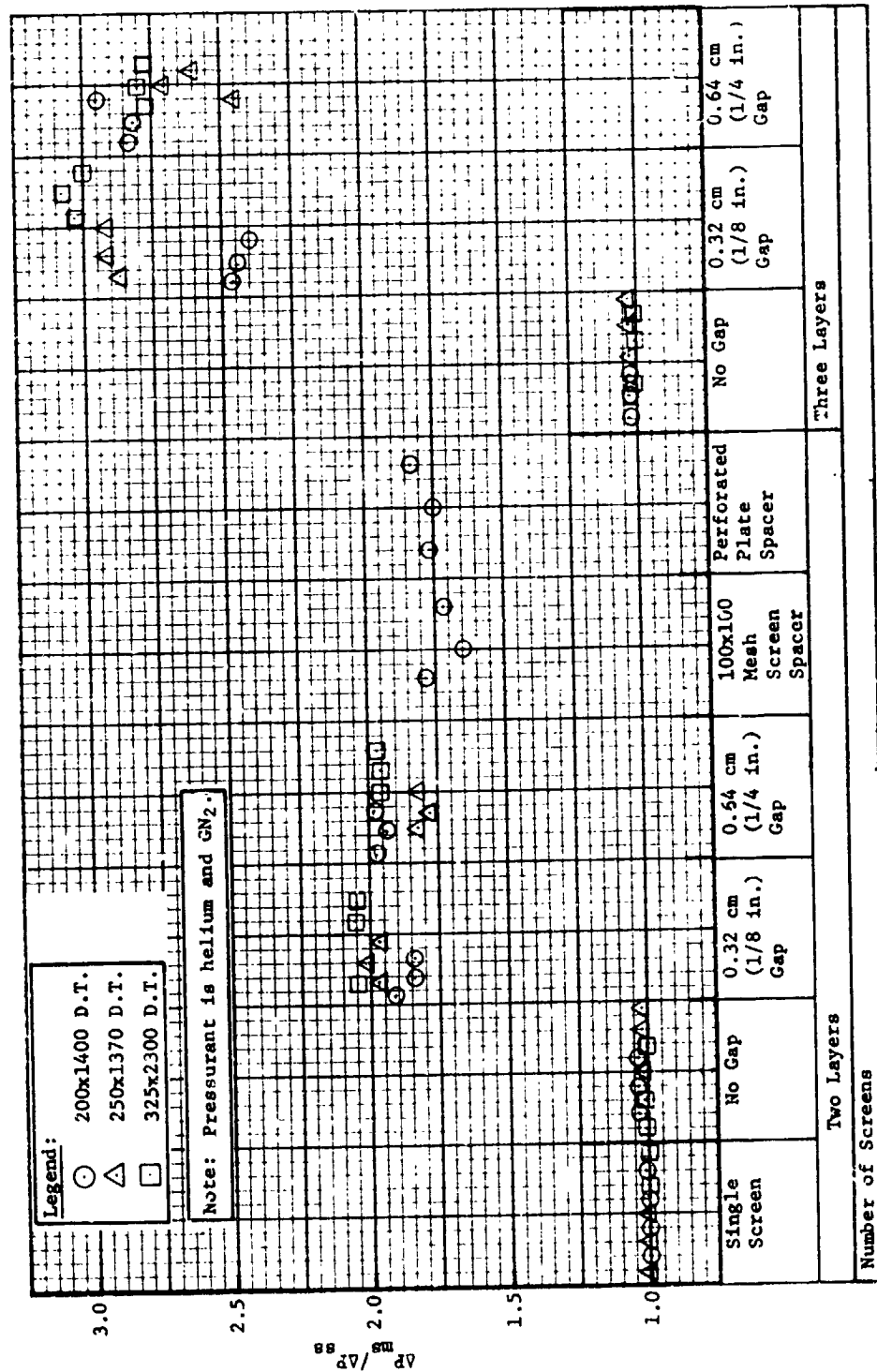
Fig. II-20 Methanol Screen Layering Bubble Point Data
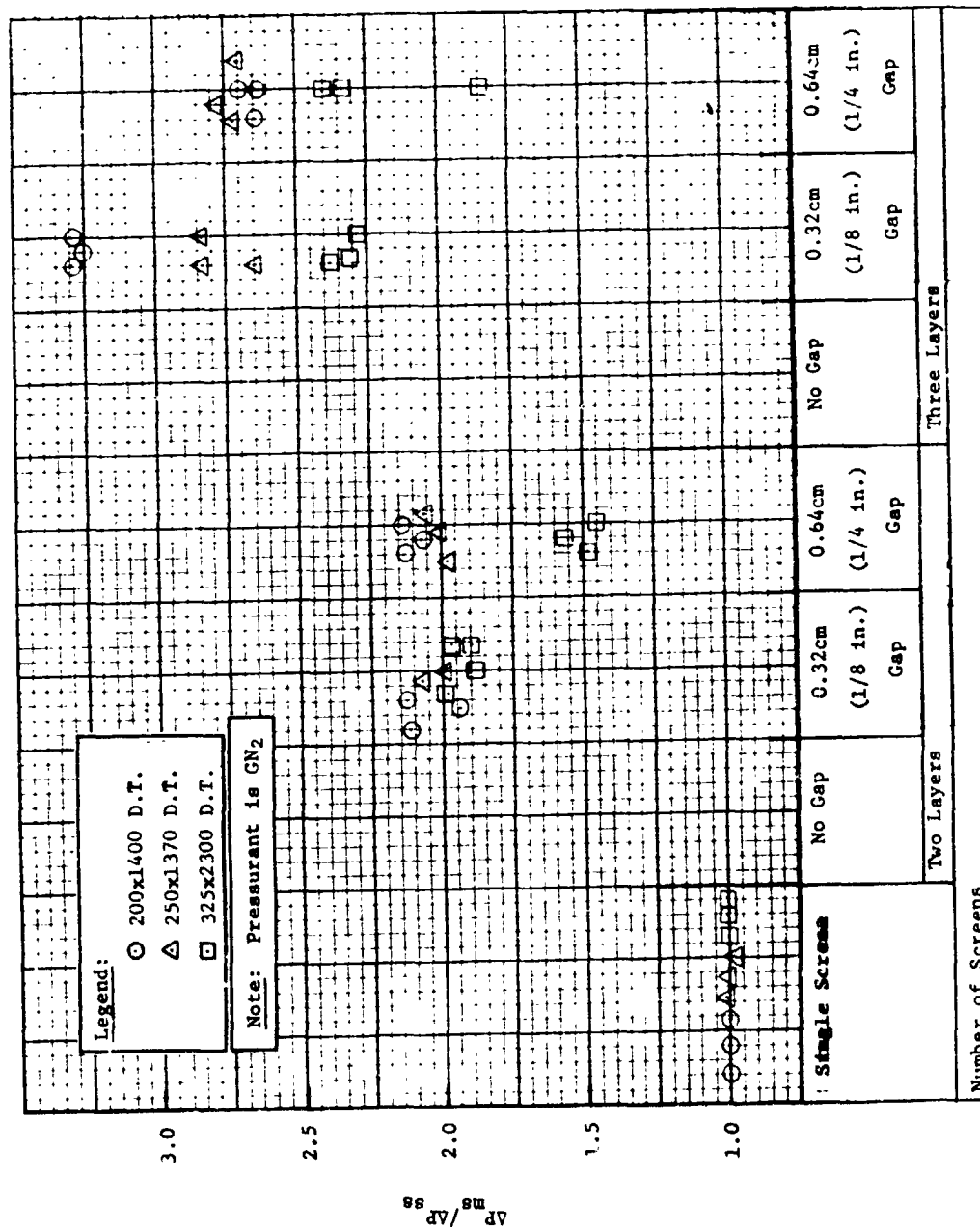
Fig. II-21 LN_2 Screen Layering Bubble Point Data

Double screen samples separated by coarse screen (100x100 mesh square weave stainless steel screen, which exhibits a bubble point in methanol of approximately 5.08 cm (2 in.) water gage) and perforated plate exhibited about 1.75 times the bubble point of a single screen. It is interesting to note that it was appreciably more difficult to ensure wetting of the lower screen in the pair separated by perforated plate. Maintaining screens not adjacent to the liquid in a wetted condition was the main problem encountered in these tests.

d. *Conclusions* - Layered screens with separation appear to provide additive bubble points, as long as the separation thickness is much greater than the radius of a screen pore. This spacing may be effected by perforated plate, coarse mesh screen, or other lightweight porous material of sufficient thickness.

The tests indicate that double and triple layered systems behave similarly. The problem with multilayered screen systems appears to be in maintaining those screens out of direct contact with liquid and in a wetted condition. This requires maintaining a wetting source through screen wicking or capillary pumping to ensure proper operation in an actual system.

2. **Bubble Point Temperature Dependency Tests**

a. *Test Objectives* - Successful design of surface tension devices requires accurate knowledge of temperature effects on screen pressure retention capabilities. Theoretically,* the bubble point of a given screen specimen and liquid vapor interface geometry depends only on the surface tension of the wetting fluid. Hence, the bubble point of a given configuration at different environmental conditions may be related by the following formula:

$$BP_2 = BP_1 \times \sigma_2/\sigma_1 \qquad\qquad [II-2]$$

where BP = bubble point of screen,

σ = liquid surface tension.

Subscripts 1 and 2 may refer to different states of a given fluid or two different liquids. Because surface tension is temperature dependent, the bubble point for a given liquid (with constant liquid vapor interface geometry and for a given screen specimen) is also temperature dependent.

* Also verified experimentally.

II-31

Although Eq [II-2] was generally accepted, it had not been proven experimentally. This test was initiated to experimentally verify the equation for the cryogens, LN_2 and LO_2, for temperature ranges corresponding to pressures from ambient, 8.13 N/cm (11.8 psig), to 28.8 N/cm^2 (41.8 psig). Only the finest mesh stainless steel Dutch twill screens were considered. These included 325x2300, 250x1320, and 200x1400 mesh specimens. Pressurization was autogenous with the exception of a single LO_2 test, which used helium.

b. *Test Apparatus and Procedure* - The basic test article was the same as that used for the screen layering test, previously described (Fig. II-18 and II-19). Due to the higher pressures involved in this series of tests a glass dewar could not be used. The cylindrical cryogenic pressure vessel was constructed of stainless steel with a 2.54 cm (1 in.) thick plexiglass end plate for visual detection of the bubble point. The test article mounted in the cryogenic container is clearly visible through the plexiglass cover (Fig. II-22). The fine mesh screen specimen and thermocouple placement are evident as are the pressurization and vent lines, which run to the underside of the test device.

The complete test apparatus is shown in Fig. II-23 for the LO_2 test configuration. Pressure measurement instrumentation included a pressure gage for observing dewar pressure and a differential pressure transducer for monitoring screen ΔP. It should be noted that the transducer shown here was only used during LO_2 testing and replaced the water manometer used during LN_2 experiments. The manometer could not be used during LO_2 tests due to compatibility problems and safety requirements. Figure II-23 also shows the liquid temperature thermocouple and platinum sensor instrumentation leads. The platinum sensor was installed before LO_2 testing to verify the accuracy of the thermocouple measurement.

The micrometer valve was used for regulating pressurant flow from the K-bottle supply. The two remaining valves were used for venting purposes--the large valve for the stainless steel pressure vessel and the smaller valve for the test article. The vessel fill line is shown without the associated plumbing required to attach it to the supply dewar. Although the cryogenic container is shown uninsulated, several layers of foam insulation, approximately 5.08-cm (2-in.) thick, were applied before testing to minimize heat leak and reduce boiloff.

Fig. II-22 Bubble Point Test Device for Temperature Dependency Test
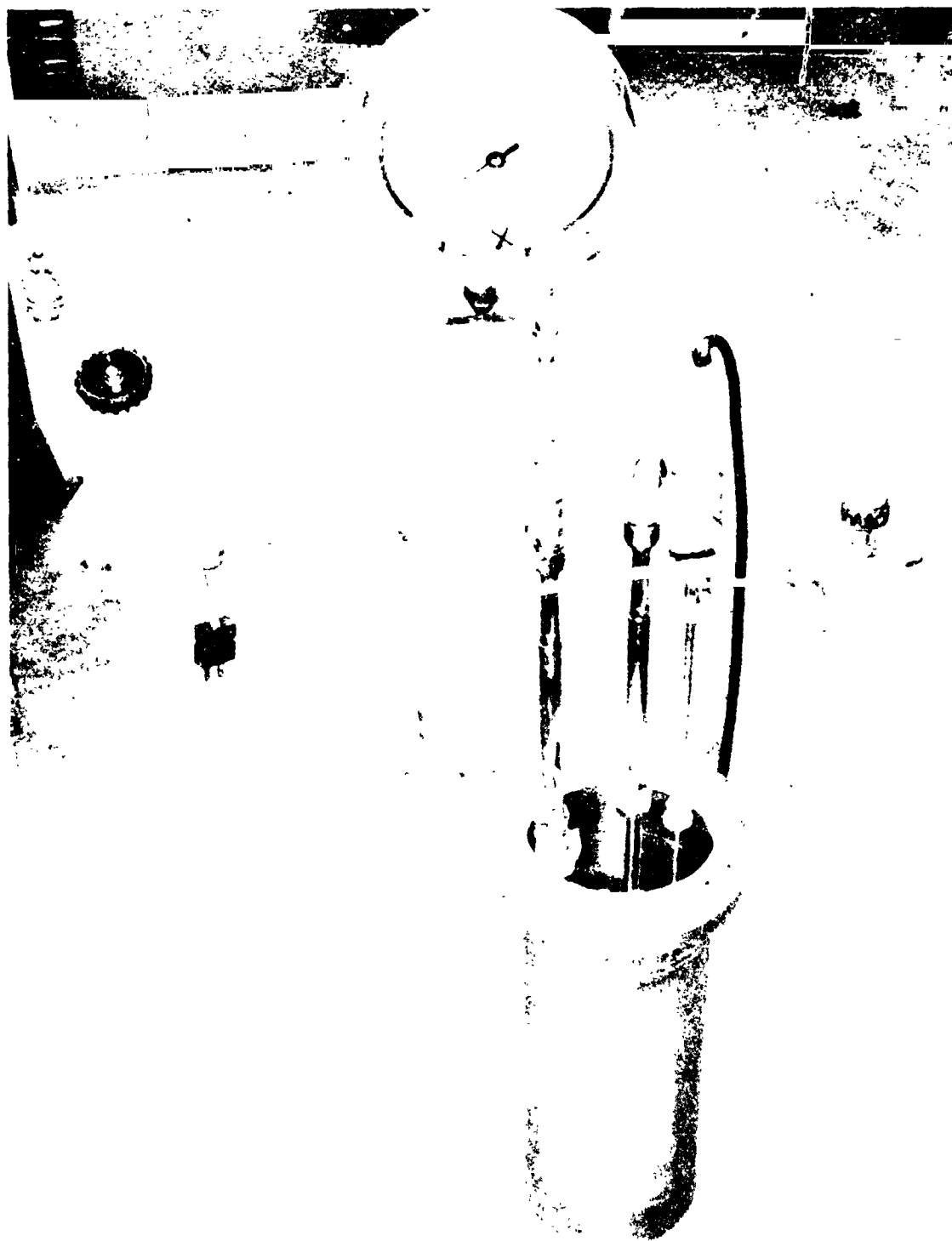
Fig. II-23   Complete Test Apparatus for Temperature Dependency Tests

The basic test procedure for both LN₂ and LO₂ tests was as follows. Initially, the container was filled with test fluid to provide a thin liquid layer above the screen (0.64 to 1.4 cm), while a small amount of pressurant flow was maintained so liquid would not fail through the screen. The dewar vent valve, which had been fully open, was adjusted to the desired test pressure. Intermittent adjustment was required to maintain the desired pressure level. At this point, gas was slowly added through the pressurization line increasing the screen reservoir pressure and, consequently, the ΔP across the screen. At the moment of first bubble breakthrough the pressure differential, liquid temperature, and liquid height were noted. Then, the pressure below the screen was vented to a point low enough to ensure rewetting of the screen, but high enough to support the liquid above the screen. This procedure was repeated to obtain several data points at the test pressure level and also at various pressure levels to obtain bubble point capability at different liquid temperatures.

Normal procedure involved running the initial tests at 28.8 N/cm² (30.0 psig) and the subsequent tests at lower pressure levels until ambient pressure was reached. This method minimized the amount of liquid condensed in the vent (pressure sensing) line because any liquid present at the highest saturation pressure would tend to vaporize as the pressure was decreased. Liquid in the vent line was undesirable because an erroneous ΔP reading would result.

Tests were performed at four different liquid saturation pressures. These pressures were 28.8 N/cm² (30 psig), 21.9 N/cm² (20 psig), 15.1 N/cm² (10 psig), and 8.13 N/cm² (0 psig). Resulting temperature ranges were 101.5°K (182.7°R) to 89.6°K (158.6°R) and 87.5°K (157.5°R) to 75.4°K (136°R) for LO₂ and LN₂ respectively. Pressurization was autogenous and pressurant temperatures were very close to saturation temperature at the screen. Helium pressurization was used for one test with LO₂.

c. Results – An empirical correlation of the LN₂ test results is shown in Fig. II-24. Experimental data are compared to predicted bubble point values for the temperature range tested. The expected range of bubble point values, represented by the solid lines, are based on Martin Marietta methanol bubble point data from Reference II-2. These data have been adjusted according to Eq [II-2] and available liquid nitrogen surface tension data. Experimental results are shown at four different temperatures for each of the three screens tested. Liquid temperatures are the measured values recorded during the tests by the thermocouple just above the screen. Some disparity in data at the same temperature may be noticed for two of the screen specimens. We believe this was caused by errors in the temperature reading, test pressure fluctuation, and difficulty in bubble point determination due to the nonquiescent liquid surface.

II-35
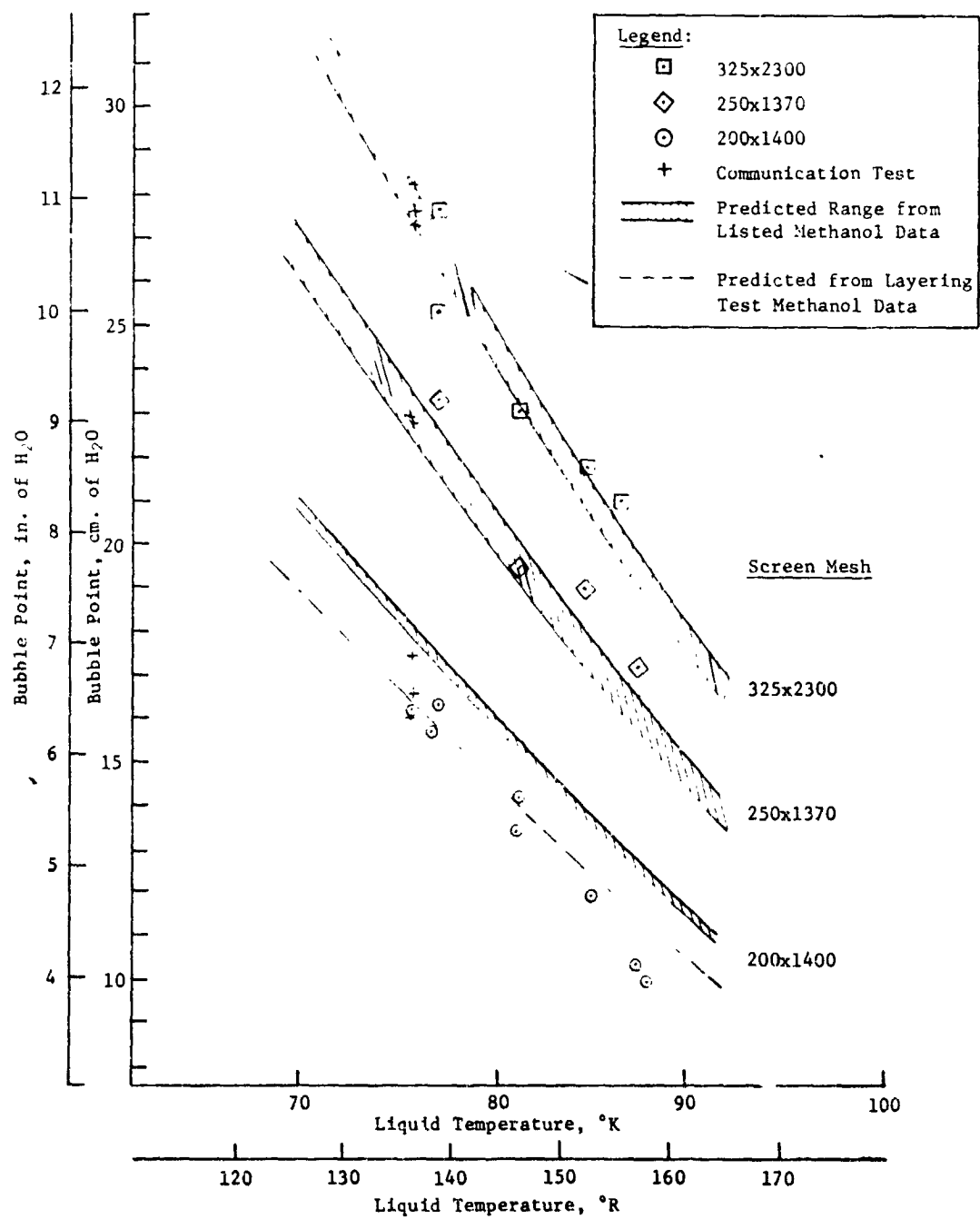
Fig. II-24 Effect of Temperature on Pressure Retention Capability in Nitrogen

The trend of the experimental data agrees favorably with the predicted bubble points. Expecially good correlation is shown for 325x2300 and 250x1370 mesh screen. Bubble point data for 200x1400 mesh screen appears somewhat lower and more erratic than predicted. However, good agreement is noted with data based on the screen layering tests previously discussed. The dashed curve represents predicted 200x1400 mesh bubble point values based on ambient methanol data obtained during the layering tests. This curve also indicates a lower trend in pressure retention capability than that shown by data from Reference II-5.

Communication screen test results (to be discussed later) support the results discussed above. Agreement with predicted values is noted for 325x2300 and 250x1370 mesh screens. However, once again, lower and somewhat more variable results are noted for 200x1400 mesh screen than were predicted. This may imply that 200x1400 mesh screen is generally less consistent than the finer meshes.

Correlation of liquid oxygen test results were less successful. These data are plotted in Fig. II-25. Predicted data were calculated, as described for LN_2, from available data for liquid oxygen surface tension. Although the data are somewhat more erratic than the LN_2 results, definite trends were established for all three screen meshes. This trend agrees with the predicted data, although a higher pressure retention capability than predicted is indicated for all screens. From a design standpoint, the data based on Reference II-5 would be conservative. The 28.8-N/cm^2 (30 psig) at 101.5°K (182.7°R) point does not support this trend, but shows a lower pressure retention capability than that predicted for all the screens tested. However, test data indicated liquid in the test article vent line during tests at this pressure, thereby causing the pressure transducer to record a lower pressure differential than actually was present across the screen. To eliminate the possibility of pressurant condensing in the system, a test was run using helium pressurant. Results showed no variation from the tests using autogenous pressurization.

Considering the correlation obtained from LN_2 test results, the LO_2 data were suspect because no logical explanation for the variance could be found. In an attempt to eliminate possible error sources, a final test series was run with a 200x1400 mesh screen. Special precautions were taken to assure that liquid was not present in the system by purging the system with pressurant. Special care was also used in bubble point determination, dewar pressure control, and temperature correlation. Results are shown in Fig. II-26. A somewhat lower bubble point value than predicted is indicated by the data, which compared favorably with LN_2 results.
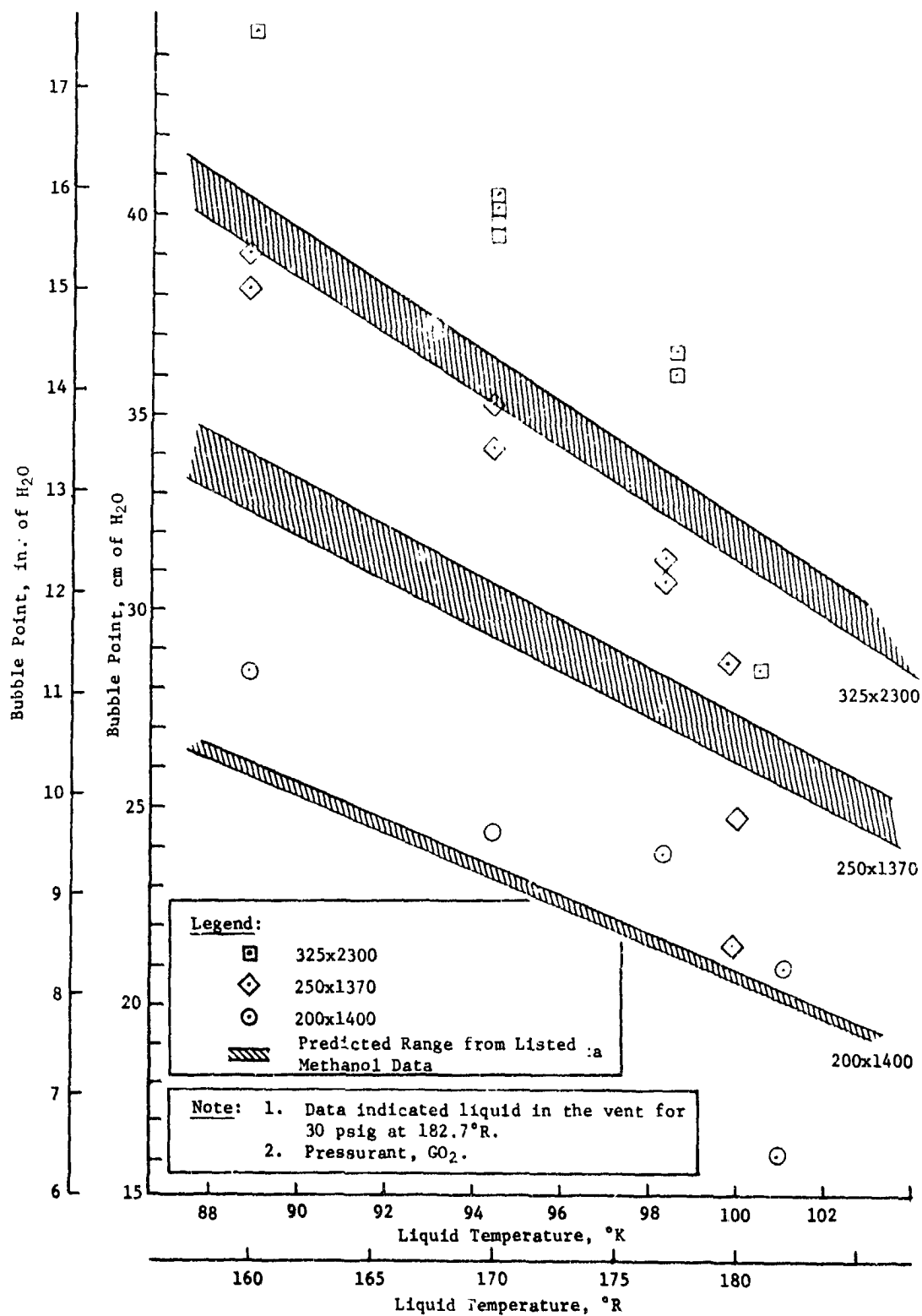
Fig. II-25 Effect of Temperature on Pressure Retention Capability in Oxygen
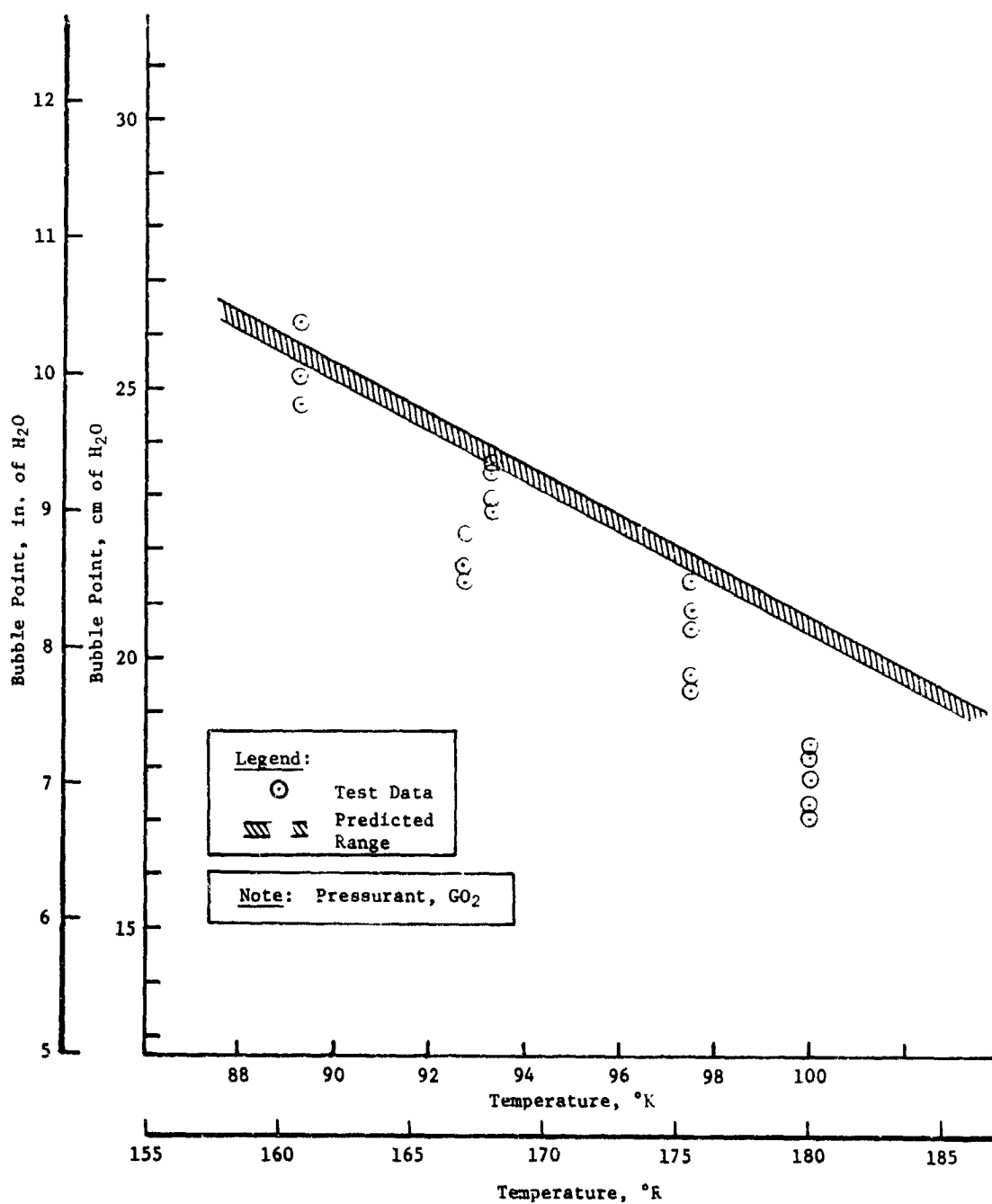
Fig. II-26 Effect of Temperature on Pressure Retention Capability
in Oxygen for a 200x1400 Mesh Screen

b. Conclusions - Bubble point correlation on the basis of surface tension is supported by the test results. Liquid nitrogen data verified the validity of Eq [II-2] for predicting bubble point variation with liquid temperature. Partial correlation of the liquid oxygen results was obtained. The remaining LO_2 data were generally higher than predicted for all the screens tested.

Considering the entire series of tests, the validity of the majority of liquid oxygen results is suspect. The disparity in the data may have several causes. These are:

1) variation in test pressure level;

2) inability to determine liquid temperature accurately;

3) difficulty of bubble point determination due to high boiloff rates;

4) liquid in vent line due to pressurant condensation or failure to maintain the ΔP required to support liquid head

3. Communication Screen/Venting Tests

a. Test Objectives - Successful operation of a capillary acquisition/expulsion system depends on providing a preferential path for gas flow so that the pressure differential between two adjoining ullage regions can be controlled. This is accomplished by incorporating a wetted screen barrier (communication screen) between ullage regions and by venting the outer annulus. Communication screens are designed with a lower pressure retention capability than the controlled liquid region so that, during periods of pressurization, breakdown of the controlled liquid region barrier is precluded. Many systems require venting to prevent pressure buildup. This must be accomplished within the limits determined by the communication device to maintain proper system operation. Therefore, for proper system design, data on screen pressure loss and system venting capability is of vital importance.

The basic objectives of the communication screen/venting tests were: (1) to determine the pressure loss across a wetted screen barrier as a function of gas flow-rate and (2) to demonstrate the ability to prevent screen breakdown (gaseous or liquid breakthrough) by venting within a ΔP band. Several different screens and fluids were considered, including cryogenic and noncryogenic liquids.

II-40

The flexibility of the test apparatus allowed data to be obtained for other areas of screen performance that are important in designing screen retention devices. These included pressure drop across dry screens, multiple dry screens, and dry screen and perforated plate combinations. Also a large amount of bubble point data showing rewetting capability was obtained for all screen and perforated plate combinations tested.

b. *Test Apparatus and Procedure*

1) Apparatus - A full-scale drawing of the communication screen test article is shown in Fig. II-27. The test article was made of stainless steel with Teflon washers used to seal each side of the screen specimen. The 12 coverplate bolts compressively sealed the screen between the gaskets. The article was enclosed in a glass dewar (used in the screen layering tests). The complete test apparatus is shown schematically in Fig. II-28.

Pressurant entered the system through the micrometer valve, V1, and the flow rate was monitored by three Fisher and Porter flowmeters attached in a parallel configuration. Pressurizing gas entered the test article through a 0.47-cm (3/16-in.) stainless steel jacketed line. The test device consisted of an inner chamber in which the screen specimen was attached. This section was surrounded by an outer chamber. A perforated plate formed the bottom of the inner chamber to diffuse the pressurant. Chamber pressure was sensed and vented by the vent line which also assisted in purging the system to assure it was liquid free. This was accomplished by means of the needle valve, V4. The test article was attached to the stainless steel cover by the pressurizing and vent tubes. A silicone rubber gasket sealed the top of the dewar to the coverplate.

The pressure differential across the screen was measured by a ±0.69-N/cm^2 (±1 psid) pressure transducer or a 0 to 152.4 cm (0 to 60 in.) water manometer, or both, depending on the test configuration. These instruments sensed the difference between inner chamber vent line pressure and dewar vent line pressure. Other instrumentation included a dewar pressure gage and four thermocouples. The thermocouples measured gas temperature at the flowmeters, just below the diffuser, and just below the screen. The fourth thermocouple measured liquid temperature.

The test apparatus is pictured in Fig. II-29 and II-30. Figure II-29(a) is a closeup of the test article in the methanol and LN$_2$ test configurations. An overall view showing the flowmeters and water manometer is shown in Fig. II-29(b). Figure II-30 is a photograph of the system in the LO$_2$ test configuration.

0.47 cm (3/16 in.)

Pressurization Line

Vent Line

0.47 cm (3/16 in.)

0.95 cm (3/8 in.)

Screen

Teflon Gaskets

6.0 cm (2 3/8 in.)

8.25 cm (3 1/4 in.)

Thermocouples
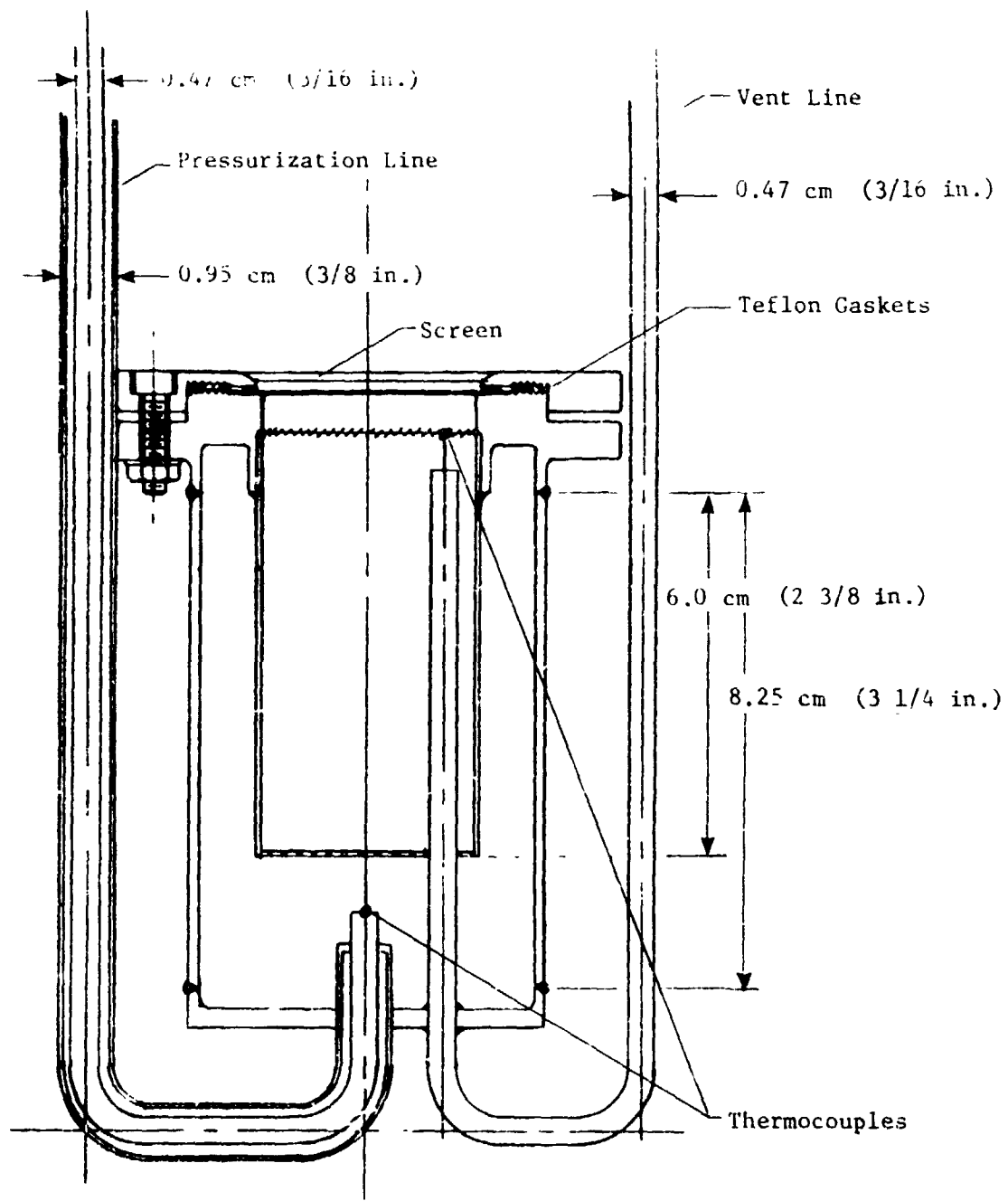
Fig. II-27   Communication Screen/Venting Test Article

II-42
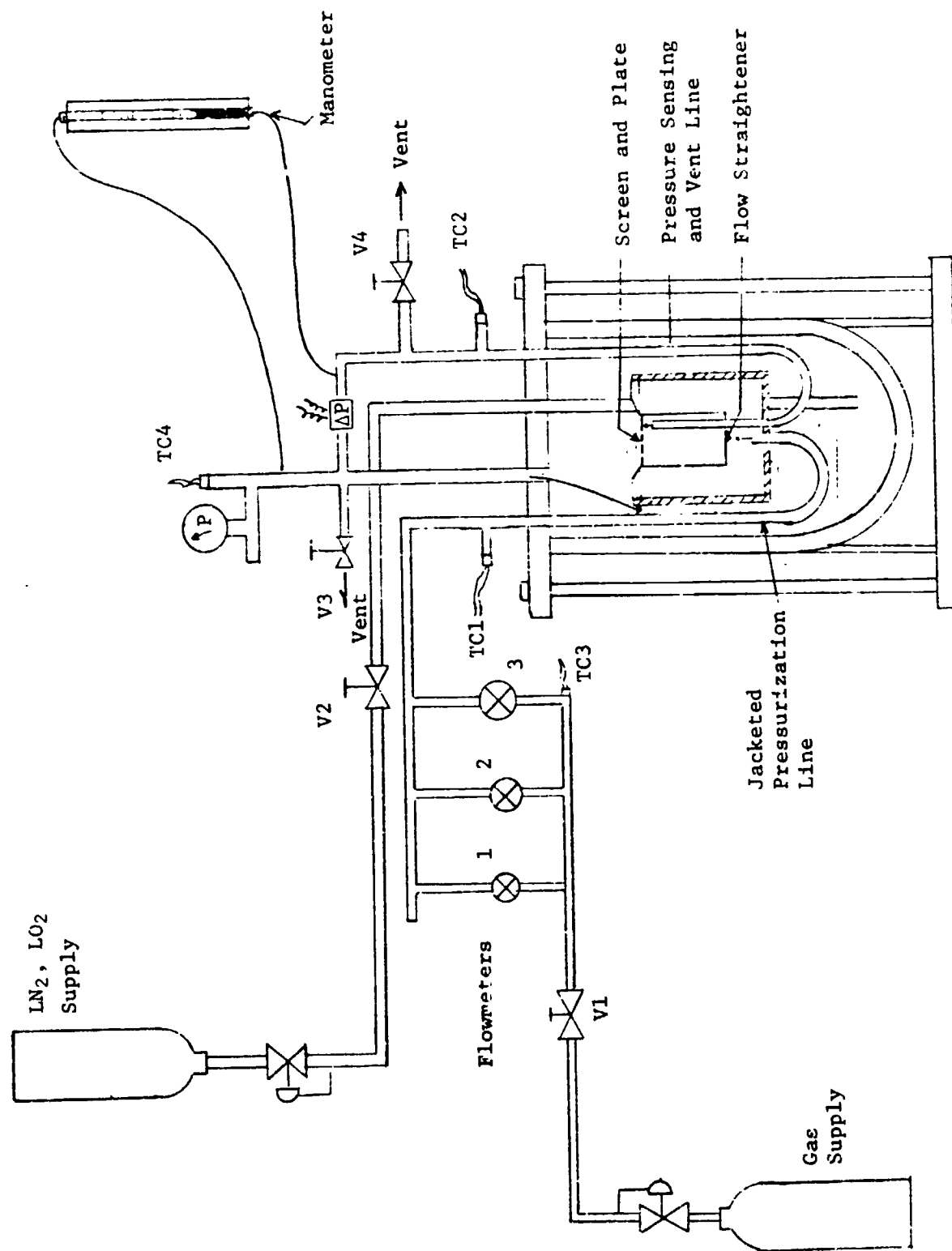
Fig. II-28 Communication Screen/Venting Test Schematic

Manometer

Screen and Plate

Pressure Sensing and Vent Line

Flow Straightener

Vent

TC2

TC4

ΔP

P

V3

V2

Vent

TC1

TC3

3

2

1

Jacketed Pressurization Line

LN₂, LO₂ Supply

Flowmeters

V1

Gas Supply

V4
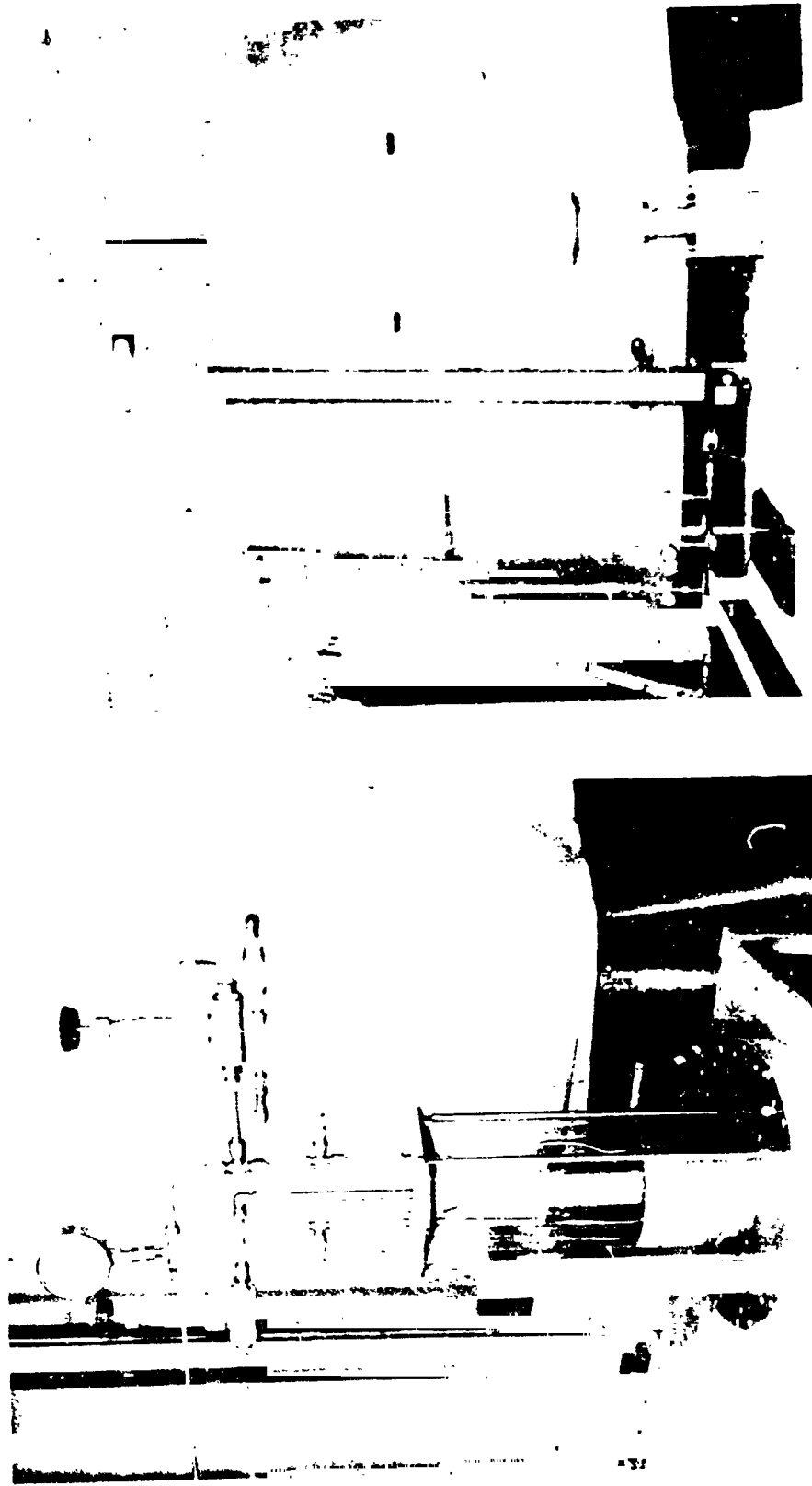
Fig. II-29   Communication Screen/Venting Test Apparatus, Methane
Test Configurations
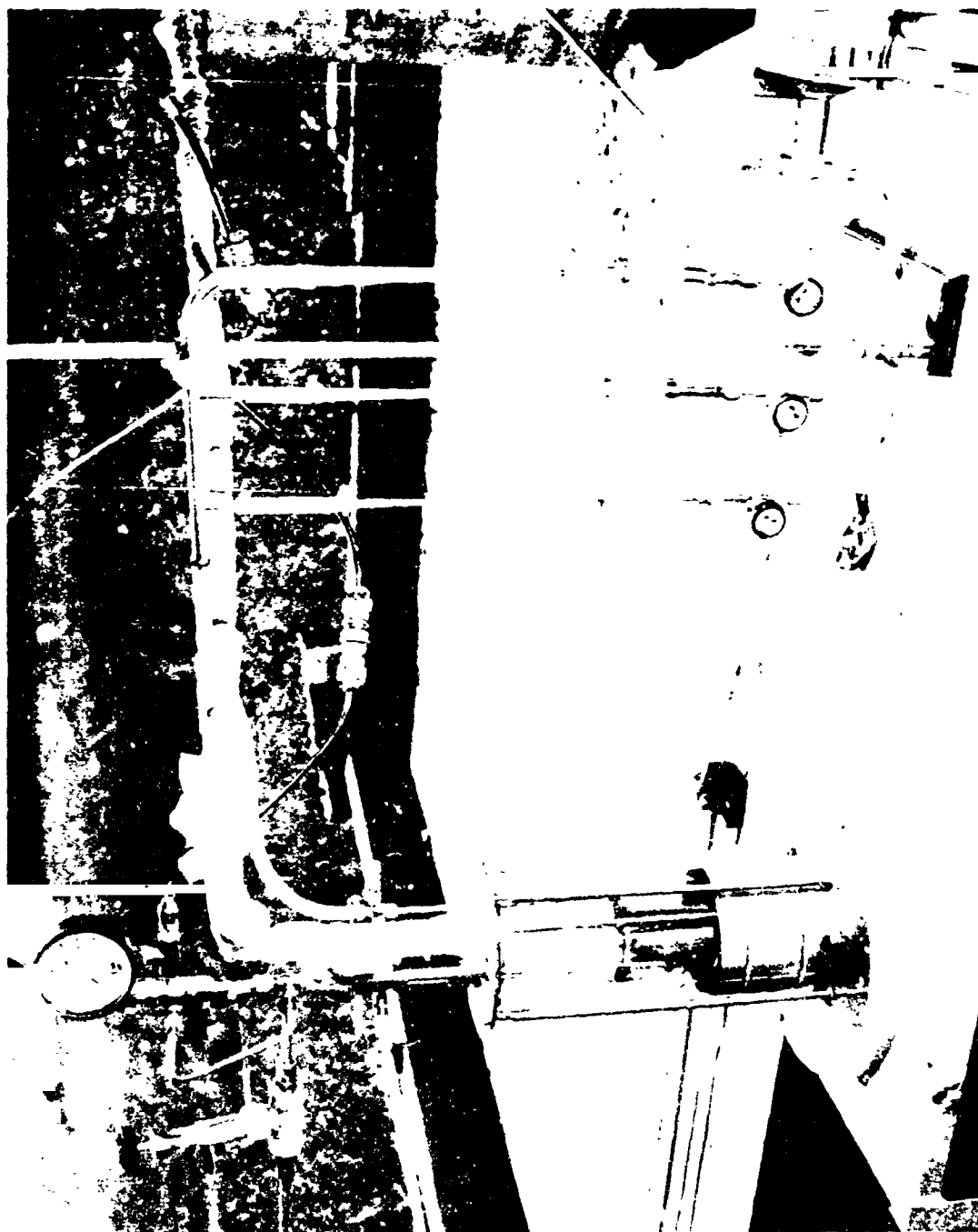
Fig. II-30 Communication Screen/Venting Test Apparatus, IO_2 Configuration

It should be noted that some instrumentation and apparatus differences existed depending on the test configuration. During initial methanol testing only the manometer was used for ΔP measurement. Following the completion of screen-only testing, both the manometer and pressure transducers were operational for all remaining methanol and LN_2 tests. Liquid oxygen testing used only the pressure transducer because of safety requirements.

c) *Test Procedure* - The basic test procedure was similar to that followed during bubble point temperature-dependency tests. Sufficient pressurant flow was initiated to prevent liquid from falling through the screen during fill. The dewar was filled with the test liquid to the desired level [approximately 0.32 cm (1/8 in.) for methanol and between 0.64 cm (1/4 in.) and 1.28 cm (1/2 in.) for cryogens above the screen]. The dewar was continuously vented to the atmosphere to prevent overpressurization and to maintain the test liquid at ambient pressure. At this point, t' ΔP across the screen was reduced to a point that ensured proper wetting of the screen. While monitoring liquid and pressurant temperatures, the system was slowly pressurized until the bubble point was reached. For cryogenic test, a continuous record of temperatures and pressure differentials was kept by strip chart recorders. As pressurant flow was increased, the pressure differential and corresponding flow rates were noted until the maximum flow capability of the flowmeters was reached. After venting the test article to ensure screen rewetting, this procedure was repeated to demonstrate data reproducibility. Subsequently, the remaining liquid was removed from the dewar and the system was changed to a new test configuration.

During cryogenic tests the system was constantly monitored for signs of liquid in the vent line. Special procedures, similar to those discussed for bubble point temperature dependency tests, were used to remedy the situation should this problem arise.

The supplementary bubble point and dry screen data presented were obtained during methanol communication screen testing. That is, bubble point data were obtained using methanol and dry screen pressure loss data were obtained immediately following methanol tests by raising the screen above the liquid level and drying it out with warm pressurant flow.

The venting test was a manual demonstration of the ability to vent within a specified ΔP band without screen breakdown. LN_2 was used as the test fluid with GN_2 pressurant. The test configuration was basically the same as for communication screen tests. With the

II-46

pressurization and dewar fill lines closed and valve V3 open, the test article vent valve, V4, was opened while monitoring the manometer. When the differential pressure dropped to a level just above that required to support the liquid head, venting was terminated causing screen ΔP to increase. Pressure was allowed to build up to a point just below the screen bubble point before venting was again initiated. This process was continued for 15 cycles while visually observing for gas breakthrough at the screen.

The reaction time of the vent valve, V1, was very slow compared to the pressurization rate. Therefore, during testing, V4 was left open and venting was accomplished by physically blocking and unblocking the exit of the vent tube.

The test specimens were all ultrasonically-cleaned stainless steel Dutch-twill screens of the following meshes: 200x1400, 250x1370, and 325x2300. Also, three different perforated plates were used in combination with the screens to determine their effect on pressure drop through wetted screens. Perforated plate data are shown in Table II-3.

Table II-3 Characteristics of Perforated Plate Tested

Plate Identifier Number	Fraction Open Area %	Hole Diameter, cm (in.)	Material	Hole Arrangement
1	51	0.35 (9/64)	Stainless Steel	Staggered, on 0.47-cm (3/16-in.) Centers
2	37	0.11 (0.045)	Stainless Steel	Not Staggered
3	30	0.16 (1/16)	Aluminum	Staggered on 0.27-cm (7/64-in.) Centers

The many combinations tested, including screens, perforated plates, test liquids, and pressurizing gases are shown in the basic test matrix of Table II-4.

The induced error in the ΔP reading caused by the thin liquid layer above the screen has been compensated for in all of the data presented. Results presented are based on a methanol temperature of 289.7°K (64°F) and saturation conditions for cryogens [P_{sat} = 8.13 N/cm^2 (11.8 psig)]. The screen diameter was 3.63 cm (1.43 in.) with a flow area of 0.001 m^2 (0.0112 ft^2).

II-47

Table II-4 Communication Screen/Venting Test Matrix

Liquid Test Configuration	Pressurizing Gas	Screen Mesh											
		200x1400				250x1370				325x2300			
		Screen Only	Screen & Plate			Screen Only	Screen & Plate			Screen Only	Screen & Plate		
			1	2	3		1	2	3		1	2	3
Methanol	GN$_2$	X	X	X	X	X	X	X	X	X	X	X	X
LN$_2$	GN$_2$		X	X	X		X	X	X		X	X	X
LO$_2$	GO$_2$ Helium					X	X	X X	X				
Dry Screen	GN$_2$	X	X	X	X	X	X	X	X	X	X	X	X
Venting Test	GN$_2$										X		

II-48

c. Results

1) Communication Screen Tests – Figure II-31 shows the response of
the wetted screen barrier to increased flow for the three screen
meshes tested. Because the screen is wetted more by gravity than by
wicking, no conclusions may be drawn regarding screen dryout. It is
evident that all screen meshes react in a similar manner. As flow
through the screen is increased, a significant increase in pressure
differential above the bubble point is noticed. At maximum flow
capacity of 0.186 m/sec (0.610 ft/sec), the differential pressure is
21.8% higher than the bubble point for a 325x2300 mesh screen.

Screen and perforated plate combinations were tested to determine
the effect of perforated plate on screen pressure retention capabil-
ity. The plate was located above the screen so that gas flowed
first through the screen and then through the perforated plate.
Data from these tests are also shown in Fig. II-31. Except for one
isolated case [325x2300 screen backed with 0.16-cm (1/16-in.) alumi-
num plate], all perforated plate data show a lower pressure reten-
tion capability than for a screen alone. Because different screen
specimens were used in each test, the data were adjusted to a common
bubble point for the same screen mesh, anticipating that a trend
would be established. The adjusted data are plotted in Fig. II-32.

Although no trends are evident as far as plate characteristics are
concerned, the pressure differential across the screen and perfo-
rated plate combination is consistently lower than for a screen a-
lone. Maximum reduction of screen pressure differential is about
5.08 cm (2 in.) of water or 8.3%.

This decrease in pressure drop may be attributed to a decrease in
the wetting capability of the screen. Pressurizing the system
forces the screen against the perforated plate, resulting in a 49
to 70% reduction in screen/liquid contact area for the perforated
plates tested. This may cause premature breakdown of some of the
pores or prevent the pores covered by the plate from completely re-
wetting.

It should be pointed out that dry screen pressure drop data (pre-
sented later) indicate an increase in pressure loss for screen per-
forated plate combinations as compared to screen alone. This re-
sult was expected because only frictional losses are involved. The
inconsistency in the two sets of data (wet and dry screen) is not
considered significant and may be explained by the different phe-
nomena affecting pressure differential.
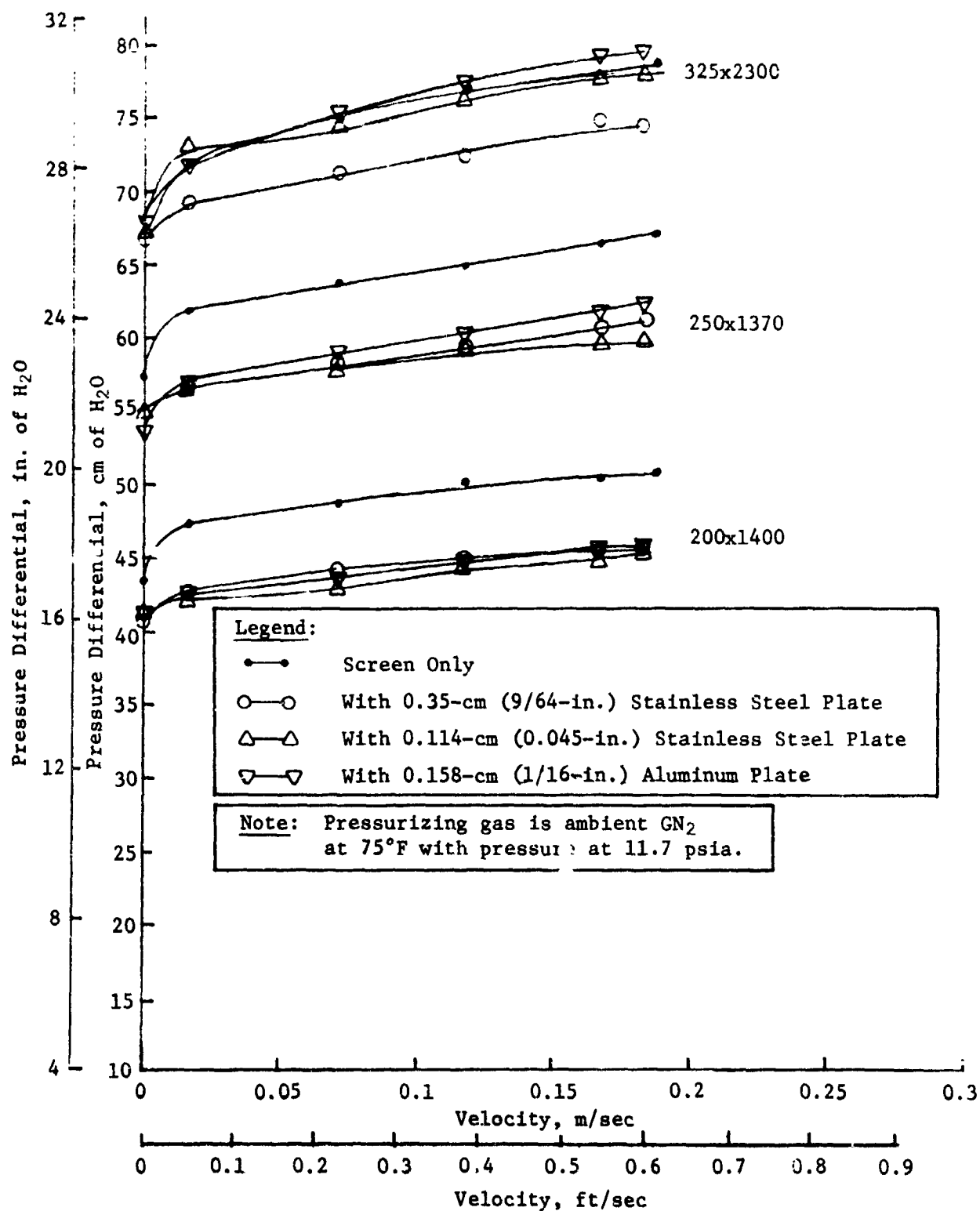
Fig. II-31 Methanol Screen and Perforated Plate Test Data

II-50
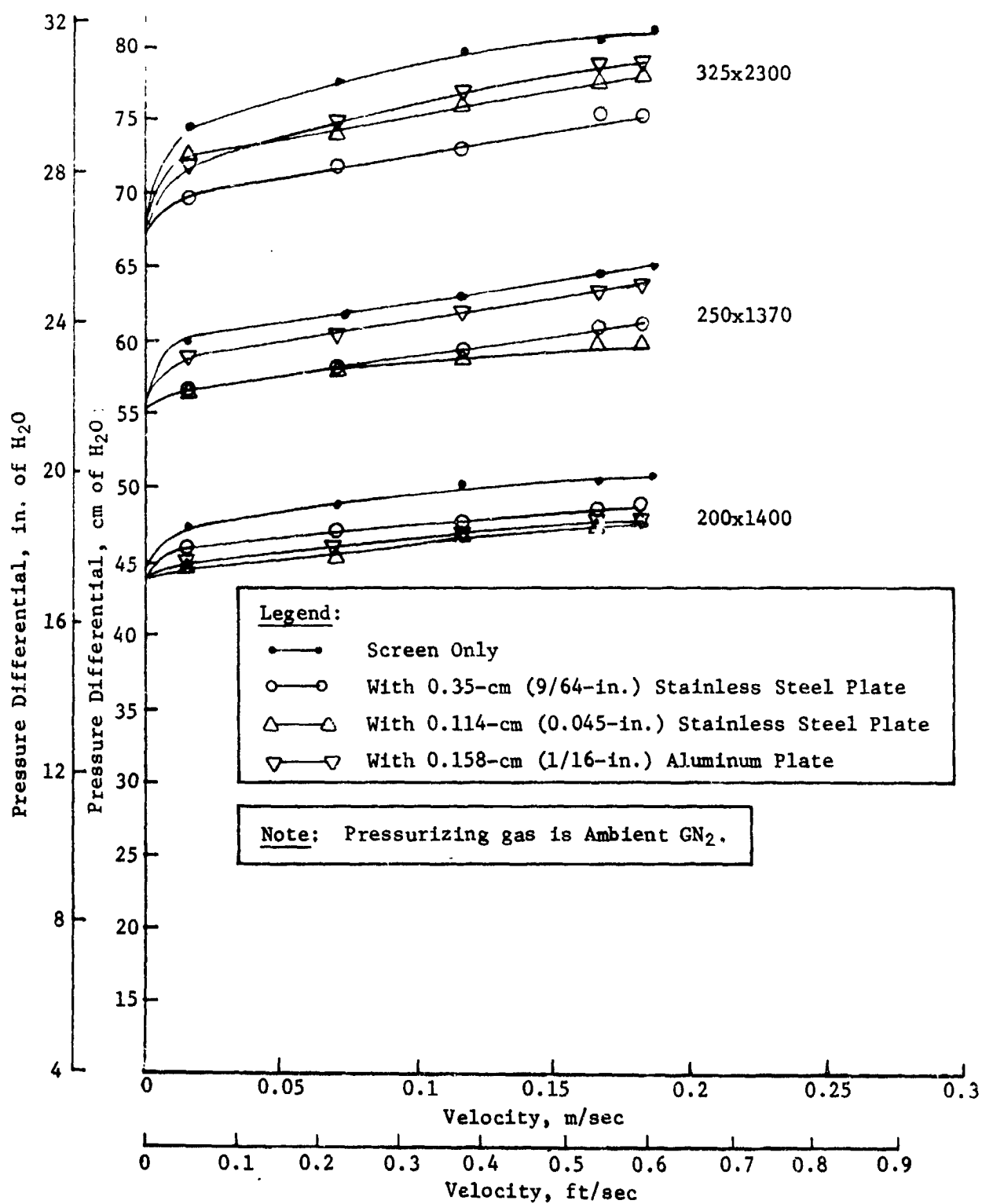
*Fig. II-32 Methanol Screen and Perforated Plate Data
Adjusted to Common Bubble Point*

Liquid nitrogen test results support those previously discussed for methanol. Pressure differentials across screen and plate combinations were lower than those predicted for the screen only configuration. Resulting data are plotted in Fig. II-33. Test data for only one screen mesh, 325x2300, were taken without perforated plate. The remaining screen-only curves were predicted from methanol data on the basis of surface tension differentials. (See previous test discussion.) Again, no trends based on perforated plate properties are evident from these curves. The data for the combination of 250x 1370 mesh screen and 0.16-cm (1/16-in.) plate are probably low because of inadequate wetting of the screen before starting the test. With this in mind, it is possible that the 0.16-cm (1/16-in.) perforated plate-screen combinations have higher pressure losses than other plates tested. This is supported by methanol data, except for 200x1400 mesh screen.

Although the pressurizing gas was ambient at the flowmeters, by the time it reached the screen it was cooled to saturated conditions. This was true for the majority of liquid nitrogen tests. However, due to initial purging of the system to assure that no liquid was present, several tests showed significant increases in gas temperature.

Tests with liquid oxygen were run using a single 250x1370 mesh screen because data acquired during methanol and LN_2 testing was sufficient to show any trends peculiar to the layering of screens. A single screen sample was used for all tests including screen and perforated plate configurations. Autogenous pressurization was used throughout most of the testing done.

Initial LO_2 test results are plotted in Fig. II-34. Once again, lower pressure differentials are indicated for screen and plate combinations than for screen alone. Also, ΔP for the 0.16-cm (1/16-in.) aluminum plate/screen combination is higher than for the other plates tested. It should be noted that data for the 0.11-cm (0.045-in.) stainless steel plate/screen configuration may be low due to improper wetting of the screen before the test.

Additional LO_2 testing was done to explain the somewhat erratic bubble point data obtained during the first test series. Unfortunately, additional problems were encountered that produced results similar to those of the bubble point temperature dependency tests. Although an explanation for the erroneous data has not been found, the problem appears to be system-related and not peculiar to the test fluid, LO_2.

II-52
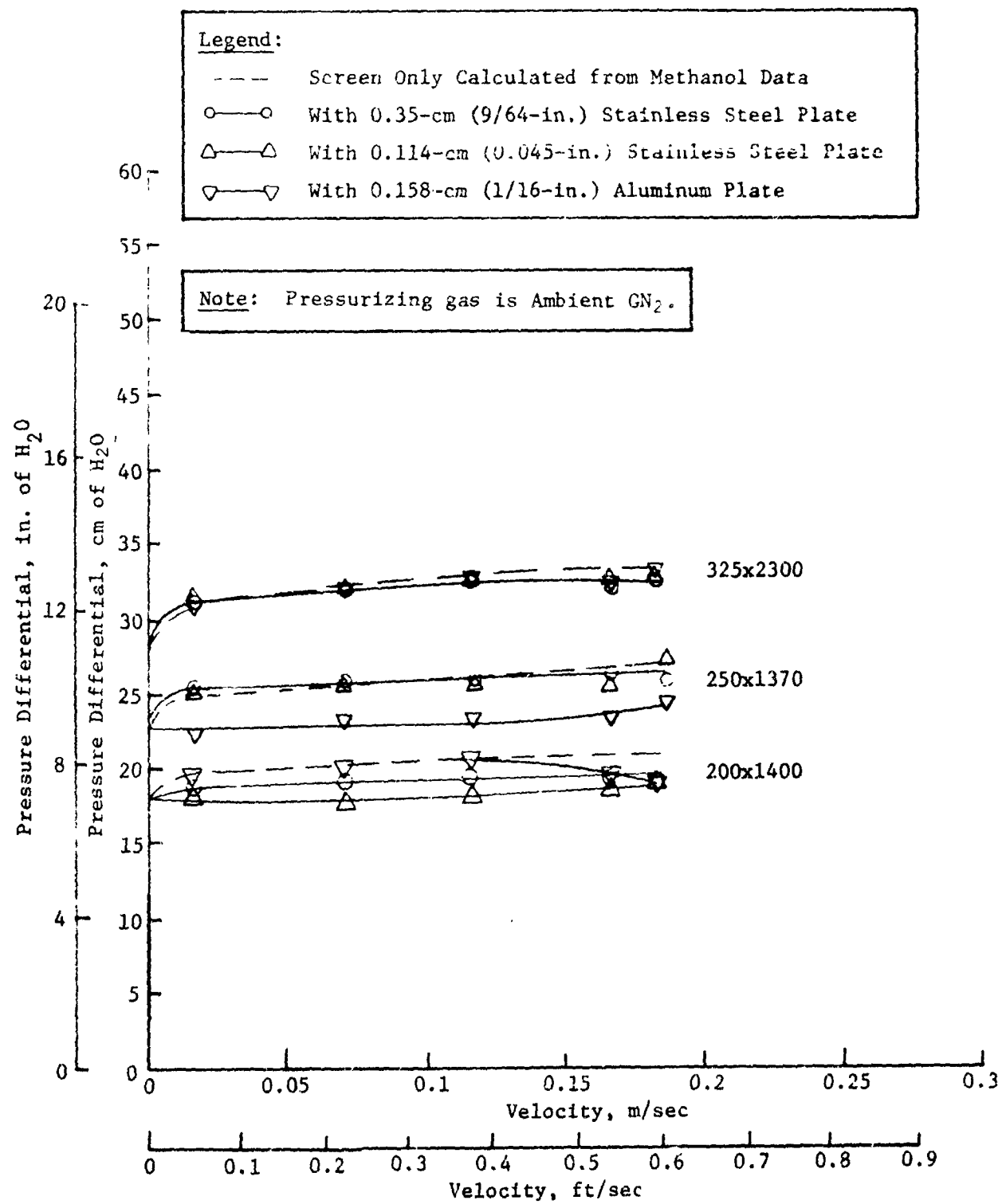
Fig. II-33 *LN₂ Screen and Perforated Plate Data Adjusted to Common Bubble Point*

II-53
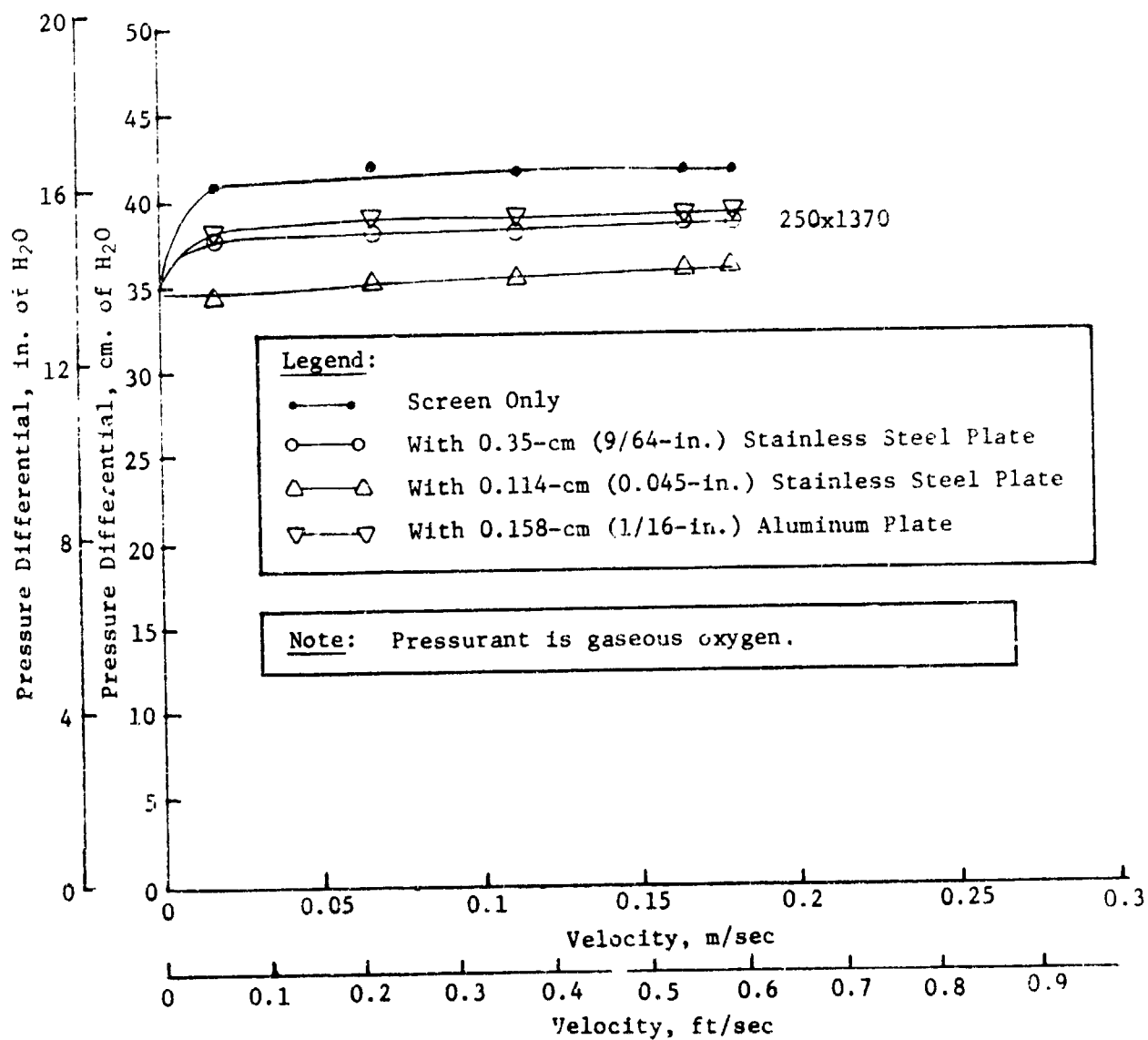
Fig. II-34 LO₂ Communication Screen Test Results

_._ _......_. _._ _-_ Venting test results are shown in Fig. II-35.
Liquid nitrogen and gaseous nitrogen were the fluids used. A 325x
2300 mesh screen with a 0.35-cm (9/64-in.) stainless steel plate
was the test specimen. It should be noted that valve V1 was closed
and was not a source of pressurization. However, analysis of test
data indicates the pressure differential across the screen dropped
to zero just before the start of the test. Apparently, this al-
lowed some liquid to drop through the screen. The residual heat in
the system from the preceding test caused this liquid to vaporize
and pressurize the system. Pressurization rates up to 0.117 N/cm^2
(0.17 psi) per second were obtained due to this phenomenon.

The upper and lower dashed lines in Fig. II-35 represent the screen
bubble point and the pressure differential required to support the
liquid head, respectively. The system was successfully vented with-
in this band for 15 cycles, representing a time of 43 seconds. The
ease with which this test was run leads to speculation that success-
ful venting with higher pressurization rates and smaller vent bands
could be attained.

_c._ _Bubble Point Data_ - As part of the curve determination and data
comparison procedures, bubble points were determined to be part of
the regular testing. A comparison of these data with existing data
is shown in Fig. II-36 for methanol. Bubble points are shown as
circular data points. The dashed lines represent the data band from
previous Martin Marietta testing (Ref II-3). The comparison is gen-
erally favorable, although some low points are noted. Earlier bub-
ble point test results suggested that some of these bands are high,
especially for 200x1400 mesh screens.

Other data are presented in Fig. II-36 in addition to ordinary bub-
ble point values. The triangular data points are "reseal" bubble
points that indicate the rewetting capability of the screen. These
data were taken after flow had been initiated through the screen.
Valve V1 was closed and the ΔP across the screen was decreased by
venting V4. As soon as all bubbles disappeared, signifying complete
rewetting of the screen, the differential pressure as indicated by
the manometer was recorded. V4 was immediately closed and V1 opened
to pressurize the system to see if an acceptable bubble point read-
ing would be indicated. These points are shown by the solid circles.
For screens only, these data represented acceptable bubble point
values. However, for screen and perforated plate combinations an
erratic and generally lower value than the bubble point was re-
corded, indicating that portions of the screen were still not wet.

Note: Test specimen is 325x2300 screen with 0.35-cm (9/64-in.) stainless steel plate.

Screen Bubble Point

ΔP Required to Support Liquid Head

ΔP across Screen, cm of H₂O

ΔP across Screen, in. of H₂O

Time, sec

Fig. II-35 ΔP, % vs Arc Results

II-56
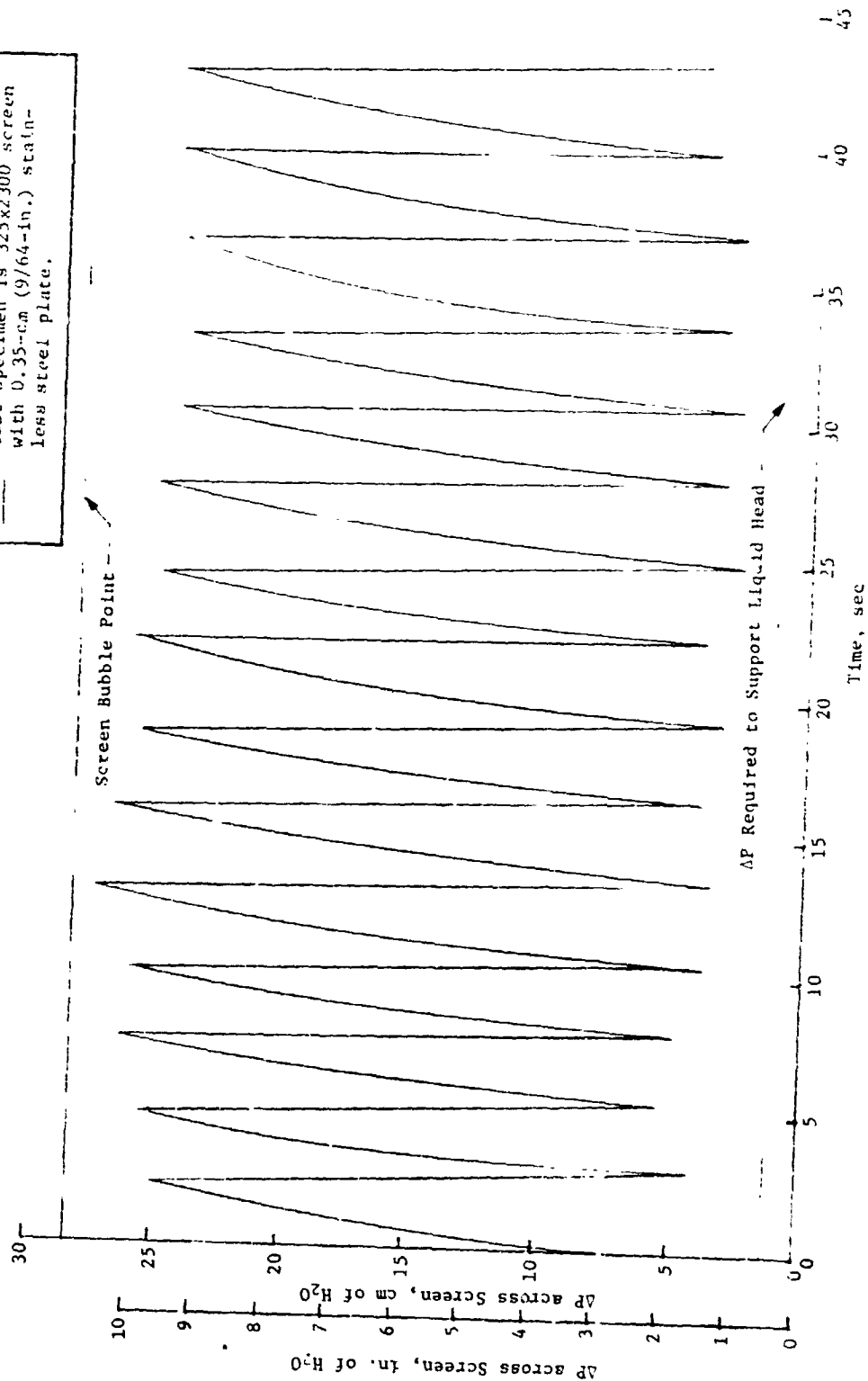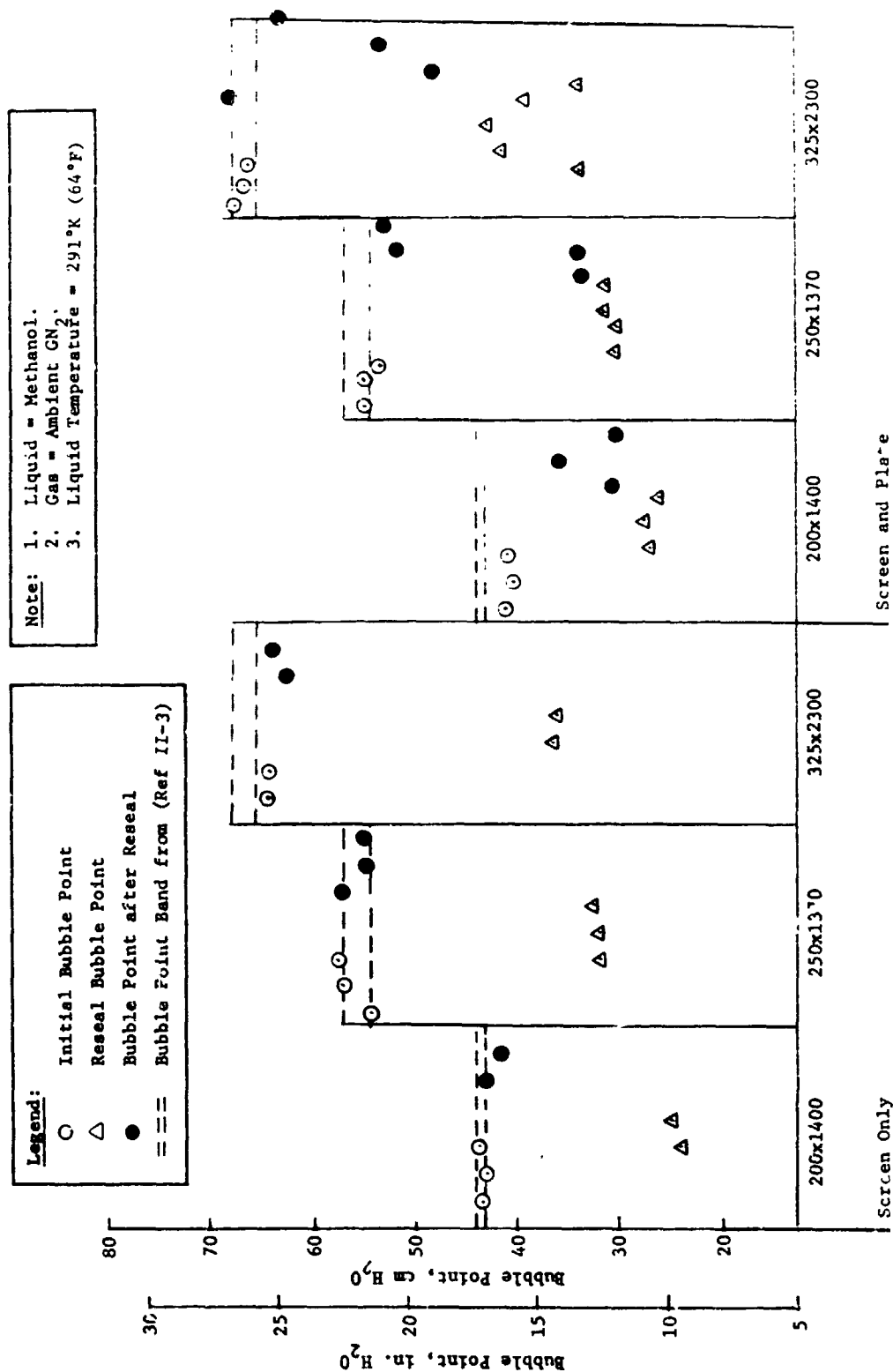
Fig. II-36 Methanol Bubble Points and Rewetting Capability

The reseal data reflect a hysteresis effect in the pressure reten-
tion capability of wetted screens. These values are generally well
below the established bubble point for the screen and indicate that
once screen breakdown has occurred, merely decreasing the ΔP across
the screen below the bubble point value will not stop gas flow
through the screen. Pressure differential at reseal generally av-
erages only 57% of the screen bubble point. Therefore, in a screen
retention device if breakdown of the screen liner occurs, the ΔP
across the screen must be decreased to at least 57% of the bubble
point to assure no further gas ingestion into the liquid region.
For a screen and perforated plate combination, the data indicate
that a reseal ΔP equal to 57% of the bubble point will not ensure a
designed pressure retention capability.

4) Nonwetted Screens - Data plotted in Fig. II-37 show the results
of the multiple dry screen test. The pressure drop ratio $\Delta P_{ms}/\Delta P_{ss}$
is plotted as a function of the number of screens and flow velocity.
ΔP_{ms} and ΔP_{ss} are the pressure drops for the multilayered screen and
single screen configurations, respectively. Data are shown for two
different flow rates and zero spacing between screen layers. Test
results for three different screens imply that pressure drop across
multiple dry screens is additive. Although some data scatter is
noted, assuming an additive pressure drop would be conservative for
the communication screen design considerations.

The validity of the test data is supported by a comparison with
McDonnell Douglas (Ref II-4) and Armour and Cannon (Ref II-5) exper-
imental results. This correlation is shown in Fig. II-38. The non-
dimensionalized parameter $\Delta P \epsilon^2 D/Q B \rho V^2$ is plotted as a function of
Reynolds Number (Re = $\rho V/\mu a^2 D$). The solid line is the Armour and
Cannon data correlation, $f = \dfrac{8.61}{Re} + 0.52$. The dashed line repre-
sents MDAC test data. The comparison indicates that MDAC experi-
enced slightly lower pressure losses than were experienced at
Martin Marietta. Data generally fit into a band bounded by Ref II-
4 and Ref II-5 test results. At lower Reynolds numbers, a deviation
from this trend is obvious. Data in this region are questionable
due to the low sensitivity of the instrumentation used. Note, how-
ever, that the correlation suggested by Armour and Cannon is suc-
cessful in aligning data points for different mesh screens.

II-58

Note: Pressurizing gas is Ambient GN_2.
No spacing between screen layers.
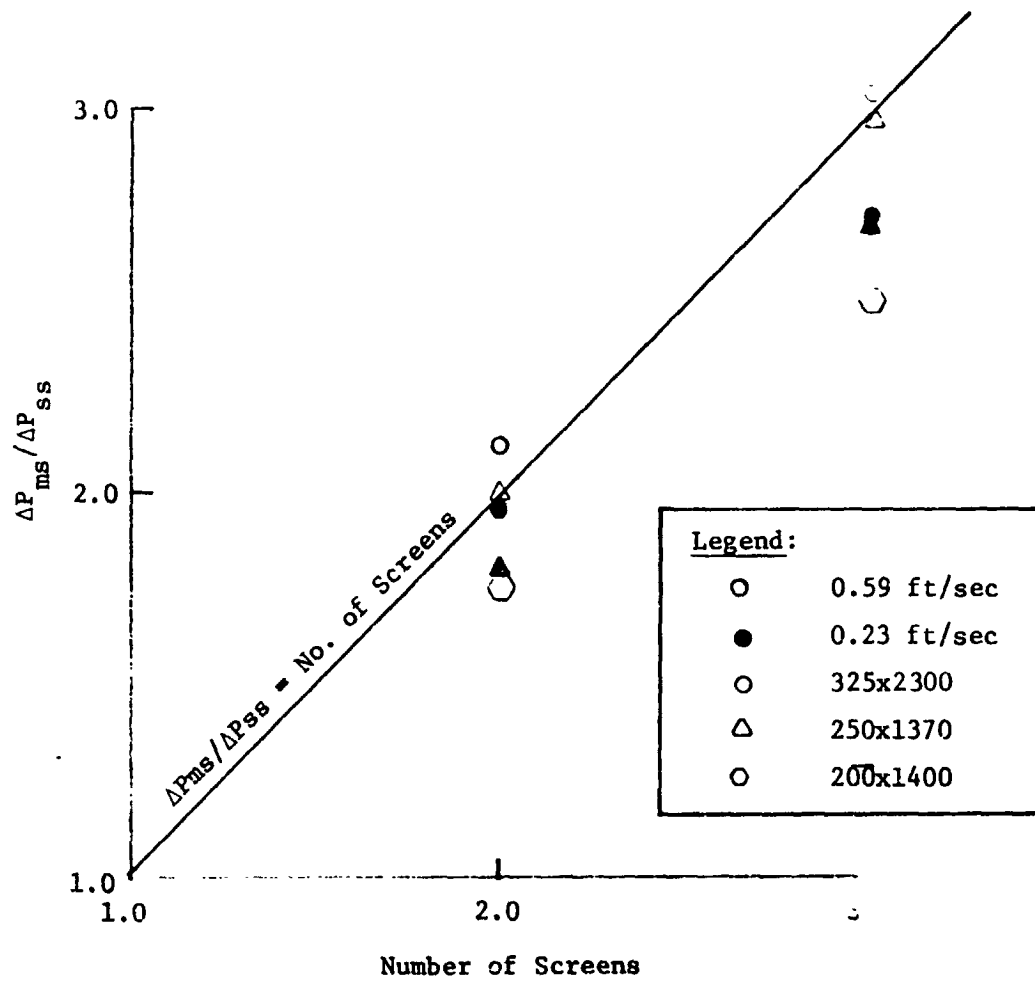
Fig. II-37 Multiple Dry Screen Pressure Drop

Screen Characteristics

Mesh Size	Q	B, m	a, 1/m	D, m	ε
375x2300	1.3	8.6×10^{-5}	108,666	1.13×10^{-5}	0.261
325x2300	1.3	8.9×10^{-5}	102,106	1.4×10^{-5}	0.297
250x1370	1.3	1.37×10^{-4}	71,438	1.7×10^{-5}	0.226
200x1400	1.3	1.52×10^{-4}	63,435	2.12×10^{-5}	0.267

Note: Gas is ambient GN_2.
Flow Diameter, D = 3.75 cm (1.48 in.)

$$f = \frac{8.61}{Re} + 0.52 \ (A \ and \ C)$$

MDAC Test Data

Friction Factor, $f = \Delta P \ \epsilon^2 D / Q B \rho V^2$

Reynolds Number, $Re = \rho V / \mu a^2 D$

Legend:

×	375x2300
△	325x2300
o	250x1370
□	200x1400

Fig. II-38 Comparison of Dry Screen Test Data with Armour and
Cannon and MDAC Correlations

II-60

The effects of perforated plate on pressure loss for flow through dry screens was also investigated. A test matrix of three screens and three perforated plates was used (Table II-4). Flow rate was also varied. The resulting data are plotted in Fig. II-39. The pressure drop for a screen and plate is higher than for a screen alone. MDAC tests indicated (Ref II-4) that correlation would involve something more complicated than simply, F_A, the fractional open area of the perforated plate. These data support that hypothesis; although a trend to lower $\Delta P_{ms}/\Delta P_{ss}$ ratios with increasing F_A is apparent.

Other trends appear to be screen and velocity dependent. Higher $\Delta P_{ms}/\Delta P_{ss}$ values are indicated at higher flow velocities although the data presented are not sufficient to be conclusive. A different data trend is indicated for a 325x2300 mesh screen, compared to data for the other screens tested. The $\Delta P_{ms}/\Delta P_{ss}$ continually decreases with increasing F_A regardless of flow rate for this specimen. However, 200x1400 and 250x1370 mesh screens consistently show lower values of $\Delta P_{ms}/\Delta P_{ss}$ at $F_A = 0.39$ than at $F_A = 0.51$. Data correlation will, therefore, involve the parameters, F_A, velocity, V, some screen properties, and possibly other variables.

d. *Conclusions* - Several conclusions important to the design of screen retention devices may be drawn from these tests. Flow through wetted fine mesh screens may cause pressure differentials as high as 1.25 times the bubble point of the screen. Flow through wet screen/perforated plate combinations exhibits consistently lower pressure losses than for wet screen alone (1.17 x BP). This added pressure differential should be considered in communication screen design.

Flow losses through dry screens may be conservatively predicted from Armour and Cannon's analysis. This is substantiated by Martin Marietta and MDAC test results. Also, from a conservative standpoint, pressure losses across multiple dry screens are essentially additive.

Results of flow through dry screen/perforated plate combinations show pressure differentials as high as 1.6 times that of the screen alone. Although a definite trend to lower pressure differentials is indicated for increasing plate open area, F_A, data are insufficient for good correlation. The inconsistency with wetted screen/perforated plate data has been previously noted and is not considered significant.

II-61
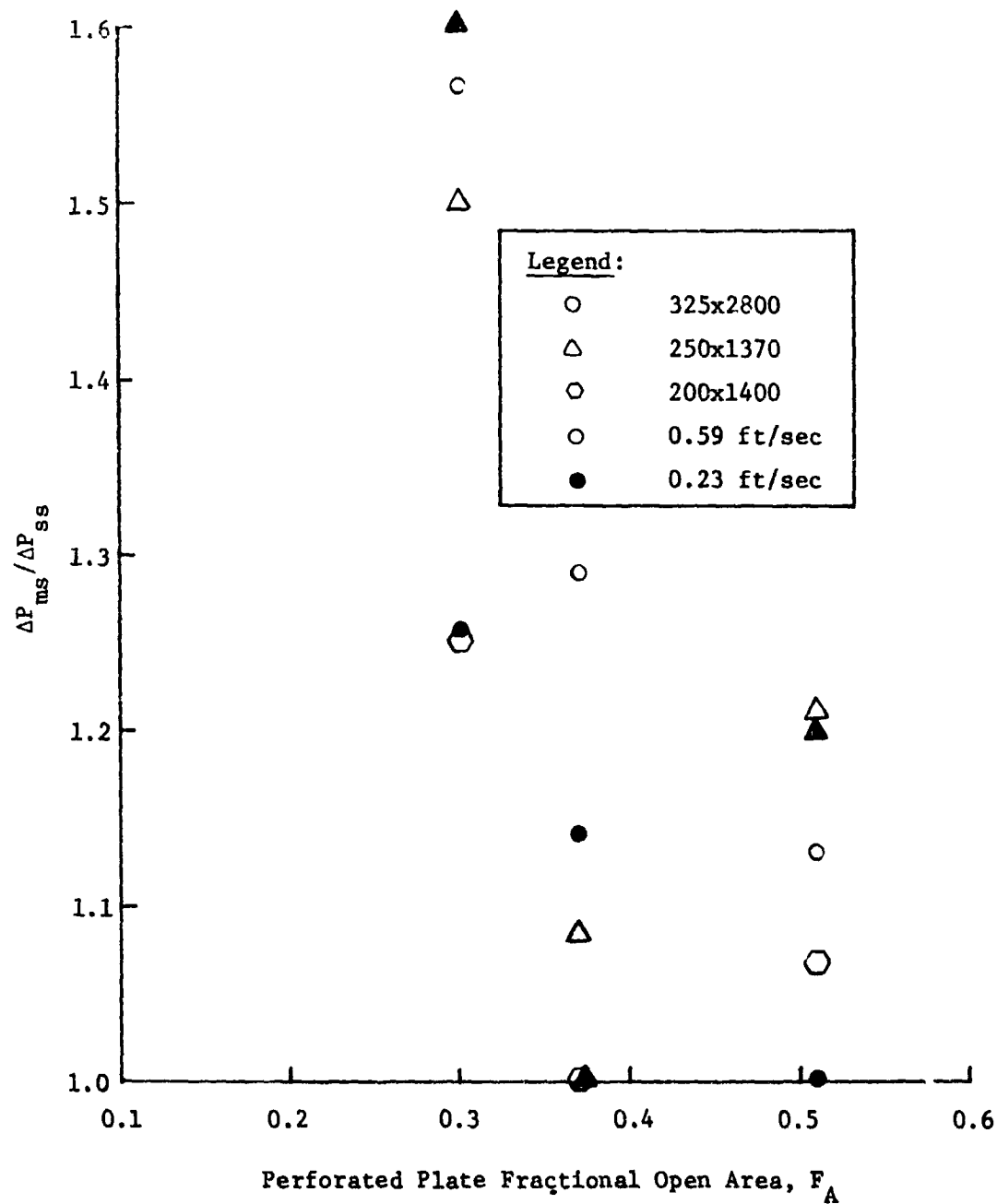
Fig. II-39   Effects of Perforated Plate on Dry Screen Pressure Loss

II-62

The cryogenic venting test was successful with pressurization rates as high as 0.19 N/cm^2 (0.17 psid) per second. Venting was achieved manually, and test results indicate that successful venting could be achieved with higher pressurization rates and narrower vent bands.

Methanol bubble points agreed favorably with previous data for the screens tested. Liquid nitrogen and much of the liquid oxygen bubble point data also agreed well with established bands.

Screen hysteresis is evident from reseal bubble point data. Complete rewetting of screens will not take place until differential pressure across the screen has been reduced to at least 57% of screen bubble point. For screen/perforated plate combinations, something less than this value is required to assure adequate pressure retention capabilities upon repressurization of the system.

4.   Wicking Tests

a.   Test Objectives - The importance of wicking to designing a
capillary cryogenic acquisition/expulsion device was discussed
in Volume II of this final report. The discussion also described
the analytical model developed for predicting steady-state wick-
ing through screens and screen/plate combinations. Due to as-
sumptions inherent in the analysis, the model approximated the
distributed heat load problem, which is of primary concern in the
design of surface tension devices. The validity of the analyti-
cal solution was supported by correlation with a computer model,
which more accurately described the physical system.

The purpose of wicking tests was to verify the analytical model
and obtain experimental data for configurations not previously
investigated. Determination of the wicking constant, K, and com-
parison with other work done were also of primary concern. Al-
though cryogenic fluids were initially of interest, it was anti-
cipated that excessive heat loads would result in meaningless
data. Therefore, the fluids, methanol and pentane, were selected
to meet the test objectives. Special emphasis was placed on
wicking in a screen/plate configuration, which is generally re-
quired by the present capillary designs. The screens tested
were the finer Dutch twill meshes, for which previous testing
failed to supply data.

b.   Test Apparatus and Procedure - The screen/plate wicking test
equipment is shown in Fig. II-40. The test section, shown sche-
matically in Fig. II-41, consisted of a stainless steel fine mesh
screen attached to a half cylinder that was formed by splitting
a 4.13x0.64-cm (1 5/8x1/4-in.) wall aluminum tube lengthwise.
Instrumentation was mounted on the underside of the plate to-
gether with three strip heaters. The scale for measuring wick-
ing distance is shown mounted along the test section. The fluid
reservoir was filled to a level that just covered the top of the
screen. The screen/plate test section was enclosed in a plexi-
glass cylinder with vacuum-jacketed plumbing designed for cryo-
genic use.

Figure II-41 shows the 26.7-cm (10.5-in.) test section and the
three strip heaters used for varying the wicking distance. The
instrumentation locations used for temperature measurement along
the wicking interface are also shown.

(a) Test Section
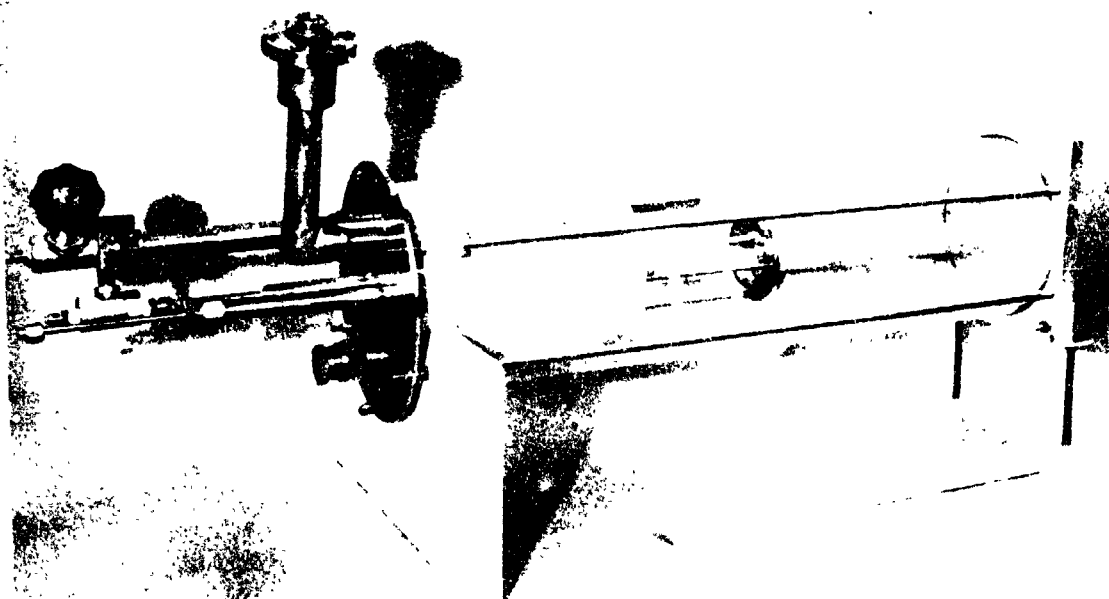
(b) Experimental Apparatus

Fig. II-40 Wicking Test Equipment, Screen/Plate Wicks

II-65

Fig. II-41 Diagram of Wicking Test Sections, Screen and Plate
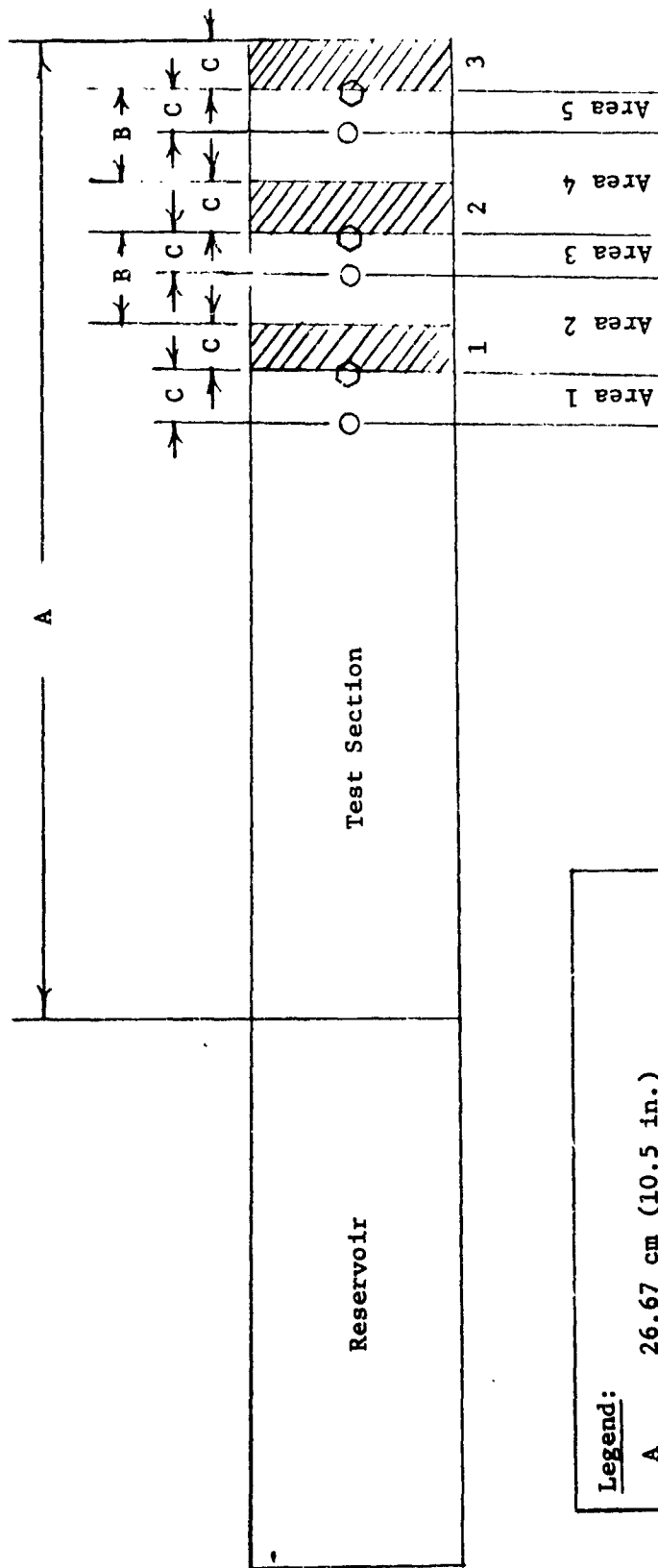
Legend:

A   26.67 cm (10.5 in.)

B   2.54 cm (1.0 in.)

C   1.27 cm (0.5 in.)

⬡   Platinum

◯   Copper Constantan Thermocouples

▨   Electric Heaters

Two ultrasonically cleaned screen specimens were used during screen/plate testing: 325x2300 and 250x1370 mesh stainless steel Dutch twilled screen. A semicircular cross section was chosen to provide a uniform gap thickness between the screen and plate. The screen was attached by spotwelds at the inside edge of the plate, which created an unwanted reservoir of liquid along the length of the screen. The effect was to increase the wicking potential of the systems, resulting in an approximately parabolic interface profile. To minimize the induced error, the wicking length was measured at the top of the semicircular test section.

The test equipment was modified to test screen wicks as shown in Fig. II-42. Basic modifications involved only the test section, which consisted of a single screen with instrumentation mounted as shown in Fig. II-43. The screen wicks tested were 2.54x10.16 cm (1x4 in.) rectangular sections of 325x2300 and 200x1400 Dutch twill screen. Each specimen was ultrasonically cleaned and attached as shown in Fig. II-42(a). Since the screen test section was an extension of the reservoir screen, support was necessary only at the far end, as shown. This arrangement assured that wicking was due entirely to the screen test section because additional wicking due to attachment was precluded.

Instrumentation included heaters and temperature sensors for each test section. An additional thermocouple recorded the liquid reservoir temperature. Other equipment included a DC power supply, ammeter, and voltmeter for each heater circuit from which power, and ultimately heat load, were calculated. Two of these units are shown in Fig. II-42 (b).

Procedure - Tests were run using both methanol and pentane. Before testing, the system was flooded with liquid and then drained, leaving a small depth of liquid to ensure a relatively saturated atmosphere. The liquid level in the reservoir was maintained even with the top of the screen during testing to minimize hydrostatic head effects.

Referring to Fig. II-41, screen/plate wicking data were taken by adjusting the power to Heater 1 until the interface separating the wet and dry sections of the wick was located in Area 1. Heaters 2 and 3 were then regulated until the temperature gradient along the dry portion of the screen was zero. At equilibrium, the wicking length, power readings, and temperature measurements were recorded. At this point all heaters were turned off to allow the wick to completely rewet. Data were taken in a similar manner for a stable interface in each of the five areas shown in the schematic. In Areas 2 and 3, Heater 2 was used to locate the
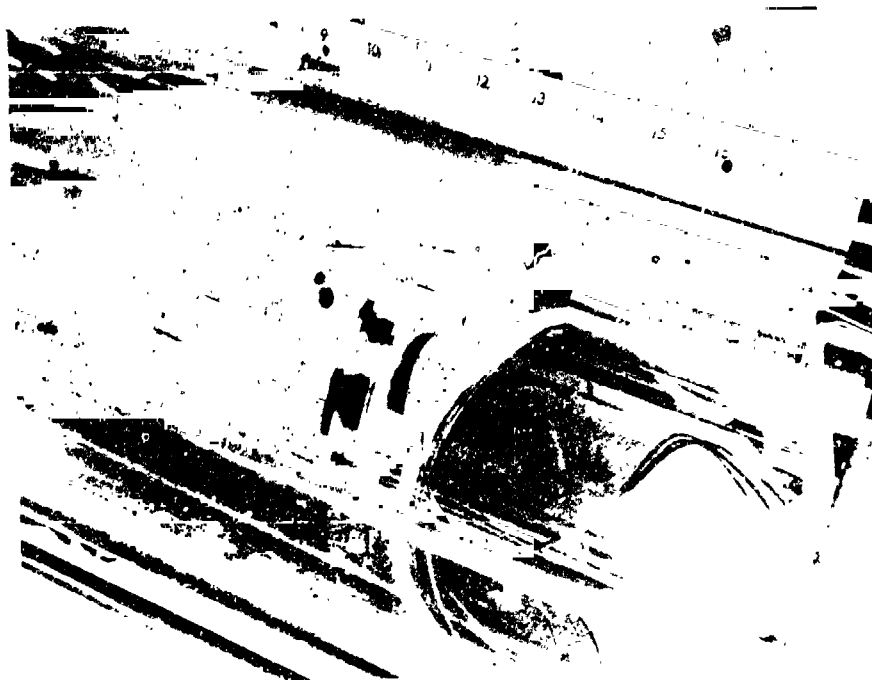
II-67

(a) Test Section

(b) Experimental Apparatus

Fig. II-41. Winding-test apparatus, general view.
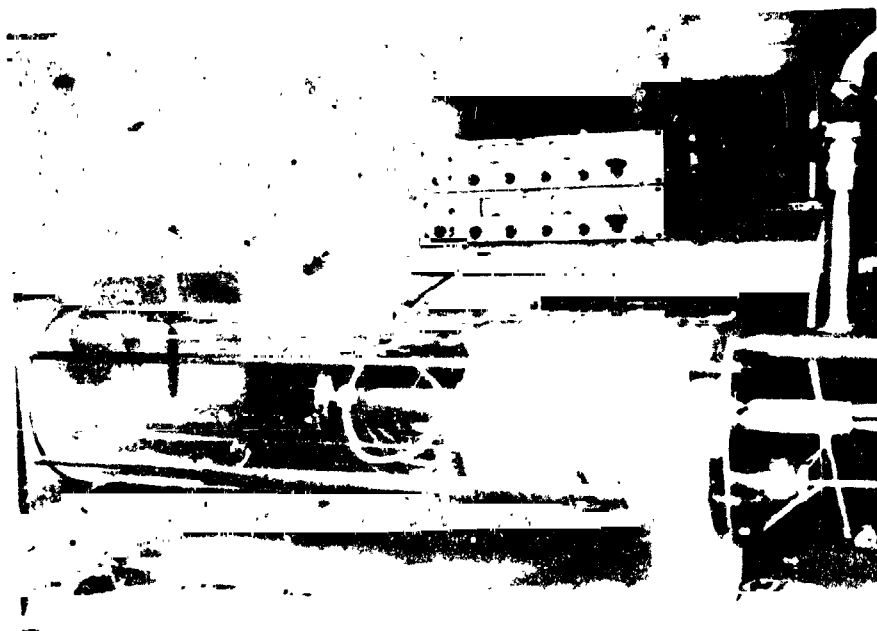
II-68
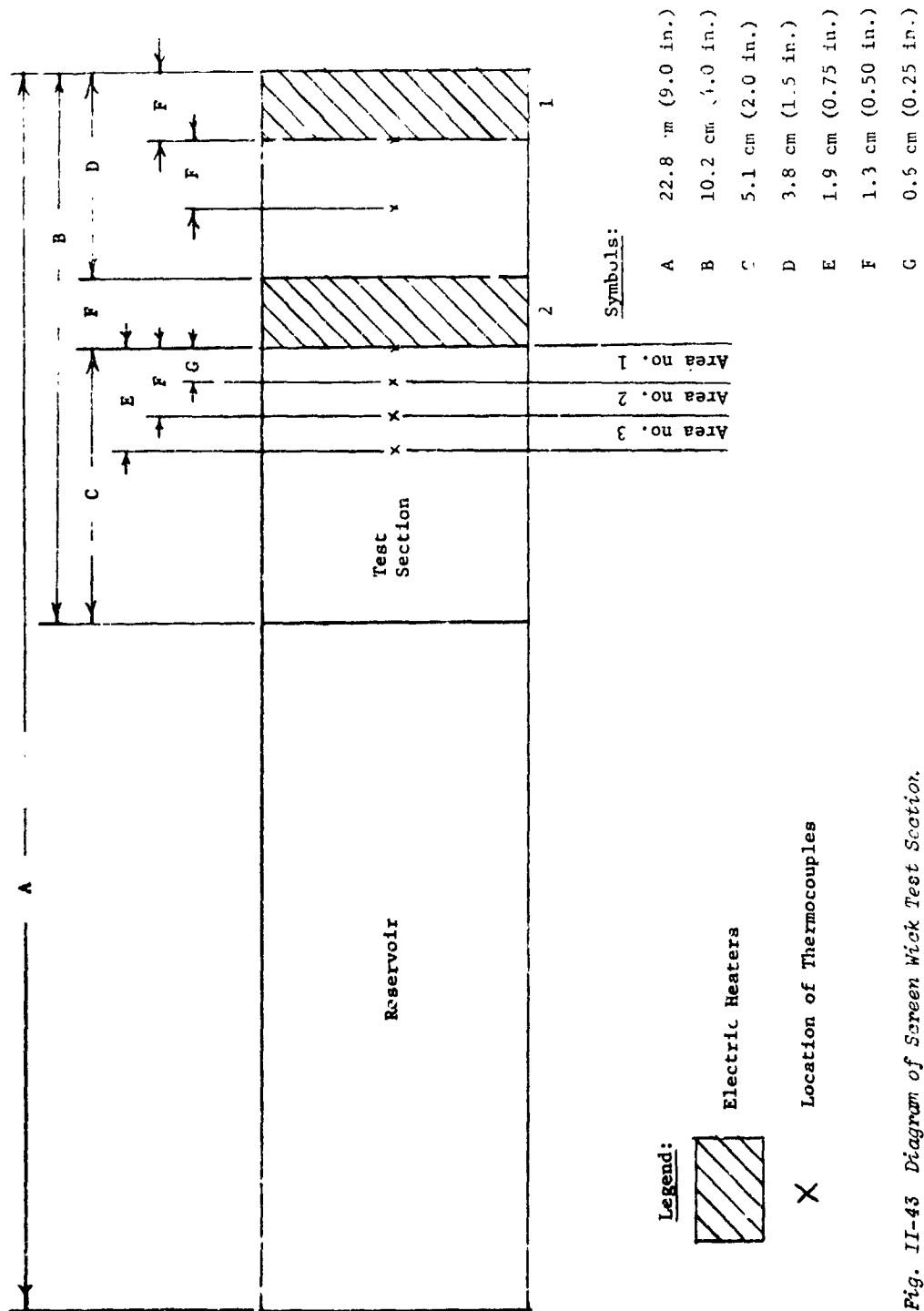
Fig. II-43 Diagram of Screen Wick Test Section.

Symbols:

A	22.8 cm (9.0 in.)
B	10.2 cm (4.0 in.)
C	5.1 cm (2.0 in.)
D	3.8 cm (1.5 in.)
E	1.9 cm (0.75 in.)
F	1.3 cm (0.50 in.)
G	0.6 cm (0.25 in.)

Legend:

Electric Heaters

X   Location of Thermocouples

wicking front and Heater 3 became the guard heater. The interface in Areas 4 and 5 was located using Heater 5. To show reproducibility, two additional runs were made, providing data for each of the five interface locations. A similar procedure was followed for screen wick tests.

c. Results - Useful test data could not be obtained with methanol because of the corrosive nature of the fluid. Severe corrosion of the aluminum plate caused pitting and clogging on the wicking surfaces and resulted in erratic and unpredictable results. Consequently, only pentane results are presented.

Data analysis involved determining the heat per unit of time, q, input to the liquid from the heater power readings. This computation assured that the contribution of the guard heaters was negligible. However, corrections for heat losses due to convection, radiation, and liquid subcooling were estimated with the help of temperature readings. Conduction losses were assumed to be minor. The heat flux was determined using the surface area of the wick tested and plotting it against the corresponding dryout limit, S. Test data for screen and screen/plate configurations are shown in Fig. II-44 through II-46 for the three screens tested.

As the graphs show, data for both configurations were not obtained for all screen specimens. Screen and screen/plate data were obtained only f ' the 325x2300 mesh sample. For the 250x1370 screen, only screen/plate data were taken and for 200x1400 mesh only screen wick data were obtained. Experimental data from different areas of the test section are denoted by different symbols on the graph. As discussed previously, some error in heat input to the test fluid was anticipated. Estimates indicated that the losses would vary from 5 to 44% of the power input to the system as indicated by instrumentation. However, most of the tests showed losses of 10% or less. Only data from these tests were considered reliable and are presented here.

Several important points may be noted from the experimental data. First, a significant increase in wicking distance is indicated for screen/plate wicks as compared to screen alone. A heat flux of 1.26×10^3 W/m² (4×10^2 Btu/hr-ft², resulted in a wicking distance of approximately 0.228 m (0.75 ft) for both sets of screen/plate data shown (325x2300 and 250x1370 mesh screens). Screen wicks exhibit considerably lower wicking ability: i.e., for a heat flux of 31.5 W/m² (10 Btu/hr-ft²), the wicking distance was approximately 0.0304 m (0.1 ft) for 325x2300 and 200x 1400 mesh screens. As will be seen later, this results in more than an order of magnitude increase in wicking distance for a screen on a plate as compared to a screen wick at the same incident heat flux.

II-70
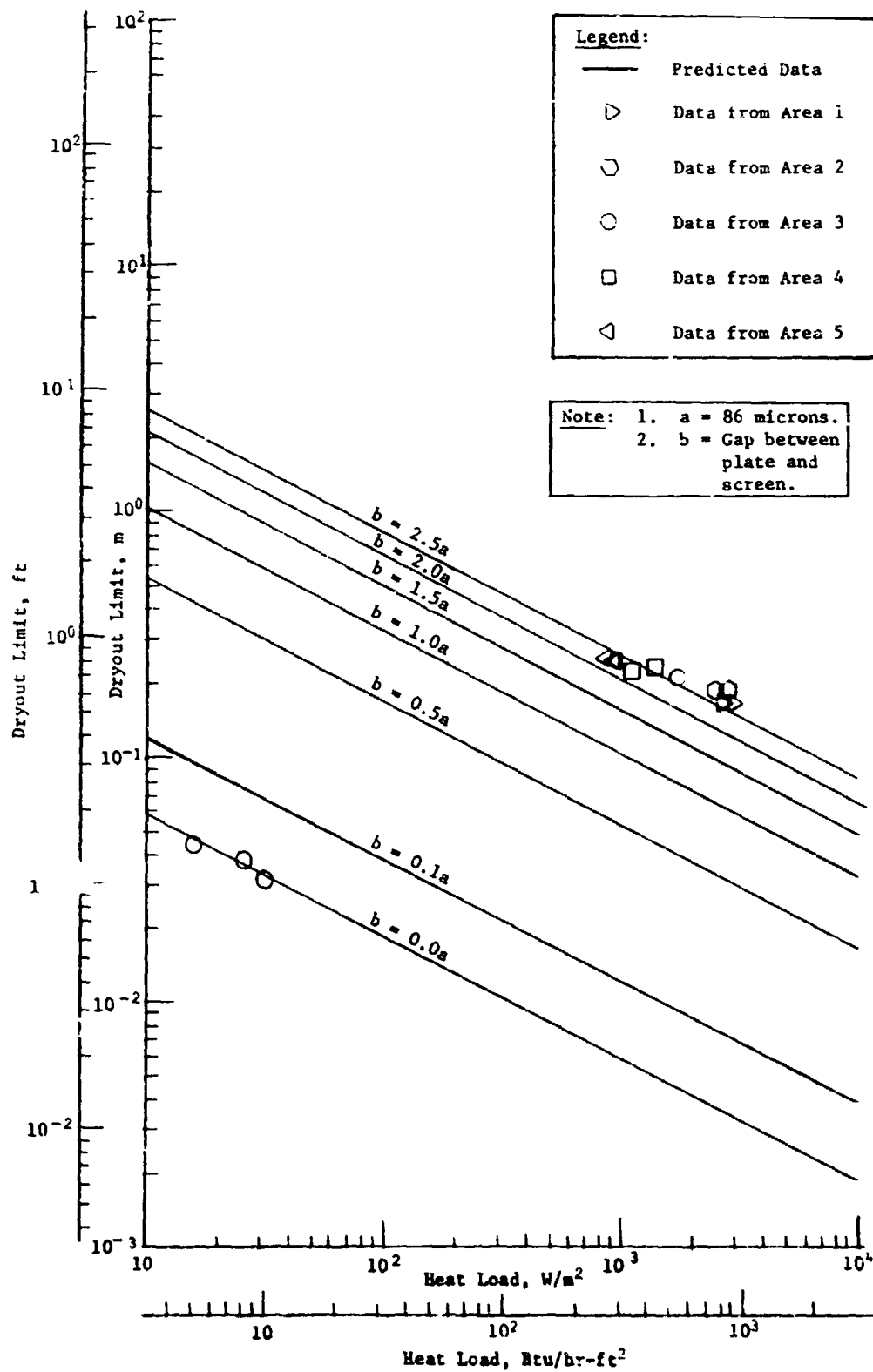
Fig. II-44 *Dryout Limits for Pentane with 325x2300 Screen on a Plate*
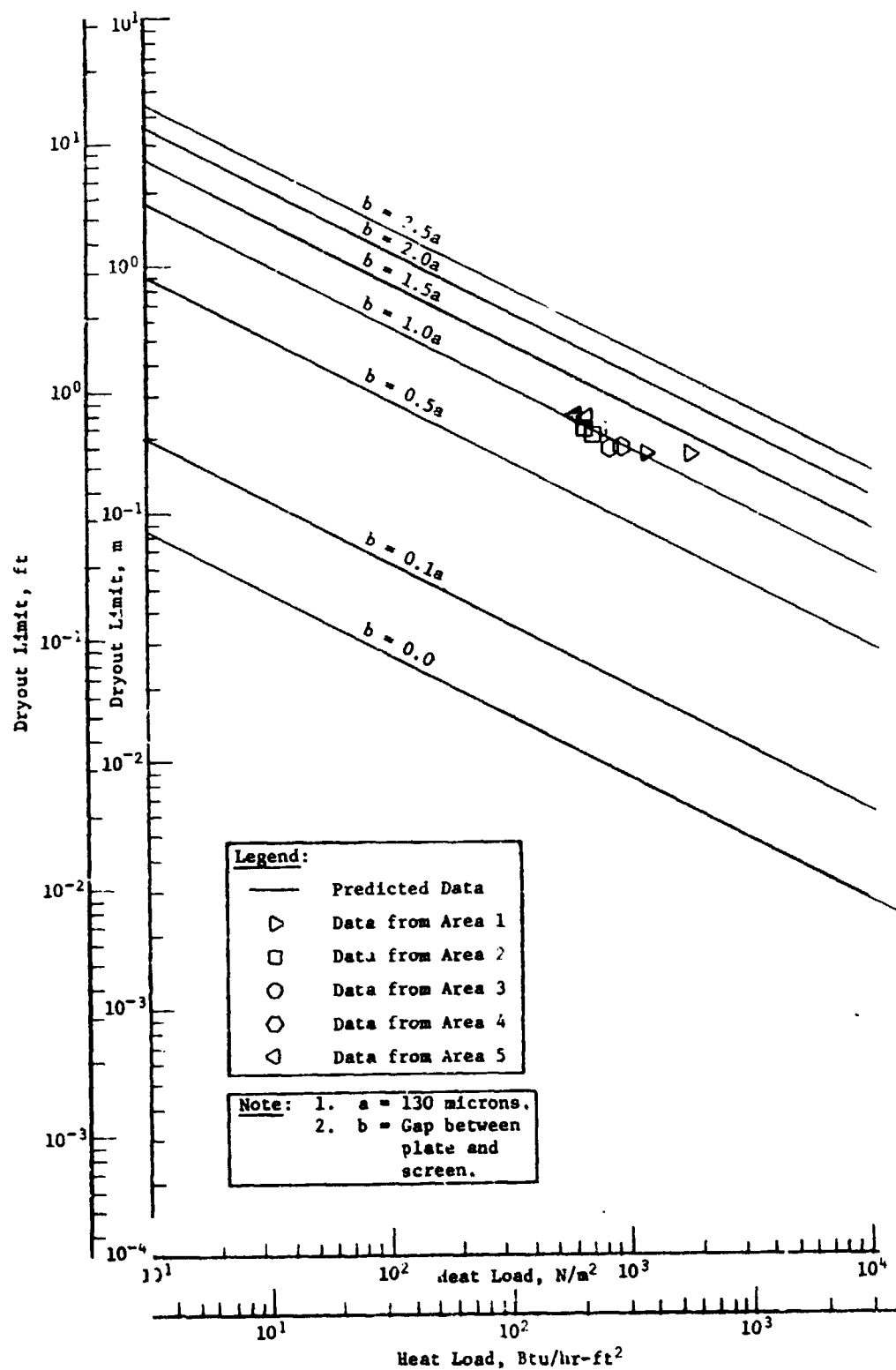
Fig. II-45 Dryout Limits for Pentane with 250x1370 Screen on a Plate
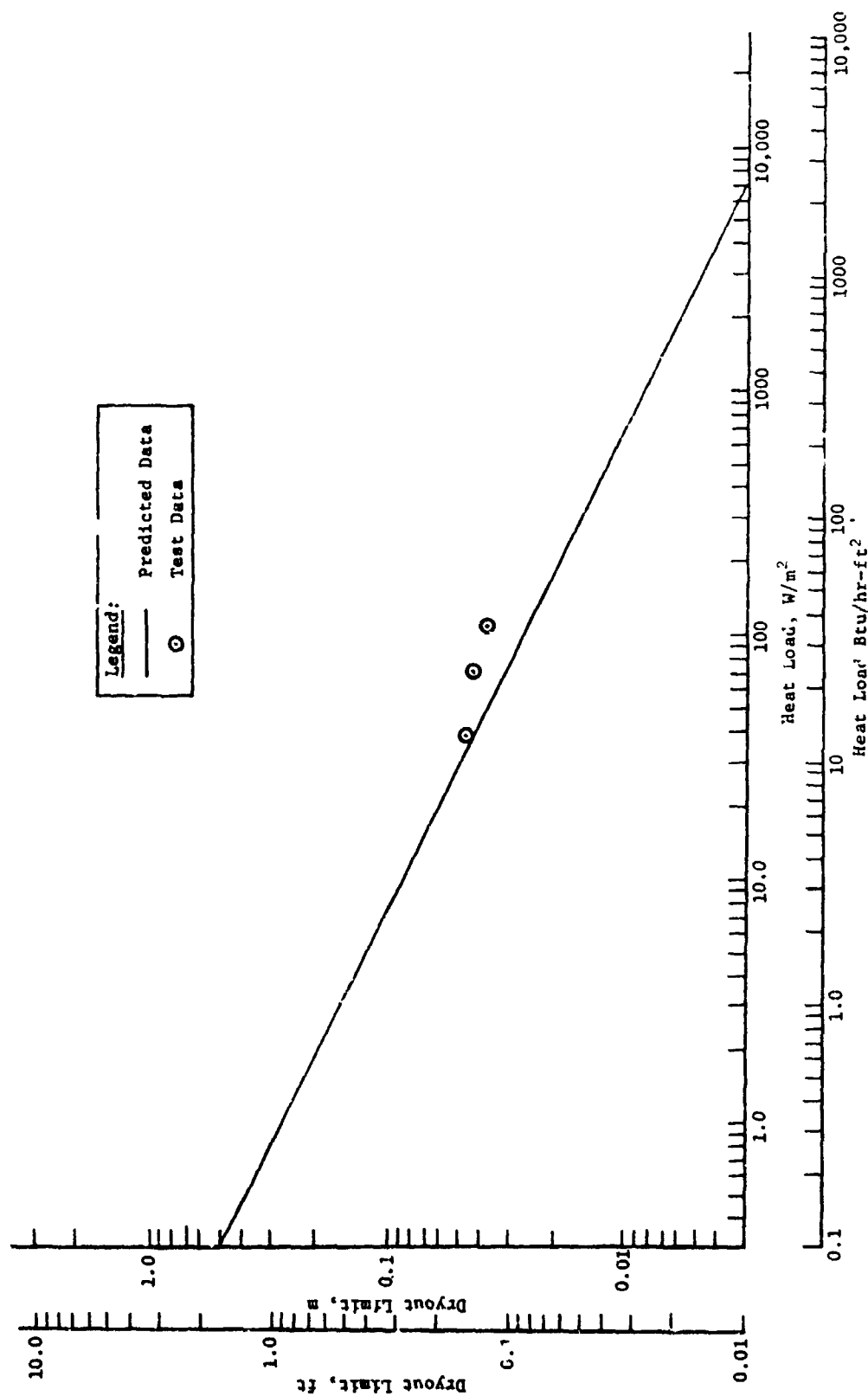
Fig. II-46 Dryout Limits for Pentane with a 200x1400 Screen

Legend:

— Predicted Data
⊙ Test Data

Heat Load, W/m²

Heat Load, Btu/hr-ft²

Dryout Limit, m

Dryout Limit, ft

II-73

Second, an increase in wicking potential is indicated for the
coarse 200x1400 mesh screen over that recorded for the 325x2300
mesh specimen. This increase is consistent with the effect noted
for screen/plate wicks because the larger pores and capillaries
for coarse mesh screen are somewhat analogous to the channel
formed in the screen/plate configuration.

Third, it is interesting to note that for the same heat flux,
both sets of screen and plate wicking data (two screens) indi-
cate approximately the same wicking distance. This implies that
the screen contributed little to the total wicking potential in
this configuration. Correlating the experimental data with the
analytical expression developed for dryout length, S, produced
an average value of the wicking constant, K. The wicking equa-
tion, as defined in Volume II, is

$$\sqrt{\frac{\rho g_c \; h_{fg} \sigma K \; (a + b)}{Q \mu}} \qquad\qquad [\text{II-3}]$$

where S = the dryout limit of the wick, m (ft).

$$K \quad = \frac{C\phi \; a + b^2/6}{a + b}, \qquad\qquad [\text{II-4}]$$

ϕ = porosity of the screen,

a   = thickness of the screen, m (ft),

b   = thickness of the gap between the screen and plate, m (ft),

Q   = heat flux, W/m^2 (Btu/hr-ft^2),

h_{fg} = heat of vaporization, J/kg (Btu/lbm),

μ = viscosity, kg/m-sec (lbm/ft-sec),

σ = surface tension,

ρ = density, kg/m^3 (lbm/ft^3),

$$C \quad = \frac{4 \; Da^2}{D_{bp} \; A_w}.$$

II-74

The resulting K values are shown in Table II-5. Data from Ref II-6 and II-7 are also shown. Good agreement is noted between Martin Marietta test results and Ref II-6 for a 200x1400 Dutch twill screen (K values of 1.8×10^{-7}, compared to 1.2×10^{-7}). Although no other direct correlations are possible, similar trends are indicated for Martin Marietta data and other work done. Increases in the wicking constant and, therefore, the wicking capability, are indicated for configurations that form geometric chan-nels through which additional wicking may occur. For the screen/plate and layered screen data (shown in Table II-5), increases in K of almost two orders of magnitude are noted over the wicking in screens.

Table II-5 Comparison of Wicking Constants

Screen Configuration	Constant K, m (ft)
Martin Marietta Test Results	
325x2300 Mesh Screen on a Horizontal Plate	2.56×10^{-5} (8.4×10^{-5})
250 x 1370 Mesh Screen on a Horizontal Plate	1.00×10^{-5} (3.3×10^{-5})
200x1400 Horizontal Screen	5.48×10^{-8} (1.8×10^{-7})
325x2300 Horizontal Screen	4.57×10^{-8} (1.5×10^{-7})
Other Work	
200x1400 Horizontal Screen (Note 1)	3.65×10^{-8} (1.2×10^{-7})
Four Wraps of a 150 Mesh Screen on a Vertical Tube (Note 2)	2.62×10^{-6} (8.6×10^{-6})
Four Wraps of a 325 Mesh Screen on a Vertical Tube (Note 2)	7.62×10^{-7} (2.5×10^{-6})
Three Wraps of a 325 Mesh Screen on a Vertical Tube (Note 2)	3.65×10^{-7} (1.2×10^{-6})

Note: 1) See Ref II-6.
      2) See Ref II-7.

The K values previously presented (See Vol II, Chapter II.) were used in Eq [II-3], to generate the analytical curves shown in Fig. II-44 and II-45. Dryout limit is shown as a function of heat flux for various gap thicknesses, b, for 325x2300 and 250x 1370 screens. A range of gap thicknesses from b = 0.0a (screen only) up to 2.5a (a = screen thickness) are shown. It should be noted that curves for 325x2300 screen are based on the experimental wicking constant for a horizontal screen. Since corresponding data were not available from 250x1370 tests, the value of K (K = Cϕ for screen) was calculated from data presented in Reference II-7.

Several interesting points are shown by Fig. II-44 and II-45. Large increases in wicking distance are predicted for screen/ plate wicks as compared to screen wicks. An increase of about two orders of magnitude is shown in Fig. II-44 for the maximum gap thickness that agrees favorably with experimental data. Also, increased wicking potential is shown for the coarse 250x1370 mesh screen and is consistent with trends indicated by experimental results. Note the correlation for 325x2300 screen between theoretical and experimental results. Test results for screen alone clearly fall along the analytical curve for b = 0.

The relative magnitude of gap thickness that can be expected is shown by the cluster of screen/plate data along the analytical curves in Fig. II-44 and II-45. The values of b indicated are 1.0a and 2.5a for 250x1370 and 325x2300 screen, respectively. Considering values of screen thickness, a, these numbers correspond to absolute gaps of 130 microns and 215 microns, respectively.

The effect of gap thickness, b, on wicking is evident from Eq [II-4]. The wicking constant K is a function of two terms: one depending on screen properties and the other on the gap thickness squared. As b increases, the b^2 term becomes predominant and wicking becomes essentially independent of the screen wicking constant, C. Consequently, the curves presented for 250x1370 screen should be unaffected by the screen wicking constant, C, in the range of b values indicated by the experimental data.

d. *Conclusions* - Several conclusions important to the design of capillary propellant acquisition/expulsion systems are evident from results of these wicking tests. Wicking, a relatively slow phenomena in fine mesh screen, may be increased an order of magnitude or more by backing the screen with a material that forms

additional wicking channels. In this configuration wicking becomes independent of screen mesh and depends on the gap thickness between the screen and backing material. Based on these test data, gap thickness, b, can be expected to vary from 130 to 215 microns with significant increases in wicking.

Based on data for 200x1400 and 325x2300 Dutch twill screen, coarse mesh screen shows better wicking properties, compared to those for the finer meshes. This is in agreement with Reference II-6.

Based on experimental data correlation, the analytical model appears to be representative of the distributed heat load wicking problem important in screen retention devices. Predicting dryout limits for screen and screen/plate wicking configurations for the liquids and heat loads of interest may be achieved with reasonable accuracy.

5.   Screen Pressure Drop Tests

a. *Test Objectives* - The pressure drop associated with the flow
of a fluid through fine mesh screens is of primary concern in the
design of a surface tension device. Capillary acquisition/expul-
sion systems based on the DSL concept resupply the liquid annulus
(or channels) during expulsion by flow of liquid from the bulk
region through fine mesh screen into the liquid annulus. At low
ullage volumes, the liquid screen contact area and, consequently,
the area of flow, is large and pressure drop is small. However,
as tank depletion is approached, the area of flow becomes small
and the corresponding pressure drop due to the flow of propellant
through the screen is no longer negligible. Flow through multiple
screens as well as different screen meshes is, therefore, of
interest.

As originally outlined, these tests were to include gas as well
as liquid as the test fluid. However, since data on gas flow
(GN_2) was obtained during the communication/venting test series
only liquid tests were conducted during this phase. The purpose
of the test was to experimentally determine the pressure loss
associated with the flow of water through fine mesh Dutch twill
screen. Triple and double screen layers as well as single screens
were tested, with attention given to the effect of screen spacing
on the test results.

b. *Test Apparatus and Procedure* - A schematic of the test appa-
ratus is shown in Fig. II-47(a). Tap water was used as the test
fluid and was filtered through a 325x2300 fine mesh screen be-
fore flowing into the test section. The test section consisted
of one, two, and three layers of fine mesh Dutch twill screen.
The pressure differential across the test section was measured
by an inclined manometer as shown in Fig. II-47(b) and a 0 to
6.9 N/cm^2 (0.to 10 psig) pressure gage was used to monitor system
pressure.

Volumetric flow rate was determined by dividing the liquid volume
collected in a graduated cylinder by the time period required to
collect the measured volume. By knowing water temperature and
test section flow area, 4.45 cm^2 (0.69 $in.^2$), the flow velocity
could be determined. A thermocouple was available for measuring
water temperature. The Dutch twill screens tested were 200x1400,
250x1370, and 325x2300 mesh. For double and triple-layered screen
tests, spacings of 0.16 cm (1/16 in.) and 0.48 cm (3/16 in.) were
investigated.

II-78

V3 0.64 cm (1/8 in.) Hoke

Inclined Manometer

Flexline

V1 0.64 cm (1/4 in.) Globe

0 to 6.9 N/cm² (0 to 10 psig)

P_2

0.64 cm (1/4 in.) Globe

V2

To Water Tap

Filter (325x2300 Mesh)

Catch Tank

Graduate

(a) Test Section

Hoke Needle Valve

Flexlines

Heavy, Small-Bore Class Tubes

50.8 cm (20 in.)

0.25 cm (0.1 in.) Craduations

30°

Horizontal

0 to 6.9 N/cm² (0 to 10 psig)

Can Be Flexlines
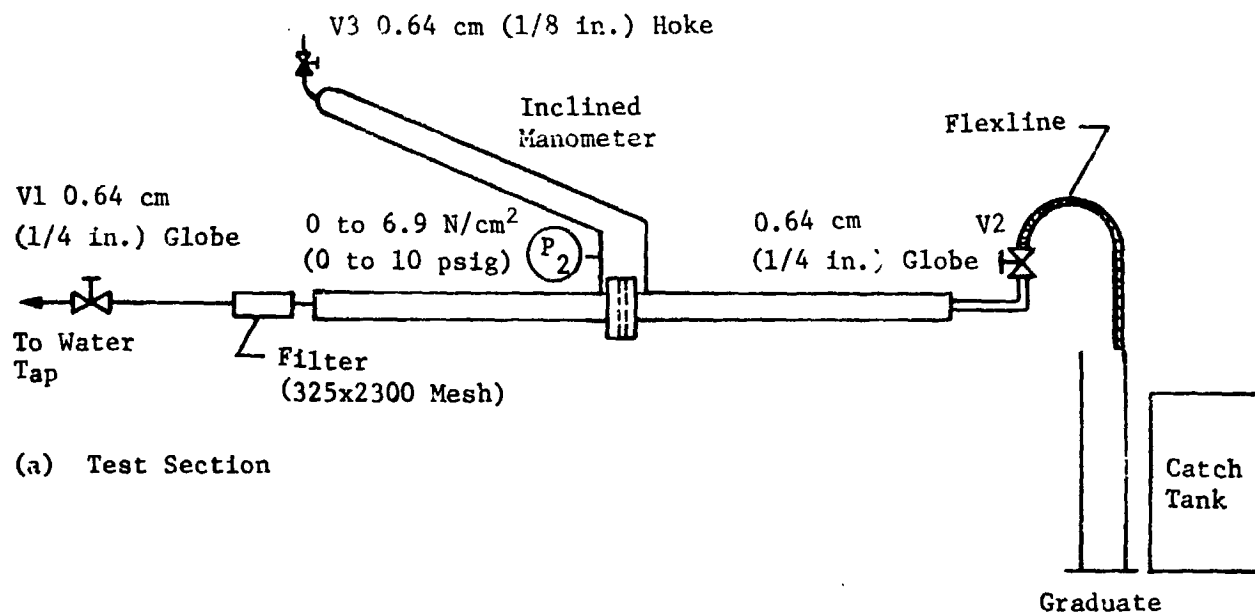
Test Section
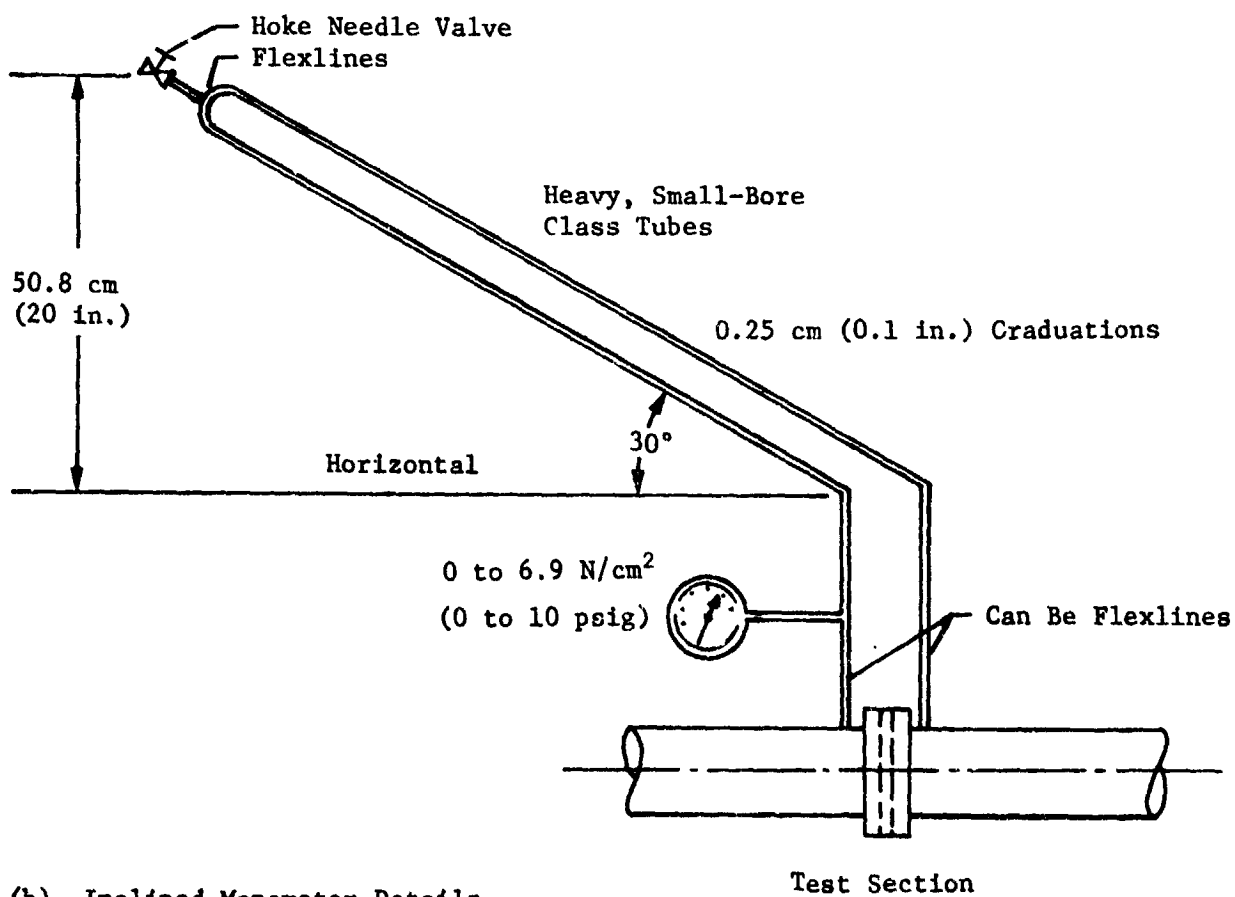
(b) Inclined Manometer Details

Fig. II-47 Test Setup Schematic for Liquid ΔP Tests

The basic test procedure involved opening valve V2 one turn and then adjusting system pressure to approximately 0.69 N/cm^2 (1 psi) using V1. [See Fig. II-47(a).] The liquid level was positioned in the manometer using V3, and the flowrate adjusted to give a ΔP of about 1.27 cm (0.5 in.) H$_2$O. The flowrate was then determined by moving the flexible dischar e line from the catch tank to the graduated cylinder and recording the time and corresponding volume. System pressure, ΔP, and water temperature was also noted. This procedure was followed for increasing pressure differential until the manometer limitation was reached.

c. Results – Figures II-48 through II-50 show the test results for the three different screen meshes tested. Pressure differential is plotted as a function of fluid velocity for water at 297°K (75°F). Results for one, two, and three layers of screen with different spacings are shown for each screen. Data for two layers of 200x1400 mesh screen, with a spacing of 0.48 cm (3/16 in.) was erroneous and is not shown. Pressure differentials from 5.33 cm (2.1 in.) H$_2$O to 44.5 cm (17.5 in.) H$_2$O for a velocity range of 0.28 cm/sec (0.11 in./sec) to 3.48 cm/sec (1.4 in./sec) are presented. Note the straight line correlation as predicted from previous theoretical and experimental work (Ref II-5). Also, flow losses increase with the number of screen layers as expected.

Further data analysis shows good correlation with the results presented in Subsection 3. Figure II-51 shows this comparison in a plot similar to Fig. II-38. The solid symbols represent GN$_2$ pressure drop data and the open symbols represent single screen data using water as the test fluid. Good agreement between GN$_2$ and water data is shown. Once again, Martin Marietta results are bounded by Armour and Cannon $\left(f = \dfrac{8.61}{RE} + 0.52 \right)$ and MDAC experimental data. A consistently lower trend is suggested by both GN$_2$ and water data compared to the Armour and Cannon correlation. This agrees favorably with the experimental data for Dutch twill screen (Ref II-5).

Figure II-52 shows the increase in pressure loss associated with flow through multiple screen layers. Again the ratio $\Delta P_{ms} / \Delta P_{ss}$ is plotted as a function of the number of screens for velocity of 1.27 cm/sec (0.5 in./sec). Results indicate that larger $\Delta P_{ms} / \Delta P_{ss}$ ratios are obtained for fine mesh screens. This is consistent with GN$_2$ data. However, a somewhat higher trend is indicated for water data, so that assuming the pressure drop across multiple screens is additive is no longer conservative for 325x2300 and 250x1370 mesh screens.
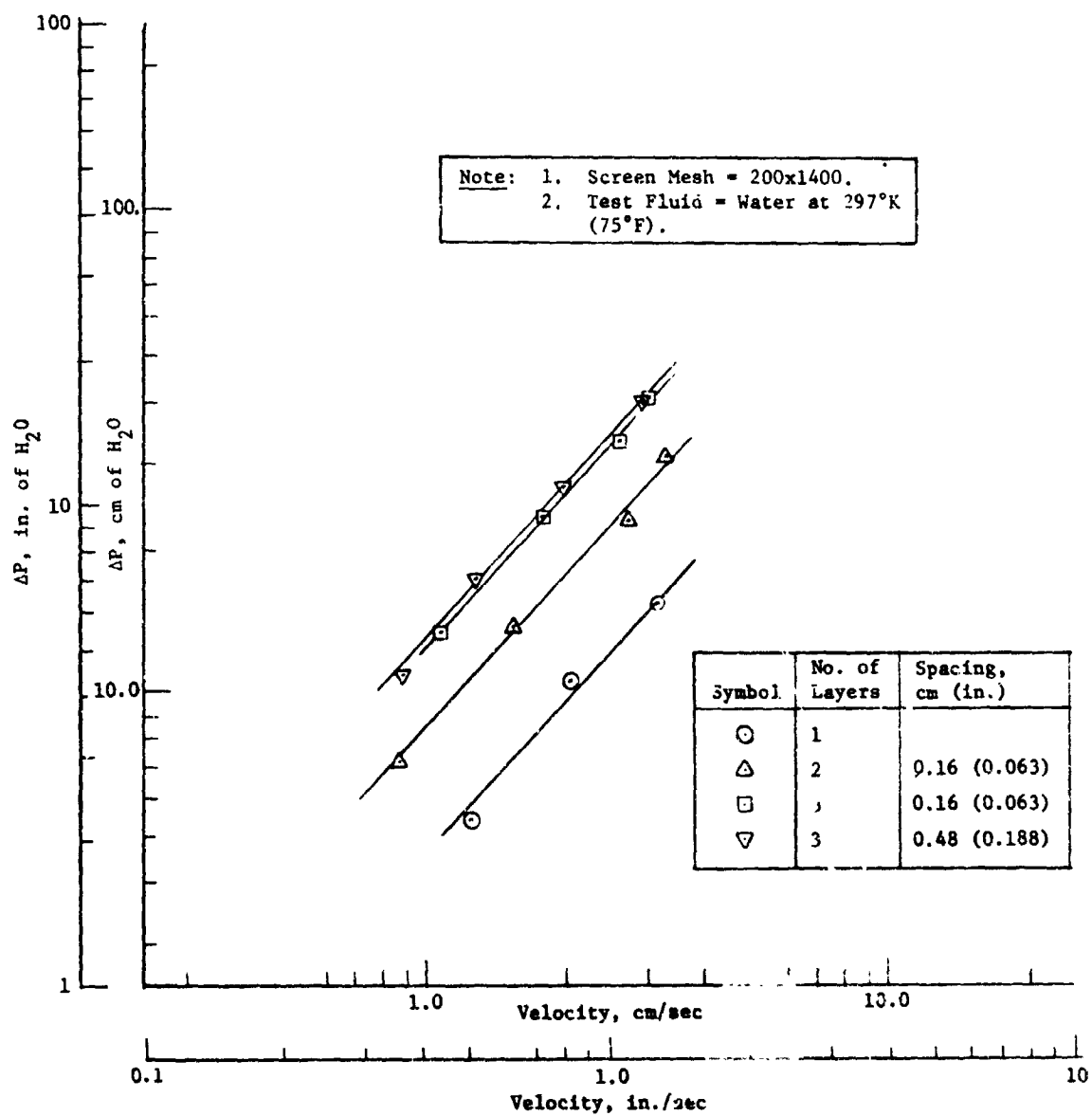
Fig. II-48   Pressure Drop vs Liquid Approach Velocity for Single and
Multiple-Layer Dutch Twill Screen, 200x1400 Mesh
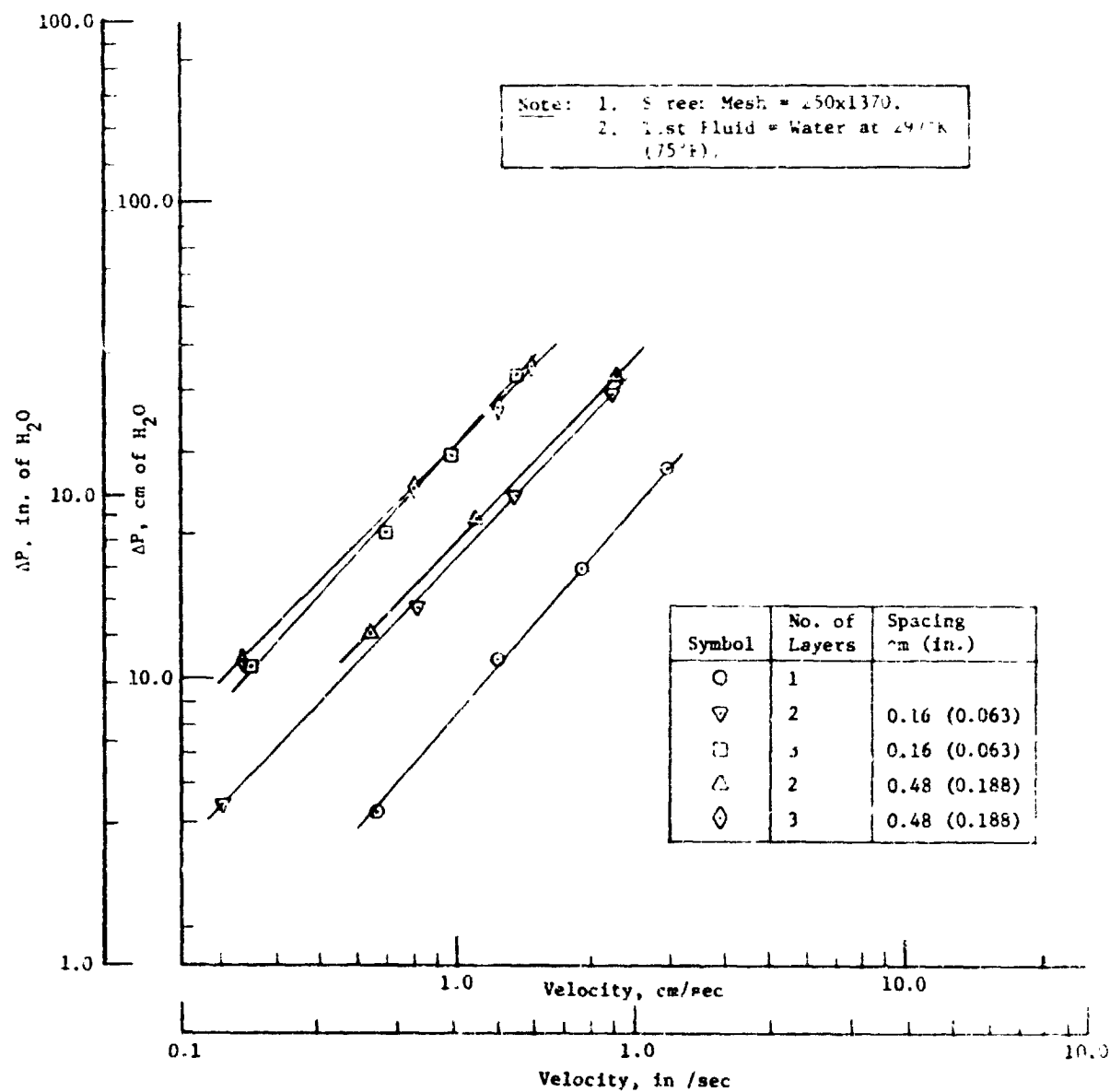
Fig. II-49 Pressure Drop vs Liquid Approach Velocity for Single and
Multiple-Layer Dutch Twill Screen, 250x1370 Mesh
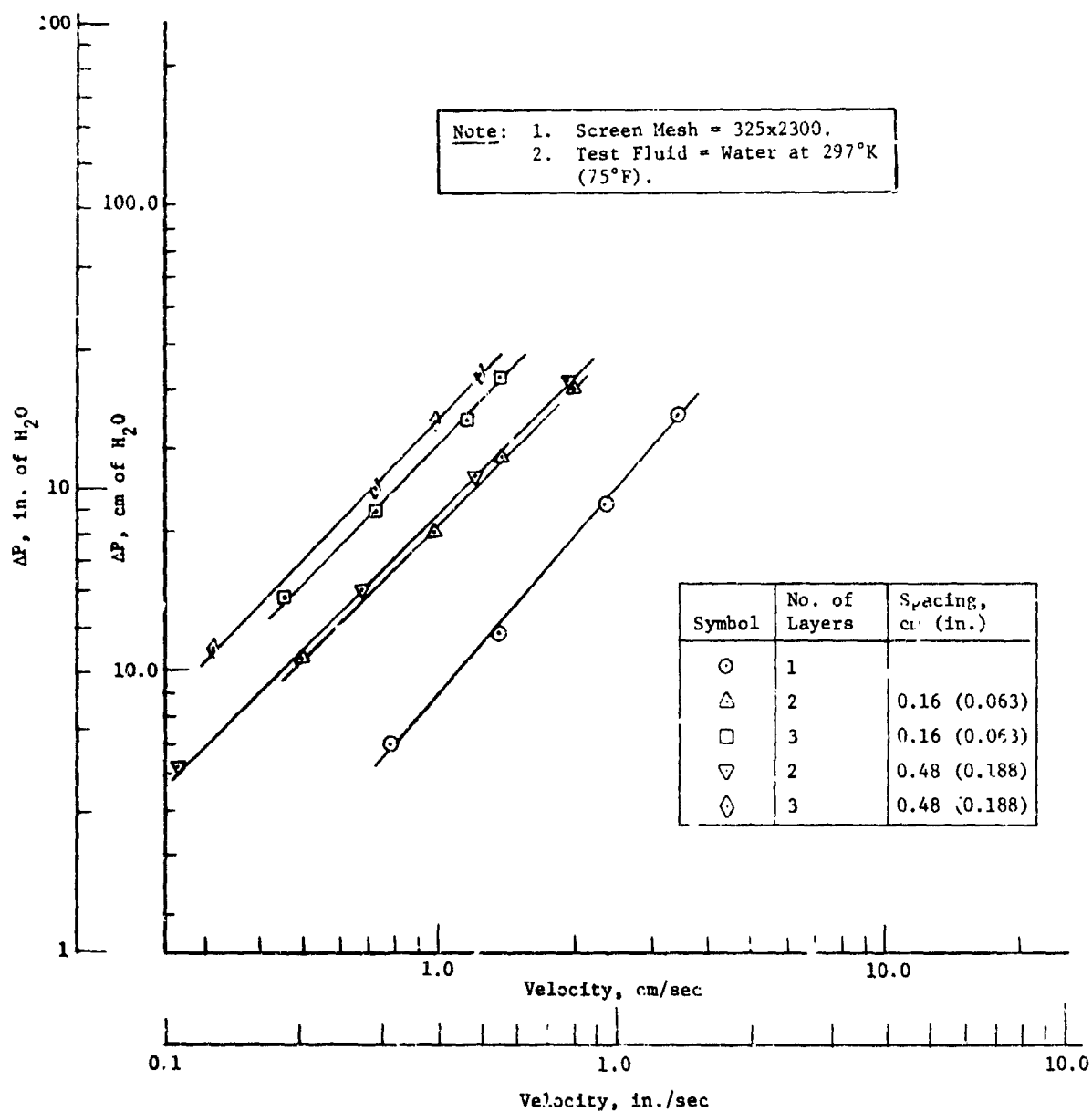
Fig. II-50 *Pressure Drop vs Liquid Approach Velocity for Single and Multiple Layer Dutch Twill Screen, 325x2300 Mesh*

SCREEN CHARACTERISTICS					
	α	D, m	a, 1/m	D, m	ϵ
375x2300	1.3	8.6×10^{-5}	108,666	1.13×10^{-5}	0.261
325x2300	1.3	8.9×10^{-5}	102,106	1.4×10^{-5}	0.297
250x1370	1.3	1.37×10^{-4}	71,438	1.7×10^{-5}	0.226
200x1400	1.3	1.52×10^{-4}	63,435	2.12×10^{-5}	0.267

$$f = \frac{8.61}{Re} + 0.52 (A + C)$$

MDAC Test Data

Legend:

◐	375x2300
△	325x2300
○	250x1370
□	200x1400

Communication/Venting

● GN_2 Test Data

○ Water Test Data

Friction Factor, $f = \Delta P \epsilon^2 D / \alpha B \rho V^2$

Reynolds No., $Re = \rho V / \mu a^2 D$
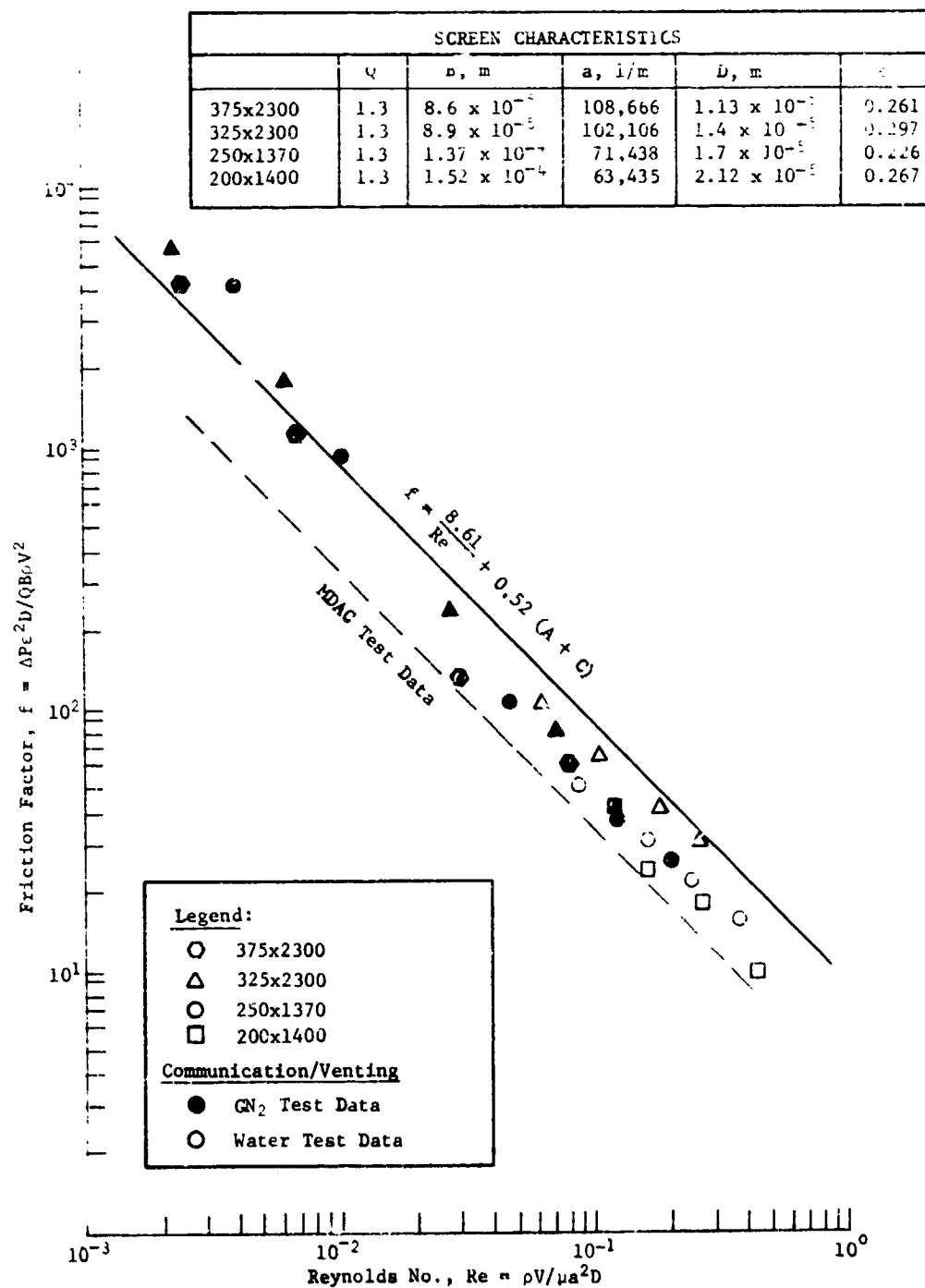
Fig. II-51 Nondimensional Correlation of Water Pressure Loss Data
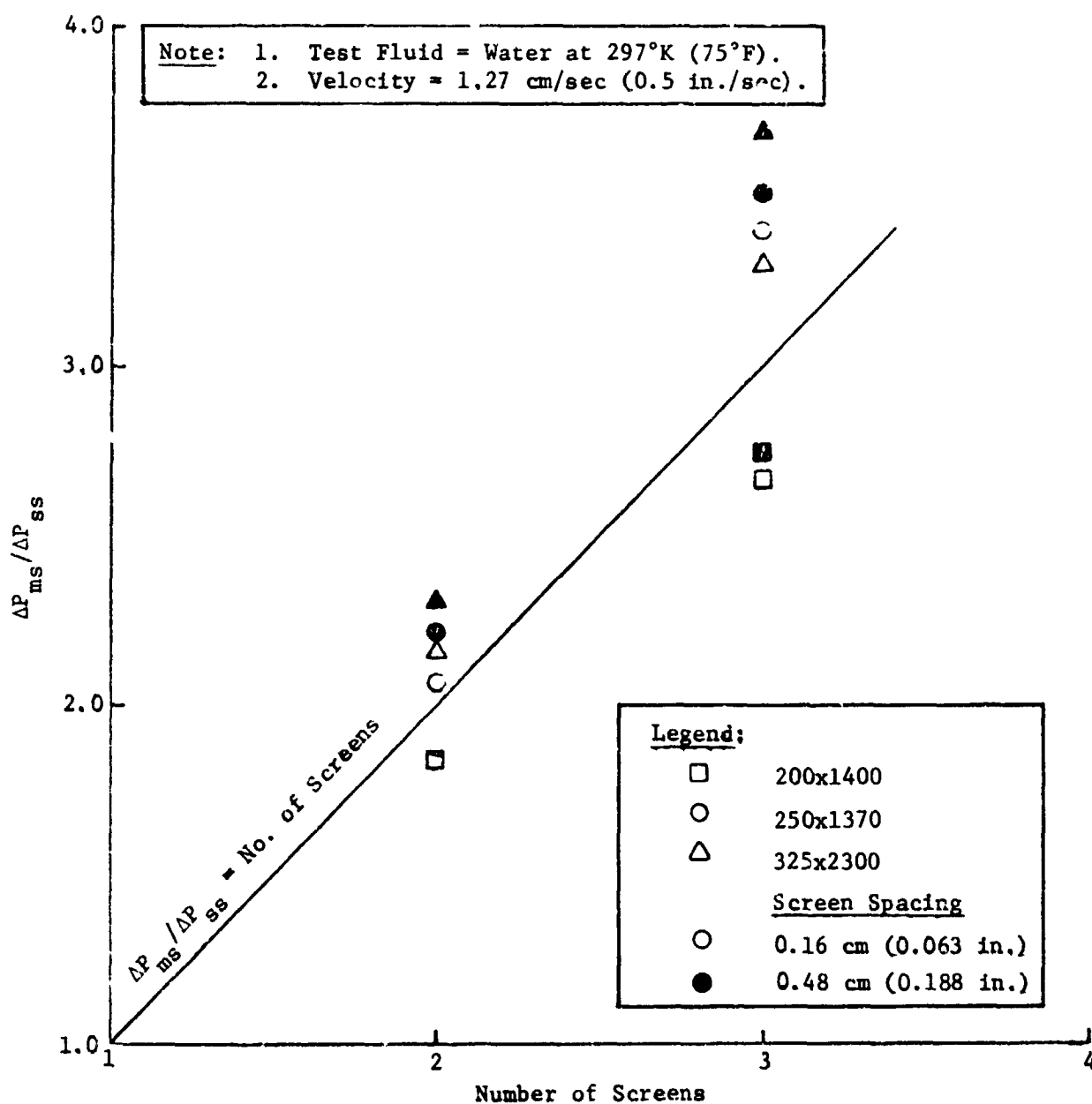
Fig. II-52 *Multiple Screen Pressure Drop Results*

A trend that may explain this inconsistency is suggested from closer examination of the data. Noting that the solid and open symbols represent the large and small screen spacings, respectively, pressure drop consistently increased with increased screen spacings for each of the three screens tested. Extrapolation of this trend indicates lower ratios of $\Delta P_{ms}/\Delta P_{ss}$ for a zero spacing multiple screen configuration. This was the geometry of the GN_2 test specimens. However, the reason for this increase in pressure drop with increased spacing thickness is not apparent.

d. Conclusions - Single screen test results agree favorably with the gaseous nitrogen data run during the communication screen/venting test. Once again, good correlation is noted based on Armour and Cannon's analysis, although their empirical correlation $\left(f = \dfrac{8.61}{RE} + 0.52 \right)$ appears conservative. For the test fluids and experimental conditions investigated, an approximate 40% reduction in the pressure loss was noted for the experimental data, compared to the correlation in Ref II-5.

From the previous GN_2 tests, the results indicated that the measured values of $\Delta P_{ms}/\Delta P_{ss}$ were on or below the predicted condition $\left(\Delta P_{ms}/\Delta P_{ss} = \text{number of screens} \right)$. Figure II-52 shows that for the water tests, values of $\Delta P_{ms}/\Delta P_{ss}$ were higher than predicted for two of the three screens tested. Also the deviation above the predicted condition increased with the number of screens, screen spacing, and screen mesh. The reason for this deviation is not readily apparent and further evaluation would require additional data for different screen spacings and numbers of screen layers.

II-86

6.   Screen Structural Characteristics Tests

a. *Test Objectives* - The DSL designs presently proposed under
the cryogenic phase of NASA Contract NAS9-12182 use perforated
plate to give structural support to the fine mesh screen. The
use of perforated plate was based on the assumptions that the
screen could not support the pressure load environment without
structural failure (i.e., excessive plastic deformation or screen
rupture). However, there was no experimental data available
that defined the structural capability of fine mesh screens.
Since the use of perforated plate causes a considerable weight
penalty, tests of the structural capability of fine mesh screens
were needed to determine the necessity for added structural sup-
port.

The purpose of these tests was to provide experimental data on
the structural capability of fine mesh screens. Test data were
also used to verify the mathematical model developed during this
task. The tests and the mathematical model were to characterize
the specific loading case of uniform pressure acting on a circu-
lar flat screen segment.

b. *Apparatus and Procedure*

1) Apparatus - Experimental data were obtained by uniform pres-
sure loading of flat circular sections of the various screens
tested. Basically, three types of tests were run: (1) static
loading tests, (2) cyclic loading tests, and (3) rupture (ulti-
mate loading) tests. The test apparatus was basically the same
for all tests conducted.

The experimental apparatus is shown in Fig. II-53 and II-54.
Sections of the various fine mesh screens were positioned between
two 20.24-cm (8-in.) diameter rings, which were in turn clamped
together by 12 clamping bolts (the smaller bolts in Fig. II-53
and II-54). Pressure was supplied through a regulating valve
from below into the base of the apparatus to deliver a uniform
load to the bottom surface of the screen. A thin sheet of plas-
tic was used to cover the bottom surface of the screen sample to
prevent the pressurant from flowing through the screen and to
provide a seal between the screen and lower ring. Pressure was
monitored with a highly accurate pressure gage, while screen de-
flection (the amount the screen surface moves perpendicularly
above its unloaded position) was measured with a dial indicator.
Both air and nitrogen were used as pressurants. The mounting sup-
port for the dial indicator was designed to allow the dial indi-
cator to measure deflection both in the radial and angular direc-
tions.

Fig. II-53 Screen Deflection Apparatus, Assembled

Fig. II-54 Screen Deflection Apparatus, Disassembled

II-88

Some changes in the experimental system were required for the cyclic loading test. Pressure sensing was accomplished by a pressure switch, which, in turn, commanded two solenoid-operated valves. One valve controlled the supply of pressurant while the other controlled the venting of the base or reservoir of the apparatus. When the supply valve was open, the vent valve was closed and vice versa. A timer was connected into the circuit to allow adequate venting time, while the regulating valve provided the proper pressurization rate. The approximate length of one cycle (pressurize, vent, start of repressurization) was 14 to 20 sec.

Two different screen clamping techniques were used as shown in Fig. II-55. Technique (a), used in initial testing, employed flat rings that were capable of exerting forces only in the vertical direction. This provided no means of eliminating the initial sag and waviness in the screen specimens, which resulted in inconsistent data. This problem was eliminated by using the beveled rings shown in Technique (b). With this configuration, the sample was drawn to the sides during clamping which eliminated the initial sag and prevented inconsistent zero readings and nonrepeatable data. The preloading associated with this clamping technique had little effect on the test results.

The majority of the screen specimens were the same size as the clamping rings, 20.3 cm (8 in.) in diameter. However, some testing was done with 15.2-cm (6-in.) diameter screens to establish the dependency of deflection on screen radius. This was accomplished by inserting two machined aluminum rings, 15.2 cm (6 in.) inside diameter, between the clamping rings of the test apparatus. The test specimen was inserted between these rings and clamped into position.

All the screens tested were fine mesh Dutch twill screens in the as-received condition. Three different stainless steel screen meshes were tested: 325x2300, 250x1370, and 200x1400. Aluminum screen of 200x1400 mesh was also tested.

2) Procedure - Three types of tests were run to obtain sufficient data for empirical and analytical correlation and to determine any degradation in screen performance caused by the test loads. These included static deflection, cyclic loading, and rupture tests.

For static deflection testing, the screen test specimen and plastic sealant were mounted in the test apparatus and secured by tightening the 12 clamping bolts with sufficient force to prevent screen
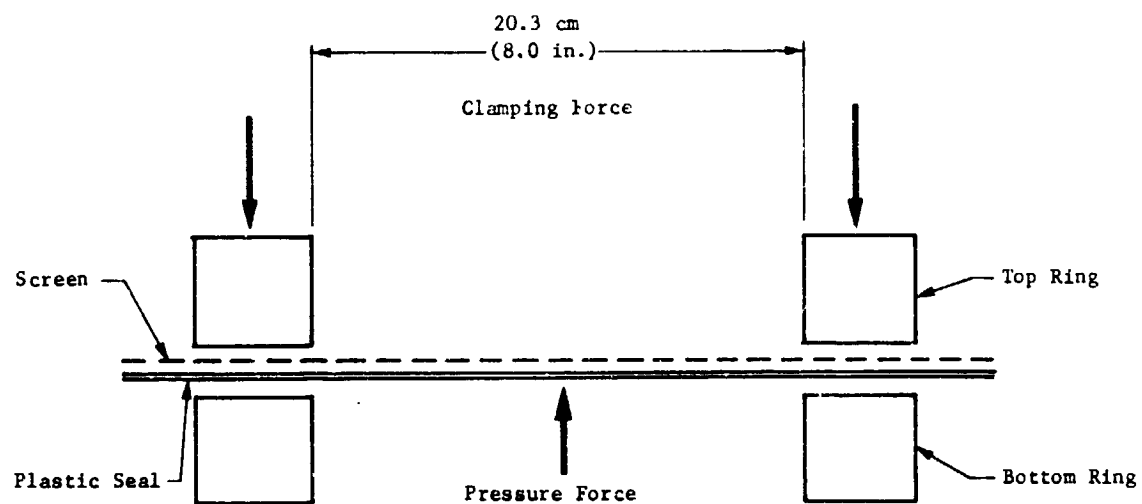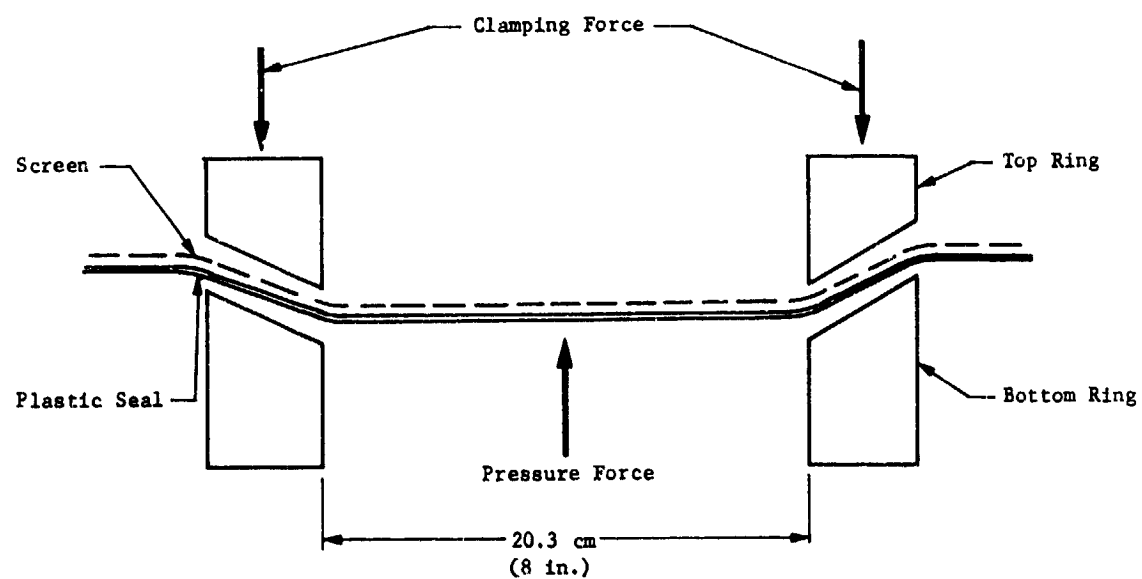
Fig. II-55 *Screen Clamping Techniques*

slippage. The dial indicator was zeroed and the pressurant intro-
duced using a microvalve. Pressure increments of 0.069 N/cm^2
(0.1 psi) were used as indicated by the Heise gage, with maximum
pressure depending on screen and test. During the initial test
sequence, pressures as high as 3.14 N/cm^2 (4.5 psig) were used
for 325x2300 screen. After the ultimate load of the screens had
been more clearly defined, deflection measurements were made at
pressures as high as 11.2 N/cm^2 (16 psig). Deflections were meas-
ured at the center of the specimen and at distances of 2.54 cm
(1 in.), 5.00 cm (2 in.) and 7.62 cm (3 in.) from the specimen
center in both the warp and shute wire directions.

Cyclic loading tests subjected a sample of 325x2300 stainless
steel screen to a pressure of 0.757 N/cm^2 (1.1 psi) for 101,987
times. Deflection at the center of the screen was measured
periodically (approximately every 5000 cycles) to monitor any
degradation in structural capability. The bubble point of the
screen sample was measured before and after cycling to determine
any effects on pressure retention capability. This was also done
for several of the screen deflection test specimens.

Rupture tests were conducted to determine the screen's deflection
transition point, see Paragraph c.1. Samples of 325x2300, 250x
1370, and 200x1400 stainless steel and 200x1400 aluminum Dutch-
twill screens were tested. Each sample was individually installed
in the testing apparatus and pressurized until either screen rup-
ture occurred or until the screen's plastic deformation was severe
enough to terminate the test. A light ruler was fixed to the
top at the center of the screen samples in place of the dial in-
dicator and was used to measure W_o (screen deflection at the

center) because the indicator could possibly be damaged during
screen rupture.

The test data helped to define screen behavior and were used to
obtain empirical correlations of screen deflection dependency on
ΔP and radial distance. These correlations were used to refine
the analytical model into workable equations capable of predicting
deflections that agreed with test results for circular uniformly
loaded screen sections.

c. Results

1) Static Deflection Tests - Initial static deflection test results are shown in Fig. II-56 and II-57. Screen deflection is shown as a function of pressure differential and screen radius, r, for three different screen samples. As can be seen from Fig. II-56, deflection at the center of the screen follows a one-third power dependency on pressure differential up to a transition point where the slope of the curve changes (i.e., for the same increments in pressure the increment in deflection is larger, instead of smaller, than the previous increment in deflection). This transition point seemed to correspond to a point where a permanent set in the screen became noticeable. However, clamping techniques used in this sequence of tests made measurement of a permanent set very difficult due to the initial sag present in the sample.

Empirical correlation for the three screens tested resulted in the following equation for maximum screen deflection:

$$W_o = K \, \Delta P^{1/3} \qquad\qquad [II-5]$$

where

W_o = screen deflection at center of screen,

ΔP = pressure differential across screen, resulting in a hoop stress,

K = screen constant

Considering the number of wires and their diameter in the warp and shute directions, for Dutch twill weave the shute wire direction should have greater strength. However, test data for the three different screen samples showed little difference in deflection for the two directions, indicating that the screen behaves as an isotropic medium. Consequently, an average of the data in both directions was used to obtain the plot in Fig. II-57. The ratio of screen deflection at various radial positions to deflection at zero radial distance (center of screen, i.e., maximum deflection) is shown as a function of the ratio of radial distance to the radius of the screen sample [10.16 cm (4 in.)]. This nondimensional plot was useful in developing mathematical models for the screen. Based on this graph the dependency of deflection on radial distance can be approximated by the curve.

II-92
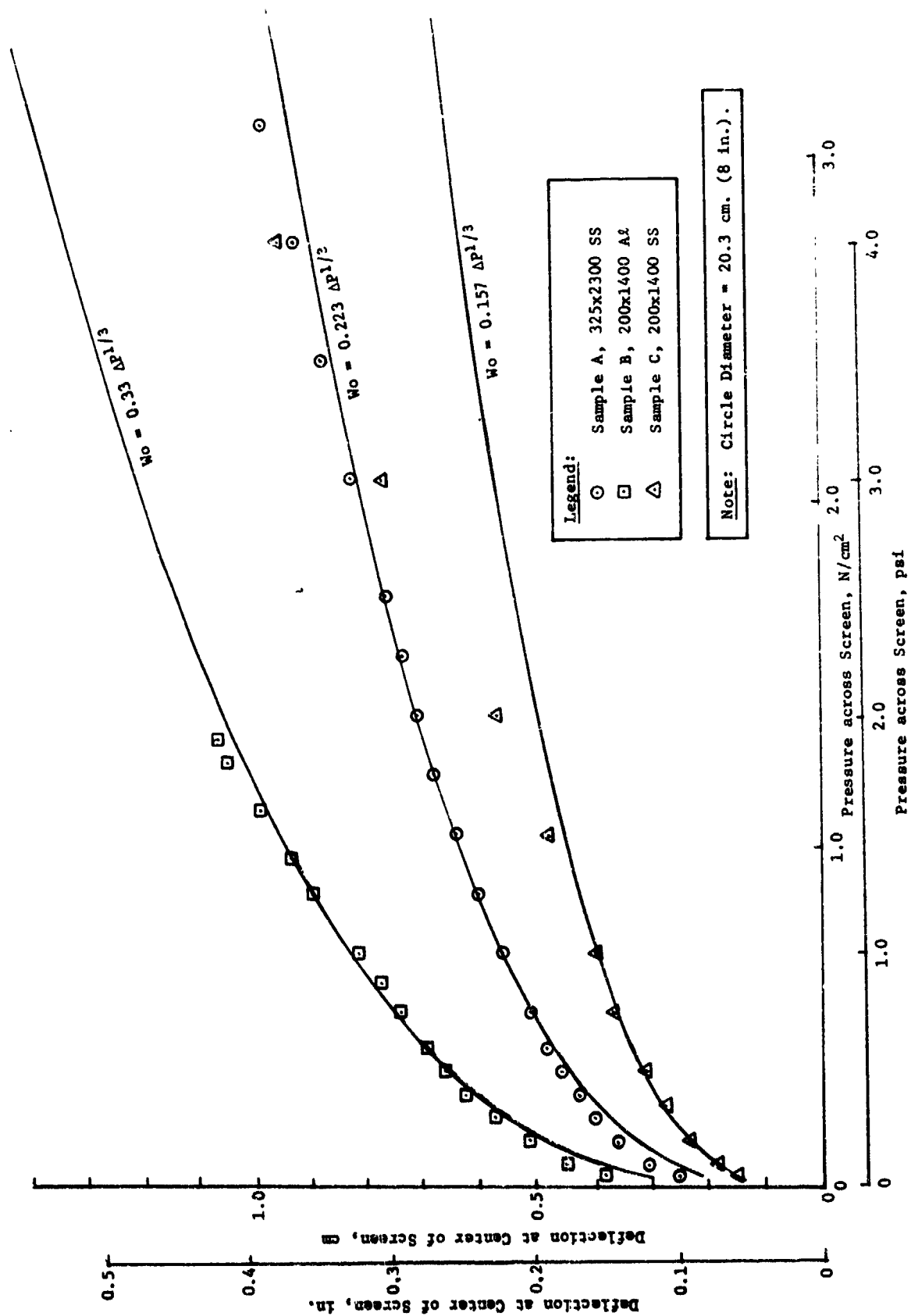
Fig. II-56 Center Screen Deflection vs Pressure for Three Dutch Twill Screens

II-93
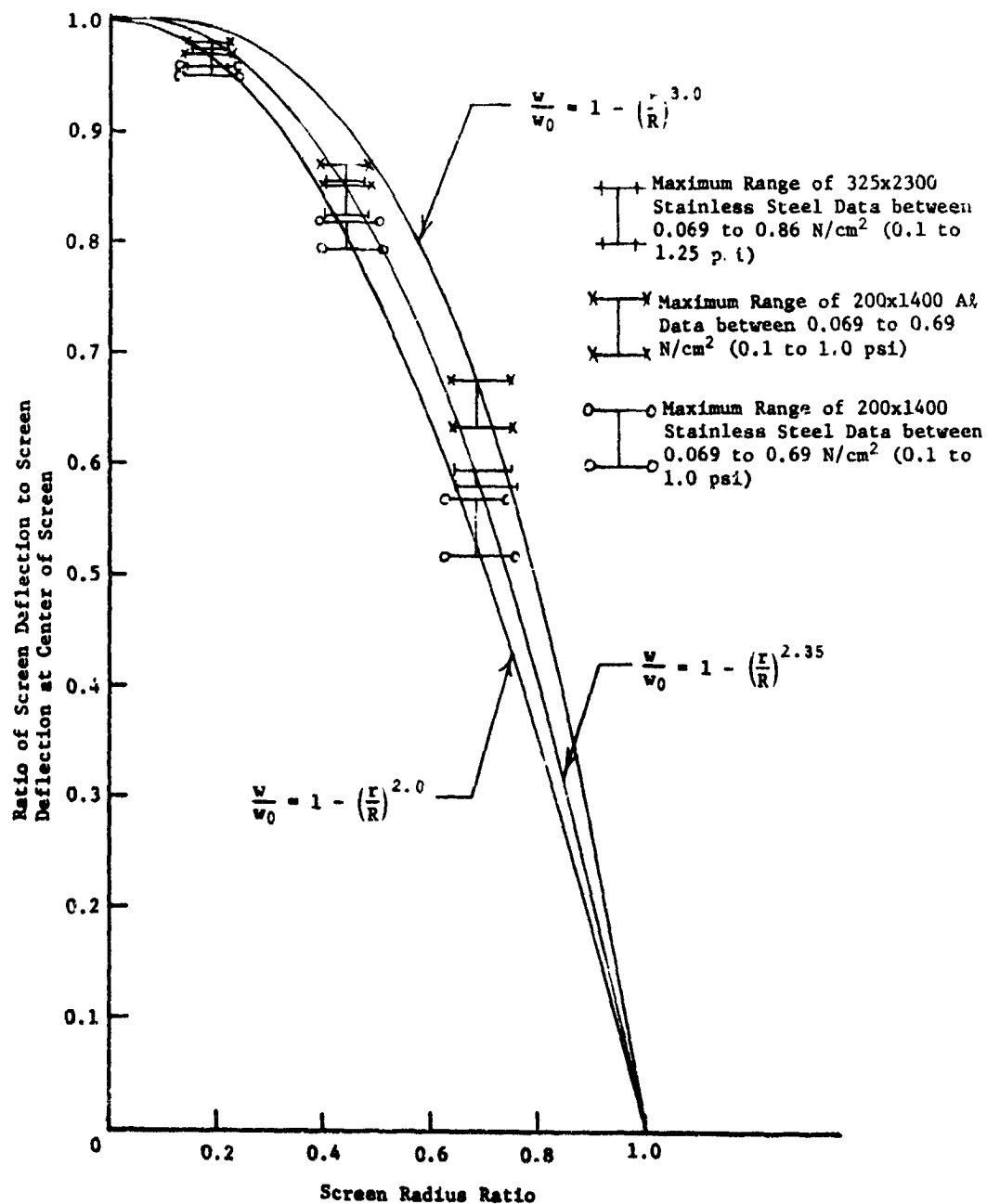
Fig. II-57 Dependency of Screen Deflection on Radius

The figure contains the following annotations:

$$\frac{w}{w_0} = 1 - \left(\frac{r}{R}\right)^{3.0}$$

Maximum Range of 325x2300 Stainless Steel Data between 0.069 to 0.86 N/cm^2 (0.1 to 1.25 p.i)

Maximum Range of 200x1400 Aℓ Data between 0.069 to 0.69 N/cm^2 (0.1 to 1.0 psi)

Maximum Range of 200x1400 Stainless Steel Data between 0.069 to 0.69 N/cm^2 (0.1 to 1.0 psi)

$$\frac{w}{w_0} = 1 - \left(\frac{r}{R}\right)^{2.35}$$

$$\frac{w}{w_0} = 1 - \left(\frac{r}{R}\right)^{2.0}$$

Y-axis: Ratio of Screen Deflection to Screen Deflection at Center of Screen

X-axis: Screen Radius Ratio

$$W/W_o = 1 - (r/R)^{2.35}$$

where

r = radial distance from center of screen,

R = screen sample radius, 10.16 cm (4 in.),

W = deflection at r,

W_o = deflection at r = 0

Subsequent tests, run after rupture testing was complete, indicated that higher loadings than were initially used could be safely applied. Also, beveled clamp rings were used to see if repeatable data could be obtained. Figure II-58 is representative of the data obtained. Data are shown for tests using flat ring and beveled ring clamping techniques for 325x2300 Dutch twill screen. Note that the two sets of data using beveled rings are consistent and agree with the initial set of flat ring data. However, subsequent samples tested with flat rings showed significant data scatter.

The higher ΔP loadings shown by Sample 5 indicate that a transition point does exist as noted during the initial series of tests. For a 325x2300 screen, this occurred at a ΔP of approximately 3.44 N/cm^2 (5 psia).

Figure II-59 shows experimental data for the 15.2-cm (6-in.) diameter circular screen test. Two samples of 250x1370 stainless steel screen were tested using flat clamping rings and a method of zeroing the dial indicator which agreed with beveled ring clamping data. Using this method, the dial indicator was positioned at the edge of the screen sample, instead of in the center. The data were fairly repeatable with this method. Two predicted curves derived from the 20.24-cm (8-in.) diameter data are shown in Fig. II-59. Both curves are based on a screen deflection dependency on radius, R, of R$^{4/3}$. This type of dependency is a result of the mathematical model that was developed from the test data.

2) *Cyclic Loading Test* - The 325x2300 stainless steel screen sample seemed to be totally unaffected by the cyclic testing. Deflection at the center of the screen varied by only 0.00178 cm (0.0007 in.), from 0.7531 cm (0.2965 in.) to 0.7513 cm (0.2958 in.), during the entire 101,987 cycles. Also no permanent deflection was observed, indicating that the deflection transition point of the screen was not exceeded.
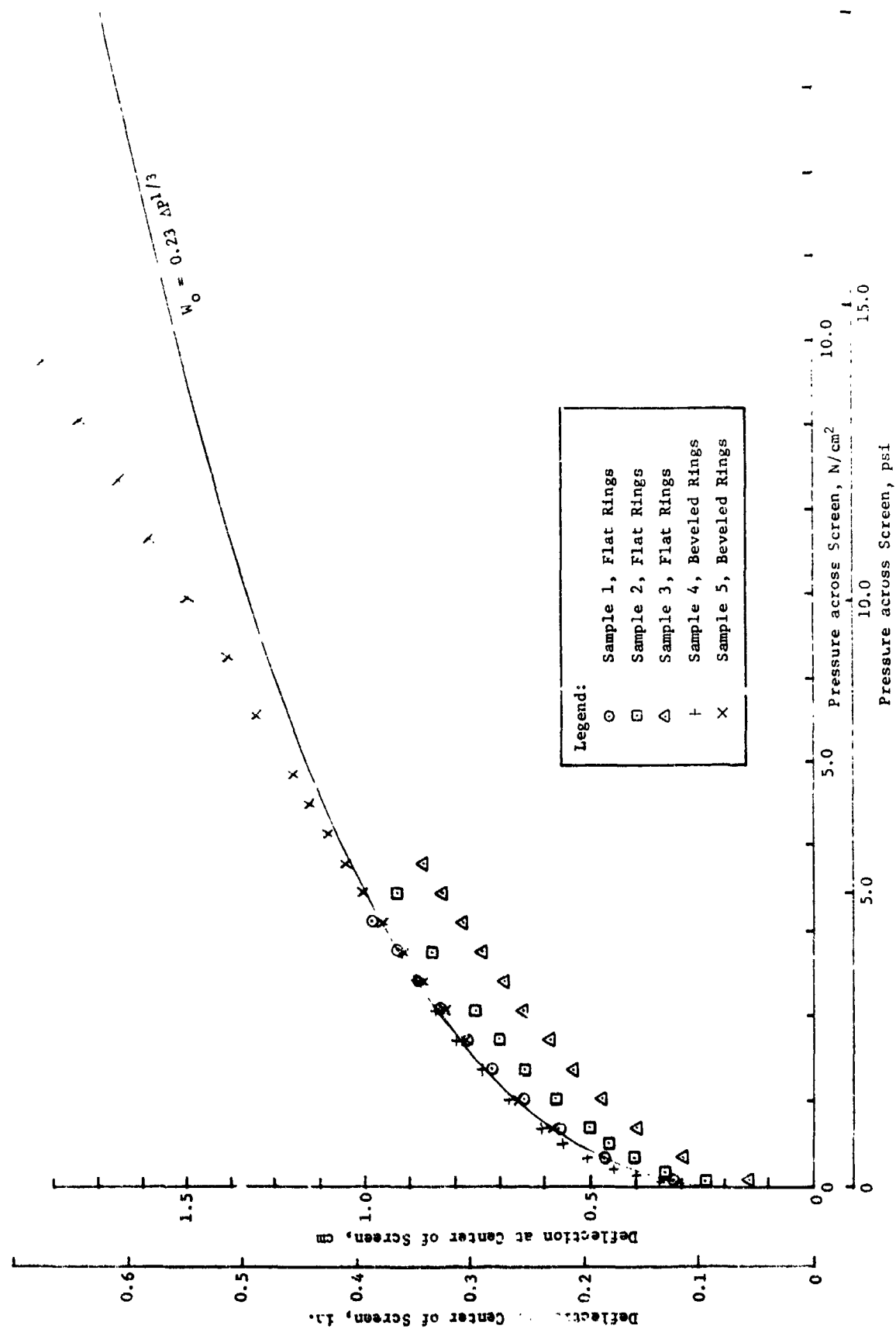
Fig. I-58 Static Loading Deflection Measurement Tests for 325x2300 Stainless Steel Screen

Legend:

⊙	Sample 1, Flat Rings
▢	Sample 2, Flat Rings
△	Sample 3, Flat Rings
+	Sample 4, Beveled Rings
×	Sample 5, Beveled Rings

$W_o = 0.23 \ \Delta P^{1/3}$
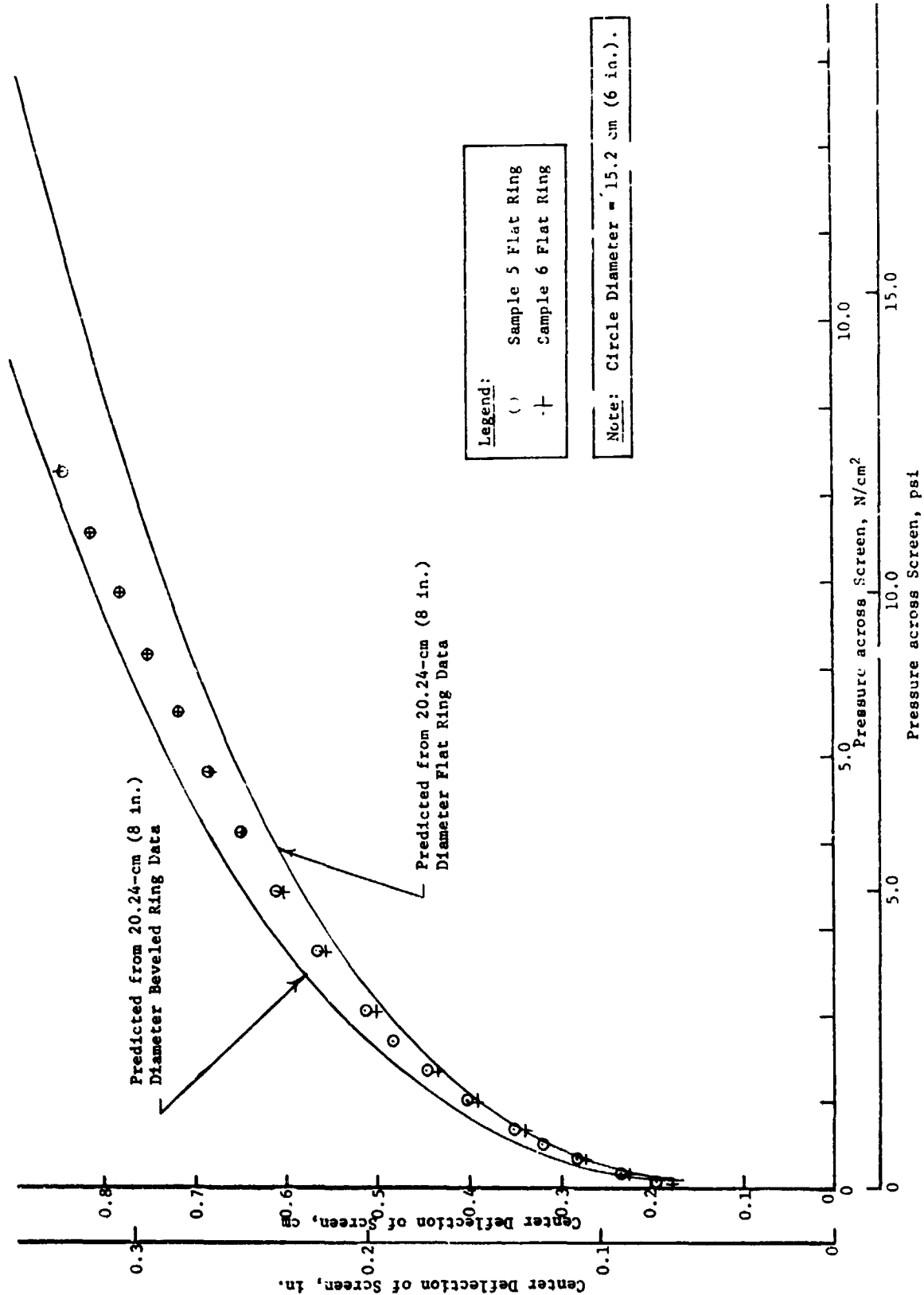
Fig. II-59 Screen Deflection Data for 15 cm (6 in.) Diameter Screen Specimen, 350x1370 Stainless Steel

In addition to determining whether fine mesh screen could support a pressure load without severe plastic deformation or rupture, the ability of the screen to support a pressure load without bubble point degradation was also investigated. Before and after the initial test series, all of the sample were bubble point tested. This included the screen samples, shown in Fig. II-56, as well as the cyclic loading screen specimen. Table II-6 summarizes the bubble point data. There was no significant bubble point degradation observed even for the static load test specimens, which sustained definite plastic deformation.

Table II-6   Bubble Points of Initial Test Specimens

Sample	Screen Type	When Measured	Bubble Point in Methanol, cm H_2O (in. H_2O)	Remarks
A	325x2300 Stainless Steel	Before Testing	60.4 (23.8)	
		After Testing	63.7 (25.1)	
B	200x1400 Aluminum	Before Testing	43.9 (17.3)	At edge of sample
		After Testing	23.5 (9.25)	In a flaw
			44.9 (17.7)	Away from flaw
C	200x1400 Stainless Steel	Before Testing	40.6 (16.0)	
		After Testing	37.8 (14.9)	
Cycling Test Sample	325x2300 Stainless Steel	Before Testing	58.9 (23.2)	Near edge
			61.5 (2)	Near edge
		After Testing	56.4 (22.2)	At center, but in a seam
		.	59.2 (23.3)	At edge of sample
			60.4 (23.8)	At edge in wrinkled area
			61.4 (24.2)	Across boundary of sample

3) Rupture Test - Rupture test results are summarized in Table II-7. Note the high pressure differentials required for rupture of the stainless steel screens. Results show that rupture loads are well above the deflection transition points indicated during the static deflection test and in some cases almost two orders of magnitude greater than the bubble point of the screen. Note that a differential pressure of 31 N/cm^2 (45 psia) failed to rupture the 200x1400 mesh stainless steel screen.

Table II-7 Rupture Test Data Summary

Screen Type	Rupture Pressure, N/cm^2 (psi)	Approximate Center Screen Deflection at Failure, cm (in.)	Remarks
325x2300 Stainless Steel	19.3 (28.0)	2.5 (1.0)	
250x1370 Stainless Steel	31.0 (45.0)	3.0 (1.2)	
200 x 1400 Stainless Steel	31.0 (45.0)	6.1 (2.4)	Tested terminated at this pressure, before screen ruptured
200x1400 Aluminum	3.4 (4.9)	2.0 (0.8)	

In addition to the failure data obtained during rupture testing, additional information was obtained from the 200x1400 stainless steel sample. Figures II-60 and II-61 show the specimen after testing. The very uniform surface created (Fig. II-60) supports the initial test data, which indicated that fine mesh screen acts as an isotropic rather than an orthotropic medium. The other significant result obtained is shown in Fig. II-61. As can be seen, the screen thinned out the most at its center indicating that the maximum strain and, therefore, the maximum stress occurs at the center of the screen for a circular geometry. Therefore, any model developed for the fine mesh screen must also predict that the maximum strain and stress be at the screen center for circular geometries.
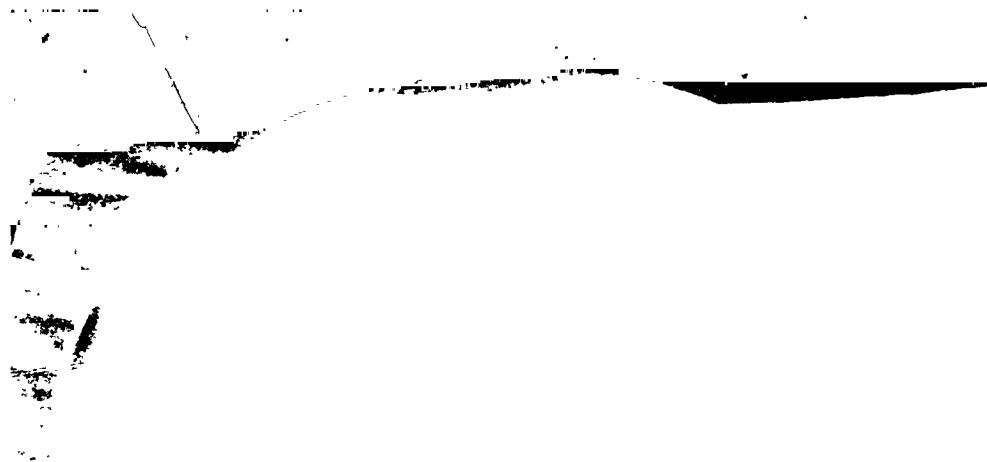
Fig. II-60 200x1400 Stainless Steel Rupture Specimen after Having 31 N/cm^2
(45 psi) Across It, Center Deflection Approximately 6.0 cm (2 3/8 in.)

Fig. II-61 200x1400 Stainless Steel Rupture Specimen, Light Projected through
Screen Showing Opening Up of the Weave After Testing

II-100

4) *Empirical-Analytical Correlation* – The equations presented
in Volume II Chapter II to define unsupported screen character-
istics are the result of the analytical analysis performed as
part of the screen structural capability study. Correlating
these equations with the experimental data resulted in the K
factor and design curves also presented in the Volume II dis-
cussion. Experimental correlations with the analytical equa-
tion defining screen deflection in circular segments developed
the following equations for the different screens tested.

$$W_o = 0.220 \; \Delta P^{1/3} \quad \text{for 250x1370 stainless steel} \qquad [II-7]$$

$$W_o = 0.235 \; \Delta P^{1/3} \quad \text{for 325x2300 stainless steel} \qquad [II-8]$$

$$W_o \simeq 0.175 \; \Delta P^{1/3} \quad \text{for 200x1400 stainless steel} \qquad [II-9]$$

$$W_o = 0.260 \; \Delta P^{1/3} \quad \text{for 200x1400 aluminum} \qquad [II-10]$$

The approximate sign is used in Eq [II-9] because only data from
one sample were available. In addition, these data were obtained
using the 20.24-cm (8-in.) flat clamping rings and the old dial
indicator zeroing procedure discussed previously under the test
program.

d. *Conclusions* – The structural integrity of fine mesh screens
was characterized by this series of tests and analyses. Struc-
tural factors (screen moduli and critical stresses) were identi-
fied for four types of fine mesh screen so that structural de-
sig s incorporating a number of different loading conditions
could be made. In addition, a mathematical model characterizing
the structural strength of fine mesh screen was developed for the
specific loading case of uniform pressure acting on a flat screen
segment. This specific model was confirmed experimentally by
testing. The following conclusions can be drawn from the work
performed to identify unsupported screen structural characteris-
tics:

1) Fine mesh screen behaves as an isotropic medium rather than
   as an orthotropic medium and can be mathematically modeled as
   such.

2) An upper design limit can be determined for fine mesh screen
   and used for structural screen designs.

3) Fine mesh screen offers considerable structural strength if uniformly loaded as flat screen segments (no radius of curvature).

4) Fine mesh screen offers practically no structural strength if loaded in a buckling mode.

5) The proposed DSL designs can be modified so that practically all perforated plate can be eliminated.

7.   Octosphere Deflection Tests

a. *Test Objectives* – The DSL concept of propellant management has
at least two problems associated with it for which the octosphere
configuration may offer a solution. The first of these is the need
for foraminous liners that are lightweight and can withstand the
external application of pressures approximately equal to the bubble
point of the screen. Second, this barrier must, as nearly as prac-
tical, conform to the geometry of the enclosing tank. Generally,
propellant tanks will be spherical or hemisphere/cylinder configu-
rations because of their favorable volume-to-weight ratios. This
requires the formation of capillary liners with hemispherical
shapes.

Forming hemispheres from flat stock is not an unusual technology
and there are companies that specialize in drawing or spinning
these shapes. However, when the additional requirement of porosity
is added, an otherwise routine operation becomes very difficult.
The spinning process, for example, develops great stress in the
metal blank, particularly around the edge. A porous material, such
as perforated sheet, will invariably crack in these high-stress
areas. Shell type structures called polygonal domes solve this
fabrication problem with little weight penalty.

The octosphere, as previously described in Volume II, Chapter II,
is an eight-sided member of the polygonal dome family whose sur-
faces are joined at an angle of 157.5° to approach a sphere in
appearance, surface area, and volume. Comparing an octosphere with
a volumetrically-equivalent sphere (Volume II, Fig. IV-2) results
in only a 4.5% increase in surface area and, consequently, a 4.5%
weight penalty as compared to the sphere. This number can, of
course, be reduced by increasing the number of sides. This type of
structure is desirable because fabrication problems are signifi-
cantly reduced without an appreciable weight increase.

Since the primary purpose of such a shell in a capillary acquisi-
tion/expulsion system is structural support of the fine mesh
screen, the structural adequacy of the configuration is of primary
importance. The purpose of deflection tests was to determine the
structural characteristics of a 25.4-cm (10-in.) perforated plate
octosphere subjected to a uniform buckling load. This load was a
uniform pressure differential, related to the bubble point of the
communication device in a dual-screen liner system. The results
from these tests could be used to verify the analytical methods and
model presented in Chapter II of Volume II.

b. *Test Apparatus and Procedure* - Two octosphere shells were fabricated from 24-gage, 0.064-cm (0.025-in.) thick, and 28-gage, 0.041-cm (0.0156-in.) thick, stainless steel perforated plate. A description of perforated plate material is given below:

28 Gage	24 Gage
304 Stainless Steel	304 Stainless
0.102-cm (0.040-in.) hole diameter	0.114-cm (0.045-in.) hole diameter
0.041-cm (0.0156-in.) thickness	0.064-cm (0.025-in.) thickness
23% open area	37% open area
0.2-cm (5/64-in.), holes staggered	No. 3 1/2 holes, not staggered

A drawing of the octosphere bench-test models is shown in Figure II-62. Photographs of the 24-gage model (Fig II-63) show external and internal construction features. The girth ring, gore sections, and support ribs are visible in the two views shown.

The perforated plate shell was sealed with Mylar sheets glued to the structure to produce an airtight system without increasing the structural capability of the model. The open end of the test item was placed on a hard flat surface and sealed so as not to effect deflection readings during testing. Eight dial indicators were used to measure deflection of each gore section from the girth ring to the dome cap. A pressure gage was used to record octosphere internal pressure. The octosphere was evacuated during testing to impose the uniform buckling loads of interest. A photograph of the complete test setup is shown in Fig. II-64. Note that the article was evacuated from the underside to prevent any additional loading that would result from hardware weight on the dome of the shell. Clearly visible are the points on each gore section where deflection measurements were made. The numbers shown are inches above the girth ring. Also each of the eight segments was assigned a letter, A thru H, clockwise in sequence as viewed from above. This assisted in mapping deflection of the surface as a function of pressure differential.
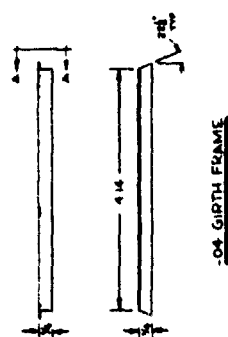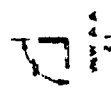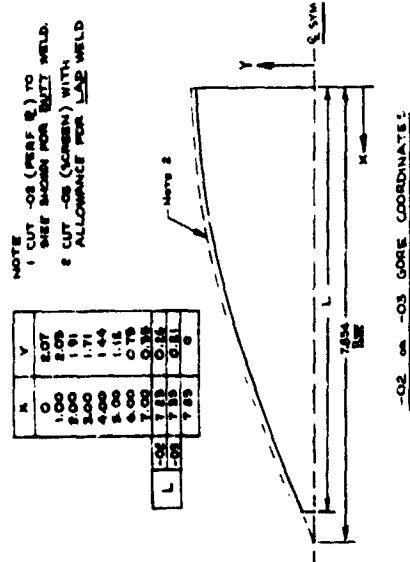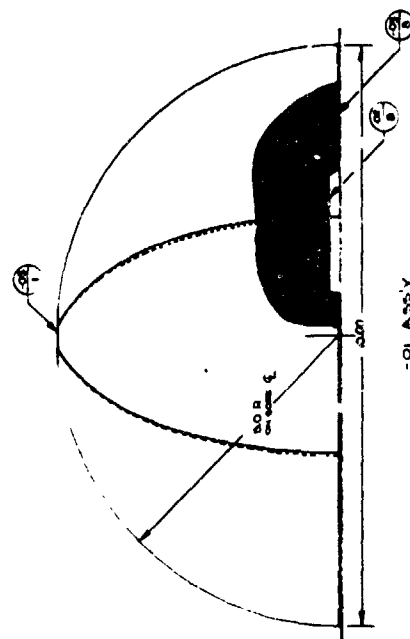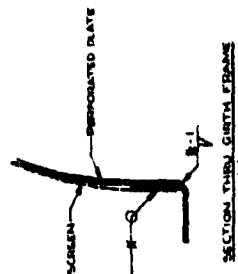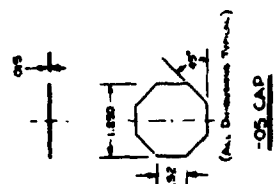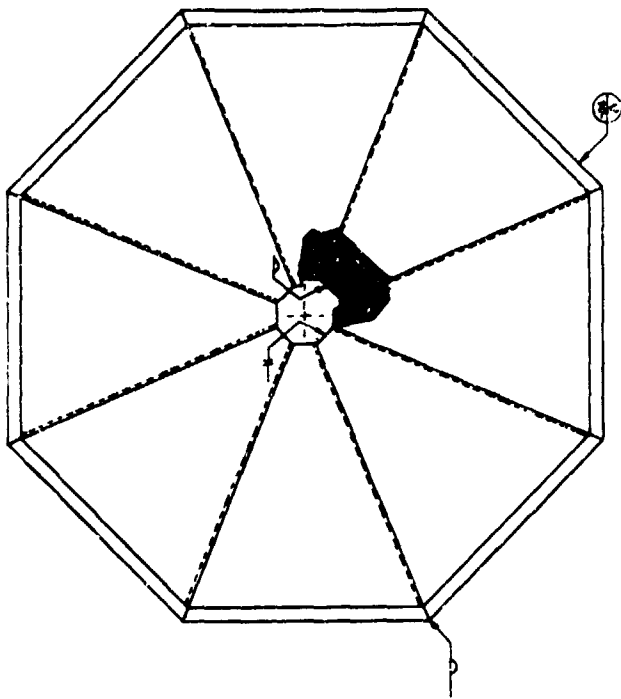
Fig. II-62 Octoephere Screen Assembly Drawing
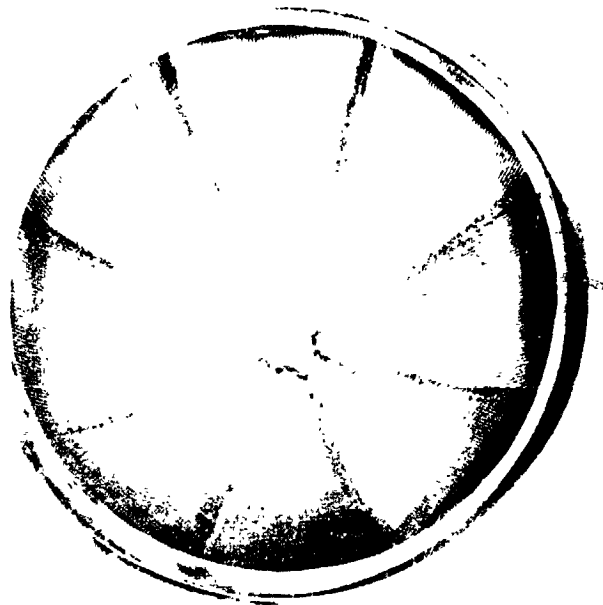
(b) Internal View
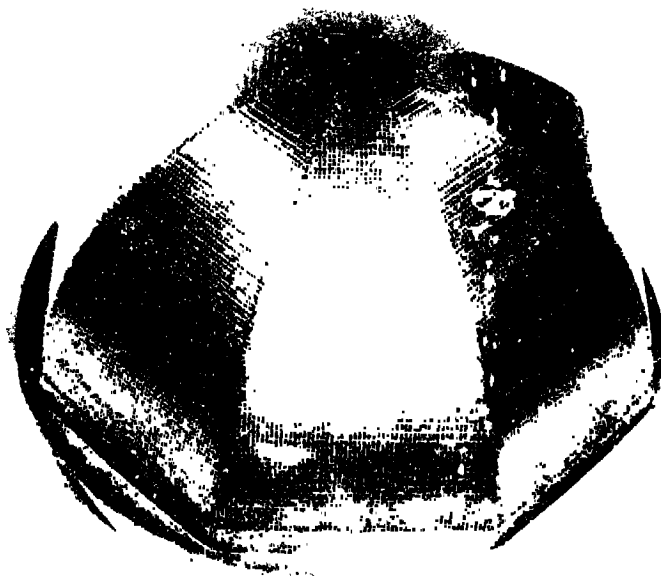
(a) External View

Fig. II-63 Octosphere Bench Test Model
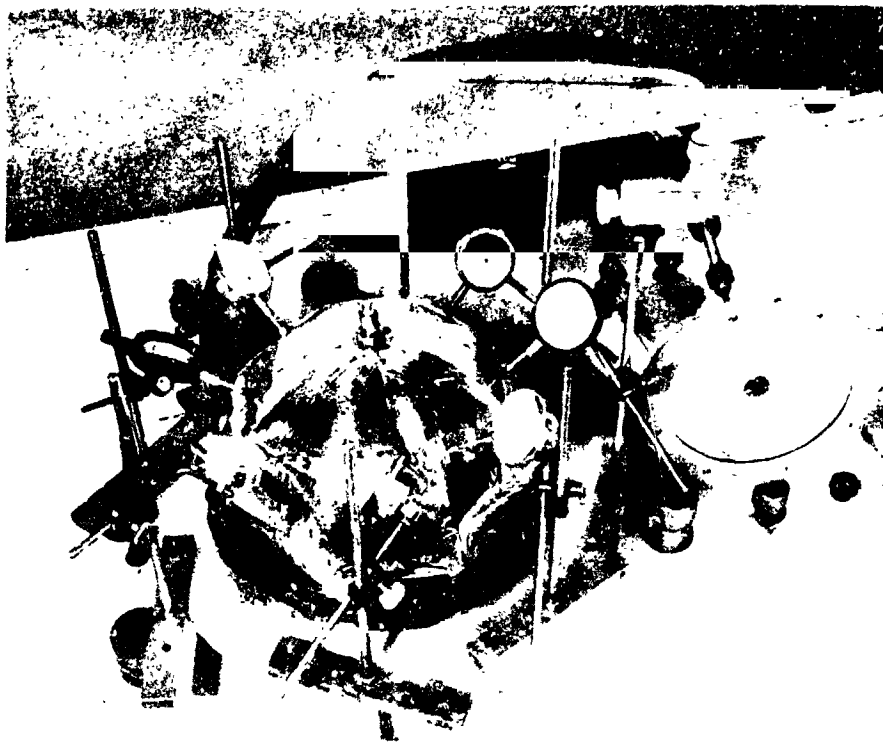
Fig. II-64   Octosphere Deflection Test Configuration

Both models were deflection tested in a similar manner. The dial
indicators were zeroed using a small ΔP to seat the Mylar cover.
The shell was then evacuated to 550-mm of mercury and deflection
readings taken at each segment 1.27 cm (1/2 in.) above the girth
ring. This was repeated for pressures of 500 and 450 mm Hg.
These pressures correspond to pressure differentials of 0.8 (1.1),
1.47 (2.1), and 2 14 N/cm^2 (3.1 psi) for an ambient pressure of 610
mm Hg. Deflection data were taken as a function of ΔP, as pre-
viously discussed. This procedure was followed using 1.27 cm (1/2
in.) increments until the top of the dome was reached and mapping
of the shell was complete. For the 24-gage octosphere, only four
segments (A, C, E, and G) were mapped, while data were taken for
all 8 segments during testing of the 28-gage model.

A failure test was also run using the 28-gage specimen to obtain
some correlation with the predicted ultimate strength of the shell.
The pressure differential was simply increased until failure oc-
curred, noting the pressure when the shell collapsed. This test
was documented on 16-mm black and white film.

c. Results – Deflection test results showed that uniform pressure
loads as high as 2.14 N/cm^2 (3.1 psid) could be sustained without
significant deflection of the octosphere shell. Figures II-65 and
II-66 show deflection curves for the 24- and 28-gage test models,
respectively. The data shown are for the panel of each model that
registered the maximum deflection.

Both figures show increased deflection with larger buckling loads.
A maximum deflection of 0.05 cm (0.020 in.) and 0.025 cm (0.01 in.)
was recorded for the 28- and 24-gage models, respectively, for a
pressure differential of 2.14 N/cm^2 (3.1) psid. These deflections
are small and pre.ent no design problems because pressure differen-
tials of this size will rarely be encountered in an actual system.
The maximum deflections shown indicate that the deflection for the
28-gage model will be twice that of the 24-gage octosphere. This
is generally supported by the data presented in Fig. II-65 and II-
66. These deflections did not exceed the elastic limit of the
material since no permanent deflection was noticed after loading
was removed. Deflections of 0 to 0.0013 cm (0.0005 in.) were re-
corded after the internal pressure was returned to ambient.

For a uniformly constructed and fabricated octosphere, shell de-
flection curves should be the same for each segment of the struc-
ture. However, due to nonuniformity in construction, such as welds,
weak and strong sections will exist throughout the structure,
causing deflection to be more or less random throughout the model.
This is substantiated by test data for both perforated plate shells.
A comparison of curves for different octosphere segments shows de-
flection to be completely random with negative deflections in cer-
tain cases. Also no trend is evident for deflection as a function
of distance from the girth ring. These effects are attributed to
the nonhomogeneous nature of the fabricated structures.

Failure test results indicate that the structure is predictable
from a stress standpoint. An analysis was made based on a homo-
geneous uniform shell to predict the ultimate loading capability
of the 28-gage octosphere. Based on this analysis, a maximum pres-
sure differential of 10.33 N/cm^2 (15 psid) could be sustained. The
maximum pressure recorded during the test was 6.5 N/cm^2 (9.5 psid).
This was significantly less than the predicted value because the
effect of fabrication is to introduce weaknesses into the struc-
ture that were not considered in the theoretical analysis. It is
instructive to point out that the failure model was not constructed
using advanced fabrication techniques. Seams and joints were
butted and spot welded. Present techniques would ensure increased
structural integrity and result in higher ultimate loading capabil-
ities than theoretically predicted.

II-108
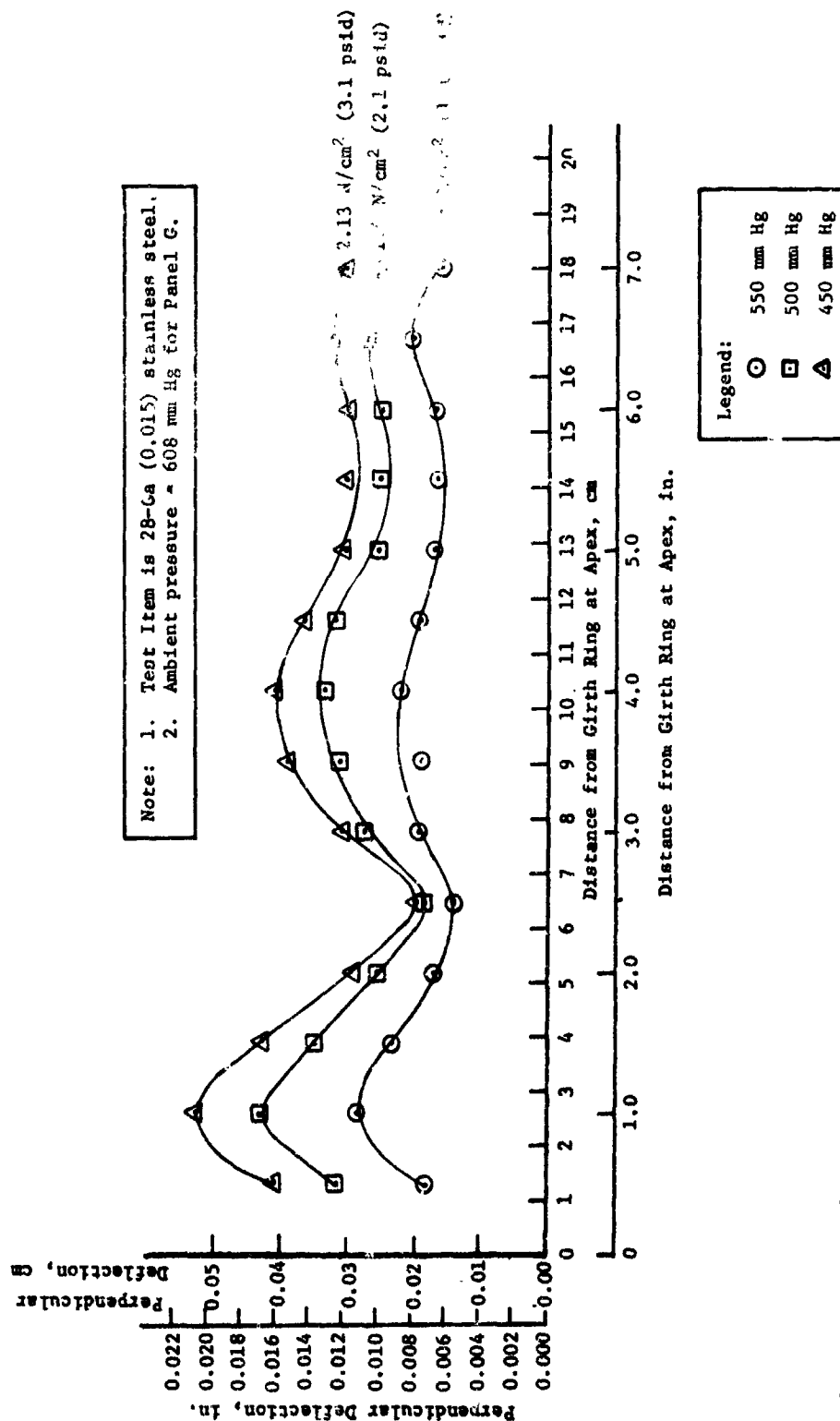
Fig. II-85 Octosphere Structural Test Results, 28 Gage Stainless Steel

601-11
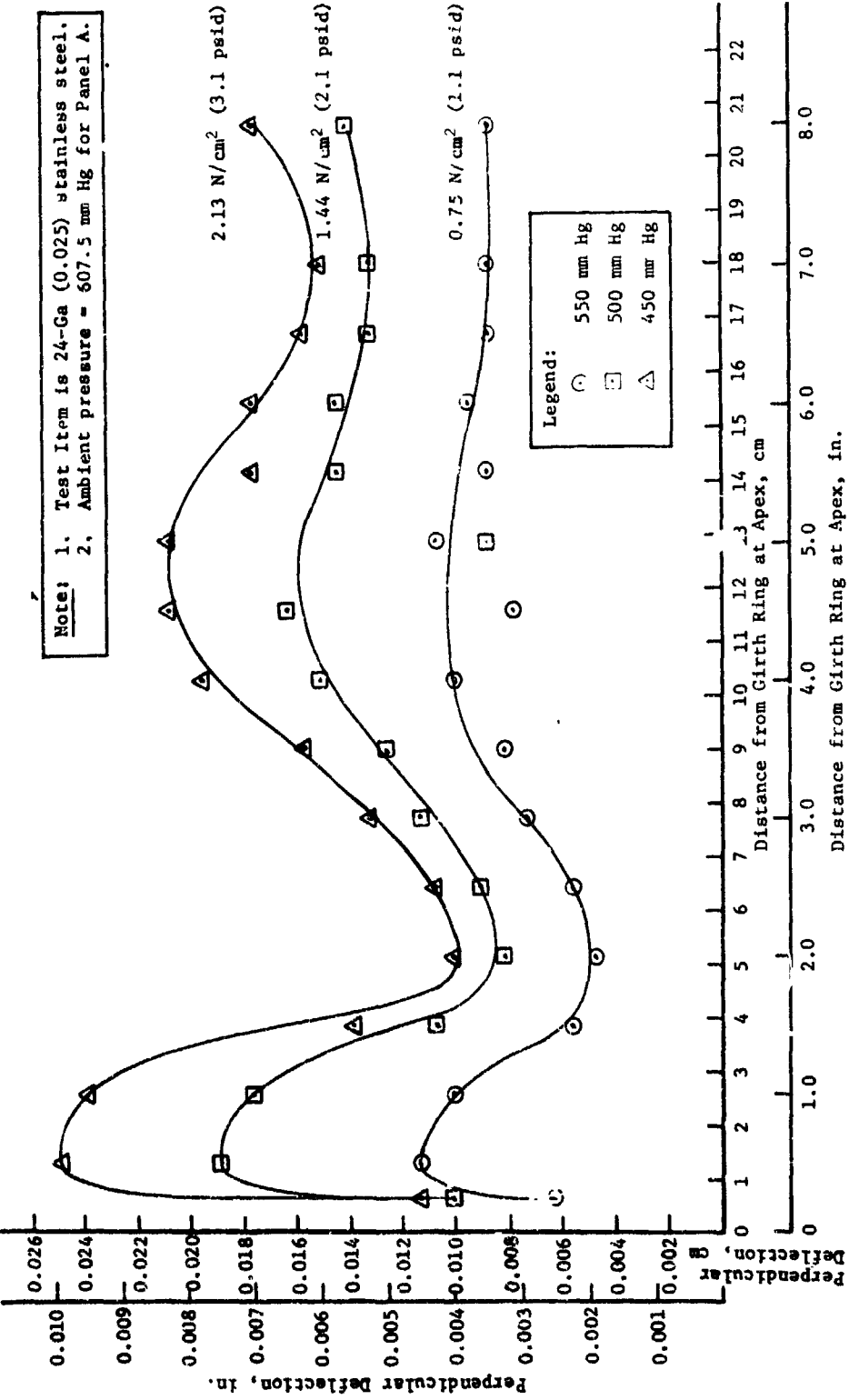
Fig. II-66 Octosphere Structural Test Results, 24 Gage Stainless Steel

l. Conclusions - Polygonal domes appear to be the geometric solution to the construction of fine mesh screen and support structure domes. Fabrication problems are significantly reduced with a minimal weight increase.

Test results verify the structural integrity of this type of dome shell when subjected to a uniform buckling loads. For pressure differentials as high as 2.14 N/cm^2 (3.1 psid) the maximum deflection recorded for the two 25.4-cm (10-in.) octospheres was 0.05 cm (0.020 in.) with no permanent deflection evident. Consequently, no structural problems are foreseen for this type design on encountering the loads anticipated in an actual system.

Failure test results indicate that this type of structure may be successfully modeled to establish design criteria. Advanced manufacturing techniques should strengthen the test models so that the ultimate load carrying capability approaches the theoretical value.

8. Boiling at the Screen Test

a. Test Objectives - In a DSL system, if the possibility of slightly superheating the liquid exists, the most likely place for such boiling to occur is at the outer screen where the maximum superheat is limited by the bubble point of the communication screen. The limited data available on the required superheat to initiate boiling indicate a high sensitivity to the nature of the solid surface. A wetted screen surface with vapor on one side would seem highly susceptible to boiling at a low superheat. No data existed for this condition.

The objective of this test was to determine the liquid superheat that can be sustained at a screen surface with vapor on one side. The question to be answered by this series of tests was whether or not boiling could be initiated at superheats corresponding to pressure differences less than the bubble point of the fine mesh screen. If boiling occurred, an added limitation would be imposed on system operation and quantitative data would be necessary. If boiling did not occur, the bubble point would remain the major design criterion for preventing gas ingestion into the controlled liquid region of a capillary cryogenic acquisition/expulsion device.

c. Test Apparatus and Procedure. - A diagram of the test setup is shown in Fig. II-67. The test was performed in a dewar that permitted visual observation of vapor bubble formation. For this reason, the test article was an inside-out configuration, in which the inner volume simulated the outer vapor annulus of a dual-screen-liner system. A small heater located in the screen liner simulated ambient heating. A bubbler was connected between the two chambers to limit the maximum ΔP across the screen. This device served the same function as the communication screen in a dual-screen-liner, but the ΔP was easily adjusted by changing the position of the submerged inlet tube. A nonvolatile liquid was used in the bubbler.

Because of the difficulty in accurately measuring the small temperature differences involved, the superheat was determined in terms of a pressure difference. This limited the required instrumentation to a voltmeter for measuring power input to the heater and a pressure gage to establish the starting conditions for the test. A pressure transducer was used to monitor the pressure differential across the screen liner.

The test apparatus is shown in Fig. II-68 and II-69. Figure II-68 shows the vertical test section, which consisted of a single liner of 325x2300 mesh stainless steel Dutch twill screen. Liner diameter and length were 2.54 cm (1 in.) and 30.5 cm (12 in.), respectively. The screen liner is shown inside a 7.62-cm (3-in.) diameter Pyrex cylinder. Figure II-9 shows the test article mounted in the Pyrex dewar, which is covered with tape to reduce the amount of radiative heating to the cryogenic liquid. Only a narrow slit was left uncovered for visual observation of gas in the liquid region. The fluids tested were liquid nitrogen and liquid hydrogen.

The procedure consisted of filling the transparent dewar to a suitable level with the cryogen, immersing the test article fill-tube, and allowing the apparatus to cool down with all valves open. The valves were then closed until a slight positive pressure built up in the dewar, at which time Needle Valve A was opened to fill the outer chamber to the desired level. This valve was then closed, and Needle Valve B was adjusted to establish the vent rate necessary to maintain the dewar at the desired initial pressure with power applied to the heater at the desired rate. When a relatively steady-state condition had been achieved, Dump Valve C was opened while the apparatus was observed visually for bubbles in the liquid annulus. The restriction in the fill-tube minimized the amount of liquid rising in the annulus after the sudden depressurization. Subsequent tests with an increasing immersion depth in the bubbler established the critical ΔP at which either boiling starts or screen breakdown occurs.

Fig. II-67 Schematic of Test Apparatus to Investigate Boiling at Screens
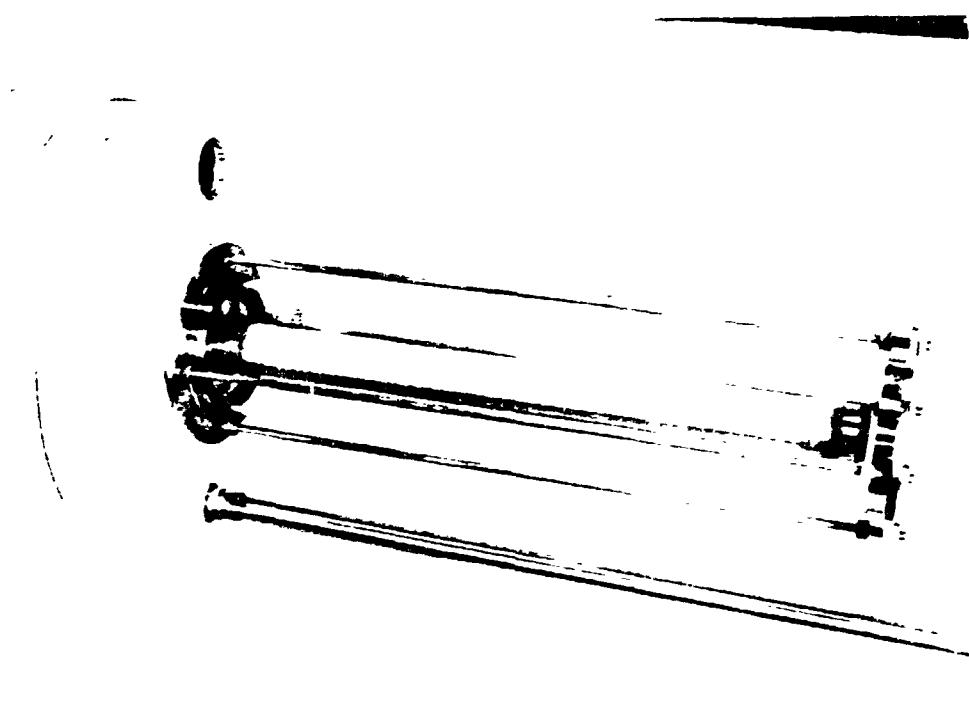
Fig. II-68 Boiling at the Screen Test Section

c. *Results* - Difficulties in obtaining good test data were limited
to qualitative rather than quantitative results. Due to the large
ambient heat loads, the heater was rarely used during testing. For
the majority of the tests, only a decrease in pressure was neces-
sary to superheat the liquid. This did not alter the test proce-
dure, however, because the only effect was to reduce the vent rate.

Liquid nitrogen and liquid hydrogen tests yielded similar results
although the increased boiloff with liquid hydrogen made gas deter-
mination in the liquid region even more difficult than for LN_2. In
general, the presence of gas in the liquid region coincided with
the differential pressure between the two regions (liquid and vapor)
approaching the established bubble point capability of the screen.
This seemed to indicate that the superheat associated with LN_2 and
LH_2 bubble points (27.4 cm of H_2O for LN_2 and 5.6 cm H_2O for LH_2)
was not sufficient to initiate boiling in the liquid region. How-
ever, problems during testing made reliable results difficult to
obtain.

d. *Conclusions* - Test results indicated that boiling at the screen,
because of a sudden decrease in pressure (venting), is not a problem
for the pressure differentials considered   The ΔP's considered cor-
responded to the bubble point of the 325x2300 mesh stainless steel
screen liner in the test fluids LN_2 and LH_2. Test results were in-
conclusive and should be verified by further testing.

II-114
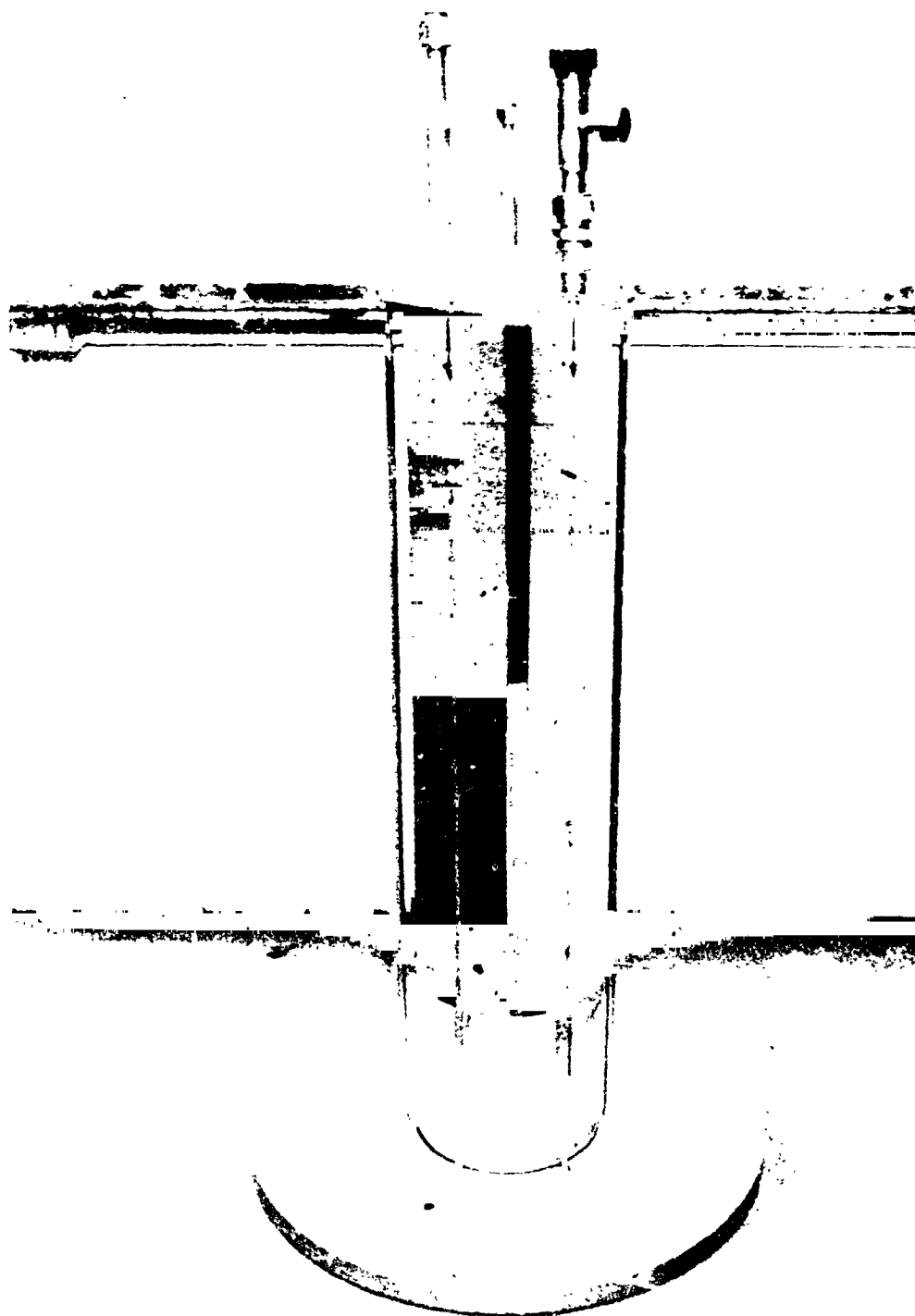
Fig. II-69   Test Apparatus for Investigating Boiling at the Screen

9.   Bubble Point Testing through Nonvisual Techniques

a. Test Objectives - The present reliability and reusability re-
quirements of spacecraft, such as Shuttle, impose a difficult de-
sign problem for propellant acquisition/expulsion systems. On this
basis, a completely passive system, such as a capillary screen de-
vice, is most attractive. However, from a reliability standpoint
the system must be checked periodically to assure no degradation in
system performance has taken place. For a fine mesh screen surface
tension device this requires bubble point verification of all screen
hardware. This will require special techniques for systems such as
the DSL, which cannot be removed from the tankage.

The purpose of this experiment was to verify techniques for inspect-
ing the retention capability of a capillary system using the Trans-
parent Expulsion Demonstration Device (TEDD). It was intended that
these test results be used as a basis for nonvisual determination of
the bubble point capability of large-scale capillary acquisition/ex-
pulsion systems.

b. Test Apparatus and Procedure

1) Apparatus - The test apparatus consisted of a capillary screen
device and a bubble point test facility. The test device was the
TEDD model used in KC-135 low-g expulsion tests. The low pressure
test apparatus (LPTA) (shown in Fig. II-70) included (1) first-
stage regulator and gage, (2) second-stage regulator and gage, (3)
four test pressure gages, and (4) various flow-control valves. The
gages were Dwyer Magnahelic types, which have 2% accuracy, are
easily calibrated, and are not sensitive to moderate overpressure.
A schematic of the entire test apparatus is shown in Fig. II-71.

All lines were 0.64-cm (1/4-in.) stainless steel tubing with the ex-
ception of the lines connected to the end plates of the model.
Tygon tubing was used for this application because of its noncorro-
sive properties and because its flexibility allowed the shake-turn
movement of the tank needed to ensure wetting of the screens. This
required lines approximately 1.53 m (5 ft) long.

Methanol was used to wet the capillary screens in the TEDD model. A
15.1-ℓ (4-gal) methanol storage tank was used, along with a heavy
duty pump, to supply methanol to the test article. Nitrogen gas
saturated with methanol gas was used as the pressurant to prevent
screen dryout due to methanol evaporation. This mixture was ob-
tained by bubbling nitrogen gas through liquid methanol collected
at the bottom of a 45.7-cm (18-in.) long, 37.8-ℓ (10-gal) tank. The
nitrogen/methanol gas ullage formed was fed from the outlet of this
tank to the LPTA. The pressure inside the ullage was checked with a
13.8-N/cm^2 (20-psig) gage positioned near the outlet.

II-116
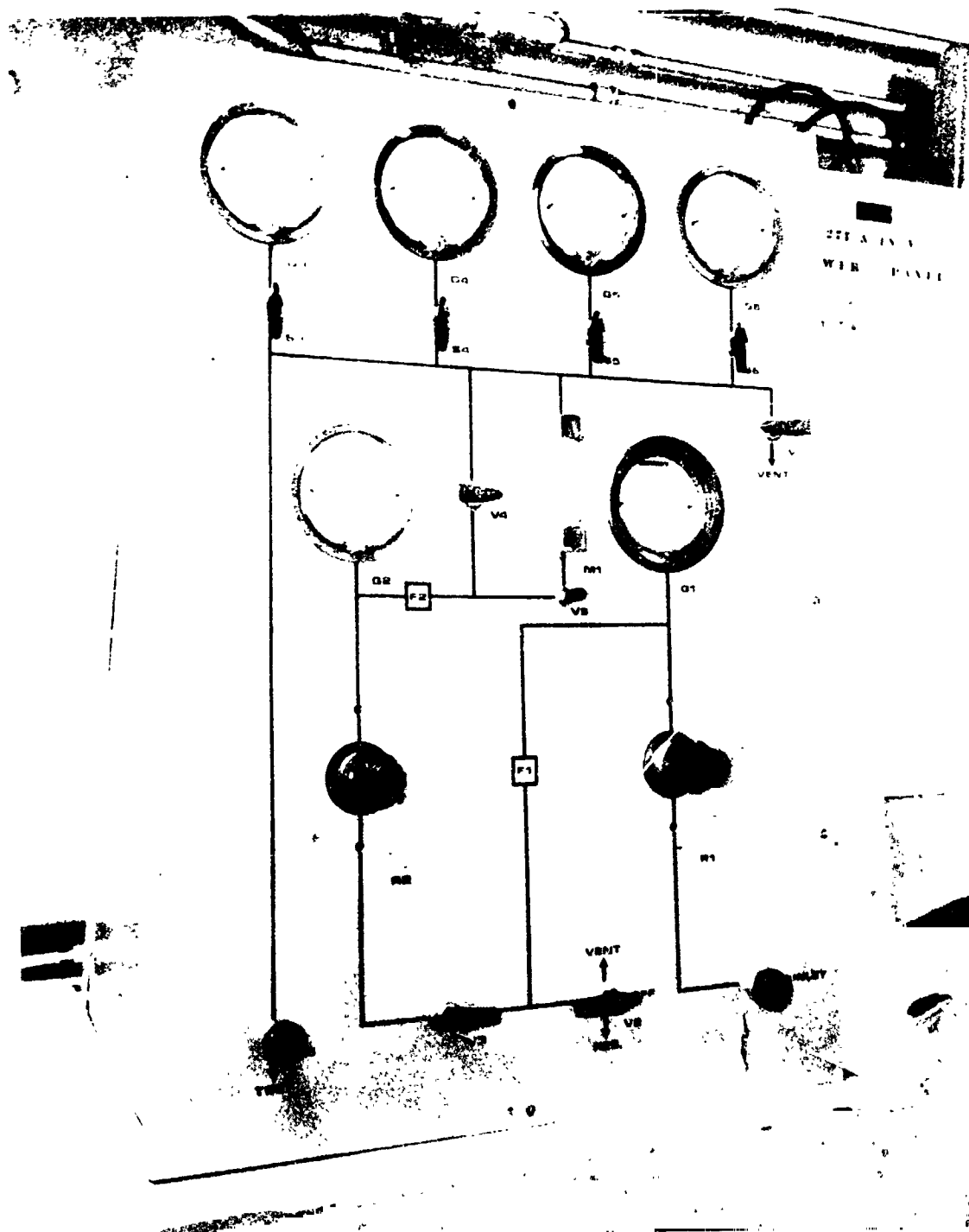
Fig. II-70 Low-Pressure Test Apparatus
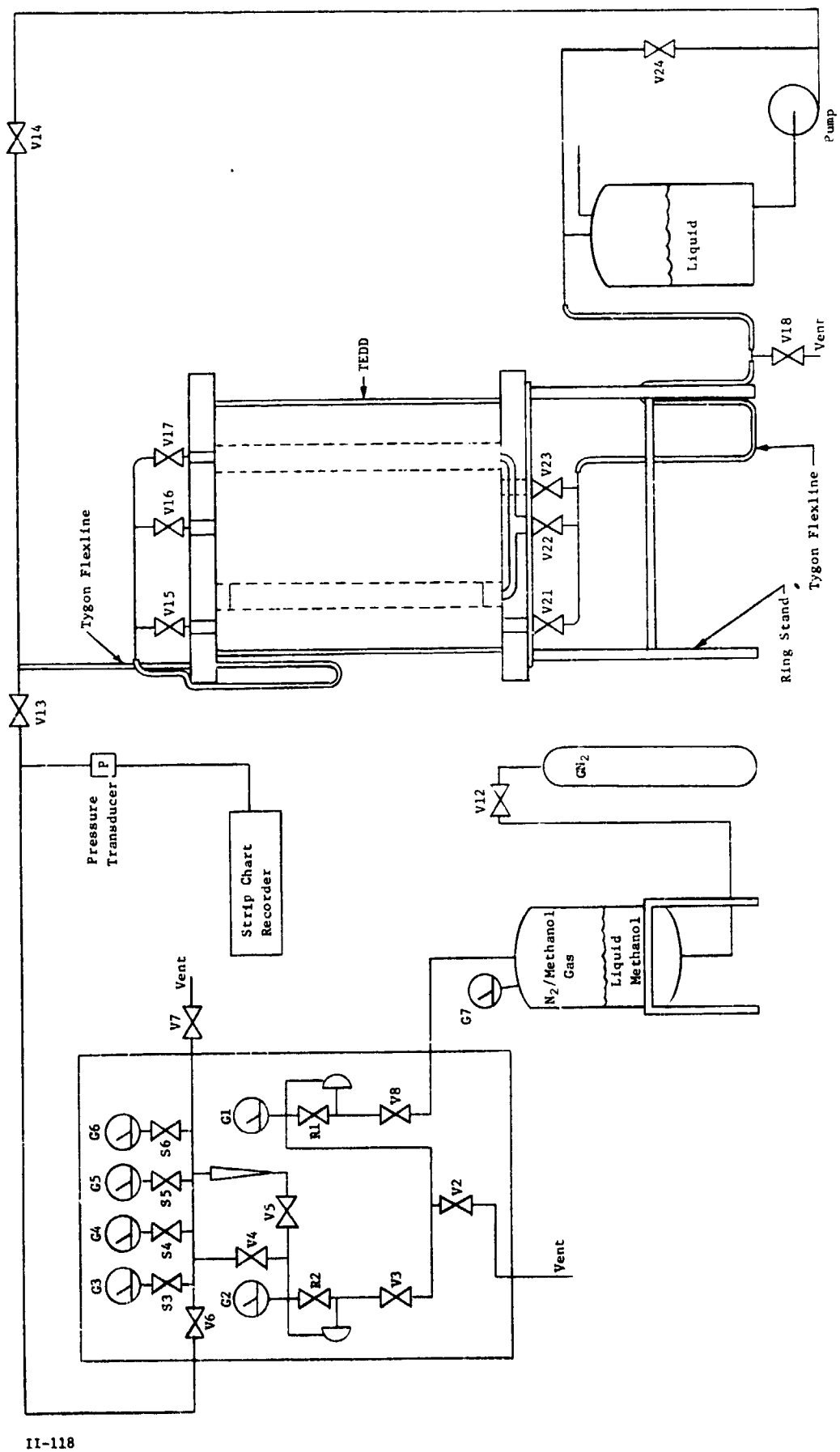
Fig. 11-71 TEDD Model Bubble Point Test Schematic

2) *Procedure* - Nonvisual bubble point testing of the TEDD model required that the screens be wetted, regions be pressurized to their specific values, and the pressure changes recorded when screen breakdown occurred.

Wetting the screens was accomplished first by pumping methanol to the TEDD model and then shaking the model until methanol was forced into all the screens. Visual observation of the screen wetting was done by looking through the end plates. The small amount of liquid left in the tank allowed rewetting of the screens just before bubble point determination.

The test article was pressurized to obtain a ΔP across the screen being tested. This was accomplished by opening and closing the inlet valves when the appropriate pressures were reached.

Nonvisual determination of the bubble point was based on the results of the communication/screen venting tests. Bubble point data from these tests revealed that the ΔP across the screen would increase to some peak ΔP and then decrease to a steady-state value. The difference between peak and steady-state ΔP is a function of pressurization rate; i.e., the higher the pressurization rate the more overshoot and the bigger the difference between peak and steady-state values. For very small pressurization rates, the peak and steady-state values will essentially coincide and the bubble point is obvious. Where significant differences between peak and steady-state ΔP's exist the actual bubble point is approximately the mean of these values. A typical bubble point trace is shown in Fig. II-72.

c. *Results* - Data obtained from the TEDD model tests show the same basic curve shapes that are characteristic of the bubble point tests performed on 5.08-cm (2-in.) diameter screen sections. Bubble point test curves snow a gradual buildup of pressure, a pressure maximum or peak, and then a drop followed by constant pressure levels similar to the trace in Fig. II-72. However, for these tests, the results indicated the maximum or peak value of the curve appeared to be more representative of the actual bubble point. This difference is attributed to the inability of the screens to stay in a wetted condition once screen breakdown has occurred. This caused lower steady-state values than would normally be recorded if the screens remained wetted as in the communication/ screen venting tests. Test results are shown in Fig. II-73.
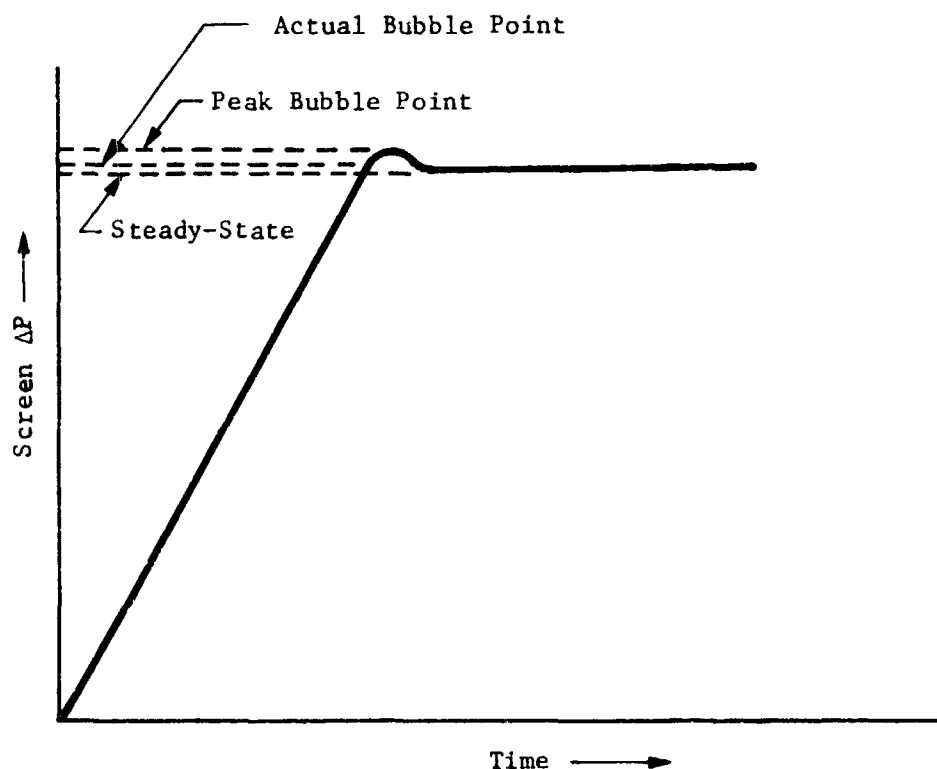
Fig. II-72 Typical Fine Mesh Screen Bubble Point Response

To obtain the bubble point value before screen dryout occurred, a pressurization rate of 100 cc/min was used in the three screen tests. This rate was high enough to obtain good data quickly, but low enough so that pressurant impingement on the screen had minimal influence on screen breakdown from dryout. Since screens could not be continuously wetted with this system, this pressurization rate is important in bubble point determination.

The bubble point data obtained showed that under ideal screen retention conditions, deviations from the acceptable bubble points for the communication and outer liquid annulus screens occurred consistently. Deviations ranged from 1.7 cm (0.67 in.) H_2O over the acceptable bubble point for the communication screen to approximately 1.77 cm (1/2 in.) H_2O below the standard bubble point value for the outer liquid annulus screen. Acceptable data ranges for as-received 325x2300 and 250x1370 screen are 63 to 68 cm (24.80 to 26.75 in.) and 53.6 to 58 cm (21.10 to 22.83 in.) H_2O, respectively. Flaws within the capillary network may have influenced the screen retention capabilities.

t = 5.1 cm/min (2 in./min)
Communication Screen (250x1370)

t = 5.1 cm/min (2 in./min)

Outer Liquid Annulus Screen (325x2300)

t = 5.1 cm/min (2 iu./min)

Inner Liquid Annulus Screen (325x2300)
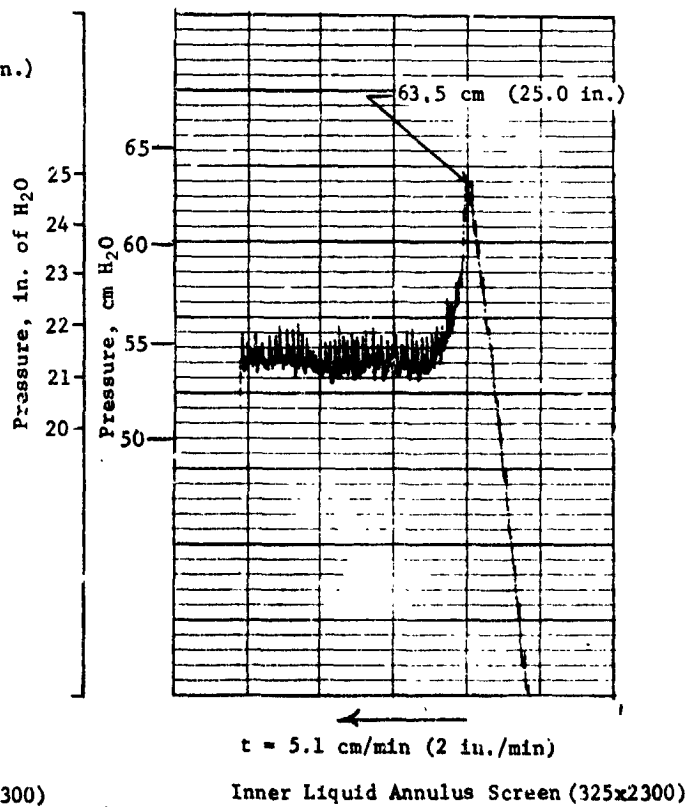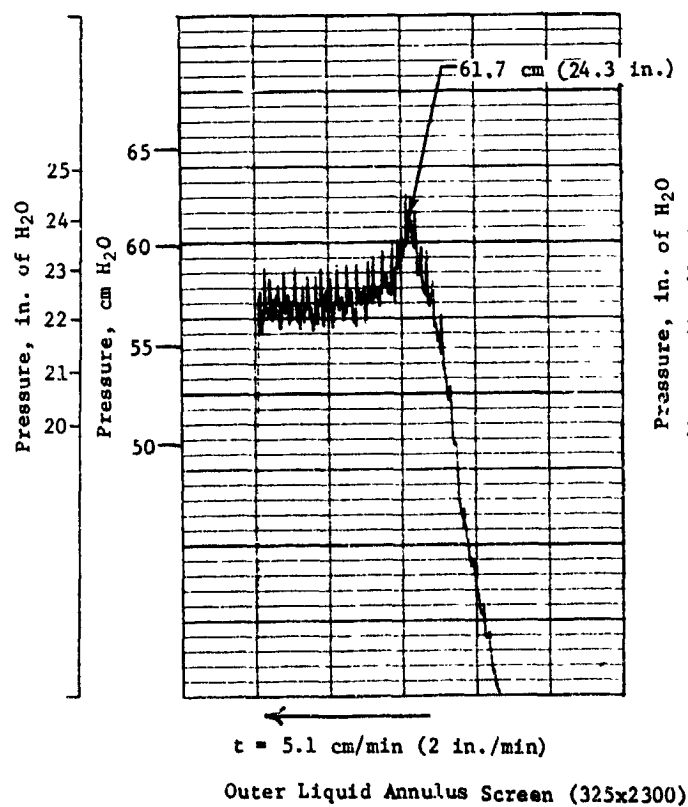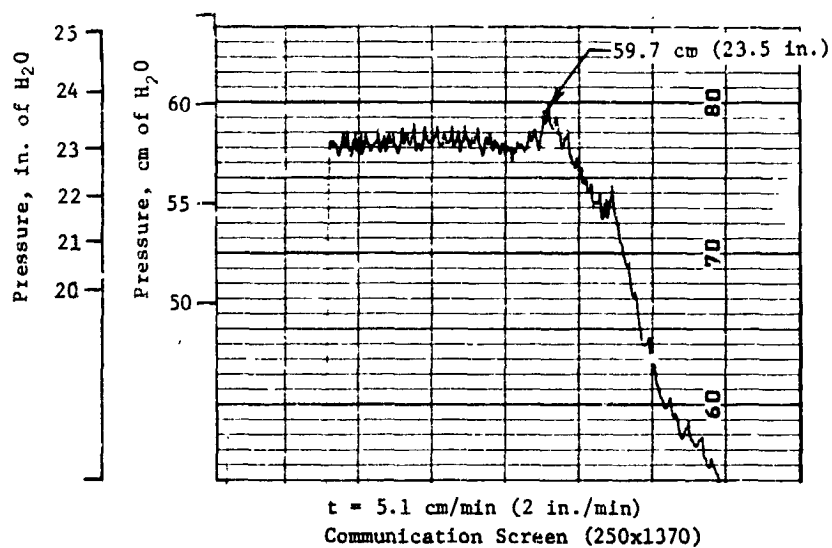
Fig. II-73 Nonvisual Bubble Point Test Results

II-121

Weave discrepancies, screen cleanliness, and cold solder joints are major factors causing inconsistent bubble point data. Since joining techniques and cleanliness standards were eliminated as possible sources of error, weave discrepancies seem to be the prime cause of the deviations in data.

The main problem that occurred during the tests was screen dryout. This problem was corrected when the pressurant flow rate to the tank was increased. A reduction in the expulsion rate would allow more time for the methanol to drain from the screen and cause screen dryout. Therefore, by increasing the pressurant flow rate, good data was obtained in a short period of time before screen dryout occurred. The optimum pressurization rate is the lowest that can be used and still prevent screen dryout.

d. *Conclusions* - A systematic method of bubble pointing a capillary acquisition/expulsion device using the nonvisual technique can be established. Low pressurization rates provide the most accurate bubble point determination, provided the fine mesh screens do not dry out. Techniques used to check the functional operation of a similar device could incorporate the basic procedure used for TEDD. Methods and procedures would be changed to compensate for the differences in size, weight, and geometry of the tank capillary device.

10. **Transparent Feedline Tests**

a. *Test Objectives* - The selection of a passive surface tension device, as the preferred storage tank design, made a passive screen liner the most logical concept for feedline conditioning. Experimental data on capillary feedline performance was necessary to compare passive concepts and was to be obtained from the 3.9-m (12-ft) long LN_2 feedline model. Schedule slippage of these tests and the immediate need for verification of the screen liner system dictated the testing a second, less sophisticated feedline model so that selection of the best concept could be accomplished during Task II.

The primary purpose of these tests was a qualitative demonstration that the screen liner feedline concept is a valid, workable system. This was accomplished by demonstrating: (1) gas-free liquid flow with a vapor-filled outer annulus and (2) a stable liquid/gas interface during static venting conditions. Noncryogenic liquids were used to check out hardware and procedures. A transparent feedline was used to allow visual observation and documentation of the tests; 16-mm color film recorded the ability of the fine mesh screen liner to maintain phase separation during both flow and nonflow conditions.

b. *Test Apparatus and Procedure*

1) Test Apparatus – The test setup consisted of the transparent
feedline test section, supply and receiver tanks, plumbing, and
control components. The test section consisted of a 1.9-cm (3/4-
in.) diameter by 101.6-cm (40-in.) long screen core with 7.62-cm
(3-in.) glass extensions on each end so the fluid state inside the
core could be observed. The screen liner consisted of a layer of
325x2300 mesh Dutch twill screen wrapped around a 1.9-cm (3/4-in.)
diameter perforated copper tube. The liner was fabricated in two
50.8-cm (20-in.) sections that were brazed together to form the
completed feedline. Tubular sections were brazed on each end of
the screen core and sealed by O-rings to each of the glass exten-
sions.

The liner assembly was encased in a Pyrex glass tube, 7.62-cm (3-
in.) in diameter and 122-cm (48-in.) long. This formed a vapor
annulus much larger than would ordinarily be used and simplified
instrumentation installation. The Pyrex tube was sealed by two
aluminum end plates with 1.9-cm (3/4-in.) aluminum tubes on each
end. Pressure taps were available in each end plate for monitoring
and controlling the vapor-annulus pressure. The entire assembly
was proof tested at 17.2 N/cm^2g (25 psig) to yield a working pres-
sure of 6.89 N/cm^2g (10 psig). Photographs of the liner assembly
are shown in Fig. II-74(a) and (b).

Two different test fluids were used. First, for the flow test, a
fluid with a normal boiling point at or near ambient conditions was
desirable to preclude vaporization problems. Based on this and
other considerations such as surface tension, Freon 11 was selected
[normal boiling point of 297.7°K (76°F)]. Second, venting tests
required sufficient boiloff to assure pressure buildup in the vapor
annulus. For this application a fluid with a normal boiling point
below ambient temperature was needed. Freon 114 met this require-
ment [normal boiling point of 277°K (39°F)] and was selected for
this series of tests. The basic test apparatus was the same for
both fluids.

A schematic of the complete test apparatus is shown in Fig. II-75.
The basic components, supply tank, feedline section, and reservoir
(catch tank) are shown with the necessary plumbing and instrumenta-
tion. The supply tank was a stainless steel pressure vessel, 26.7
cm (10.5 in.) inside diameter with hemispherical end domes and a
barrel section, 20.3-cm (8-in.) long. Instrumentation included a
supply tank pressure gage, three differential pressure gages, a
feedline absolute pressure gage, and six thermocouples for measuring
fluid temperatures at various points in the system. Differential
pressure was measured to give screen ΔP, pressure loss in the feed-
line, and ΔP across the vent microvalves MV2 and MV3 to aid in cal-
culating vent flow rates. However, the two latter measurements
were suspect because of Freon contamination of the gages.
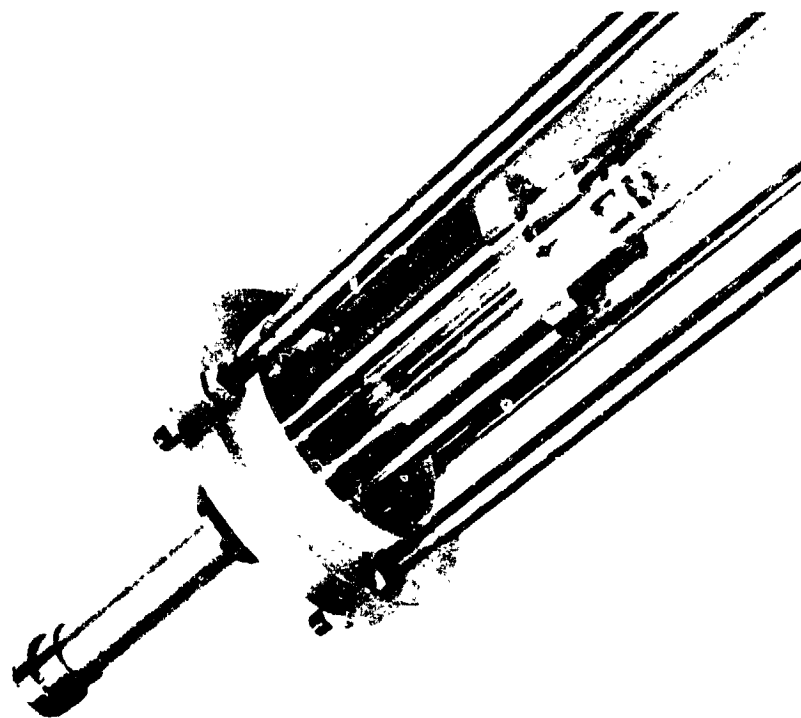
(b) Liquid Core Sightglass
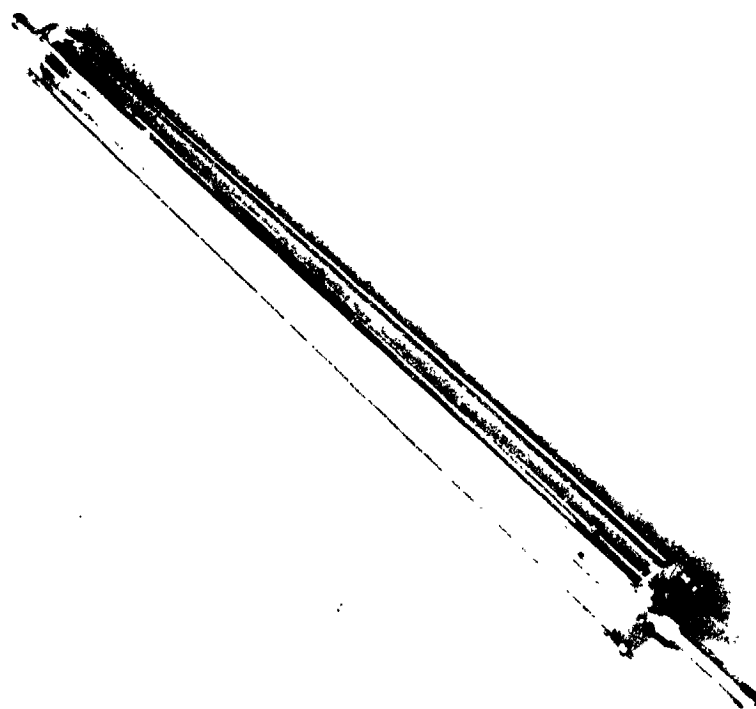
(a) Total Feedline Section

Fig. II-74 Transparent Feedline Test Section
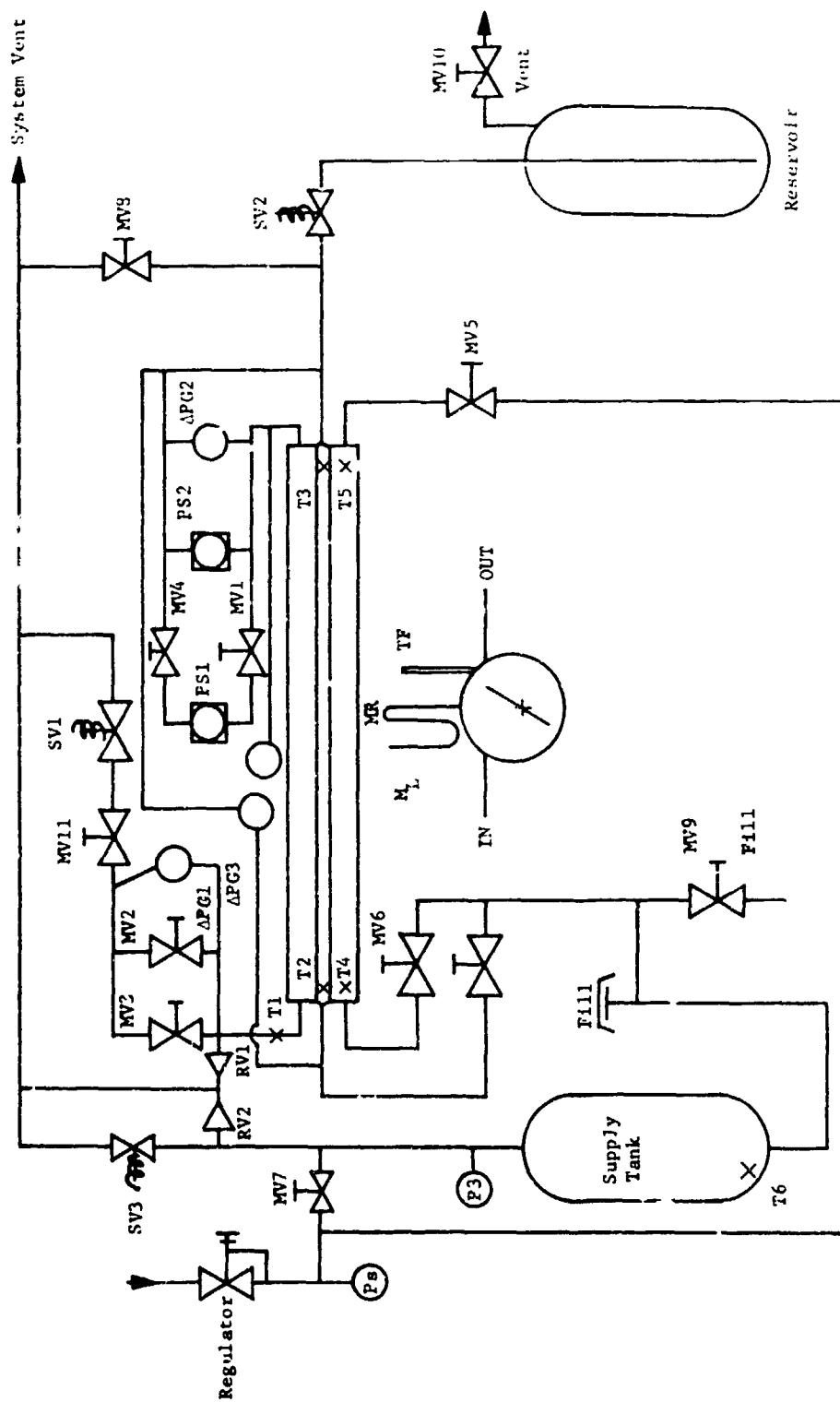
Fig. II-75 9.6-cm (40.9 in.) Feedline Schematic

The test configurations for flow and venting tests are pictured in Fig. II-76 and II-77, respectively. Essential components of the test setup are shown with the exception of the liquid catch tank. The supply tank, feedline, and instrumentation panel can be seen mounted on a compact pallet with the plumbing and hardware necessary for successful test operation. Figure II-77 shows the system insulated for the venting test. This was done to minimize heat leak into the system other than through the feedline vapor annulus. Even with the insulation, a cold GN_2 purge was eventually required to nullify feedline end effects, which caused gas formation in the liquid core. Supply tank pressurization was accomplished using gaseous nitrogen from the facility supply. Although not evident in the photograph, the feedline was inclined slightly to allow observation of any gas present in the liquid core region at the outlet sightglass.

Preliminary tests indicated that gas in the liquid core region had pressure differentials significantly less than the bubble point of the screen liner. Subsequent bubble point tests of the feedline were made by filling the vapor annulus with liquid and pressurizing the inner core with gas. This revealed that the ΔP capability of the system was about 7.6 cm (3 in.) of water with Freon 11, which is much less than the expected screen capability [approximately 53.5 cm (21 in.) of H_2O]. A leak was found at the O-ring seals at each end of the test section. After repair with a suitable sealant, the tested bubble point was 39.9 cm (15.7 in.) of H_2O or 75% of normal. This degradation was attributed to the brazed joint in the center of the feedline test section where initial breakdown consistently occurred.

2. *Procedure* - Before test, the entire feedline test section was filled with liquid at a pressure sufficient to maintain a single-phase liquid. This corresponded to system pressures of 10.3 to 13.8 N/cm^2 (15 to 20 psia) for both series of tests (flow and venting). Liquid was then purged from the vapor annulus by nitrogen gas, while maintaining a positive pressure difference between the annulus and core regions. This established a stable liquid/vapor interface at the screen without exceeding the screen bubble point.

Dynamic flow testing included flow rates of 33.2 to 83.2 kg/hr (73.2 to 183 lbm/hr) using Freon 11 at a temperature of 293°K (68°F). After loading liquid into the system, the pressure was increased to achieve the desired flow rate while maintaining a stable liquid/vapor interface. At steady-state conditions, flow rate, pressure differentials, and temperatures were noted. During tests, the liquid state was continually monitored by observing the inlet and outlet sightglasses. This procedure was repeated for several flow rates in the test range.

II-126
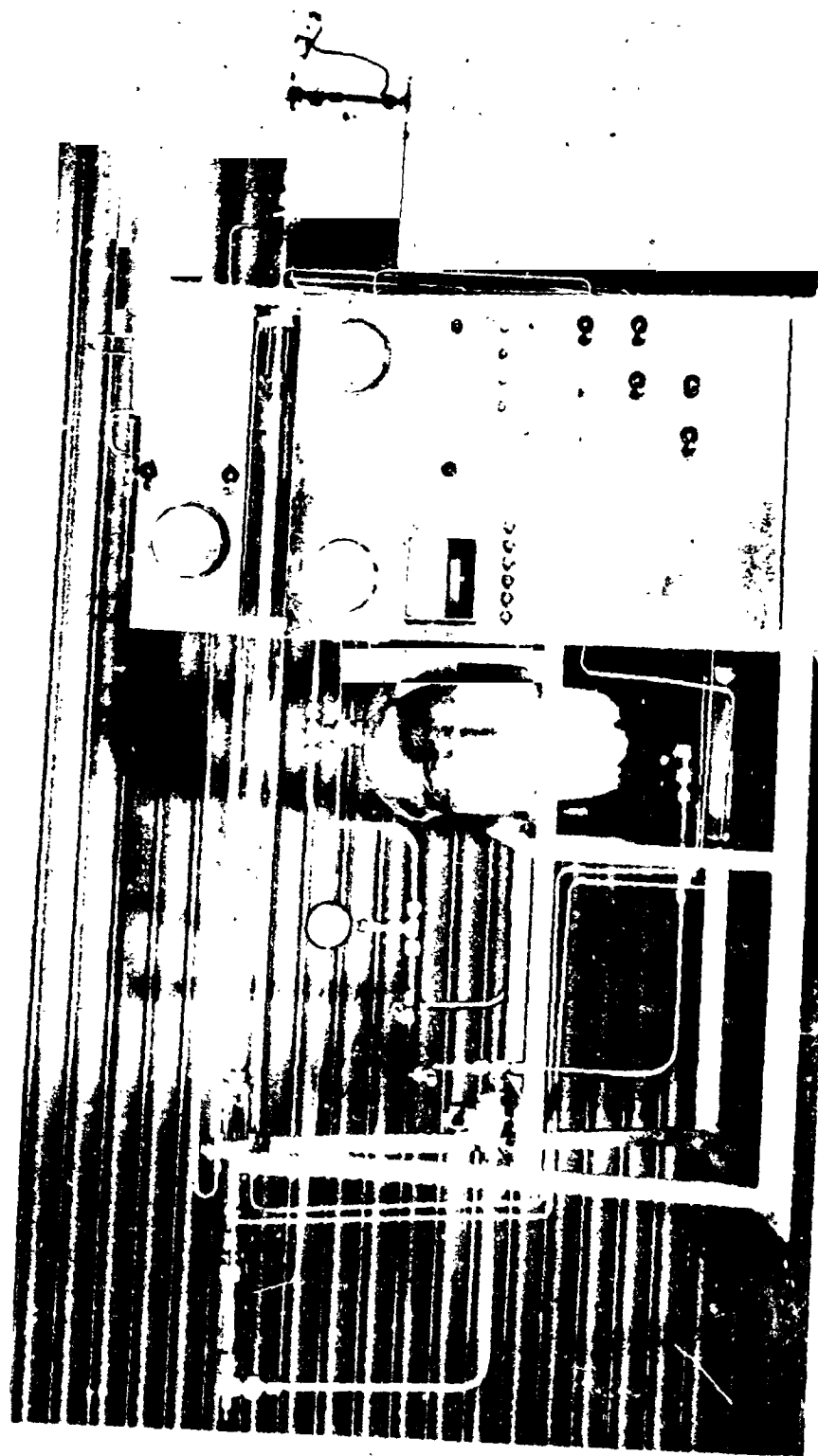
Fig. II-7. Transparent Feedline Test Apparatus, Flow Test Configuration
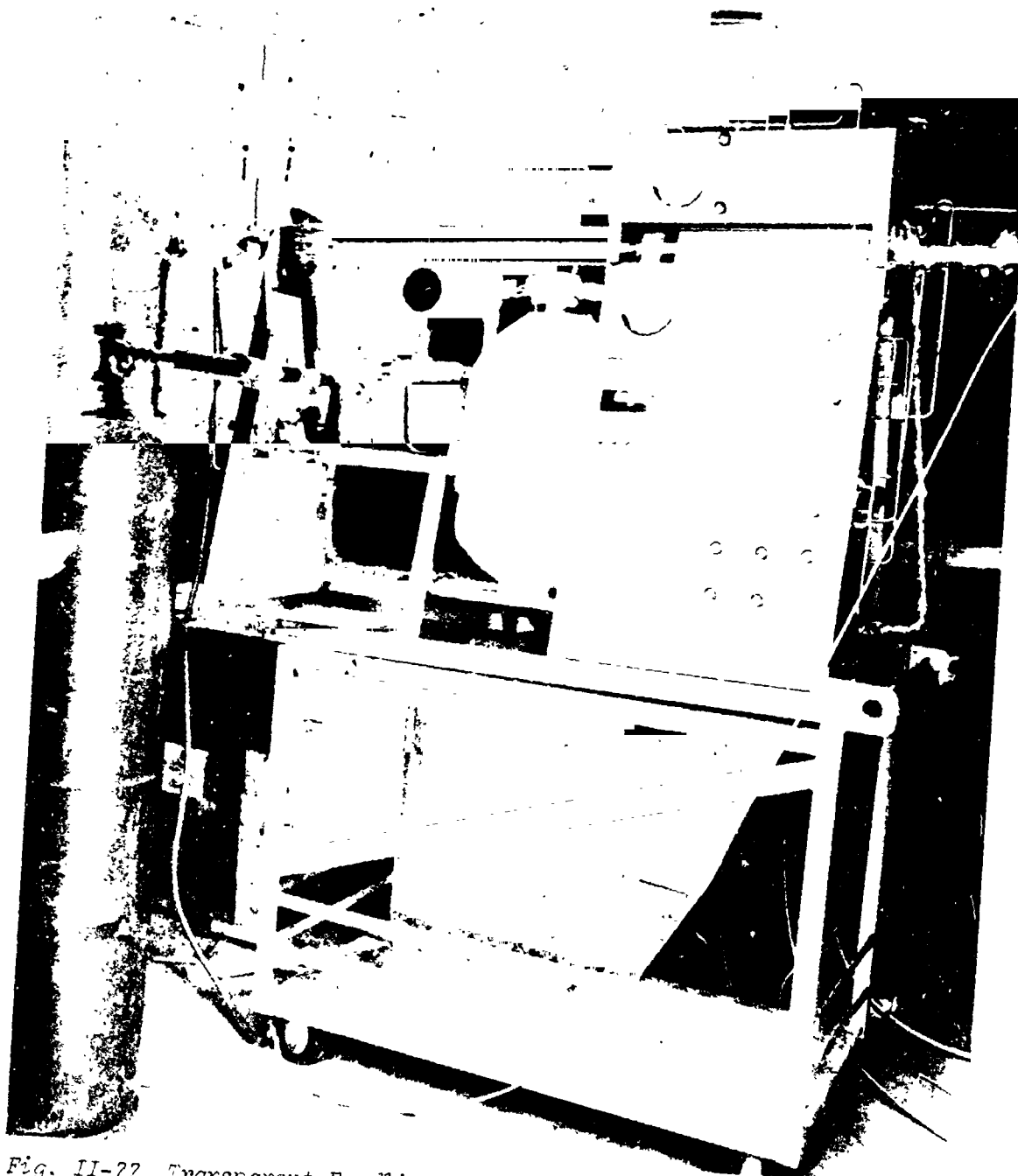
Fig. II-77 Transparent Feedline Test Apparatus, Venting Test
Configuration

II-128

Venting tests used Freon 114 at temperatures between 272 and 277.6°K (30 and 40°F). With downstream valves closed for a no-flow condition, the upstream valves remained open to maintain communication between the supply tank and feedline test section. This allowed continuous supply of liquid to the feedline core to replace the liquid vaporized at the screen surface. An external heat load was applied to the test section with a heat gun because ambient thermal loading was not sufficient to produce significant venting rates. However, even in the insulated configuration, the end effects produced gas in the liquid region as observed at the inlet sightglass. This heat leak was nullified by a cold GN_2 insulation purge at each end of the feedline test section.

Intermittent venting was accomplished by a pressure switch, solenoid vent valve, and appropriate hardware, which formed an automatic vent system. Vent flow rate was adjusted using a microvalve upstream of the solenoid vent valve. The pressure switch used resulted in vent bands of 2.54 cm (1 in.) of water. During venting, the liquid core was observed for presence of vapor, temperatures were noted, and the vent flow rate recorded periodically. This was repeated for varying heat loads resulting in vent rates of 0.057 to 0.142 m^3/hr (2 to 5 ft^3/hr).

c. Results - Dynamic flow tests successfully expelled gas-free liquid from the capillary feedline test article. Initial tests were plagued by O-ring leakage and gas was observed in the liquid core. Following system repair, successful results were obtained with pressure differentials of 17.8 to 25.4 cm (7 to 10 in.) of water across the screen liner. Horizontal gas-free liquid expulsions were obtained for the range of flow rates stated, while maintaining a positive pressure difference between the annulus and screen core that were less than the bubble point of the screen liner. These results were obtained with a vapor-filled outer annulus and indicate that pressure drops associated with the test flow rates were equal to or less than the corresponding ΔP across the screen liner [17.8 to 25.4 cm (7 to 10 in.) of water]. Temperatures varied little from the 293°K (68°F) liquid reading.

Quantative data for frictional flow losses in the screen liner were not obtained because of instrumentation problems. The differential pressure gages did not function properl. after liquid was forced into the mechanism. This was true of gage $\Delta PG3$ (Fig. II-75), which measured the pressure difference between the inlet and outlet of the feedline liquid core. Consequently, empirical correlation of fine mesh screen friction factors was not possible.

Successful venting was achieved while maintaining single-phase Freon 114 in the liquid core. The vent valve opened at a ΔP of 22.8 cm (9 in.) of water and closed at 20.3 cm (8 in.) of H_2O for a vent band of 2.54 cm (1 in.) of water. Although heat loads were not measured experimentally, venting rates corresponded to heat fluxes of 57.7 to 144.2 W/m^2 (18.3 to 45.8 $Btu/hr-ft^2$), which are considerably greater than values expected in a flight system. Temperature variations during venting were minimal and generally saturated at the test pressure. Both venting and flow tests were documented on 16-mm color film.

d. Conclusions - The 101.6-cm (40-in.) transparent feedline model successfully demonstrated the feasibility of the single liner concept. Erratic thermal loads and source pressures required continual control adjustments at times to minimize ΔP fluctuations and flow instability. However, an actual system would not be plagued by these problems and system operation could be stabilized over a wider range of operations than during testing.

The important point demonstrated by these tests was that a capillary feedline system can maintain a single-phase liquid core during venting and flow conditions. Detailed quantitative data necessary for designing an operational system are anticipated during cryogenic testing of the 3.8-cm (12-ft) feedline system. (See Chapter V.)

11. Structural Penetration Tests

a. Test Objectives - The need for verifying the bubble point integrity of mechanical penetrations through fine mesh screen was discussed in Volume II (Fabrication and Cleaning Techniques). The purpose of these tests was to determine the effect of the selected penetrations on the bubble point capability of a screen/perforated plate barrier. In addition, the effects of thermal cycling were evaluated using the same criterion. In order to effect the most stringent test, a stainless steel 325x2300 mesh screen was used. Two penetration sizes were investigated, 0.64-cm (1/4-in.) tubing and 7.62-cm (3-in.) pipe.

b. Test Apparatus and Procedure - Three types of penetrations were fabricated for testing: (1) the pressed type, in which the parts were forced together with a hydraulic press, (2) the screwed type, which is torqued together, and (3) the riveted type. Figures II-54 and II-55 in Volume II showed details of the mechanical penetrations tested. The perforated plate, screen, and copper gasket were compressed between two flanges that were welded to the 0.64-cm (1/4-in.) tubing or 7.6-cm (3-in.) pipe.

A 0.64-cm (1/4-in.) model was designed for each of the three penetrations tested. This represented the smallest size that could be conveniently fabricated and tested. The 7.6-cm (3-in.) model was chosen as the largest size that might have practical application. It was concluded that a 3-in. screwed type penetration would not be practical due to weight considerations and because it becomes increasingly difficult to develop sufficient torque to properly seat the gasket for these large fittings. A 7.6-cm (3-in.) riveted model was not designed because it is believed that the riveted joint, if proved practical, could be readily scaled up from 0.64-cm (1/4-in.) to 7.6-cm (3-in.). Consequently, only a pressed configuration was tested for the larger fitting.

The 0.64-cm (1/4-in.) penetrations were mounted on screen/perforated plate discs, which were 6.04 cm (2.375 in.) in diameter. Similar discs, 17.62 cm (6.838 in.) in diameter, were used for the 7.6-cm (3-in.) test article. The test article is shown in Fig. II-78. Two 0.64-cm specimens were tested for each mechanical penetration configuration. Riveted, screw type, and pressed penetrations are shown from left to right, respectively. Also pictured is the single 0.95-cm (3/8-in.) aluminum tube and gasket specimen that was tested. This was a screw type penetration that was tested for comparison purposes using 200x1400 mesh aluminum screen.

Fig. II-78 Structural Penetrations Tested

The test specimens were bubble pointed in appropriate fixtures using the low pressure test apparatus (LPTA) described in Subsection 10. A typical bubble point test setup is shown schematically in Fig. II-79. The test configuration is pictured in Fig. II-80. The LPTA is shown with the 0.95-cm aluminum and 7.6-cm stainless steel test specimens mounted in their respective bubble point fixtures.

Fabrication of the test articles involved applying sufficient pressure to assure seating of the gasket. Pressed fit configurations used a force of 22,200 to 26,700 N (5000 to 6000 lbf) for the smaller penetration and 267,000 to 356,000 N (60,000 to 80,000 lbf) for the 7.6-cm (3-in.) specimen, more than the force required to move the ring. For all screw type penetrations a torque of at least 135.6 J (100 ft-lb) was used.

Each penetration assembly was bubble pointed at each step of the fabrication process. Following complete fabrication, each test specimen was subjected to thermal cycling in liquid nitrogen and liquid hydrogen and the assembly was bubble point checked at the end of the warmup period. Bubble pointing was accomplished by covering the screen with methanol and pressurizing below the screen assembly using the LPTA. The liquid height was sufficient to cover the entire penetration assembly.

c. *Results* - Test results are summarized in Table II-8. Bubble points for all test specimens are presented at different stages of assembly and after thermal cycling. Although a reduction in pressure retention capability was noticed during some LH_2 thermal cycling tests, the data generally showed that penetrations may be made without affecting the pressure retention capability of the system. In only one instance did insertion of the penetration assembly decrease the bubble point of the screen/perforated plate laminate. The data seem to indicate that the problem lies in seating the metal gasket inserted between the screen and penetration assembly flange, although no patterns are evident. No differences in results are noted for the aluminum and stainless steel assemblies.

d. *Conclusions* - Test results show that mechanical penetrations through screen and perforated plate laminates may be fabricated without significant degradation in the pressure retention capability. All systems tested remain candidates for this application. No differences were noted for stainless steel and aluminum configurations. The choice of one penetration type over another should be based on fabrication considerations and requirements for the particular application.

II-132
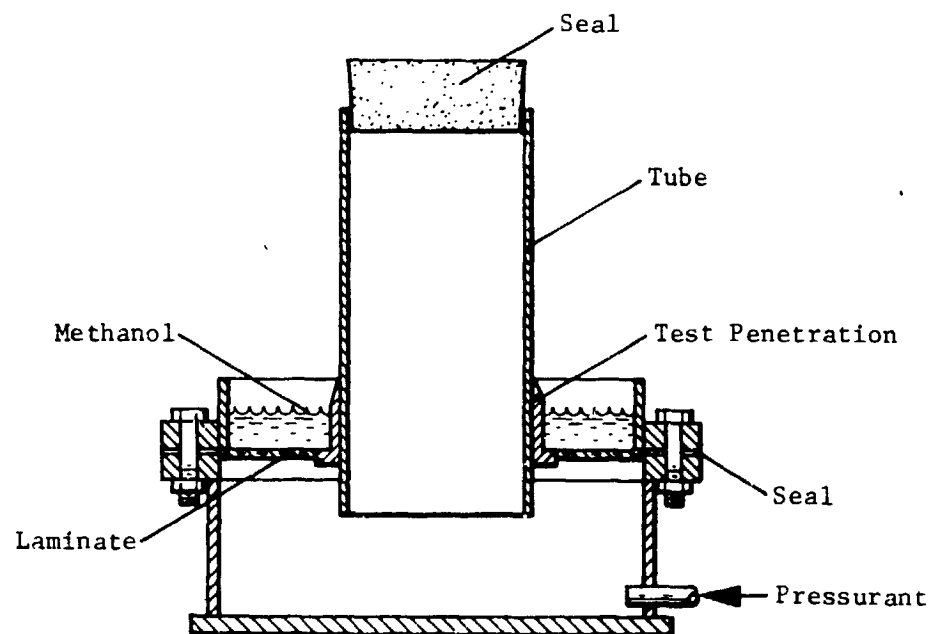
Fig. II-79   Typical Bubble Point Test Setup
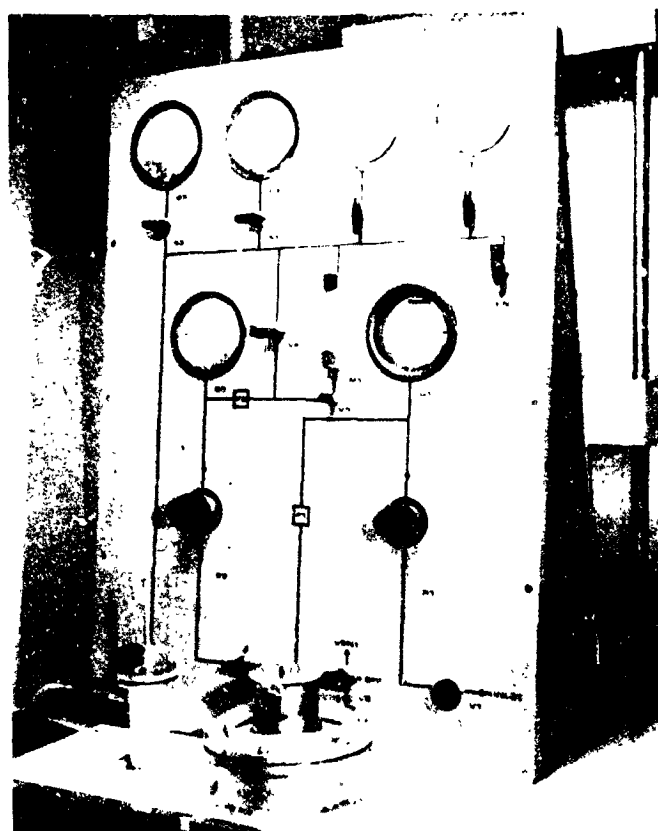
Fig. II-80   Bubble Point Apparatus for
Structural Penetration Test

Table II-8 Structural Penetration Test Results

	Pressed			Riveted		Screw Type		
	0.64-cm (1/4-in.) Stainless Steel		7.6-cm (3-in.) Stainless Steel	0.64-cm (1/4-in.) Stainless Steel		0.64-cm (1/4-in.) Stainless Steel		0.95-cm (3/8-in.) Aluminum
Operation	A	B		A	B	A	B	
Screen	65.5 (25.8)	62.5 (24.6)	62.7 (24.7)	63.5 (25.0)	63.5 (25.0)	66.5 (26.2)	64.3 (25.3)	41.9 (16.5)
Assembly	65.5 (25.8)	62.5 (24.6)	62.7 (24.7)	50.8 (20.0)	63.5 (25.0)	66.0 (26.0)	64.3 (25.3)	41.9 (16.5)
Tube Installed	65.5 (25.8)	63 (24.8)	62.7 (24.7)	50.8 (20.0)	63.5 (25.0)	66.0 (26.0)	64.0 (25.2)	42.9 (16.9)
LN$_2$ Soak	65 (25.6)	62.7 (24.7)	62.7 (24.7)	48.7 (19.2)	66 (26.0)	66.5 (26.2)	64.3 (25.3)	42.6 (16.8)
LH$_2$ Soak	58.4 (23.0)	62.2 (24.5)	50.8 (20.0)	48.2 (19.0)	63.5 (25.0)	66.0 (26.0)	61.5 (24.2)	39.9 (15.7)

Penetration Bubble Point, cm (in.) of H$_2$O

12. Vibration Test

a. *Test Objectives* - Design of capillary retention devices re-
quires accurate knowledge of pressure retention capability
under all conditions that will be imposed on the system. The
effect of a flight vibrational environment on the performance of
a capillary propellant management system is of major concern.
Although recent work indicated a lowering of pressure retention
capability (Reference 1I-8), sufficient work in the area of vi-
brational effects on fine mesh screen was not available.

The purpose of the vibration test was to provide a qualitative
demonstration of vibrational effects on the performance of a screen
retention device. Both sinusoidal and random vibration effects
were evaluated for the frequency ranges and acceleration levels
that represented worst-case flight environment. Oscillation in
the horizontal and vertical axis were investigated while monitoring
methanol expulsions for premature gas ingestion. Expulsion as
well as non-expulsion tests were planned to characterize vibrational
effects and related phenomena.

b. *Test Apparatus and Procedure* - The test device was the TEDD
Model that had been successfully tested during KC-135 aircraft
tests (refer to Fig. II-8). This cylindrical transparent DSL de-
vice allowed visual monitoring of methanol expulsions for prema-
ture screen breakdown during periods of induced oscillation. The
model, mounted in the minus 1-g outflow configuration, was vi-
brated both vertically and horizontally.

Additional test equipment included a pump and methanol reservoir
for filling and draining the test model. A schematic of the test
system is shown in Fig. II-81. Instrumentation included a manometer
to determine system outflow pressure and monitor screen liner ΔP
during vibration tests. Accelerometers were located on the model
to monitor the vibrational environment of the device and deter-
mine the acceleration amplification.

Figure II-82 shows two photographs of the test article mounted on
the shaker platform in the vertical test configuration. Two views
of the regulator and pressure gage used to decrease the GN_2 supply
pressure to a safe level for pressurizing the test article are
shown. The vertical manometer measured absolute system pressure
or screen ΔP by adjusting valves located at the top of the model.
The micrometer valve was used for final regulation of pressurant
to obtain the desired outflow rate. A toggle valve provided con-
stant pressurization rates and, consequently, constant outflow
times during each test.

II-135
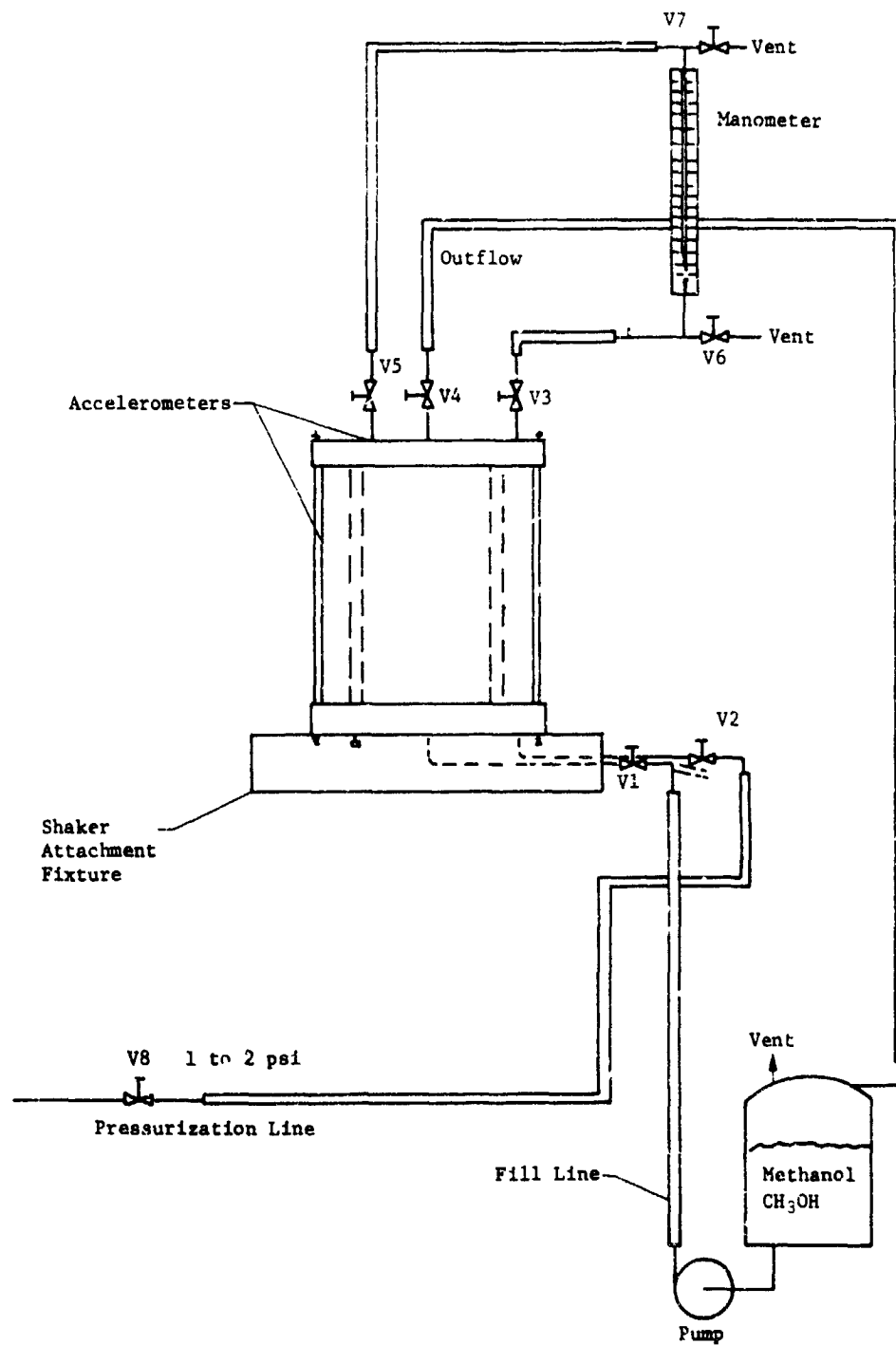
Fig. II-81   TEDD Model Vibration Test Schematic

(a) Front View
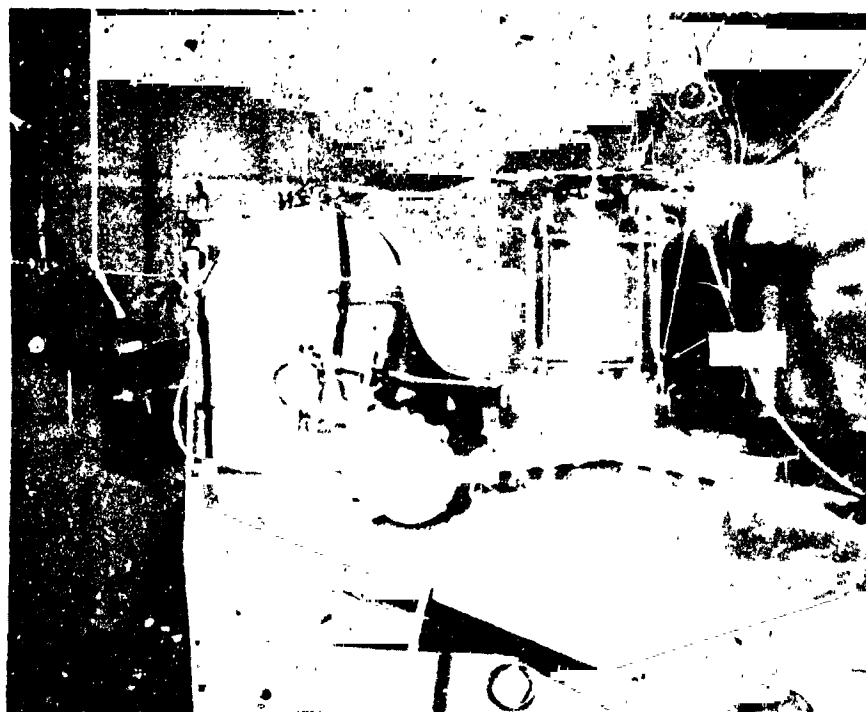
(b) Rear View

Fig. 11-82 Vibration Test Apparatus - Vertical Axis

Figure II-83 shows all components of the system mounted in the
horizontal test configuration. The liquid in the outer annulus
was generally expelled before the frequency sweep was started.
Note the two accelerometers located on the slide plate which
recorded the shaker input acceleration. In the vertical test con-
figuration these transducers were located on the shaker attach-
ment fixture (Fig. II-82(b).

Fig. II-83   Vibration Test Apparatus - Horizontal Axis

Both sinusoidal and random vibrations were evaluated. Although
random vibration is more representative of the actual flight
environment, sinusoidal vibrations are more severe from the stand-
point of inducing resonance. This may be significant because a
predominant frequency may exist at various vehicle locations.
Also, harmonic motion (sinusoidal vibration) is more easily analyzed
than the more complicated random inputs.

Sinusoidal vibrations encompassed the frequency range, 5 to 2000 Hz,
for the acceleration levels of 0.5, 1.0, 1.5, 2.0, and 3.0 g. This
range of energy input should exceed that expected in an on-orbit

II-138

environment. During testing, the shaker displacement was
limited to 1.02 cm (0.4 in.) because of safety requirements.

Random vibration input included a range of accelerations, 2.0 to
6.0 g rms, within the spectrum shown in Fig. II-84. Thus curve
was obtain from Ref II-4. The vibration environment represented
by this curve (22 g rms) is more severe than the levels anticipated
for an on-orbit system such as Space Tug or Shuttle OMS. Expulsion
tests during random vibration were run in both the vertical and
horizontal axes.
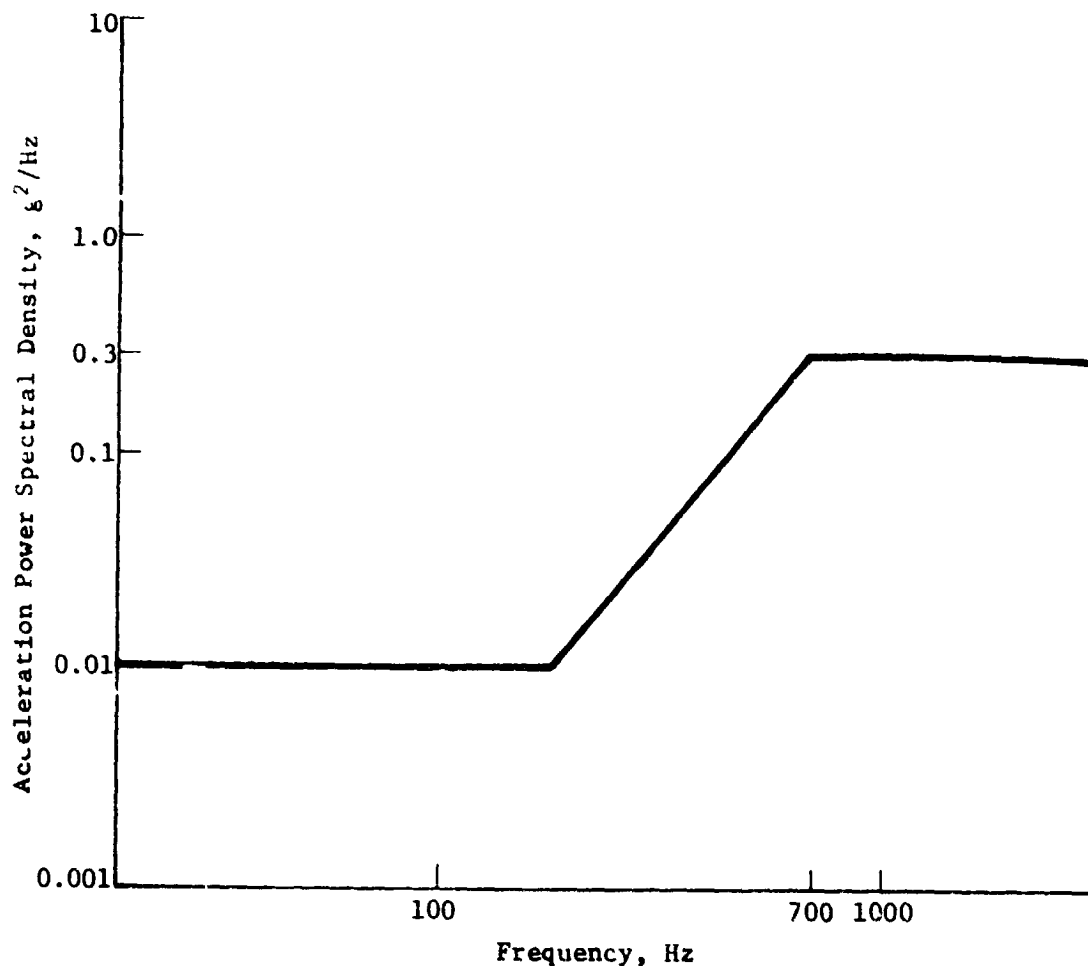
Fig. II-84   Random Vibration Power Spectrum

Both outflow and nonoutflow tests were conducted. The purpose of the nonoutflow tests was to simplify the analysis of the results. Expulsions increased the complexity of the test due to the variance of the screen pressure differential during outflow. Nonoutflow tests were run with the bulk region full of liquid.

The test procedure was varied for different types of tests. Nonoutflow tests and random vibrations were essentially independent of time, which simplified the test procedure. Sinusoidal expulsion tests were time-dependent and required a more involved procedure to meet the required objectives.

Random vibrations were not used during the nonoutflow tests. The general procedure required the TEDD model to be filled with methanol using the test hardware shown in Figs. II-82 and II-83. The model was filled and expelled so that the vapor annulus was void of liquid and the bulk region was completely filled before starting the vibration. The TEDD was pressurized to obtain the desired screen ΔP. Subsequently, all valves were closed to obtain the required vapor annulus/bulk region pressure differential on the manometer. At this point, the system was sinusoidally vibrated (horizontal position only) through the stated frequency range at constant acceleration levels. The sweep time was approximately 2 minutes. During test the liquid outflow region was visually monitored for gas ingestion and the frequencies noted where breakdown occurred.

Expulsion tests were run in a similar manner with some variations caused by the imposed time dependency. The micrometer valve was adjusted to obtain bulk region outflow times of about 2-1/4 minutes [corresponding to a pressure of 0.91 N/cm^2 (1.3 psig)] before starting the test. This expulsion time was maintained throughout testing and allowed the 2-minute vibration (sinusoidal) frequency sweep to be completed before terminal breakdown of the capillary system.

Preparation for the expulsions tests involved filling TEDD as before, leaving a small level of liquid in the vapor annulus. With the manometer monitoring the pressure differential, outflow was initiated. When the vapor annulus was emptied of liquid and expulsion from the bulk region had started, harmonic vibration was initiated at a constant g-level (0.5 g). During the test period, the outflow region was monitored for gas ingestion, breakdown frequencies, and screen ΔP. This was repeated for accelerations of 1.0, 1.5, 2.0, and 3.0 g for the vertical and horizontal test configurations.

II-140

Random vibration tests were run in a similar manner. The ... of Fig. II-84 was used for acceleration levels of 2.6, 3.5, 3.5, 5.0, 6.0, and 8.0 g rms in the vertical and horizontal axes.

Several horizontal expulsion tests were documented on 16 mm ... film.

Bo Criteria - The effect of a vibrational environment on the pressure retention capability of a screen device is assumed to be twofold if effects on physical interfacial properties such as surface tension, adhesion, and cohesion are considered negligible. First, the variation in buoyant force with acceleration may affect the stability of the liquid-gas interface (Bond number criteria). Second, the alteration of the pressure field by the acceleration head, ρ_{gh}, may exceed the screen bubble point and cause failure of the capillary barrier. Either or both of these phenomena may cause the liquid/vapor interface in fine mesh screen to fail because of the varying accelerations of a vibrational environment.

The effect of the first phenomenon may be determined by applying the Bond number criteria. The Bond number for a totally wetting liquid is defined as:

$$Bo = \frac{\rho a r}{\sigma}$$ [II-11]

where ρ = liquid density

   a = acceleration

   r = hole (pore) radius

   σ = liquid surface tension.

Previous contract work (Ref II-9) determined critical Bond numbers of 0.84 for perforated plate and 0.45 for square-weave screen. Bond numbers larger than the critical value indicate an unstable condition, while smaller numbers assure a stable interface. For a 325x2300 Dutch-twill screen in liquid methanol, an acceleration of 10 g results in a Bond number of 1.68×10^{-4}. This indicates that for the test configuration the Bond number is not an important stability criterion, and the acceleration head (ρ_{gh}) will be the dominant factor affecting screen bubble point. This is indicated by test results of Ref. II-8.

Figure II-85 shows amplification of the input acceleration at the different accelerometer locations and g levels. Note that increased loading over input is shown for sinusoidal vibrations while very little variation in the input vibration levels was noted during random testing. Amplification factors range from 4.7 to 11.3 with an average value of 6.5. The data indicate that amplification increases with vertical distance toward the top of TEDD. Consequently, accelerations much higher than input may be acting on the screen and liquid during sinusoidal tests.

Test results are discussed below according to the type of vibration input.

1) *Sinusoidal Vibration Tests* - Both nonexpulsion and expulsion tests were run using harmonic vibration inputs. Figures II-86 and II-87 show system response to sinusoidal vibrations in the vertical and horizontal axes independent of liquid expulsion. Gas ingestion into the liquid outflow is denoted by broken lines and is shown as a function of frequency at various input acceleration levels. The important points shown by these data are: (1) breakdown during sinusoidal testing was frequency dependent and (2) breakdown frequency bands corresponded to resonance periods as indicated by the accelerometers located on the test model. These resonance bands are also shown in the plots.

During the 2-minute tests, the duration of breakdown was only approximately 15 sec and did not continue throughout the tests as indicated by other work (Ref II-8). A stable gas/liquid interface was reestablished with gas-free liquid outflow within a frequency band of several hundred Hertz. Subsequent static tests also indicated that the observed vapor ingestion was caused by breakdown of the liquid/vapor interface and not by a structural failure of the model. Frequency scans in both directions, 5 to 2000 Hz and 2000 to 5 Hz, for the 3 g case in Fig. II-86 indicate essentially the same breakdown frequencies with some hysteresis effects. Every interval indicating gas ingestion corresponded to a resonant period with one exception. The resonances during the latter part of tests (1200-Hz vertical axis and 1800-Hz horizontal axis) had little effect on capillary performance. This is attributed to the very small amplitudes at these frequencies. Data correlation for nonexpulsion and expulsion tests are presented below.

II-142
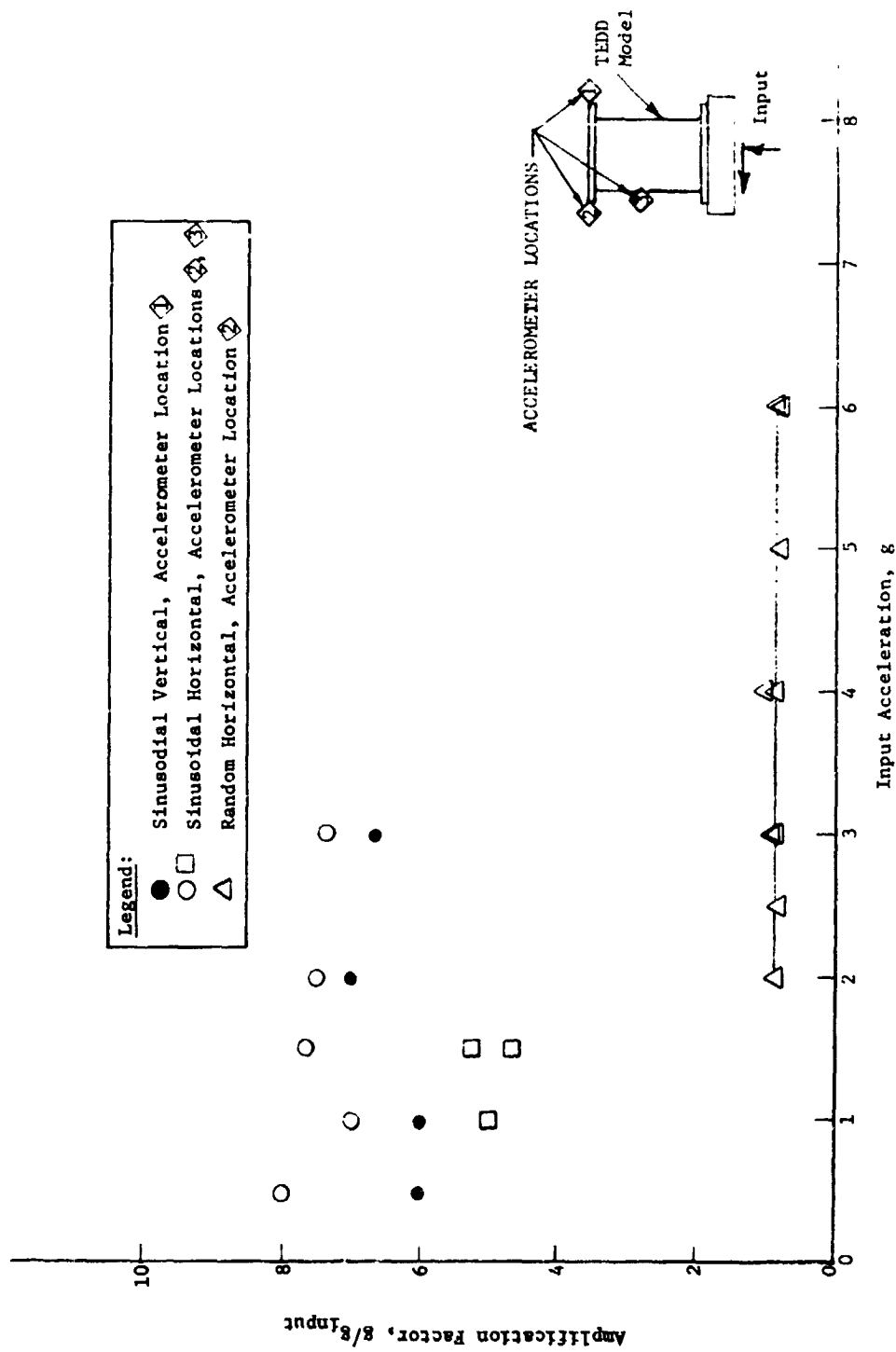
Fig. II-85 Maximum Amplification of Input Acceleration at Various Accelerometer Locations
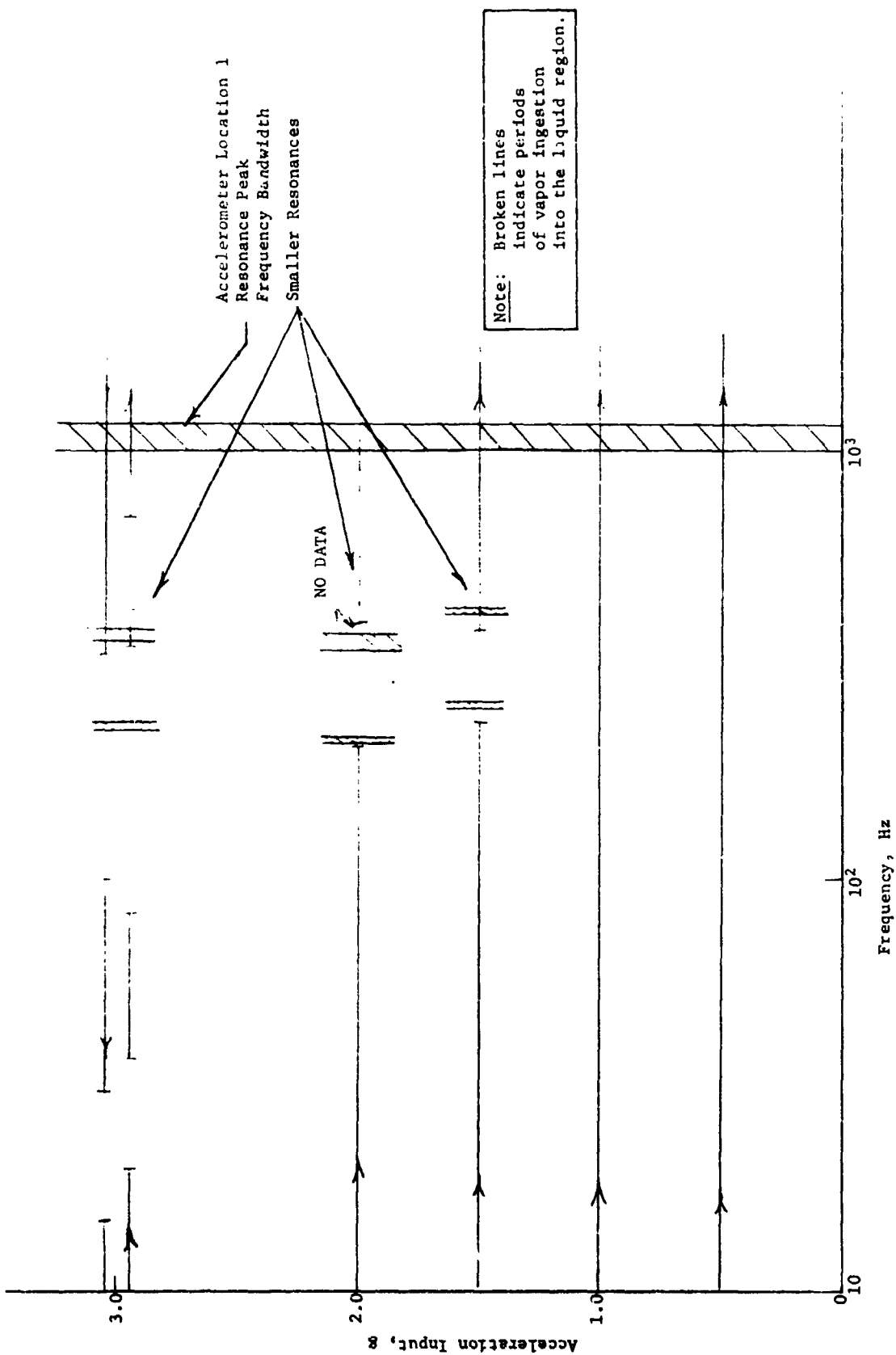
Fig. 1-86 *Gas Ingestion Frequency Dependence, Vertical Sinusoidal Vibration*
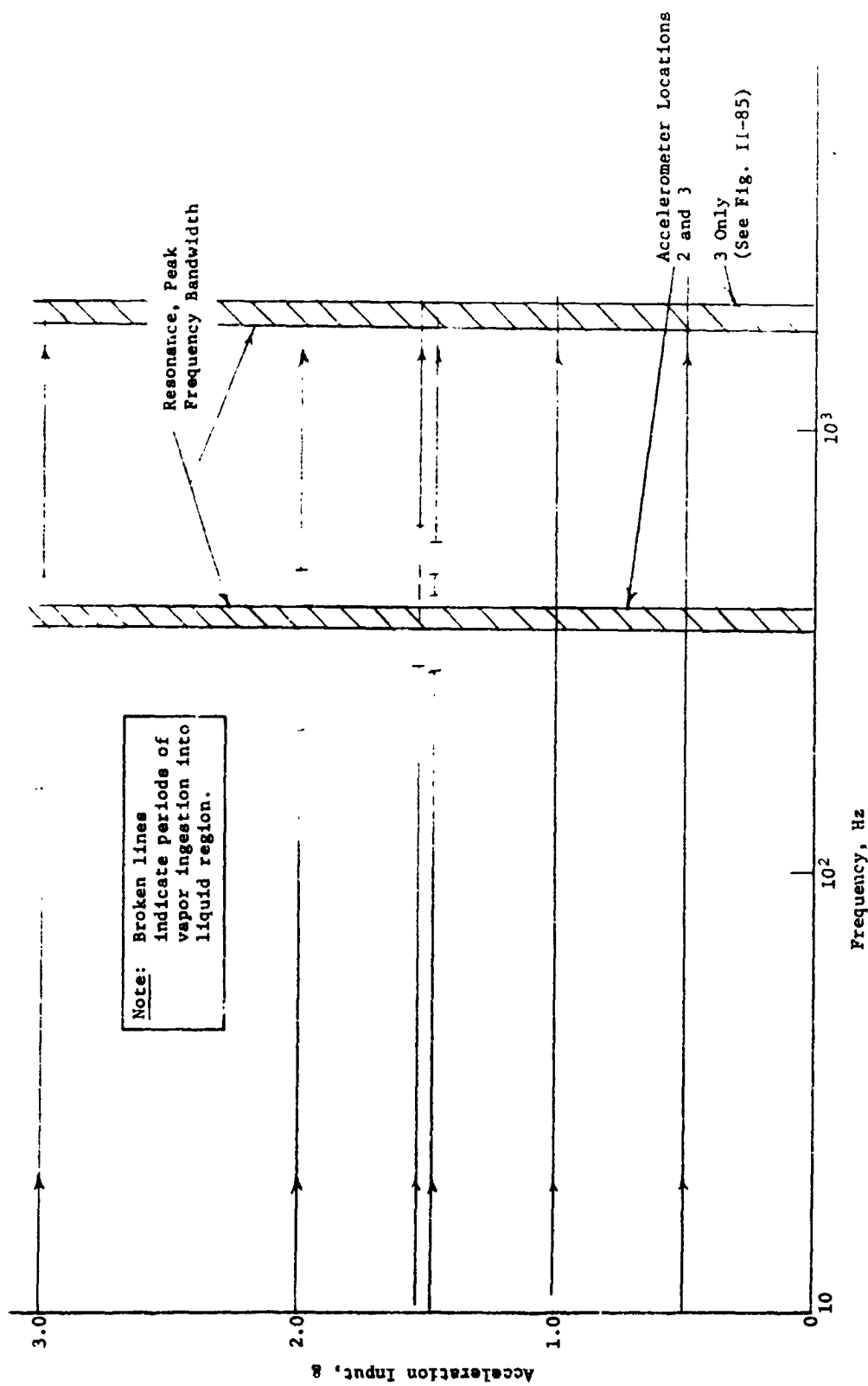
Fig. II-87 Gas Ingestion Frequency Dependence, Horizontal Sinusoidal Vibration

a. Nonexpulsion Tests - Figure II-88 shows the results of the nonexpulsion tests. Data are shown for sinusoidal vibration of the model in the horizontal axis with the bulk region full of liquid and the vapor annulus depleted. The graph shows acceleration as a function of vapor annulus-bulk region pressure differential (ΔP). Experimental data for 1.0, 1.5, 2.0 and 3.0 g at various ΔP's are plotted. Two acceleration levels are shown for each set of data. The lower value indicates input and the higher value was recorded by instrumentation during periods of screen failure. Curves showing the theoretical g required to force liquid into the vapor annulus and ingest gas into the liquid annulus, based on a hydrostatic head correlation, are also shown.

Points 1 and 2 on Fig. II-89 represent the most likely places for gas ingestion and liquid dropout, respectively, due to the 1 g gravitational field. For the liquid annulus, interface stability and hydrostatic stability are described by Eq [II-12] and [II-13], respectively.

$$BP \geq \Delta P + \rho gh_2 \qquad\qquad\qquad [II-12]$$

$$\Delta P \geq \rho g_0 h_1 + \rho gh_2 \qquad\qquad\qquad [II-13]$$

where

BP = screen liner bubble point,

$\Delta P = P_v - P_b$

ρ = liquid density,

P_v = vapor annulus pressure,

P_b = bulk region ullage pressure,

g_0 = gravitational acceleration,

g = induced sinusoidal vibration.

Equation [II-12] must be satisfied to prevent gas from entering the outflow region of the system. Equation [II-13] applies when liquid dropout is of interest. Considering only the equality signs, these equations were solved for acceleration level, g, as a function of ΔP and plotted in Fig. II-88.

II-146
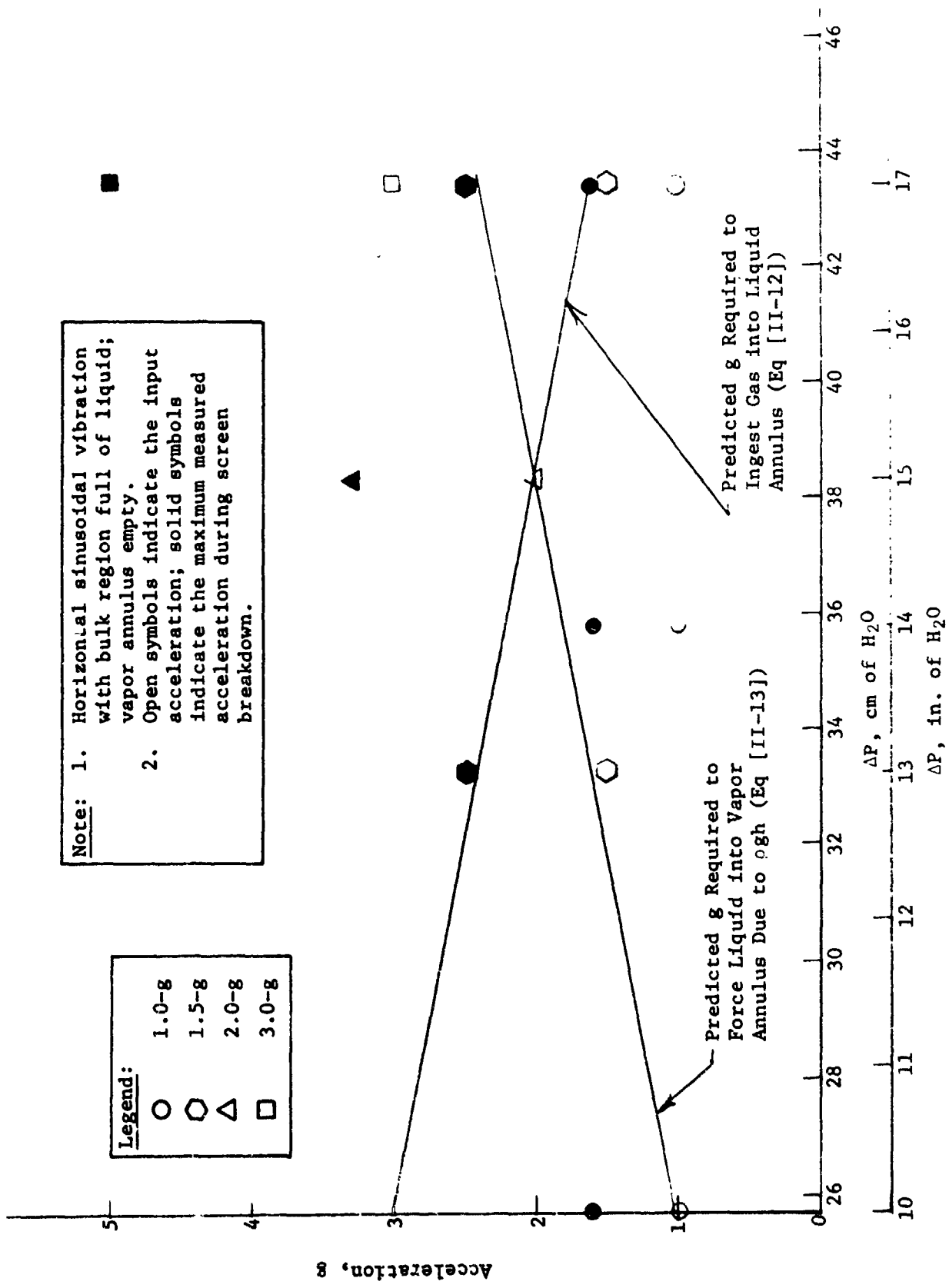
Fig. II-88 TEDD Model Nonoutflow Vibration Test (See Note 1)
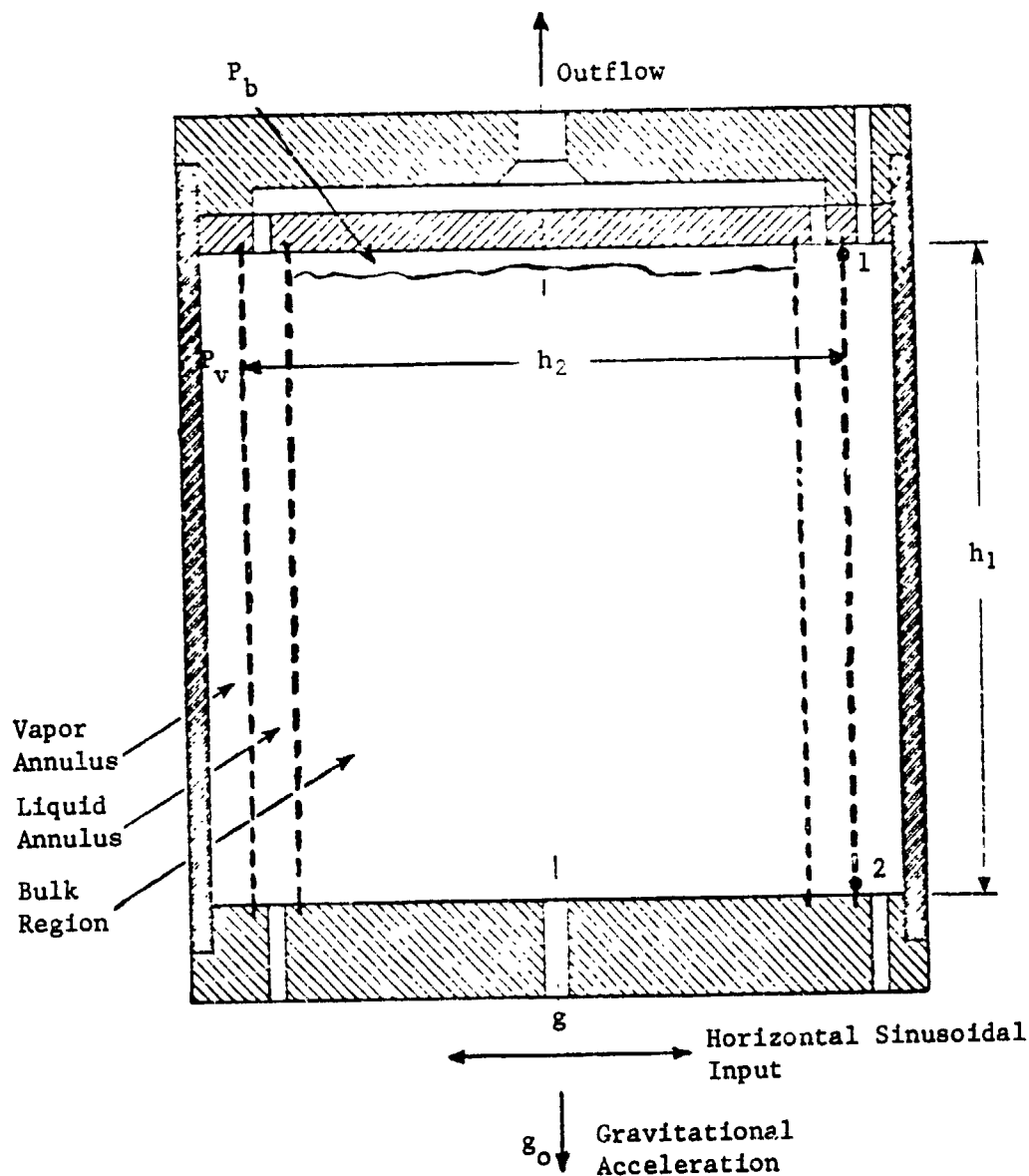
Fig. II-89 TEDD Model Schematic

Experimental data correlated well with theoretical predictions.
For liquid dropout, only the 2.0- and 3.0-g tests forced enough
liquid into the vapor annulus to be visually discernible. This
agrees well with the predicted values since data are well above
the curve of Eq [II-13]. Other data points are noted above the
curve indicating that some liquid should have been forced into
the vapor annulus. These data points are considered to be on the
verge of breakdown because there was no visible liquid in the outer
annulus.

Equation [II-12] describes the vapor ingestion into the liquid annulus. The initial pressure differential plus the induced hydrostatic head must not exceed the bubble point of the liquid annulus screen liner. Referring to Fig. II-88, five of the seven data points are above the predicted curve, indicating that gas ingestion should have occurred. This correlation is valid since gas ingestion was recorded in these cases. The 1.0-g [ΔP = 25.4 cm (10 in.) H_2O] data point also is consistent with the hydrostatic analysis because breakdown was not noticed during this test. However, the remaining 1.0-g data point [ΔP of 35.6 cm (14 in.) H_2O] is inconsistent with the predicted results because a small amount of vapor was noticed in the liquid region during the test. Since the test data point is well below either curve, neither liquid dropout nor breakdown should have occurred. Therefore, this particular data point could be in error. The small breakdown observed could have been caused by small bubbles initially trapped in the liquid annulus and released by the oscillatory motion without screen failure. Therefore, this series of tests indicates that the vibrational effect on capillary systems is hydrostatic in nature.

b) Expulsion Test Results - Expulsion tests under sinusoidal vibration were somewhat more complex and difficult to analyze. The variance during outflow of pressure differential and liquid height in the bulk region complicated the hydrostatic analysis. Pressure differential is plotted as a function of outflow time (Fig. II-90) for static and vibrated outflows. The decrease in ΔP during static outflow could be attributed to partial dryout of the communication screen. The results show that the pressure differentials decrease as acceleration levels are increased, which is consistent with increase in hydrostatic head. The curve shown for liquid height in the bulk region was extrapolated between the beginning and end of outflow. Actual liquid height may vary slightly during outflow. Since hydrostatic analysis depends on these variables, correlation of outflow results is somewhat restricted.

Sinusoidal expulsion test results are shown in Figs. II-91 and II-92 for the vertical and horizontal directions. Figure II-91 shows accelerometer readouts for 1.5-, 2.0-, and 3.0-g tests. Periods of vapor ingestion are noted for each test. The two analytical curves show the predicted g-level for gas ingestion at the top and bottom of the liner as a function of expulsion time. A good correlation was obtained between the predicted and measured periods of breakdown. This is illustrated in Fig. II-91 because the areas where measured values of acceleration level are
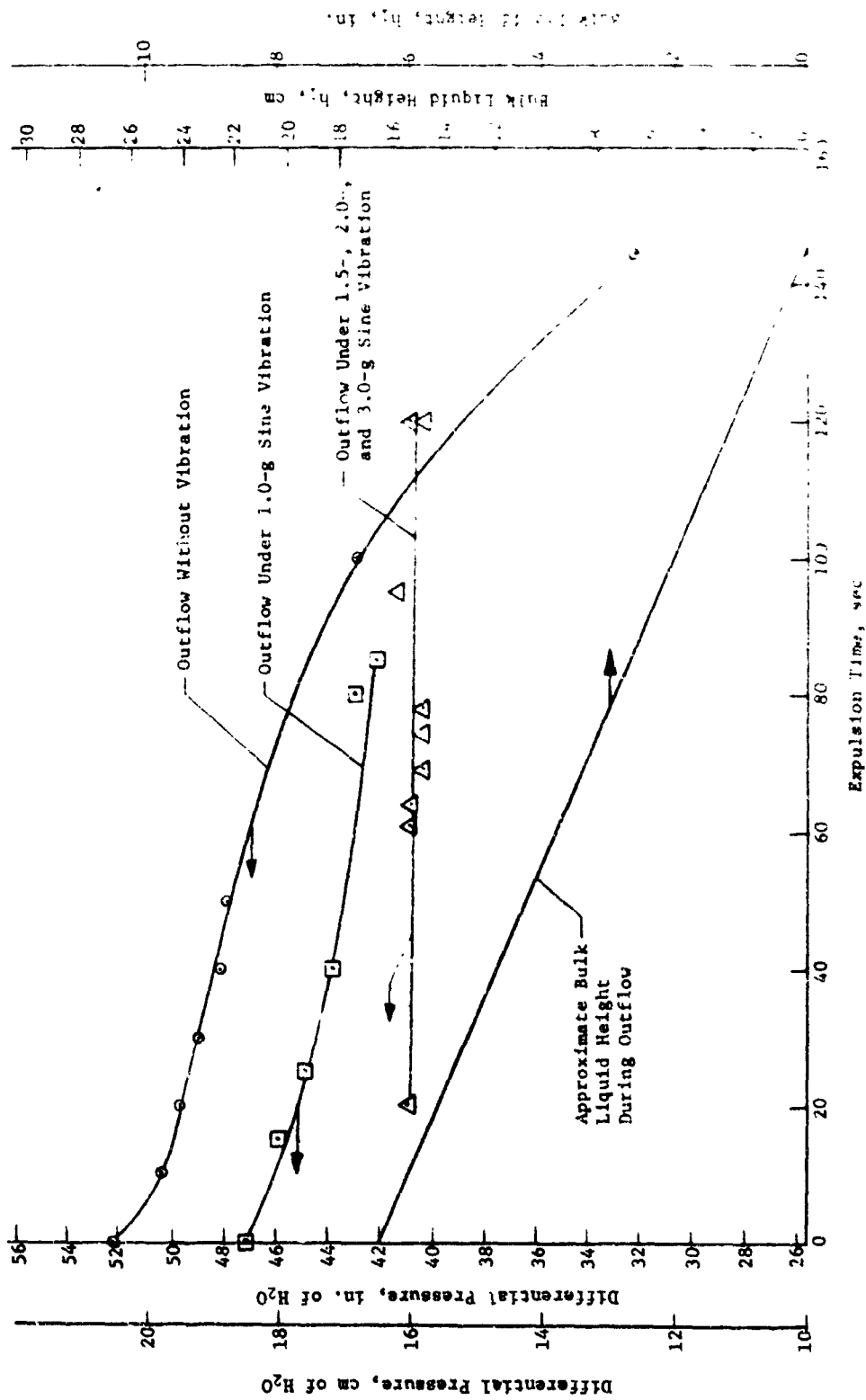
Fig. II-90 Differential Pressure and Bulk Height Liquid Height as a function of Expulsion Time.
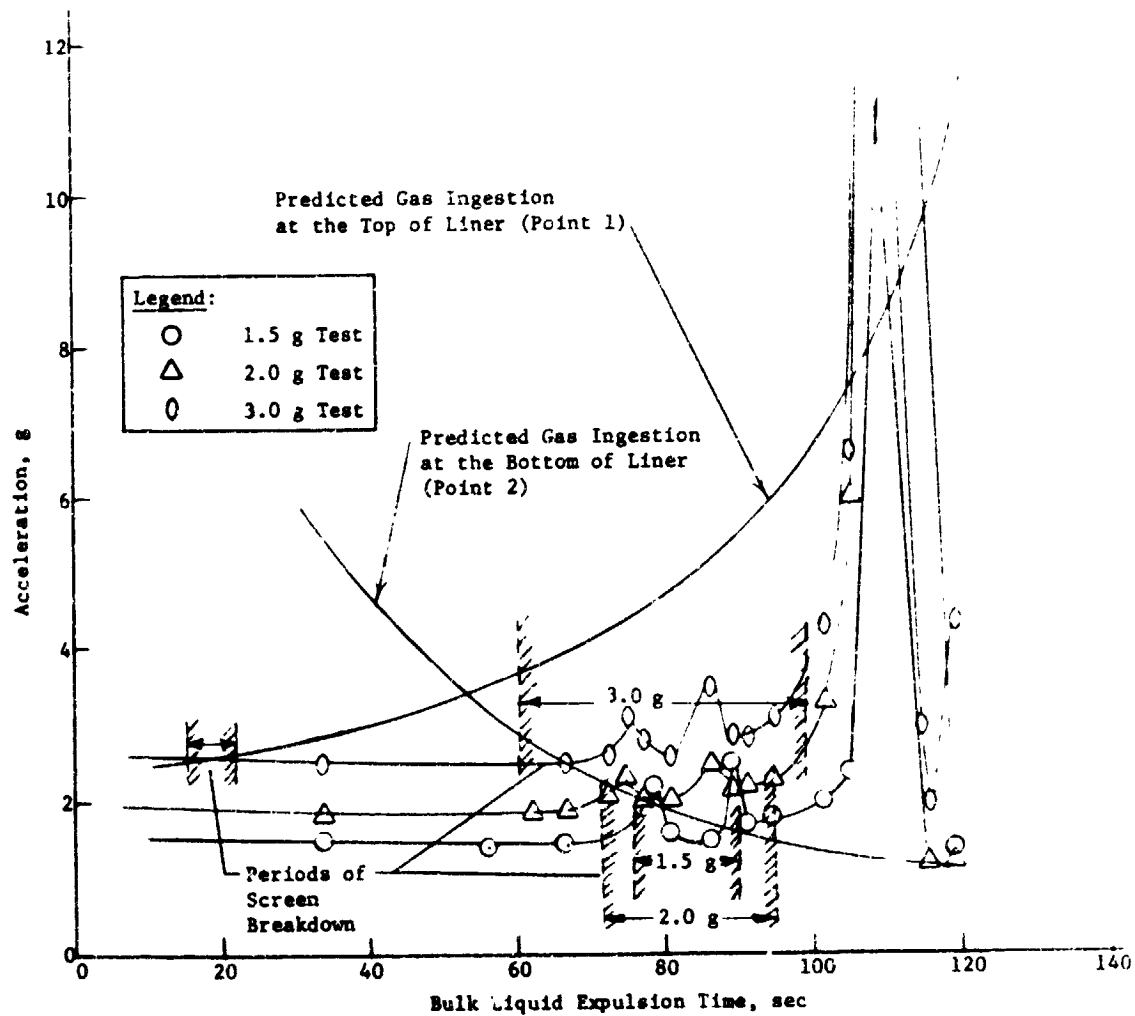
Fig. II-91 Outflow Test Data Correlation - Vertical Sinusoidal Vibration
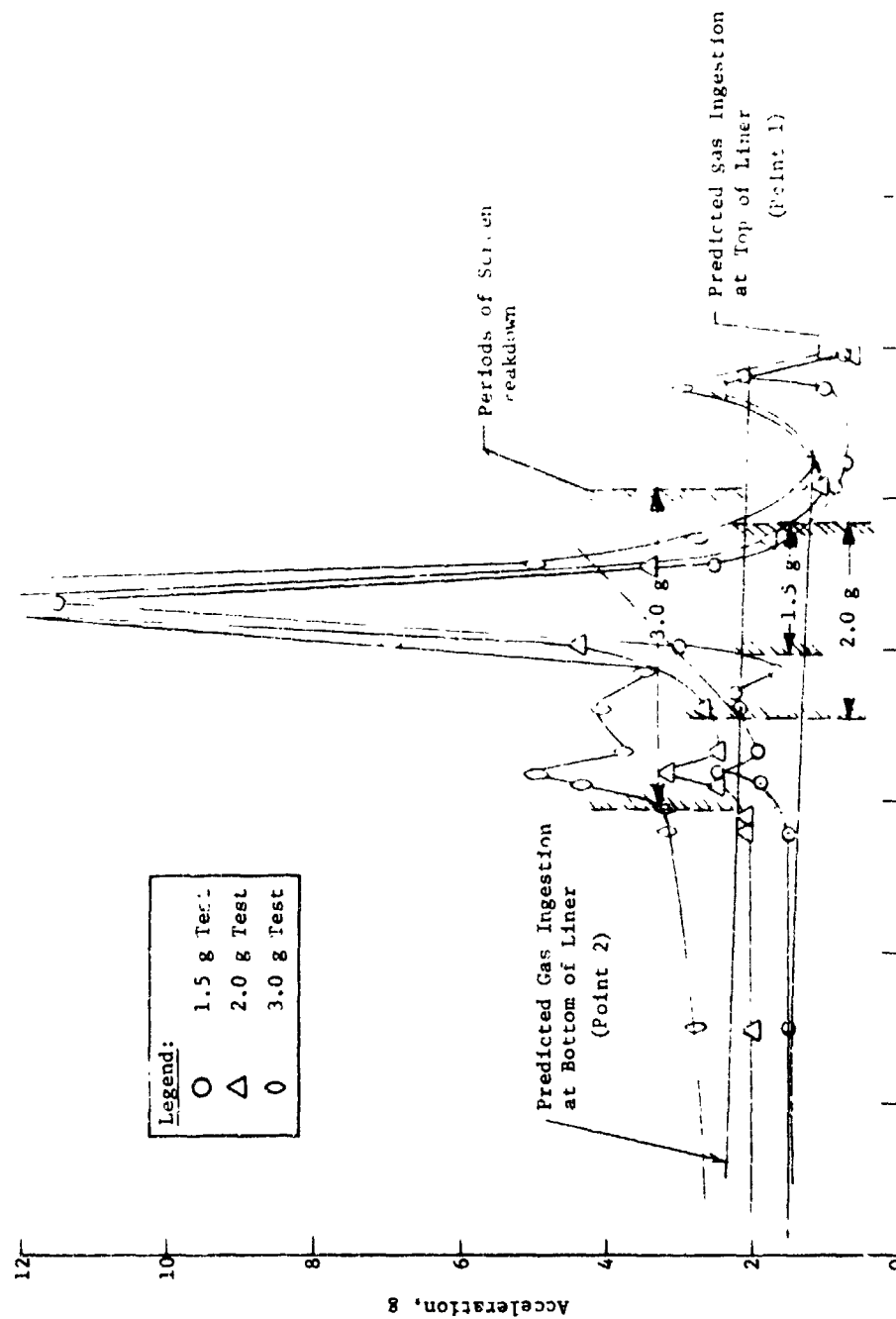
Fig. II-52 Outflow Test Data Correlation, Horizontal Sinusoidal Vibration

above the predicted curves also correspond to the recorded periods of screen breakdown. Although the measured accelerations far exceeded the values predicted to obtain breakdown during the test period, 100 to 120 sec, the system performed satisfactorily. Two explanations for this are: (1) the experimental accelerations shown may be somewhat different at the screen liquid interface than indicated at the accelerometer locations; (2) the hydrostatic effect of the induced oscillatory motion may be amplitude- and time-dependent, decreasing with both parameters so that no effect is noted at higher frequencies. Figure II-92 shows that horizontal vibration data are somewhat more erratic. Good correlation is shown at the end of breakdown and for the values predicted at the bottom of the screen liner. However, the curve that should dominate because of the lower g levels predicted (curve based on gas ingestion at top of model) indicated screen breakdown throughout all three tests until approximately 100 sec into the expulsion, which did not occur. This could be explained by a variance in ΔP and liquid height from the values used to calculate the curves.

2) *Random Vibration Tests* - Analysis of random test data is simpler since acceleration and frequency are not time-dependent. The random accelerations plotted in Figs II-93 and II-94 are 2.5 g rms inputs. This was the first acceleration at which breakdown was noticed in both the vertical and horizontal axes.

In addition to the input random acceleration and measured acceleration, Fig. II-93 shows the two predicted accelerations that would produce breakdown at the top and bottom of the screen liner. At the initial point, the predicted and the input random values are equal with the measured value slightly lower. This implies that the screens are on the threshold of breakdown. Since breakdown was observed during the test, the correlation between the predicted and experimental results was substantiated. If peak accelerations are considered rather than rms values, more than adequate acceleration was present to produce the observed breakdown. The 2.0 g rms test resulted in an accelerometer reading of 1.7 g rms (2.4 g peak, based on a sine curve), which is a marginal acceleration value for vapor ingestion as indicated by the predicted curves. No screen breakdown was noticed during this test.

Figure II-94 shows that a random acceleration of 2.5 g rms input is sufficient to cause breakdown. An input of 2.0 g rms (1.7 rms accelerometer reading) also appears to be sufficient for vapor ingestion. Both of these cases were verified by the observed
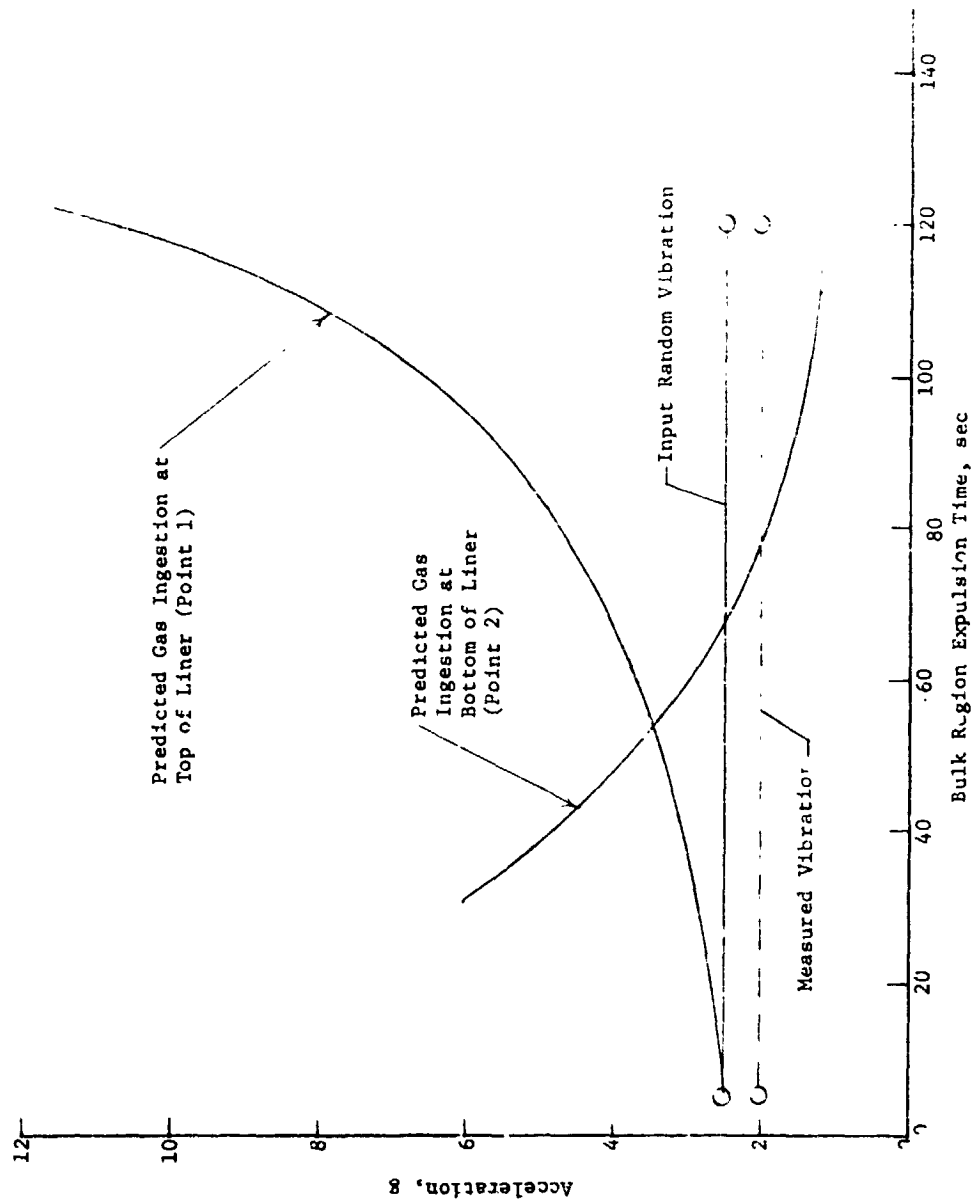
Fig. II-13 Outflow Test Data Correlation, Vertical Random Vibration
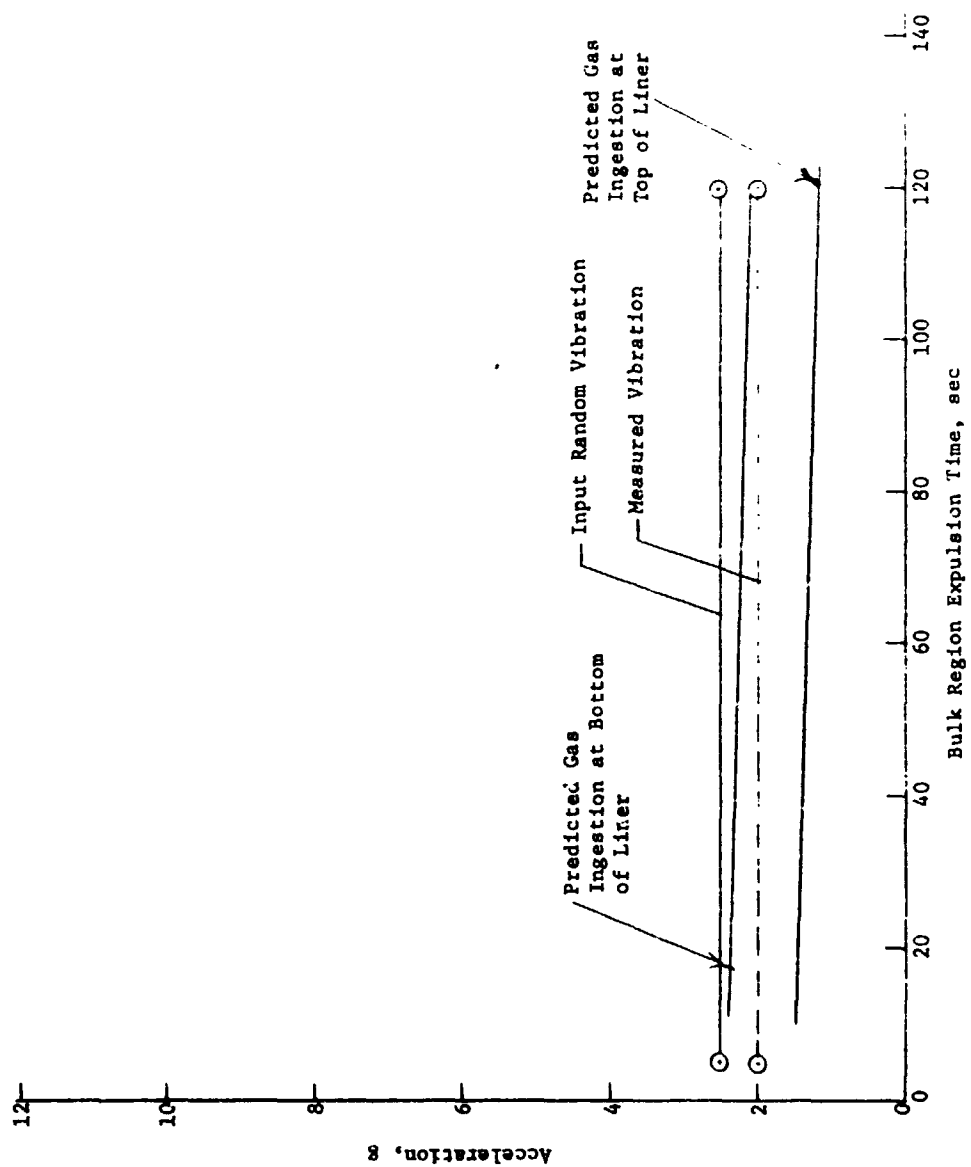
Fig. II-94 Outflow Test Data Correlation, Horizontal Random Vibration

breakdown during the tests. However, smaller pressure dif-
ferentials or larger liquid heights could shift the lower ana-
lytical curve to a higher value. Based on the data presented
here, random vibrations appear to correlate well when using a
hydrostatic analysis.

d. Conclusions - The results showed good correlation of the
measured and predicted screen liner breakdown points when using
a hydrostatic analysis; therefore, vibrational effects on capil-
lary systems may be treated hydrostatically.

The dimensionless parameters, Bond and Weber numbers, showed
that capillary forces predominated throughout the tests. The
criterion for interface stability is the screen bubble point,
which must not be exceeded by pressure variations resulting from
the vibrational environment. This conclusion is supported by
Ref II-8.

Consequently, vibrational effects create problems that can be
solved by state-of-the-art design changes, rather than developing
a new technology area for these surface tension devices. Vehicle
vibration environments must be known to determine the retention
capability of the proposed capillary systems. This may necessitate
full-scale vibration tests with flight devices because only
actual system damping and resonances can be used for accurate
hydrostatic correlation. Analytical work to mathematically define
the pressure field in the liquid during vibration would allow a
more complete understanding of the problem.

III.   SUBSCALE LH$_2$ MODEL TEST PROGRAM

A concept verification test program cannot be successful if a
satisfactory model cannot be provided as a test article. There-
fore, the first objective of the Subscale LH$_2$ Model Test Program
was to design and fabricate a suitable subscale model that was
representative of the designs proposed for the various applica-
tions discussed in Volume II. Within the constraints of a 1-g
test environment, the objective was to provide a test article
that conformed operationally, as nearly as possible, to the
full-scale flight systems.

The second objective of the program was to verify the cryogenic
system design through testing. Primary objectives of the test
program were to demonstrate the system capability to expel li-
quid and vent liquid-free vapor on demand. Secondary objectives
were to verify filling techniques, communication screen perfor-
mance, and screen rewicking.

A.   ANALYSIS AND DESIGN

Design considerations and the approach used to design the 63.8-cm
(25-in.) diameter subscale model are described here. A complete
description of this screen liner/flow channel system is presented.
The design approach that was followed is consistent with that
used under the cryogenic system design task described in Volume
II.

1.   Design Considerations

The size of capillary acquisition/expulsion model to be tested
in a 1-g bench test environment is determined almost exclusively
by the capillary retention capability of the screen. The full-
scale designs from which the test system was modeled, generally
included multiple layers of screen on the controlled liquid re-
gions but only a single layer on any screen communication de-
vice. The communication screens on the full-scale flight systems
extend essentially the full length of the device. The test mo-
del was designed, as nearly as possible, to be representative
of the full-scale systems. Therefore, the single layer communi-
cation screen retention capability determined the maximum size
of the device.

The device was designed to be tested with LH₂. The hydrostatic head retention capabilities of several screen meshes for LH_2 are given in Table III-1.

Table III-1 Hydrostatic Head
Retention Capability
of Screens in LH_2 at 1-g

	Hydrostatic Head at 1-g	
Screen Mesh (Dutch Twill)	cm	(in.)
200x1400	50.8	(20.0)
250x1370	65.2	(25.7)
325x2300	78.2	(30.8)

The table shows that the possible size range for the device and tank covers approximately 25 cm (10 in.) with the largest size being approximately 78 cm (31 in.). Given this range of device diameters, the ultimate size of the device depended on the size of available tank domes. A vendor survey revealed the best option to be a 63.5-cm (25-in.) inside diameter set of 304 stainless steel hemispherical domes. With the tank size established, the 325x2300 mesh stainless steel screen was selected because it offered an adequate margin of safety for the design. To function properly, the communication screen must have a lower bubble point than the screen forming the controlled liquid region. Therefore, two layers of 325x2300 mesh Dutch twill screen were selected as the capillary barrier for the flow channels. The hydrostatic head retention capability for two layers of 325x2300 mesh screen is twice the value indicated in Table III-1 for a single layer, providing the channels with a substantial safety factor.

Selection of the number of channels for the model was influenced by two basic considerations: (1) the desire to make the test article represent the full-scale flight systems, and (2) the need to reduce manufacturing costs where possible without compromising the design. Fabrication costs can be reduced by decreasing the number of channels, but the device must have some minimum number of channels to be a representative system. Analysis showed that no fewer than eight channels were required in the 63.5-cm (25-in.) model to adequately represent the full-scale systems.

The size of the channels depends on the capability of the communication screen to rewick the distance between the channels. For an 8-channel system, the largest octosphere that could be contained in the 63.5-cm (25-in.) diameter tank would measure 24.3 cm(9.56 in.) at the equator. The maximum wicking distance is half of that value; therefore, for any design, the maximum wicking distance would be less than 12.1 cm (4.78 in.). For the heat leaks anticipated during testing, the analyses (discussed in Chapter II, Volume II) indicated that this wicking distance presented no design problem. Consequently, the size of the channels was not determined by wicking considerations.

Because the test model was only to represent the full-scale system, rigorous scaling was not a requirement. Therefore, to simplify fabrication, the channels were designed so their cross-sectional dimensions were larger than an exactly scaled version would be. An additional consideration was the requirement for instrumentation within the channels and the need to provide sufficient space for their installation.

It was estimated that an upper limit for LH_2 outflow during tests would be approximately 0.23 kg/sec (0.5 lbm/sec). This flowrate would drain the test article in approximately 30 sec. Using the computer models discussed in Volume II, Chapter II, it was determined that eight channels, having approximately 13 cm^2 (2 in.^{2}) cross-sectional area each, would be necessary to empty the tanks at that flow rate in a -1 g attitude. Using this information, the channel dimensions were established at 7.62 cm (3 in.) wide and 1.9 cm (3/4 in.) deep. This channel has a cross-sectional area of 14.5 cm^2 (2.25-in.^{2}) and also provides sufficient size for the installation of the required instrumentation. The 7.62-cm (3-in.) wide channel, placed in the center of each panel of the octosphere, reduces the distance the communication screen must wick the liquid to no more than approximately 8.25 cm (3.25 in.) at the tank equator.

It was also necessary to consider the instrumentation requirements of the vapor annulus formed between the screen liner and the tank wall. A radius of 30.2 cm (11.9 in.) was chosen so the minimum clearance between the tank wall and the screen device would be 1.52 cm (0.6 in.) and the maximum would be 3.8 cm (1.5 in.).

2. Summary Description and Comparison

The final design is a channel/liner device in an octosphere configuration with a radius of 30.2 cm (11.9 in.). The liner was a single layer of 325x2300 mesh stainless steel Dutch twill screen. The eight channels with dimensions of 1.9x7.6 cm (3/4x3 in.), were formed of two layers of 325x2300 mesh screen. The device was enclosed in a 63.5-cm (25-in.) diameter tank. A summary of system volumes and surface areas is presented in Table III-2.

Table III-2 Subscale LH_2 Model Summary

Tank Volume	0.134 m^3	(4.734 ft^3)
Liner Volume	0.106 m^3	(3.771 ft^3), 79.5% of Tank Volume
Channel Volume	0.0093 m^3 i.e., EE = 91.3%	(0.329 ft^3), 8.7% of Liner Volume
Vapor Annulus Volume	0.028 m^3	(0.970 ft^3), 20.5% of Tank Volume
Liner Area	1.12 m^2	(12.04 ft^2)
Communication Screen Area	41.52 m^2	(447 ft^2), 37.1% of Liner Area

Figure III-1 shows assembly drawings for the instrumented test article. The instrumentation is discussed in detail in Section D.

Table III-3 compares the final test article configuration with a typical full-scale design, the OMS/RCS LH, tank for the integrated OMS system detailed in Volume II, Chapter III.

Temperature Sensor

Outflow Line (0.74 OD x 0.035 W Tube)

Electri Connect

Pressure S Line (0.12

Perforated Plate

Screen Channel

Communication Screen

To
Ou

To
In

PLAN VIEW

1.2

0.60
0.55

Temperature Se
Liqu.

Pressure Sensing
Line   (0.25 OD
Tube)

Electrical
Connector

Outflow Line
(0.74 OD x 0.035 W
Tube)

63.5 cm
(25.0 in.) ID

Electrical
Connector

Pressure Sensing
Line (0.125-OD Tube)

Perforated
Plate

Screen
Channel

Top Manifold
Outer Cover

Top Manifold
Inner Cover

Support
Tab

Up

Fig. III-1 Assembly Drc

1.2

0.60
0.55

Temperature Sensor (Typ)

Liquid Level Sensor (Typ)

Bottom Manifold
Screens

Manifold
Support Cup

Electrical
Connector

63.5 cm
(25.0 in.) ID

Pressurization & Vent
(0.75-OD x 0.35-W
Tube)

Bottom Manifold
Inner Cover
Up

Bottom Manifold
Outer Cover

Support
Tab

Up

Fig. III-1 Assembly Drawing for 63.5-cm (25-in.) Subscale Model

FOLDOUT

III-5 and III-6

Table III-3   Comparison of Integrated OMS/RCS LH$_2$ Tank with Subscale Model

	OMS/RCS LH$_2$ Tank	Subscale LH$_2$ Model
Outer Liner and Feeder Channels		
Diameter, m (ft)	3.58 (11.75)	0.585 (1.92)
Gas Annulus, cm (in.)	11.4 (4.50)	2.54 (1.0)
Communication Screen Mesh	200x1400	325x2300
Channel Screen Mesh (2 layers)	200x1400	325x2300
Perforated Plate, Percent of Open Area.	50	30
Channel Depth (at Equator), cm (in.)	2.54 (1.0)	1.9 (0.75)
Channel Width (Equator & Manifold), cm (in.)	2.69x2.5 to 8.4x8.4 (10.6x1 to 3.3x3.3)	7.62 (3.0)
Communication Screen Width at Equator, cm (in.)	27.9 (11.0)	16.6 (6.56)
Number of Channels	20	8

B.   FABRICATION AND ASSEMBLY

The detailed fabrication and assembly of the 63.8-cm (25-in.) diameter sub-scale model is presented in this section. This section also describes the critical fabrication methods that were developed and the primary problem areas encountered.

1.   Fabrication Sequence

The channels for the subscale model were fabricated as individual subassemblies and then mated to form a single 8-channel unit. Each channel was composed of a framework to which the screen and perforated plate was attached. Each frame was a welded structure composed of four components, two welded box-like channel end sections and two machined constant-radius ring sections. The individual components and a partially welded frame are shown in Fig. III-2.

Fig. III-2 Flow Channel Components

Groves were machined in both the rings and the end fittings to separate the layers of screen and perforated plate. A cross section of the channel illustrates this technique (Fig. III-3).

Flow Passage

Screen (2 Layers)

Perforated Plate (2 Layers)

Machined Ring Section
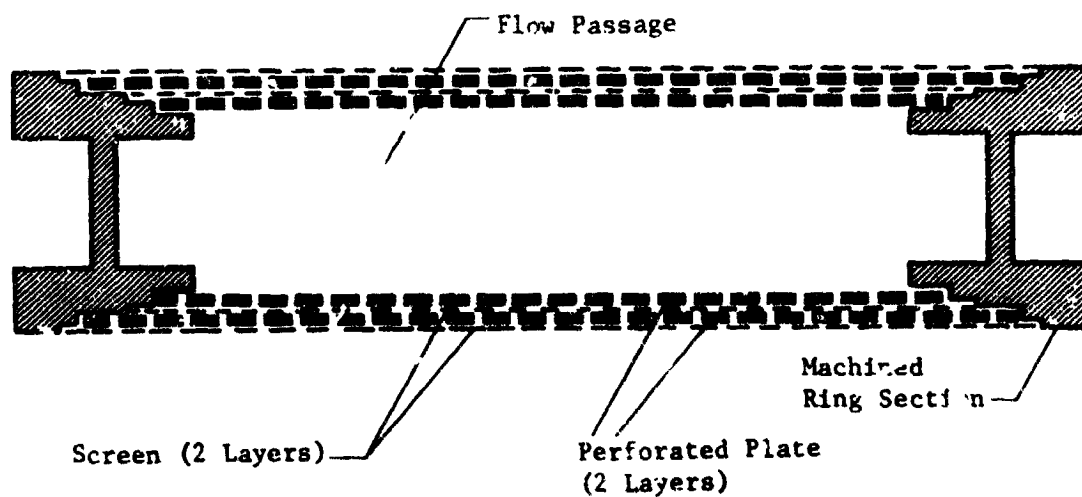
Fig. III-3 Channel Cross Section

III-8

The inner-most element of the capillary barrier on both the inner and outer surfaces of the channel was a layer of perforated stainless steel plate. The perforated plate was 0.064 cm (0.025-in.) thick with a 30% open area value. The plate was tack-welded in one groove and a layer of 325x2300 mesh stainless steel screen was soldered in the second machined groove using Eutectic 157 (96% tin, 4% silver) solder. The perforated plated served as the structural support member for the screen. A second layer of perforated plate was tack-welded in the third groove over the first screen/perforated place combination. This operation required skill to insure that the heat from the welding did not melt the solder immediately beneath the perforated plate. The final assembly step was to solder the outer screen in place in the last groove on the ring.

Because of the curvature of the channels and the spacing of the machined grooves in the rings, each layer of perforated plate and screen differed in dimension. Figure III-4 shows two channels at different stages of fabrication. The channel on the left includes the first layer of perforated plate and screen, the second layer of perforated plate has been added to the channel on the right. For the right-hand channel, a second layer of screen will complete the channel subassembly.

Fig. III-4   Flow Channel Assemblies

The eight completed channel subassemblies were welded together
at the end fittings to form a spherical cluster. This assembly
served as the framework for fabricating the remainder of the de-
vice. (See Fig. III-5). In the opening at the top of the assem-
bly, the ends of each channel can be seen. The openings at the
top and bottom of the device were enclosed with manifold covers.
These manifold covers were formed separately and joined to the
channel assembly. The outer manifold cover components of the top
and bottom manifolds are also shown in Fig. III-5 before being
joined to the channel assembly. For the purposes of this dis-
sussion, the top manifold is at the top of the device during
-1 g tests and contains the outflow line. The bottom manifold
is at the bottom of the tank during -1 g tests and is attached
to the pressurization assembly.
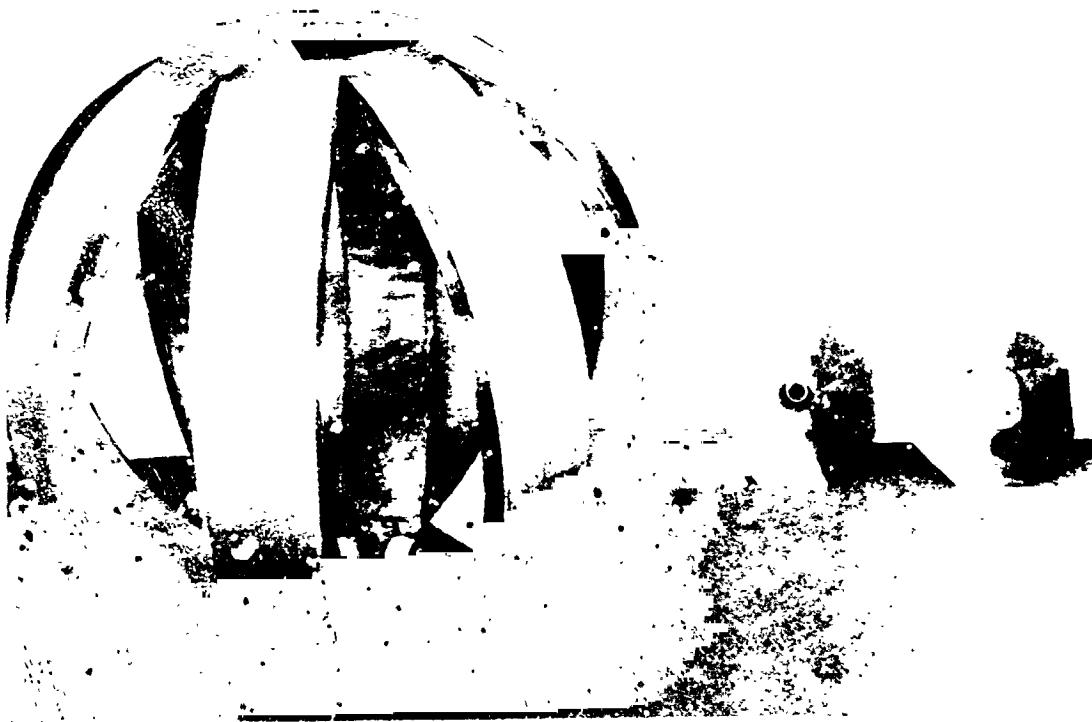
Fig. III-5 Completed Assembly of Flow Channels

III-10

The inner cover of the top manifold was fabricated of stainless steel plate and was joined to a structure to position and support the instrumentation for monitoring the bulk liquid region. This structure is shown before it was joined to the channel assembly (Fig. III-6). The instrumentation wires were fed in through the plate and out through the outflow line attached to the top manifold outer cover. The top manifold outer cover and the outflow lines were also fabricated from stainless steel and the final assembly of these components is shown in Fig. III-7.

Fig. III-6 Bulk Region Instrumentation Assembly

Fig. III-7 Completed Flow Channel and Manifold Assembly

The bottom manifold components were fabricated in the same manner
as the top manifold. However, this manifold had no outflow pro-
vision. Instead each half of the manifold had a hole for insert-
ing two layers of 325x2300 mesh screen. These screen layers
allowed draining of the entire bulk liquid region and also allowed

III-12

gas to be purged from the channels when the device is filled in the inverted position. Attached by a weld to the bottom manifold was a machined cup into which the fill/pressurization/vent line was dead-head welded. This detail is shown in Fig. III-1.

The screen device is supported in the tank by only the outflow line attached to the top manifold and the fill/pressurization/ vent line attached to the bottom manifold. The cup attached to the fill/pressurization/vent line was required as a structural support member on the bottom manifold because of the presence of the double layer of screen centered on the vertical centerline of the device. This screen prevented the direct attachment of the fill/pressurization/vent line to the device. A pressurant diffuser consisted of a number of 0.318-cm (0.125-in.) holes drilled through the walls of the fill/pressurization/vent line to allow flow into and out of the line. The diffuser was necessary to prevent direct impingement of the pressurant gas on the screen in the bottom manifold.

The final assembly procedure was completed with the fabrication and attachment of the outer screen liner. The outer liner structure was formed in eight gore sections from a 5.08-cm (2-in.) wide, 0.318-cm (0.025-in.) thick stainless steel frame and perforated plate insert tack-welded together. This panel assembly is shown in Fig. III-8. The figure also shows the 0.64-cm (1/4-in.) lip that was formed on the two longitudinal edges of each gore panel. When the panels are in position, the lips of the two adjacent panel edges butt together. The lips on the panel edges eliminated the need to butt weld the panels and allowed the much simpler lip weld to be used.

After each panel was centered over a channel on the channel assembly and tack-welded for initial positioning, the ends and edges were welded into place. This assembly is shown in Fig. III-9. The final assembly step in completing the outer liner was soldering the eight screen gore sections over the perforated plate panels. The completed screen system with the outer liner screws in place is shown in Fig. III-10. As the final step of the tank fabrication procedure, the screen device was welded into the 63.5-cm (25-in.) diameter stainless steel tank. This assembly, complete with instrumentation electrical connectors, is pictured in Fig. III-11.

Fig. III-8 Perforated Plate Gore Section
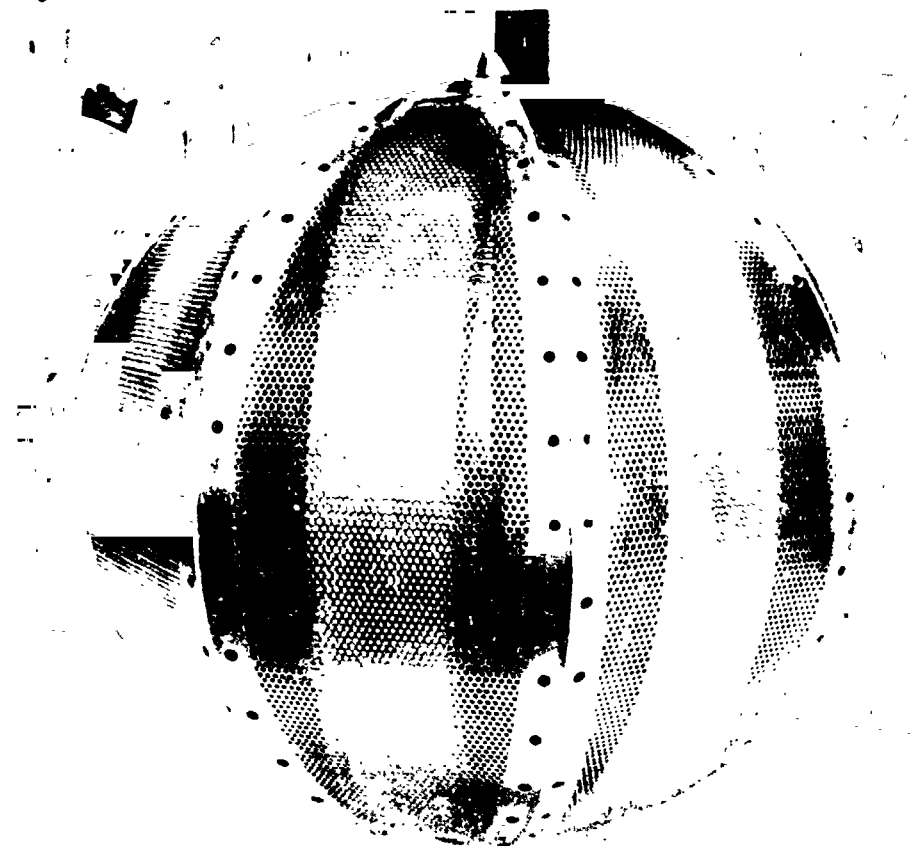
Fig. III-9 Completed Perforated Plate Gore Section
Assembly
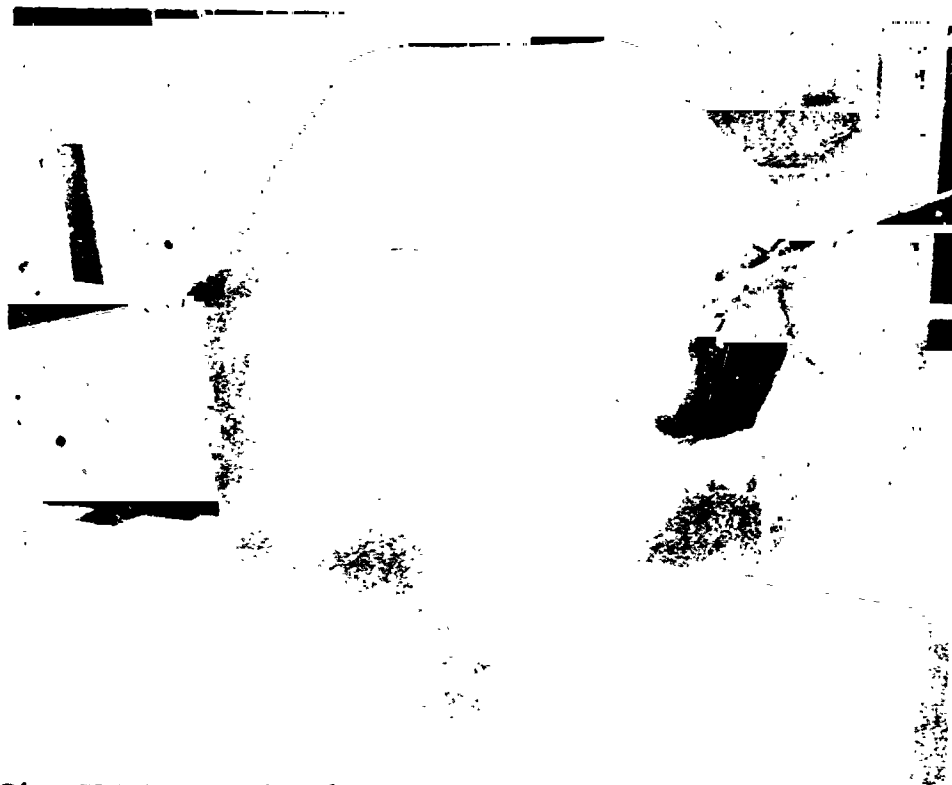
Fig. III-10 Completed Screen System
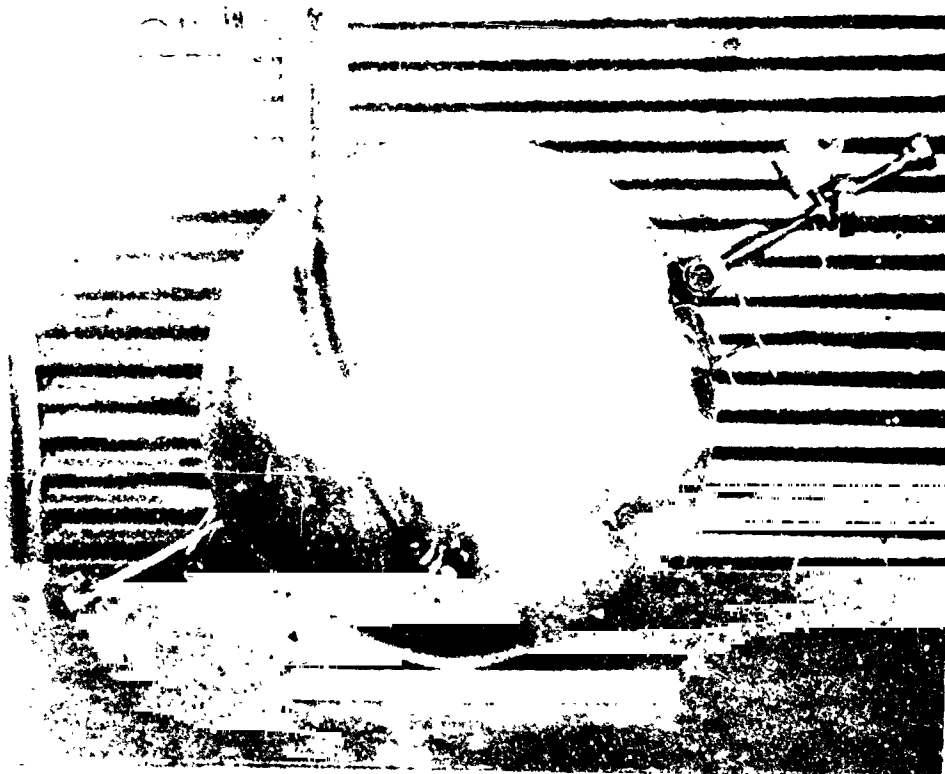
Fig. III-11 The 63.5-cm (25-in.) Diameter Tank after Final Closure Weld

The tank was suspended from the lid of a 1.83-m (6-ft) diameter vacuum chamber by three 1.27-cm (1/2-in.) diameter tubes. After completing the necessary plumbing, the tank and plumbing were both insulated. The tank was insulated using 20 alternating layers of aluminized Mylar and double nylon netting. Ten alternating layers were used for the plumbing. Figure III-12 shows the system as the insulation process nears completion.

2.   Critical Fabrication Considerations

During the analysis and design of the subscale test model, a number of critical fabrication details were identified. These critical fabrication considerations are discussed in the following paragraphs.

1)   Special tooling for manufacturing the screen device was held to a minimum. Because welding of screens generally requires special welding jigs, soldering was specified as an alternative screen attachment method. The problem associated with the soldered screen joints was the possibility of remelting the solder if subsequent welding was required near the soldered area. This was the case on the channels where two layers of screen and perforated plate were used. The second layer of perforated plate was welded in place directly over the soldered first layer of screen. To alleviate this problem, the second layer of perforated plate was made wider than the first layer of screen so the solder joint would not fall directly beneath the weld. The number of tack welds used to join the second layer of perforated plate to the channel assembly was minimized and each weld was allowed to cool before another was attempted.

2)   The eight-channel subassemblies were welded together to form the completed channel assembly. These welds occurred along the box-like channel end fittings. Here again, warpage of the assembly due to the heat of the welding process was to be avoided. To prevent warpage, or to hold it to a minimum, the channels were clamped and several short welds were used on each seam instead of one continuous weld. Each short weld was allowed to cool completely before proceeding so that heat buildup in the assembly was prevented.

Fig. III-12 Installation of MLI on the 63.5-cm (25-in.) Diameter Tank

III-17

3) For the design to function properly, the communication screen must rewick liquid if it has dried out during a pressurization event. This wicking can proceed from the bulk fluid reservoir, but the design assumed that most wicking would occur as a result of liquid flowing from the liquid-filled channels out through the communication screen. For this wicking to occur, a close fit was required between the perforated plate/fine mesh screen communication screen cover and the channels beneath it. Any gaps between the two, across which liquid could not be transferred, would prevent the necessary wicking from taking place. Great care was exercised during fabrication to assure that proper fit was achieved.

4) A similar concern was related to the placement of the screens on the device. Any location where the screen did not closely fit the supporting perforated plate offered a potential area for screen dryout. Great care was used while soldering the screen to assure a close fit.

5) Some of the sensors were positioned inside the screen portions of the device where replacement in the event of damage was nearly impossible. Therefore, all possible precautions were exercised to minimize the possibility of sensor damage.

6) Before fabricating the screen system, a technique was developed to repair damaged screens with solder. This method was also used to eliminate the small screen anomalies that occur during the weaving process, causing larger than standard pores. The ability to repair small areas of screen precludes the necessity of removing a screen if for some reason it does not meet the pressure retention specification.

7) The final closure weld on the tank equator was recognized as a potential hazard to the screen device inside. To preclude the possibility that molten metal from the weld could be sprayed onto the screen surfaces causing possible damage, a protective lip was formed on the inner edge of one of the tank hemispheres. This lip consisted of a hoop, which was welded in place, so that it extended beyond the edge of the mating hemisphere when they were joined. The hoop then served as a barrier between the closure weld and the screen device.

III-18

3. Fabrication Problems

Despite the precautions taken during the fabrication process,
some problems did occur. On two occasions after welding the se-
ond layer of perforated plate onto the channels, the solder joint
on the first screen developed cracks. The cracks developed be-
cause of the improper soldering techniques used. This produced
some leaks that required repair. The repair process involved
removing the perforated plate and again soldering the screen in
place using the proper techniques.

Although warpage of the channel assembly was prevented, some
warpage did occur while assembling the bottom manifold cover.
As a result of this distortion, the bubble point of the screen
in the center of the cover did not meet the specification. Be-
cause replacing the components involved in the assembly was im-
practical, a third layer of screen was soldered in place over
the two existing layers. This procedure restored the screen as-
sembly bubble point to an acceptable value.

During assembly, a liquid temperature sensor was damaged; how-
ever, the expense and delay associated with replacing it out-
weighed the potential benefit of the data it would have supplied.
Therefore, it was not replaced. Also during fabrication, a liq-
uid level sensor in the top manifold was damaged. The damage
occurred while the manifold cover was being welded into place and
the sensor was inadvertently shorted with the welding voltage.
The sensor was replaced by cutting out the section of the mani-
fold to which it was attached and welding a new one in place.

4. Inspection and Acceptance

Inspection and testing were performed throughout the fabrication
process to assure the quality of the device. The majority of the
acceptance testing involved bubble point checks of the various
screen assemblies.

The channel assemblies were bubble point checked three times:
(1) after soldering the first screen layer; (2) after welding
the second perforated plate; and (3) after soldering the second
layer of screen. The bubble point of the device was required to
be within specification at each of these points before fabrica-
tion could proceed.

The channels were tested by placing a rubber plug in the open
end of each channel end fitting. One plug was fitted with a pres-
surant line so the interior of the channel could be pressurized
during the test. The channels were placed in a methanol bath,
pressurized with gaseous nitrogen, and visually inspected for
leaks. A manometer was used to measure the bubble points. The
specification for acceptance was that ie layer of screen have
a bubble point of at least 50.8 cm (20 in.) of water and that
two layers of screen have at least twice that value, or 101.6 cm
(40 in.) of water. If any of the assemblies did not meet the
specifications, they were repaired as necessary to bring them
within specification.

Additional acceptance and checkout tests were conducted on the
completed screen system. The necessary plumbing was connected to
perform fill, drain, and pressurization tests in methanol. Opera-
tional tests were also performed to verify satisfactory system
operation. Figure III-13 shows a photograph of the acceptance
test system. As a result of these tests, additional solder was
placed on the screens at the ends of the channels to confine the
wicking lengths to an area where wicking was inadequate.

A final check was made after the system had been completely as-
sembled and attached to the vacuum chamber lid. This test was
a standard helium leak check to verify that there would be no
leaking from the test article into the vacuum chamber. Additional
checks were also made throughout the fabrication and assembly
process to verify the operation of the various sensors placed
in the system.
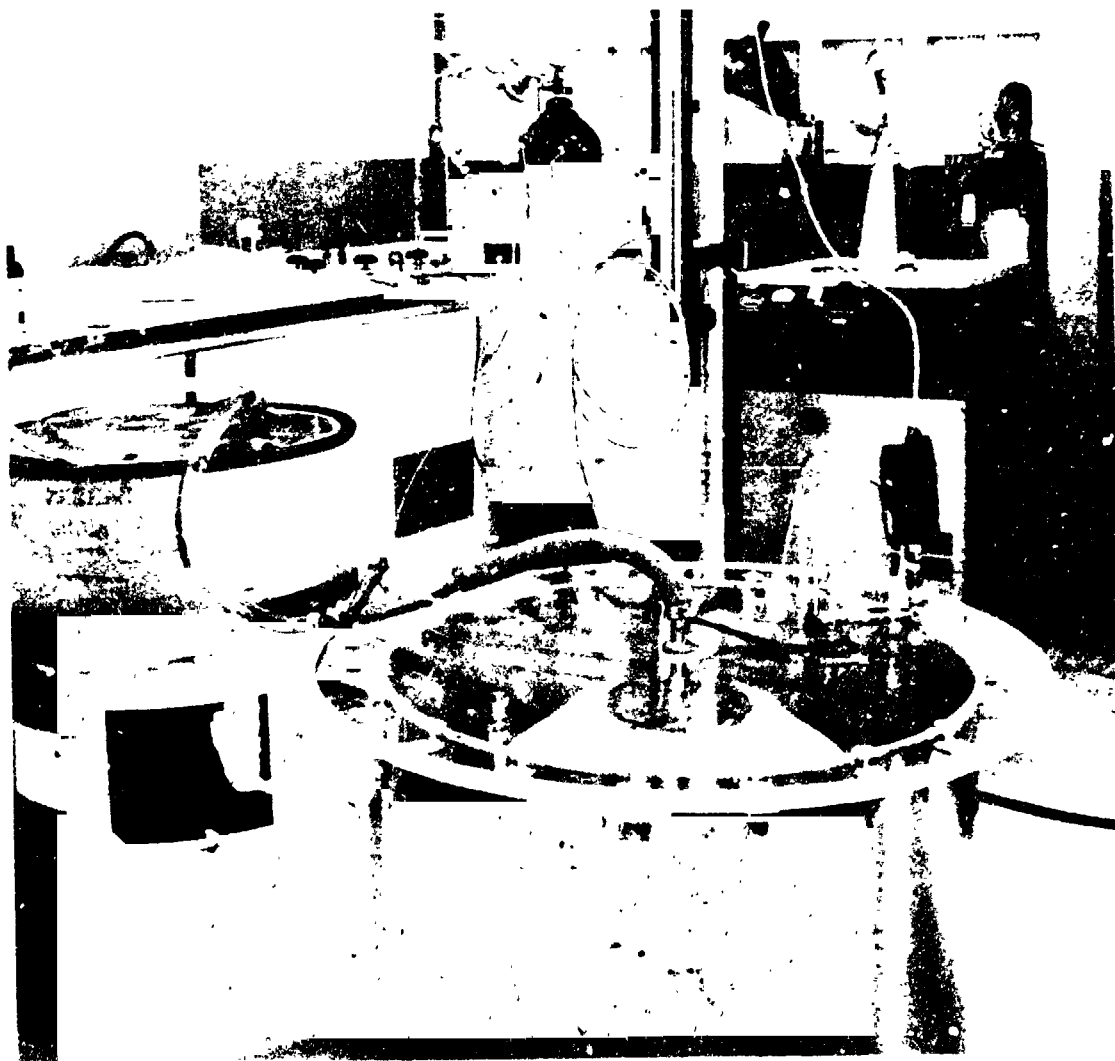
Fig. III-16 Acceptance Test System

C. TEST PLAN

The test plan for the subscale LH₂ mode' was designed to demon-
strate the capillary acquisition/expulsion system concept in the
1-g environment. The test series included pressurization, outflow,
and venting tests in addition to evaluation of filling techniques,
boiloff, and communication screen performance. The test matrix
is presented in Table III-4.

Table III-4 LH₂ Subscale Model Test Matrix

Test and Number		Liquid	N/cm^2 (psia)	Pressurization		
				Pressurant	Pressurant Temperature, $^\circ K$ ($^\circ R$)	No. of Expulsions
	1	LN_2	Vent Fill			
Fill and	2	LN_2	Vent Fill			
Boiloff	3	LH_2	Vent Fill			
Tests	4	LH_2	Vent Fill			
	5	LH_2	17.2 (25)	GH_2	88.9 (160)	1 No Vent
Pressurization,	6	LH_2	24.1 (35)	GH_2	88.9 (160)	1 No Vent
Outflow,	7	LH_2	31.0 (45)	GH_2	88.9 (160)	1 No Vent
and	8	LH_2	17.2 (25)	GH_2	260.0 (500)	1 No Vent
Vent	9	LH_2	17.2 (25)	GH_2	88.9 (160)	2 Vent
Tests	10	LH_2	17.2 (25)	GHe	88.9 (160)	1 No Vent
	11	LH_2	17.2 (25)	GHe	260.0 (500)	1 No Vent
	12	LH_2	17.2 (25)	GHe	88.9 (160)	3 Vent

1. Fill and Boiloff Tests

Demonstration of fill techniques was the primary objective of the
first four tests. Because vapor could become trapped in the con-
trolled liquid volume of the capillary system during filling,
special procedures or designs might be required. Fill tests were
to be performed using both LN_2 and LH_2.

III-22

a purpose of the boiloff rests was to determine the total heat leak to the insulated tank in the vacuum chamber. This included heat leaks through instrumentation wires and penetrations as well as incident heating through the tank insulation. This data would identify the thermal operating conditions for the test article.

The fill and boiloff rests were run in the 1-g configuration with the tank completely full of liquid (bulk region, liquid annulus, and vapor annulus). A total of four tests were planned, two with LN_2 and two with LH_2. The test article was filled through the outflow line.

2.   Minus 1 g Expulsion and Pressurization Tests

Since gas-free liquid expulsion is the primary function of the capillary acquisition/ pulsion system, these tests were to demonstrate the system's capability to function under a wide range of operating conditions. These tests would also determine any detrimental effects of the pressurization system on the capillary device. The capillary system must demonstrate stability under the hydrostatic, hydrodynamic, and thermal conditions. This includes exposing the screen to warm pressurant, which could cause screen dryout. Both gaseous hydrogen and helium pressurants were introduced at temperatures of approximately 89°K and 280°K (160°R and 500°R). System expulsion efficiency and expulsion rates were also evaluated.

3.   Venting Tests

Tests 9 and 12 (see Table III-4) were planned to demonstrate the vent capability of the DSL. The two tests were similar except for the pressurant used. During these tests, venting was to be accomplished using the automatic vent control system described in Section D. Following an expulsion period, the vent control system would be activated and data would be monitored during a 3 to 4 hour simulated coast period. The second expulsion period was planned to deplete the liquid volume to 20% of the bulk liquid volume. This expulsion event would be followed by another simulated coast with venting and then a final expulsion event to complete the test.

D. TEST SYSTEM

The test system, including the 63.5-cm (25 in.) test article,
vacuum chamber, liquid nitrogen supply dewar, and related hard-
ware is shown schematically in Fig. III-14. Major mechanical
components shown in the figure are listed in Table III-5. The
test article is pictured in the minus 1-g configurations; i.e.,
with the outflow line on top and pressurization/vent (fill and
drain) line at the bottom.

Table III-5 Test System Mechanical Components

Component*	Function	Description
PV1	Propellant fill valve	Skyvalve, 1 ¼-in., PVC-24-1S
PV2	Vent valve (throttling)	Annin, 1 ¼-in., P/N 1660
PV3	Drain/vent valve (throttling)	Annin, 1 ¼-in., P/N 1660
PV4	Vent valve (throttling)	Skyvalve, 1 ¼-in., TVC-24-1S
SV1	Vent valve	Skinner Electric Valve, 1/4-in., U52DA-052
SV2	Pressurization valve	Skyvalve, 1/2-in.
SV3	Pressurization valve	Skyvalve, 1/2-in.
SV4	Propellant outflow	Valcor, 3/4-in.
SV5	Vent valve (vapor annulus)	Hoke, 1/4-in., TY 445D
SV6	Vent valve (bulb region)	Hoke, 1/4-in., TY 445D
SV7	GHe purge valve	Valcor, 1/4-in., HV-6P-201-2-G
SV8	Isolation valve	Valcor, 3/4-in.
MV7	Isolation valve	Valcor, 1/4-in., HV-6P-201-2-G
MV8	Isolation valve	Valcor, 1/4-in., HV-6P-201-2-G
RV1	Relief valve	Republic
RV2	Relief valve	Republic
BD1	Burst disc	Fike

*See Fig. III-14.

III-24
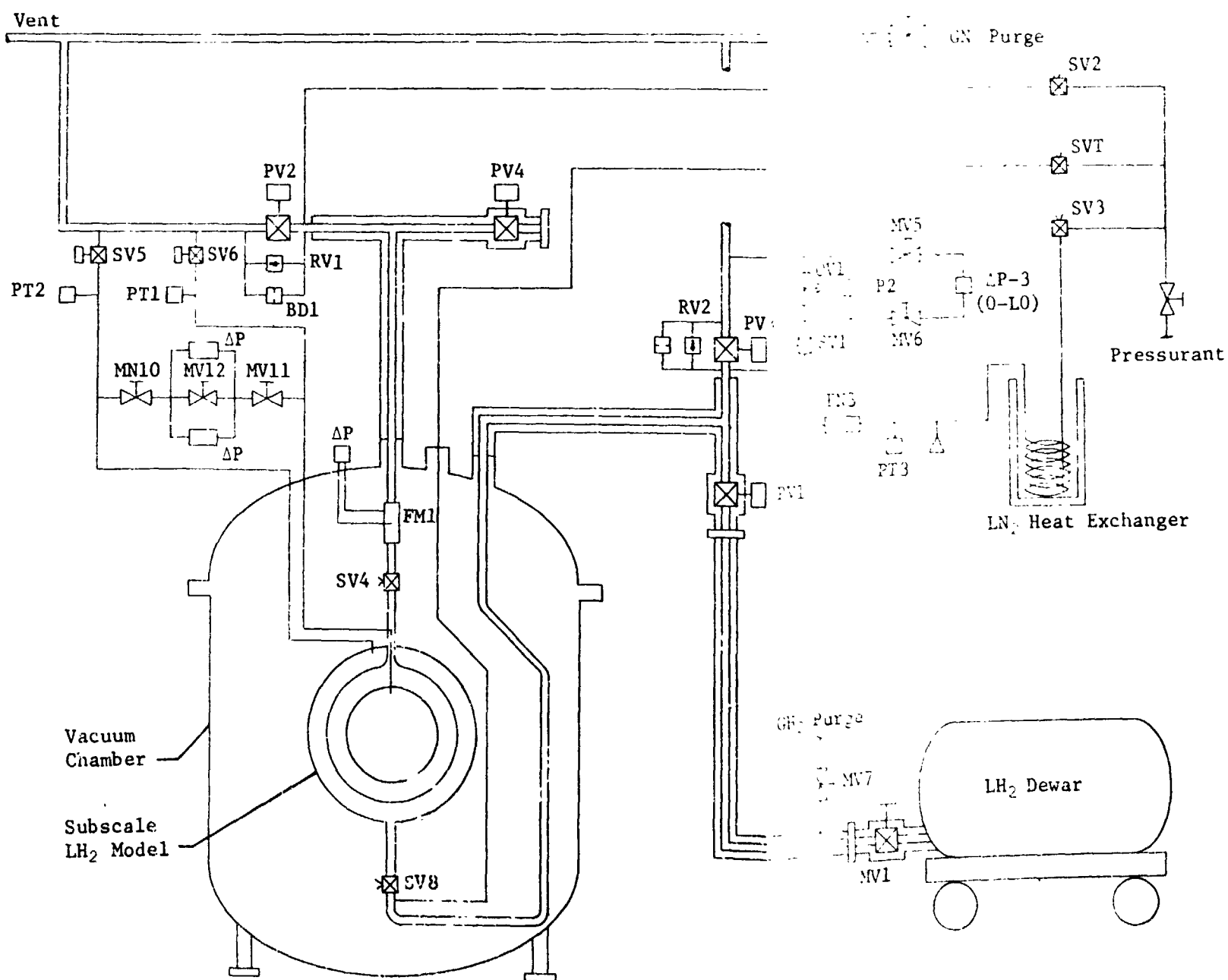
Figure III-14 Test System Schematic

III-25 and III-26

FOLDOUT FRAME

The fill and drain line was 1.9-cm (3/4-in.) OD, 0.089-cm (0.035-in.) wall, 304-series stainless steel tubing. The line was vacuum-jacketed from the supply dewar to the vacuum chamber and was sized to handle expected flight expulsions scaled down to the test model tank size. The fill valve (PV1) was a 3.17-cm (1 1/4-in.) ID vacuum-jacketed valve that was electropneumatically actuated. The drain valve, a vacuum-jacketed throttling valve, was also 3.17 cm (1 1/4-in.) ID.

The outflow line, which was also vacuum jacketed to minimize heat leak, was designed to perform as: (1) a vent system during fill or as an emergency vent should the pressurization valve fail or loss of chamber vacuum occur and (2) the system outflow line through which vapor-free liquid could be expelled. Three valves, SV4, PV4, and PV2, were installed in the outflow line to provide (1) propellant outflow; (2) venting into the vent stack; and (3) venting back into the supply dewar. These valves are described in Table III-5. The outflow line was 1.9 cm (3/4 in.) OD, 0.089-cm (0.035-in.) wall of 304 series stainless steel tubing.

The vacuum chamber enclosed the test article and related plumbing as shown in Fig. III-14. The roughing and diffusion pumps used to evacuate the chamber could operate overnight so that reconditioning the test article environment was not required periodically. The vacuum system was capable of pressures as low as 10^{-5} Torr with the test article installed.

The pressurization and fill and drain lines were common up to the point shown in the test system schematic. Upstream of this point, the pressurization system was sized for the maximum liquid outflow rate using 88.9°K (160°R) pressurant at the test article inlet. The resulting line size was 1.27-cm (1/2-in.) OD, excluding the heat exchanger section, and was fabricated of 304 series stainless steel tubing, with a 0.089-cm (0.035-in.) wall.

A heat exchanger was incorporated into the system for conditioning the pressurant to the desired temperature. The heat exchanger section consisted of 1.27-cm (1/2-in.) copper tubing coiled in a 45.7-cm (18-in.) diameter spiral. The coil was placed in an insulated container filled with liquid nitrogen for the cold gas pressurant tests. Gaseous hydrogen was supplied from K-bottles; gaseous helium was obtained from the test facility supply.

To prevent overpressurization, a relief system was incorporated in both the fill/drain and outflow systems. A relief valve and burst disc were installed in parallel with the vent valves in the fill/drain and outflow lines. The selected burst discs had a rupture pressure of 31 N/cm^2 (45 psi) gage and relief valves were set to actuate at a pressure of 34.4 N/cm^2 (50 psi) gage. All safety devices were exhausted into the vent stack.

1.   Automatic Vent System

Successfully venting the test article requires that the correct pressure differential between the vapor annulus and bulk region be maintained. For liquid hydrogen, the allowable vent band is small and depends on the hydrostatic head. A nominal value for the test article under the normal 1-g test conditions is 0.027 N/cm^2 (0.04 psi) differential. To assure venting within the required ΔP band, an automatic venting system was designed incorporating two highly sensitive differential pressure sensors. The sensors were manufactured by the Rosemount Company and have a ΔP range of $\pm$0.069 N/cm^2 ($\pm$0.10 psi) with an accuracy better than 1%.

The transducers were isolated from the rest of the system to avoid damaging them when not being used. This was accomplished by a valve tree arrangement (Fig. III-14) that incorporated three 0.64-cm (1/4-in.) HYPRO band valves (MV10, MV11, and MV12). The transducers were connected in parallel with output from one connected to a recorder. The other transducer provided the sensing output for the automatic vent control system. The electronics system between the sensor output and solenoid input was designed to provide a variable vent control band for additional system flexibility. To obtain the desired vent rate, a 0.64-cm (1/4-in.) metering valve (OV1) was installed downstream of the solenoid vent valve (SV1).

2.   Operational Considerations

This sub section describes the procedures and system considerations that were initially outlined to test the LH$_2$ subscale model. During the tests, some of these procedures had to be modified. The modifications are presented in Section F. Prior to actual testing, the entire test system was checked for proper operation including instrumentation hardware, etc. This was accomplished by a series of functional and leak tests that verified proper operation of the entire system.

a. Fill and Boiloff Tests - For these tests, the test article was installed in the vacuum chamber in the +1-g configuration. The liquid cryogen (nitrogen or hydrogen) was introduced into the tank through the outflow line. The tank was vented to the atmosphere through the pressurization/vent line. Filling was initially accomplished with the tank wall at ambient temperature. Subsequent fills were made with a cold tank. Filling was terminated when liquid level sensor, DP14, indicated liquid. Fill rates were varied by controlling the dewar pressure.

Following each fill test, a boiloff test was run with a liquid level of approximately 30%. Due to the length of time required to reach a steady-state condition (constant boiloff rate), boiloff tests were generally 6 to 8 hours. The boiloff rate was recorded using a wet flowmeter until the vent rate remained constant for two hours. The parameters that were recorded every half hour were vacuum chamber pressure, flowmeter gas inlet temperature and pressure, and test article pressure and temperatures.

b. Minus 1g Expulsion, Pressurization and Venting Tests - Pressurization and expulsion tests were run in the minus 1-g configuration following the fill and boiloff tests; this required removal of the test article from the vacuum chamber to invert the model. Since plumbing was involved, additional leak checking was required before beginning these tests to assure satisfactory system operation.

With the test article in the -1 g configuration, filling was accomplished through the pressurization/vent line. The tank was vented to the atmosphere through three lines: (1) outflow line, using SV4, (2) outer annulus pressure sensing line, using SV5, and (3) bulk region pressure sensing line, using SV6. A filled condition was indicated by monitoring liquid level sensors and pressure transducer recordings.

After the filling was complete, the tank was allowed to reach a thermal equilibrium and then the expulsion and pressurization tests were started. Fluid and tank wall temperatures were monitored to indicate thermal equilibrium.

To initiate the expulsion tests, the tank was first prepressurized to the desired tank pressure. Following the prepressurization, the pressure regulator was adjusted to the required setting and SV4 was opened to initiate outflow. Expulsion was complete when the liquid level sensor, DP9, inidcated gas.

To perform the venting demonstration, the steps for expulsion were followed as described above except that outflow was terminated when the desired liquid level was obtained. After closing SV4, the vent control system was activated and the simulated coast/vent period was monitored.
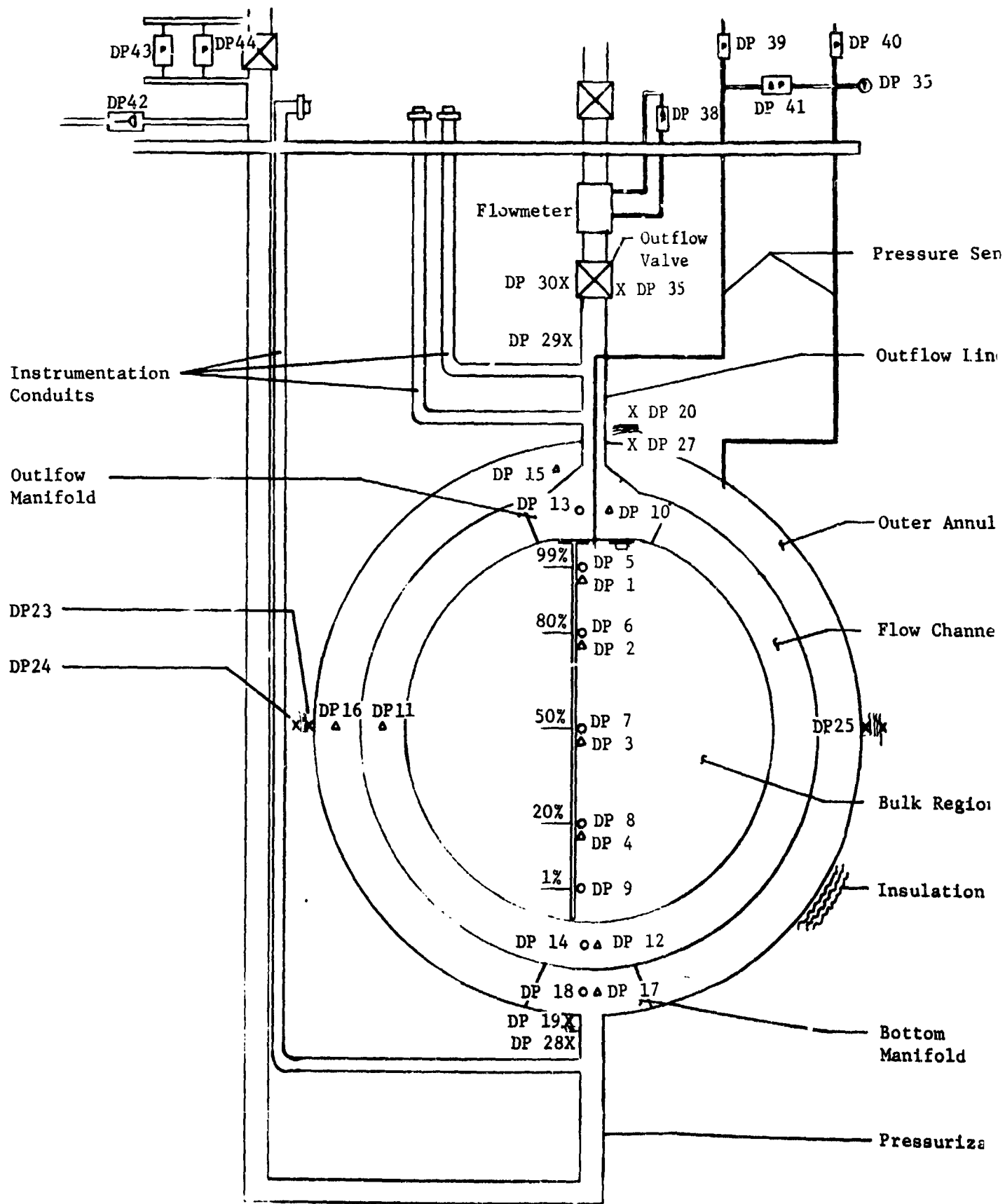
E.   INSTRUMENTATION

The test article instrumentation is shown schematically in Fig. III-15 and listed in Table III-6. The schematic shows the final configuration of the test article during the expulsion, pressurization, and venting tests.

Instrumentation consisted of five general sensor types: (1) thermocouples, (2) platinum resistance temperature sensors, (3) liquid level sensors, (4) pressure transducers, and (5) flowmeters. The sensor identification numbers are specified for each sensor (Fig. III-15 and Table III-6).

Thermocouples were selected to provide the majority of the test data because of their versatility and ease of installation. They were used for sensing temperature in areas where a high degree of accuracy was not a requirement. The thermocouples were made from 24-gage, Kapton-insulated chromel/constantan wire. For measuring tank wall temperature, five thermocouples were spot welded on the outside of the tank. Two were installed at the poles and three were located about 1.27 cm (1/2 in.) from the tank support brackets. Five insulation thermocouples were installed under the first layer of insulation opposite the tank wall thermocouples. Three other thermocouples were used to measure temperatures on the outflow valve body and coil and on the outflow line, approximately 10.2 cm (4 in.) from the tank.

Because a high degree of accuracy was desired at LH_2 temperatures, platinum resistance sensors were used to measure fluid temperatures inside the tank. Sensors with two temperature ranges were used; the first from 18.9°K to 30°K (34°R to 54°R) and the second from 12.8°K to 91°K (23°R to 164°R). Accuracy for these measurements was approximately 2% of the full range. A total of 10 platinum resistance sensors were located inside the tank. Four were located in the bulk region along the centerline of the tank. The height of the sensors corresponded to volumes of 20%, 50%, 80% and 99% of the bulk region volume. Two platinum sensors were

III-30

FOLDOUT FRAME

DP 39   DP 40

DP 35

DP 41

38

Pressure Sensing Lines

Outflow Line
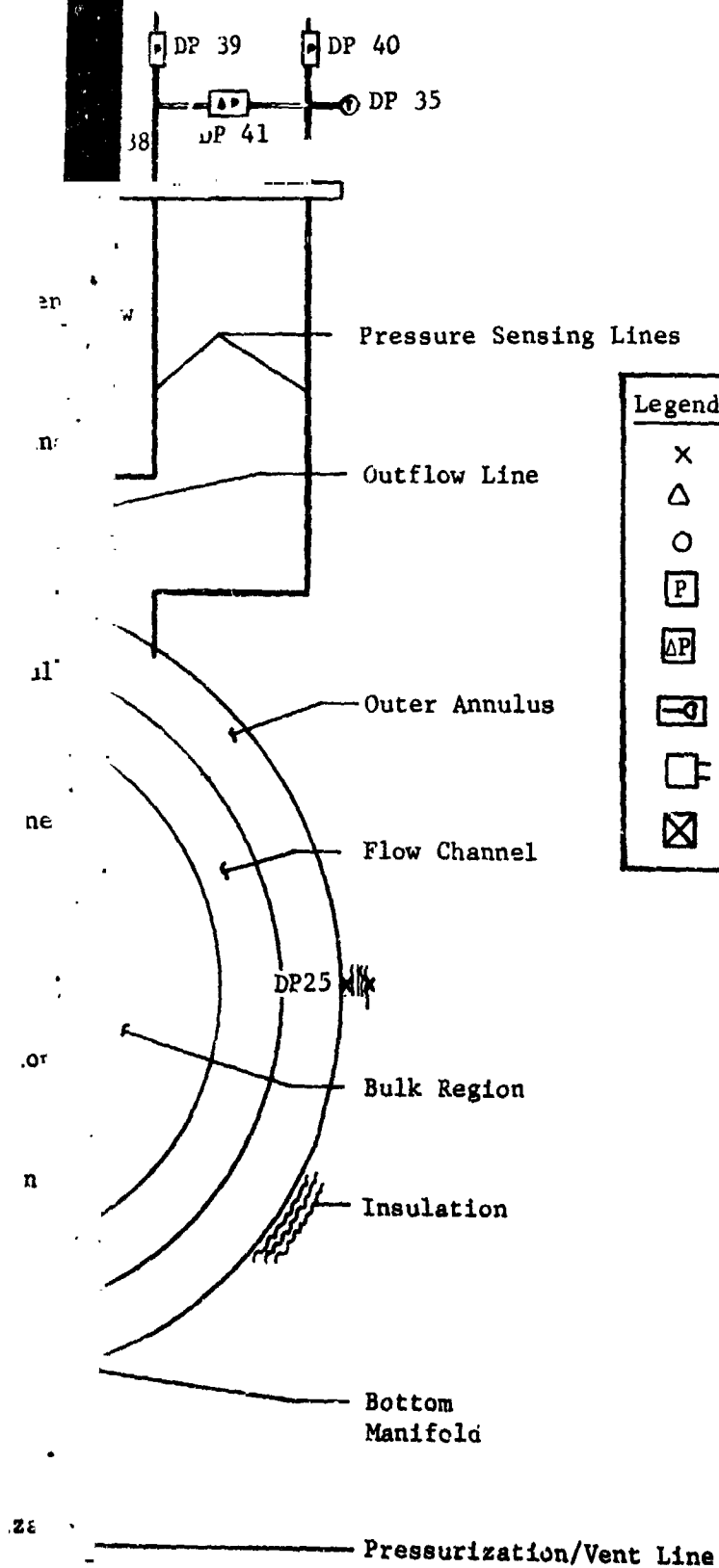
Legend:

✕	Thermocouples
△	Platinum Resistance Temperature Sensors
○	Liquid Level Sensors
[P]	Pressure Transducers
[ΔP]	Differential Pressure Transducers
[◁]	Gas Flowmeter
[□]	Annubar LH_2 Flowmeter
⊠	Valves

Outer Annulus

Flow Channel

DP25

Bulk Region

Insulation

Bottom
Manifold

Pressurization/Vent Line

Fig. III-15   Instrumentation Schematic for
Subscale LH_2 Model

III-31 and III-32

Table III-6 Test Article Instrumentation

Data Point Location*	Function	Sensor Type⁵
1	Liquid Temperature at Approximately 99% of Bulk Region Volume	A
2	Liquid Temperature at 80% of Bulk Region Volume	A
3	Liquid Temperature at 50% of Bulk Region Volume	A
4	Liquid Temperature at 20% of Bulk Region Volume	A
5	Liquid Level at Approximately 99% of Bulk Region Volume	B
6	Liquid Level at Approximately 80% of Bulk Region Volume	B
7	Liquid Level at Approximately 50% of Bulk Region Volume	B
8	Liquid Level at Approximately 20% of Bulk Region Volume	B
9	Liquid Level at Approximately 1% of Bulk Region Volume	B
10	Liquid Temperature Inside Outflow Manifold	A
12†	Liquid Temperature Inside Bottom Manifold	A
13	Gas/Liquid Phase Sensor Inside Outflow Manifold	B
14	Gas/Liquid Phase Sensor Inside Bottom Manifold	B
15	Liquid Temperature Top Vapor Annulus	A
16	Liquid Temperature Middle Vapor Annulus	A
17	Liquid Temperature Bottom Vapor Annulus	A
18	Gas/Liquid Phase Sensor at Bottom Vapor Annulus	B
19,21,23 25,27	Tank Wall Temperature	C
20,22,24,26,28	Insulation Temperature	C
29	Temperature Outflow Line	C
30	Temperature Outflow Valve (Coil)	C
31	Liquid Level Heat Exchanger, Top	D
32	Liquid Level Heat Exchanger, Middle	D
33	Liquid Level Heat Exchanger, Bottom	D
34	Flow Temperature at Heat Exchanger Exit	C
35	Temperature Outflow Valve (Body)	C
38	Outflow Meter Differential Pressure	E
39	Bulk Region Pressure	F
40	Vapor Annulus Pressure	F
41A	Communication Screen Differential Pressure	G
41B	Communication Screen Differential Pressure	G
42	Pressurant Flowrate	H
43	Flow Orifice Pressure Differential	I
44	Flow Orifice Pressure Differential	J
46	Heat Exchanger Pressure	F

*See Fig. III-15.

†DP11 was eliminated.

§The Sensor types are as listed:

A	Platinum Resistance Temperature Sensor, Rosemount Engineering Company, P/N 146L
B	Liquid Level Sensor, United Control Corporation, P/N 2641
C	Chromel/Constantan Thermocouple, Thermo-Electric Company, Inc.
D	Liquid Level Sensor, Cryogenic Research Company, Inc., Model LP-10R
E	Differential Pressure Transducer, ±5 psid, Statham Instruments, Inc., Model PM60TC±5-350
F	Pressure Transducer, 0 to 50 psia, Taber Instruments Division, Model 187
G	Differential Pressure Sensors, Rosemount Engineering Company, Model 861L1
H	Flowmeter, 0.1 to 1 gpm, Ramapo Instrument Company, Inc., Model J-1/2-SS14
I	Differential Pressure Transducer, ±10 psid, Statham Instruments, Inc., Model PM60TC±10-350
J	Differential Pressure Transducer, ±1 psid, Statham Instruments, Inc., Model PM60TC±1-350

located inside the manifolds and another sensor was installed inside one of the flow channels approximately at the equator. Temperatures in the outer annulus volume were recorded at the fololwing locations: (1) outside the outflow manifold; (2) at approximately the tank equator; and (3) outside the bottom manifold.

The liquid level sensors selected were the hot-wire type made by United Control Corporation. The selection was based primarily on previous experience which proved this sensor to be very reliable with a fast response. The fast response was particularly important because of the relatively short outflow periods. These sensors were also required to determine when gas was ingested into the liquid flow channels. A total of eight sensors were used. The two most critical locations were inside the two manifolds. One sensor was located in the outer annulus on the outside of the bottom manifold and sensed residual liquid in the outer annulus. The remaining five sensors were located in the bulk region along the centerline of the tank. Of the five, four were located approximately 1.27 cm (1/2 in.) above the platinum resistance temperature sensor. The fifth sensor, DP9, was located approximately 1.02 cm (1/2 in.) above the bottom manifold.

Two types of pressure transducers were used. One type measured absolute total pressure and the second measured differential pressure. Two 0 to 35 N/cm^2 (0 to 50 psi) atmosphere, strain-gage pressure transducers, DP39 and DP40, measured the outer annulus and bulk region pressures. The differential pressure between the outer annulus and bulk region was measured using a Rosemount Engineering transducer, DP41, with a range of ±0.069 N/cm^2 (±0.1 psi) and an accuracy of better than 1%. A second similar transducer was connected in parallel with DP41 as part of the vent control system. A strain-gage differential pressure transducer was used to measure differential pressure for the flowmeter in the outflow line, DP38.

The flowmeter that measured the outflow rate was an annubar flow element. The flowmeter was installed in the outflow line approximately 30.5 cm (12 in.) from the tank. All the pressure and thermocouple temperature data were recorded on Bristol recorders. Data from the platinum temperature sensors and liquid level sensors were recorded on a Honeywell Visicorder oscillograph.

F.   TEST RESULTS

Results from the 63.5-cm (25 in.) diameter subscale model test
program are presented in this section. The 9-week program in-
cluded boiloff tests to determine heat leak into the system and
operational tests to evaluate system fill, outflow, pressur·zation,
and venting characteristics. The test period also included the
time required to repair leaks.

1.   Boiloff Test Results

For this subscale model there were no specific design and iabrica-
tion requirements for thermal protection, i.e., insulation and
tank penetration heat leaks. Because the main objectives oi the
program did not involve thermal protection design, the insulation
and tank penetration design techniques were those normally used for
cryogenic test models rather than those normally used for flight-
qualified cryogenic tanks.

The heat flux values achieved using this approach are presented in
Table III-7. A total of four tests were conducted. The first two
tests were run with the test article in a + 1-g orientation, i.e.,
with the outflow line at the bottom and pressurization/vent line
on top. Because this was the first model test and safety procedures
called for initial system checkout tests with a less hazardous
fluid, the first boiloff test was conducted with liquid nitrogen.
Successful checkout tests were achieved and a heat flux value of
5.04 W/cm^2 (1.6 Btu/hr-ft^2) was obtained after an 8-hr test. The
second test, using LH_2, resulted in a 9.76 W/cm^2 (3.1 Btu/hr-ft^2),
which is consistent with the Test 1 value using LN_2. However,
the Test 2 value is 1.7 to 1.4 times greater than the values for
Tests 3 and 4, respectively.

The relatively high heat fluxes in Tests 1 and 2 were attributed
to three instrumentation cables that were inadvertently left un-
insulated. Following Test 2 when the test article was removed
from the chamber and rotated to the -1 g orientation, the three
cables were insulated with 10 layers of aluminized Mylar. In the
following test, Test 3, a heat flux of 5.67 W/cm^2 (1.8 Btu/hr-ft^2)
was obtained.

Table III-7 Boiloff Test Results

Test No.	Test Fluid	Tank Orientation	Heat Flux, W/cm^2 (Btu/ft^2hr)	Comments
1	LN_2	+1g	5.04 (1.6)	For Tests 1 and 2, high heat flux values were caused by three uninsulated instrumentation cables.
2	LH_2	+1g	9.87 (3.1)	
3	LH_2	-1g	5.67 (1.8)	The reduced heat flux was due to insulating the cables with 10 layers of aluminized Mylar.
4	LH_2	-1g	6.93 (2.2)	Following Test 3, the electrical connectors leaked and were replaced with 1.27-cm (1/2-in.) diameter stainless steel conduits. These conduits accounted for the increased heat flux value.

The increase in heat flux between Tests 3 and 4 was caused by replacing the three electrical connectors on the tank with 1.27-cm (1/2 in.) OD stainless steel conduits. During the first series of pressurization and outflow tests, the electrical connectors began leaking into the vacuum chamber. Testing was suspended for 10 days to repair the leaks. Repairs involved removing the three leaking connectors and replacing them with 4.3- to 4.9-m (14- to 16-ft) long conduits. The boiloff test (Test 4) was conducted before resumption of the pressurization and outflow tests.

The final heat flux value of 6.93 W/cm^2 (2.2 Btu/hr-ft^2) is considered relatively high for current state-of-the-art insulation techniques. However, this value does not affect the results of the other tests. On the contrary, it demonstrates that the DSL concept can operate satisfactorily under heat fluxes 2.3 times greater than the heat leak value used during the Phase A design effort.

2.   Fill Test Results

All fill tests were conducted with the test article in the +1-g orientation. Liquid entered the tank through the outflow line

at the bottom following the series of purges to remove all inert gases. The liquid level sensors were monitored and the time required to cover each sensor was recorded. A successful fill was achieved when all the level sensors including sensor DP14 in the top manifold, indicated liquid (Fig. III-15).

Results of the successful fill tests are presented in Table III-8. The first liquid nitrogen fill test, was accomplished in approximately 10 minutes at an average rate of 12.9 ℓ/min (3.4 gpm). The tank walls were precooled with LN_2 before fill was initiated.

Table III-8 Fill Test Results

Test No.	Test Fluid	Tank Walls	Fill Rate lpm (gpm)	Fill Time, min	Comments
1	LN_2	Cold	12.9 (3.4)	10	Successful fills were obtained under all conditions. The best approach when using LH_2 is to subcool it in the dewar before filling and then to fill at a low rate.
2	LH_2	Warm	3.4 to 4.9 (0.9 to 1.3)	25	
3	LH_2	Cold	7.6 (2.0)	17	
4	LH_2	Cold	2.3 to 3.0 (0.6 to 0.8)	45	

Tests 2 through 4 were conducted with liquid hydrogen at various fill rates. For Test 2, the tank walls were initially at ambient temperature, approximately 280°K (500°R); whereas, in Tests 3 and 4 the walls were initially at an approximate LH_2 temperature.

The two parameters that affected filling of the tank with LH_2 were the fill rate and the condition of the liquid as it entered the tank. The liquid could enter the tank as either saturated or subcooled LH_2.

In the initial LH_2 fill tests, rates approximately 2.5 times greater than those for Test 2 were attempted. At these high fill rates, liquid was forced out of the tank through the vent line before a successful fill condition was achieved. Because of the low density and viscosity of LH_2, the liquid entering through the bottom manifold would flow upward through the channels and reach the top manifold before the liquid level in bulk region reached the 50% level. This would wet the channel, top manifold, and outer liner screens and seal the bulk ullage. Without being able to vent the bulk ullage, liquid entering the tank is then diverted to the outer annulus and out through the vent line.

At the lower fill rates, the gas/liquid interface in the channels remained at approximately the same height as that in the bulk region. This kept the channel, top manifold and outer liner screens dry and allowed purging of the bulk ullage. To operate as designed the two screens in the top manifold must remain dry until the bulk region and top manifold are filled. The lower fill rates were achieved by reducing dewar pressure during fill.

Dewar pressurization was accomplished using two methods. The first method used a heat exchanger to heat and vaporize the liquid. The heat addition and vaporization raised the dewar pressure to the desired level. The second preferred method pressurized the dewar by bubbling gaseous helium through the liquid. The method not only achieved the required dewar pressure level, but also provided the desired subcooled liquid condition. Using the first method, liquid entering the tank was always saturated. Bulk region and outer annulus filling was accomplished using saturated LH_2; however, filling to the top manifold could not be completed as indicated by the liquid level sensor, DP14. The residual heat in the top manifold was sufficient to vaporize the saturated liquid. By using subcooled LH_2, the residual heat would increase the liquid temperature instead of generating vapors. The degree of subcooling that was achieved as indicated by the platinum temperature sensors was 1.65 to 2.2°K (3 to 4°R).

The results show that tank filling can best be accomplished by using a low fill rate and subcooling the liquid in the dewar prior to filling. In Table III-8, Tests 2 through 4 represent three successful LH_2 fill tests using this fill procedure.

3. Minus 1 g Expulsion and Pressurization Tests Results

These tests and the venting tests (discussed in Subsection 4) are considered to be the most significant tests conducted during the experimental verification program and represent a comprehensive evaluation of the cryogenic acquisition/expulsion system under a normal 1 g condition. The following parameters were varied during the tests:

1) tank pressure;

2) location of pressurization port;

3) type of pressurant;

4) pressurant entering temperature;

5) number of expulsion events.

III-38

Before presenting the results of the minus 1 g expulsion and pressurization tests, a discussion is required to identify the criteria for a successful test and to describe how the test data will be used to interpret the results. For a successful test, the flow channel screens must remain hydrostatically and thermally stable during the expulsion period. Any breakdown of these screens would allow gas to ingest into the liquid flow channels, which is considered an operational failure of the acquisition/ expulsion device.

During outflow, monitoring of the flow channel stability is accompl⁴ished using the liquid level sensor (DP13) located in the outflow manifold. Minor breakdowns, where several bubbles are intermittently ingested, are detected on sensor DP13 as rapid oscillations between a liquid and a gas indication. A major screen breakdown occurs when there is a steady flow of gas into the flow channels that terminates liquid expulsion. This failure mode is recorded on DP13 as a continuous indication of gas.

With DP13 used to indicate breakdown in the flow channels, the other liquid level sensors are used to monitor liquid expulsions. The liquid level sensors are uncovered in sequence to indicate gas during a normal minus 1 g expulsion.

As expulsion is initiated, liquid is first forced from the outer annulus. The outer annulus is considered to be empty when the liquid level is below the bottom screen of the bottom manifold. A small amount of liquid remains in the outer annulus, as indicated by sensor DP18, which cannot be expelled due to the loss of communication between the remaining liquid and the screen.

The first two sensor indications that the outer annulus is empty are: (1) the top level sensor in the bulk region, DP5, indicates gas and (2) the pressure differential between the outer annulus and bulk region reaches a peak value that is slightly above the bubble point of the screen liner. At this time, all other liquid level sensors in the bulk region and manifolds indicate liquid. As outflow continues, the remaining bulk region liquid level s .sors uncover in the following sequence, DP6, DP7, DP8, and finally DP9. When DP9 indicates gas, the expulsion of the tank is complete an   low and pressurization is stopped. The liquid remaining in the channels and manifolds cannot be expelled. From Table III-2, the expellable liquid volume for the test article is approximately 91.3% of the total tank volume. The liquid volume that cannot be expelled is primarily the 0.0093 m³ (0.329 ft³) contained in the channels and manifolds.

Evaluation of the communication screen liner during minus 1 g expulsion and pressurization was an important part of the test program. The differential pressure history across this liner and its ability to remain wet during pressurization and expulsion were evaluated.

Initially, the differential pressure across the liner ($\Delta P_{s\ell}$) that is recorded by DP41 is either zero or slightly greater than zero. As expulsion is initiated and the liquid level in the outer annulus begins to decrease, $\Delta P_{s\ell}$ starts to increase and reaches a maximum value when the outer annulus is empty. The maximum $\Delta P_{s\ell}$ value is equal to or slightly greater than the bubble point of the screen, which is approximately 0.055 N/cm^2 (0.08 psi). As the outer annulus is emptied, pressurant flows into the bulk region and expulsion of the bulk region begins. The $\Delta P_{s\ell}$ begins to drop consistent with the decrease in the height of the bulk liquid.

During expulsion, $\Delta P_{s\ell}$ should always be a positive value unless the screen liner dries out. If the screen liner dries out, $\Delta P_{s\ell}$ will drop to zero and the bulk liquid will flow into the outer annulus. This condition is not considered a failure mode and will not affect liquid expulsion. The minus 1-g expulsion continues with the liquid levels in the bulk region and outer annulus equal until sensor DP9 is uncovered. After pressurization is terminated, the outer liner is designed to rewick and reestablish a stable configuration.

A summary of the 10 tests conducted with the subscale model is presented in Table III-9. With the exception of Test 9, the model successfully outflowed 100% of the expellable liquid. In Test 9, 97% of the expellable liquid was outflowed before channel breakdown occurred. Additional discussion of Test 9 is presented later in this subsection. For Test 10, LH$_2$ was expelled in four short expulsion periods. The periods between the expulsion events were 5 to 10 minutes during which the conditions inside the tank were monitored without venting.

III-40

Table III-9   Minus 1-g Expulsion and Pressurization

Test No.	Tank Pressure, N/cm²	(psi)	Pressurization Port Location	Gas	Temp °K	(°R)	No. of Expulsion Events	Expellable Liquid Outflowed	Comments
1	13.8	(20)	Bottom	GH₂	89	(160)	1	100%	For all tests except 9, outflow was successfully achieved, by pressurizing through the diffuser in the tank bottom. Test 9 imposed severe pressurization conditions because the pressurant impinged directly on the screens. In Test 10, the periods between expulsion events were 5 to 10 minutes without venting. The ullage temperatures ranged between 21.1 to 30°K (38 to 54°R), except for Tests 4 and 9 where they were between 21.1 to 51°K (38 to 92°R).
2	17.3	(25)			86.1	(155)			
3	24.2	(35)			90.6	(163)			
4	31.0	(45)			94.4	(170)			
5	17.3	(25)			288.9	(520)			
6	13.8	(20)		GHe	83.3	(150)			
7	17.3	(25)			83.3	(150)			
8	17.3	(25)			27.8	(500)			
9	17.3	(25)	Top	GH₂	83.3	(150)		97%	
10	15.2 to 22.1	(22 to 32)	Bottom	GH₂	83.3	(150)	4	100%	

Results of the first four tests are presented in Fig. III-16 through III-27. The curves show histories of the tank pressure, fluid temperatures, liquid level sensors, and screen liner ΔP. The pressure histories (and therefore liquid outflow rates) in the first three tests were relatively steady. During Test 4, variations in tank pressure were caused by pressure regulator adjustments and premature depletion of the pressurant supply. Regardless of the inability to maintain a steady pressure of 31 N/cm² (45 psi) atmosphere, the test successfully demonstrated the outflow capability of the system at a high tank pressure. The average outflow rate resulting from this test was 0.0024 m³/sec (0.088 ft³/sec), which was the maximum obtained during all of the tests. For Tests 1, 2 and 3, the average LH₂ outflow rates were between 0.001 and 0.0012 m³/sec (0.036 to 0.045 ft³/sec). The pressurant flow rates listed for all but one of the tests represent the average values as measured by the Ramopo flowmeter. For Test 1 the pressurant flow rate was not recorded due to a malfunction of the recorder.

The fluid temperature histories for the first three tests were very consistent. The majority of the temperatures were within a range of 20 to 22°K (36 to 40°R). As illustrated by Figs. III-20 and III-23, one noticable effect was that the top ullage temperature began to increase slightly with an increase in tank pressure. In Test 4, a significant increase in three temperatures (DP15, DP16, and DP17) occurred. After about 30 sec, these temperatures increased from approximately 22°K (39.6°R) to 45°K (83°R). This difference between the temperature histories of
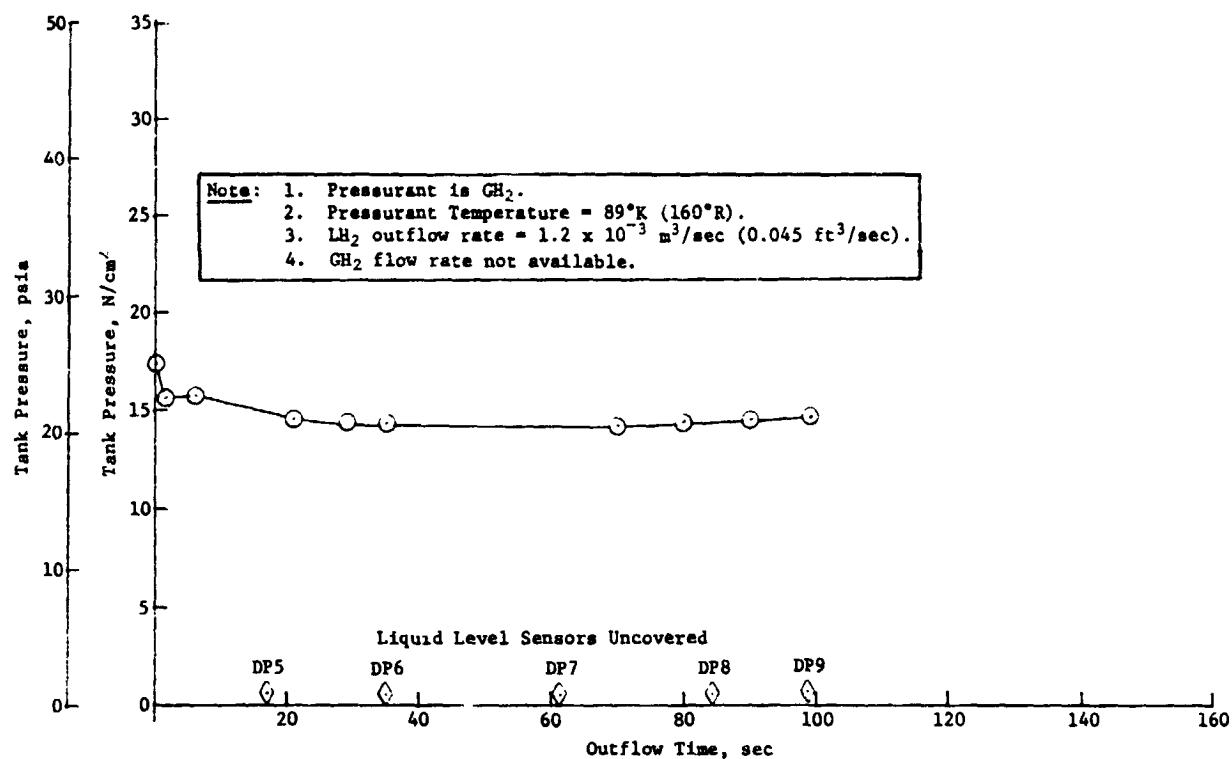
III-41

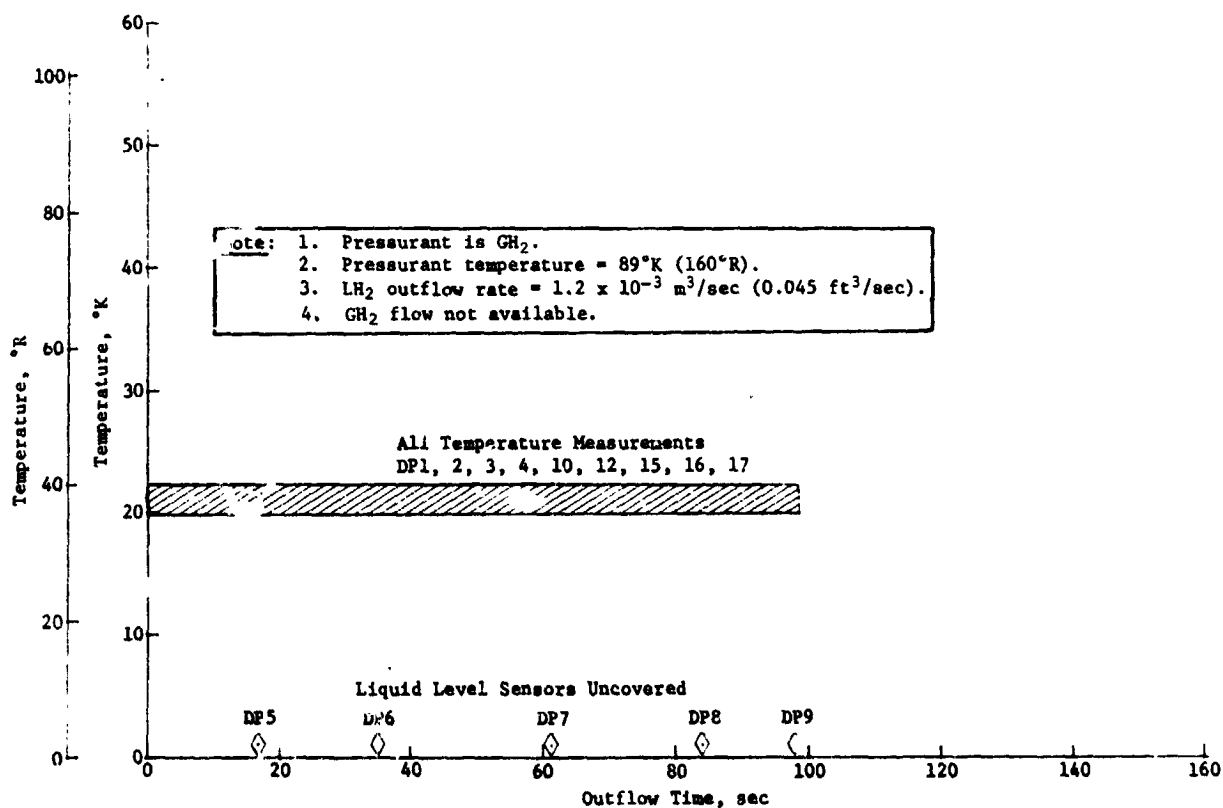Fig. III-16 Pressurization and Outflow Test Results, LH₂ Tank Pressure History, Test 1

Fig. III-17 Pressurization and Outflow Test Results, LH₂ Tank Temperature Histories, Test 1
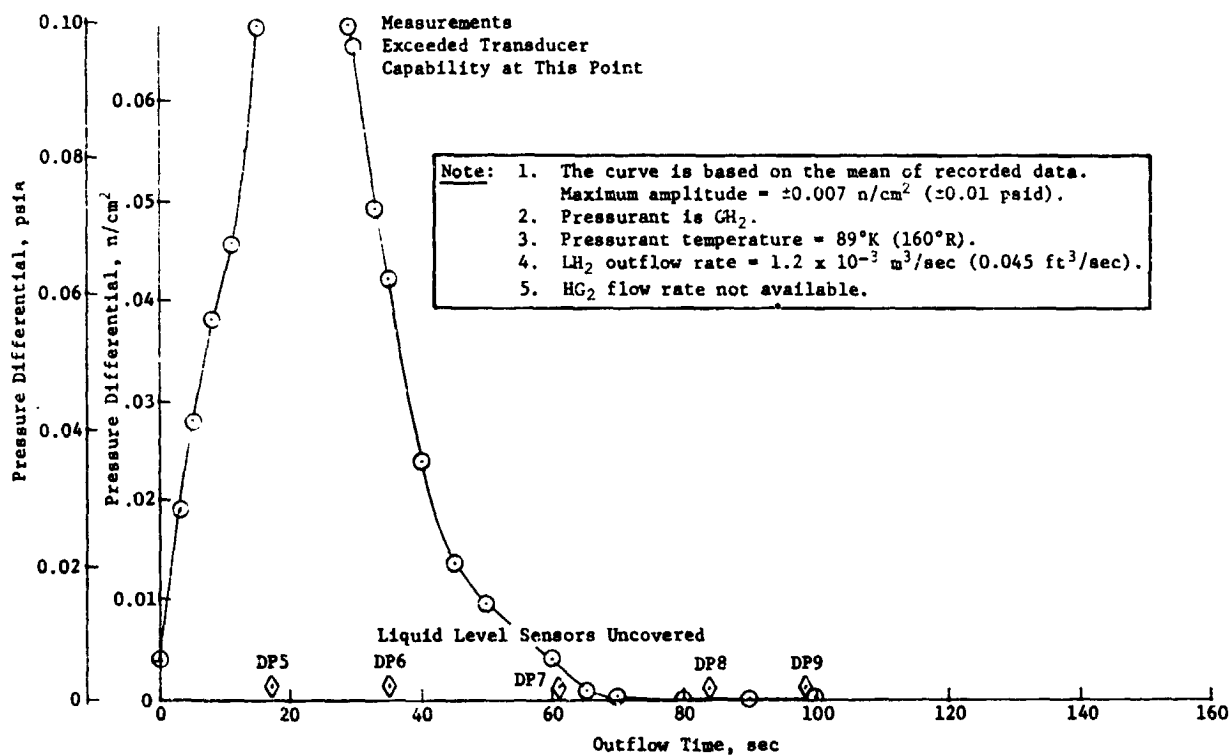
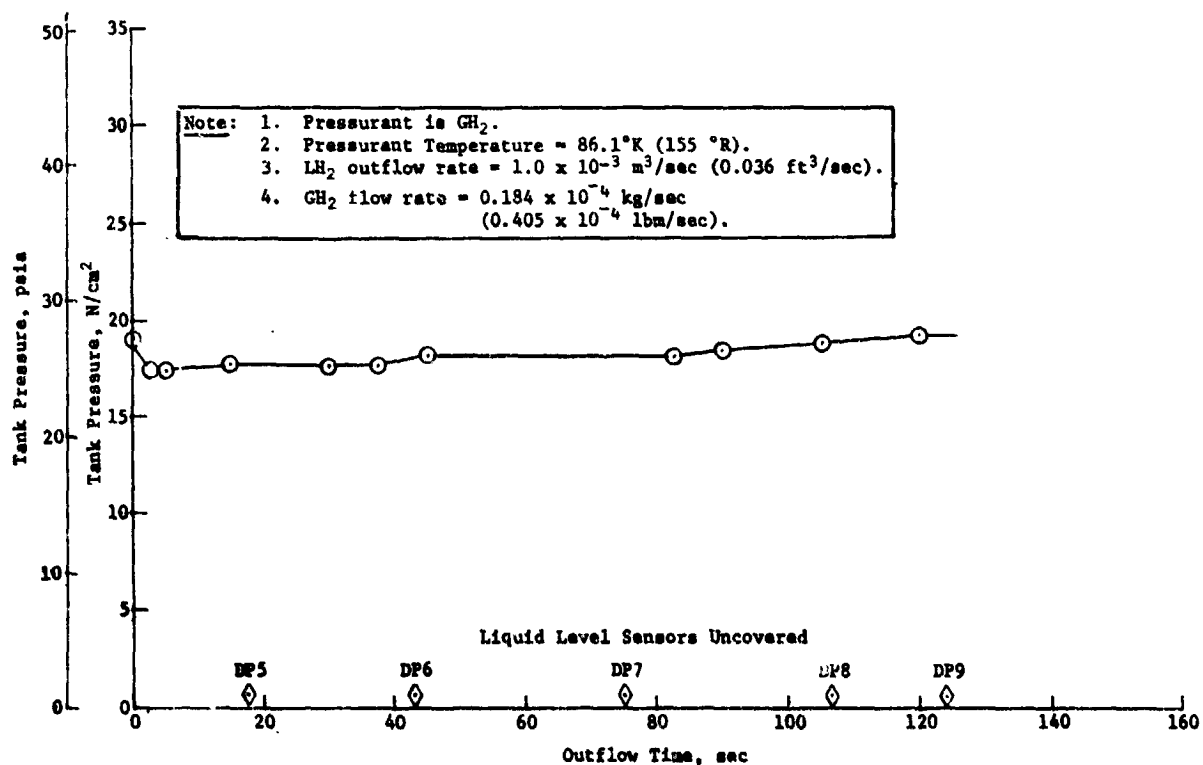Fig. III-18 Pressurization and Outflow Test Results, Vapor Annulus-Bulk Region Pressure Differential, Test 1

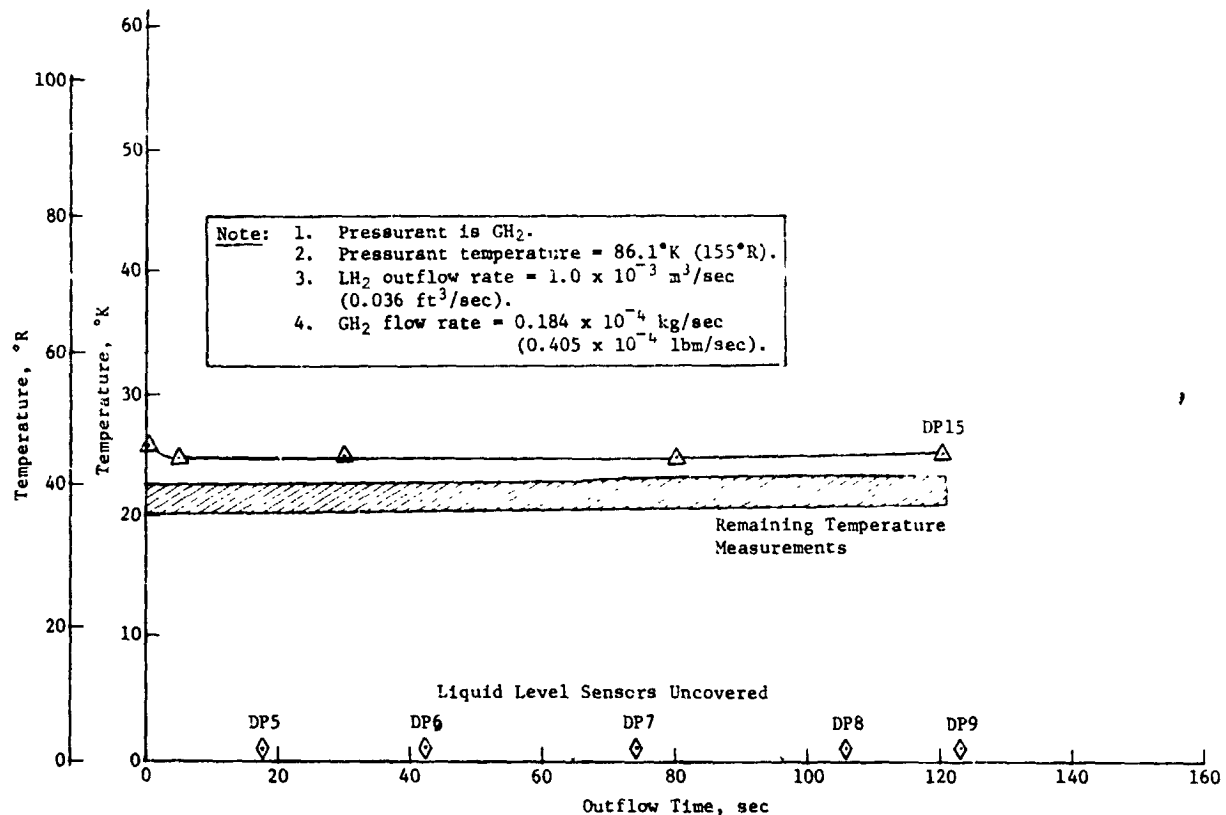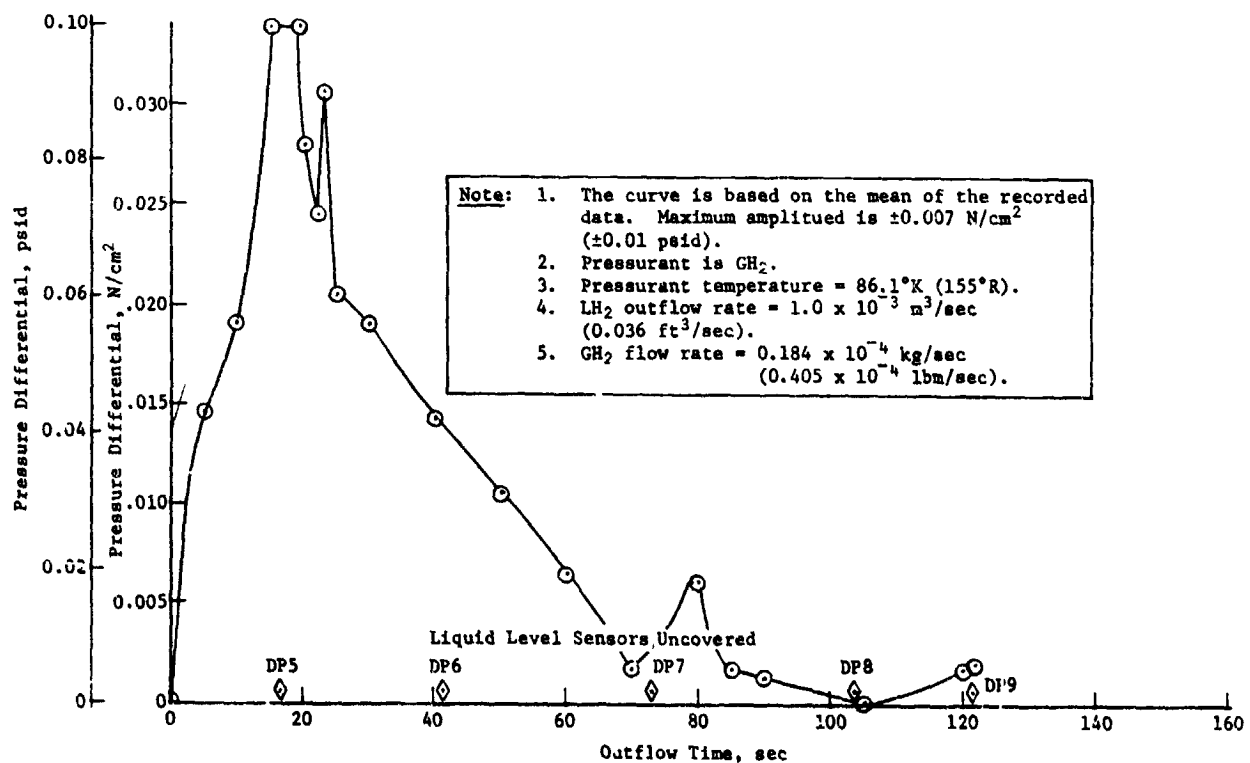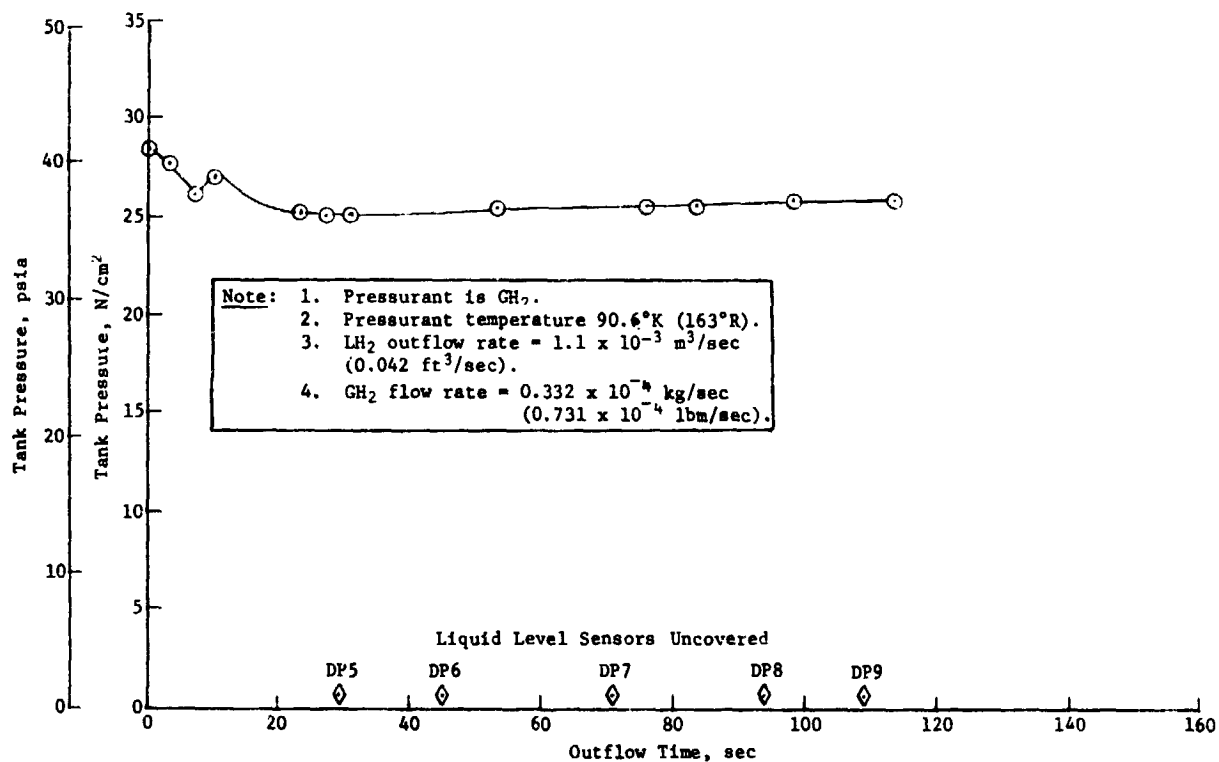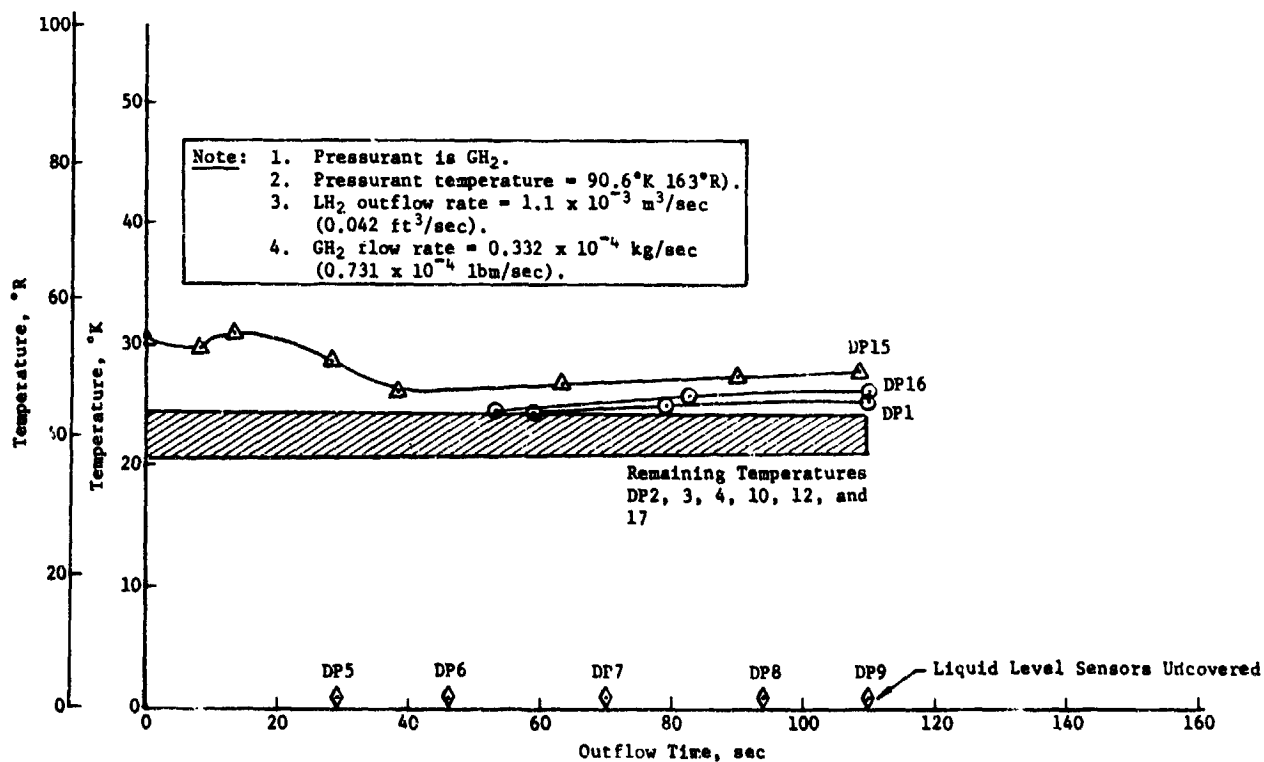Fig. III-19 Pressurization and Outflow Test Result, LH₂ Tank Pressure History, Test 2

III-43

Fig. III-20 Pressurization and Outflow Test Results, LH₂ Tank Temperature Histories, Test 2

Fig. III-21 Pressurization and Outflow Test Results, Vapor Annulus-Bulk Region Pressure Differential, Test 2

III-44

Fig. III-22 Pressurization and Outflow Test Results, LH$_2$ Tank Pressure History, Test 3

Fig. III-23 Pressurization and Outflow Test Results, LH$_2$ Tank Temperature Histories, Test 3
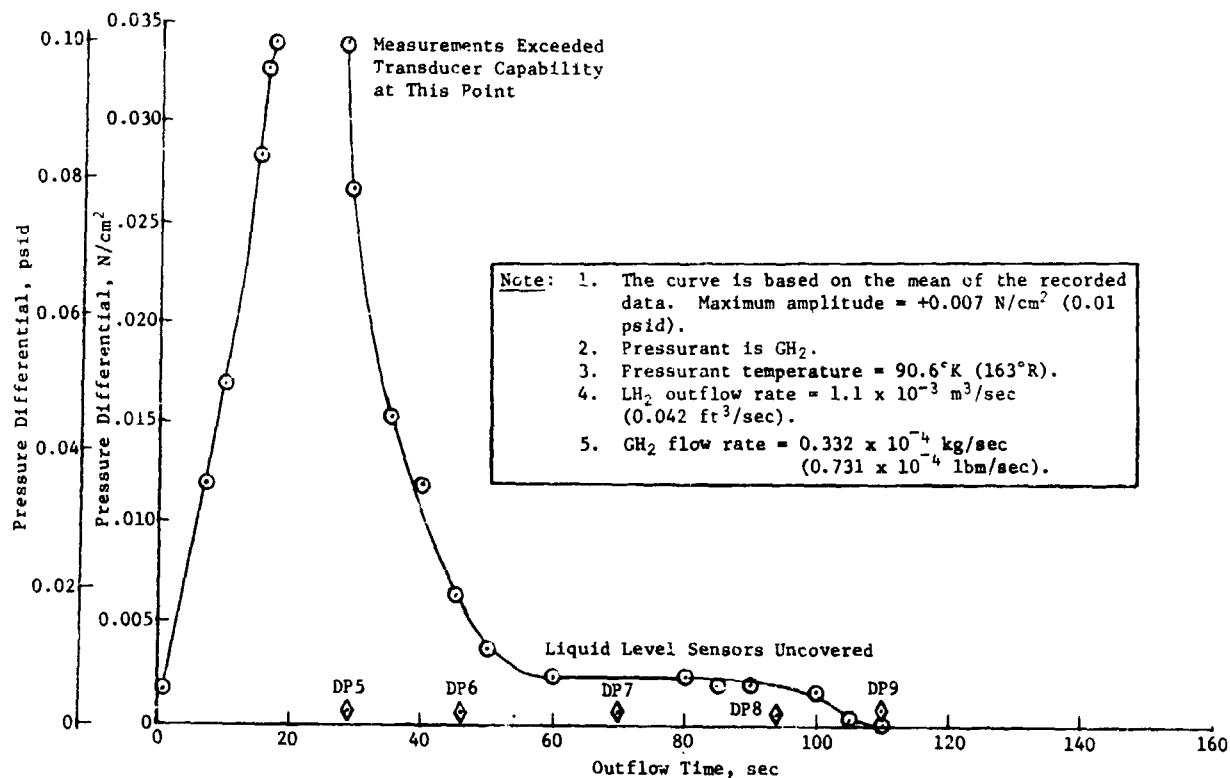
III-45

Fig. III-24 Pressurization and Outflow Test Results, Vapor Annulus-Bulk Region Pressure Differential, Test 3

Fig. III-25 Pressurization and Outflow Test Results, LH$_2$ Tank Pressure History, Test 4

III-46

Fig. III-26 *Pressurization and Outflow Test Results, LH₂ Tank Temperature Histories, Test 4*

Fig. III-27 *Pressurization and Outflow Test Results, Vapor Annulus-Bulk Region Pressure Differential, Test 4*
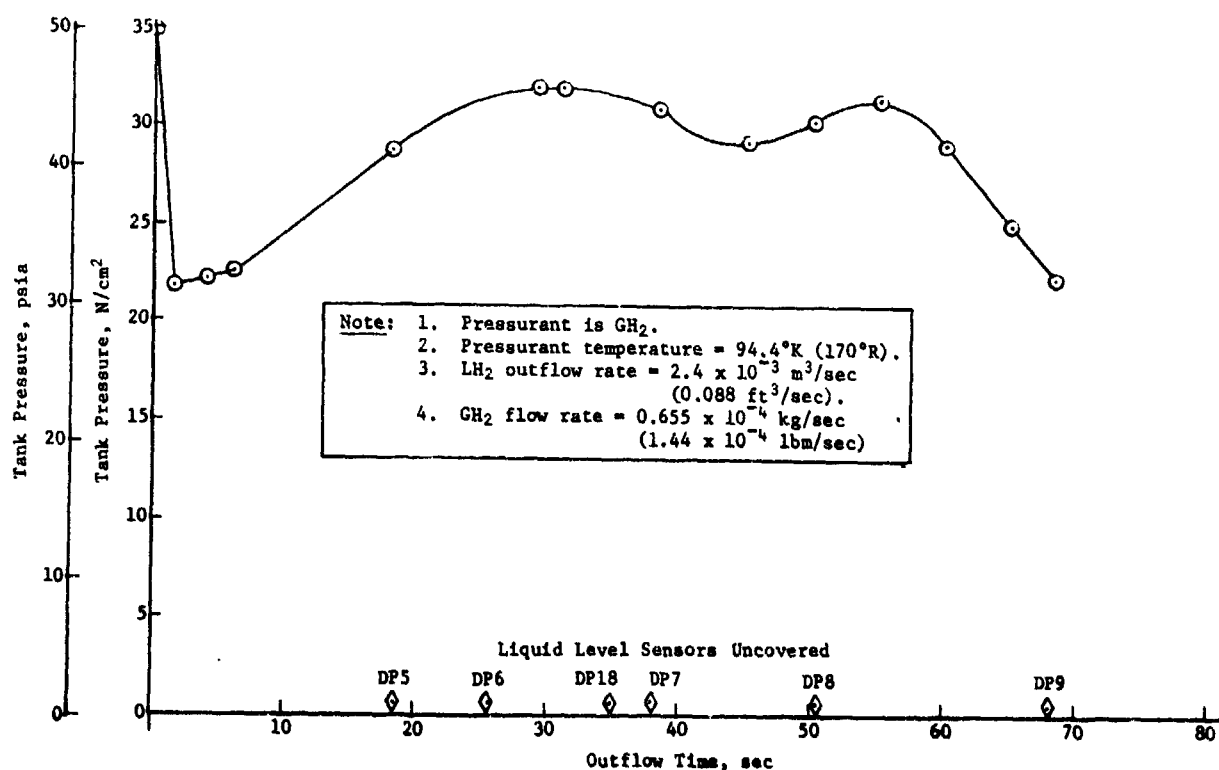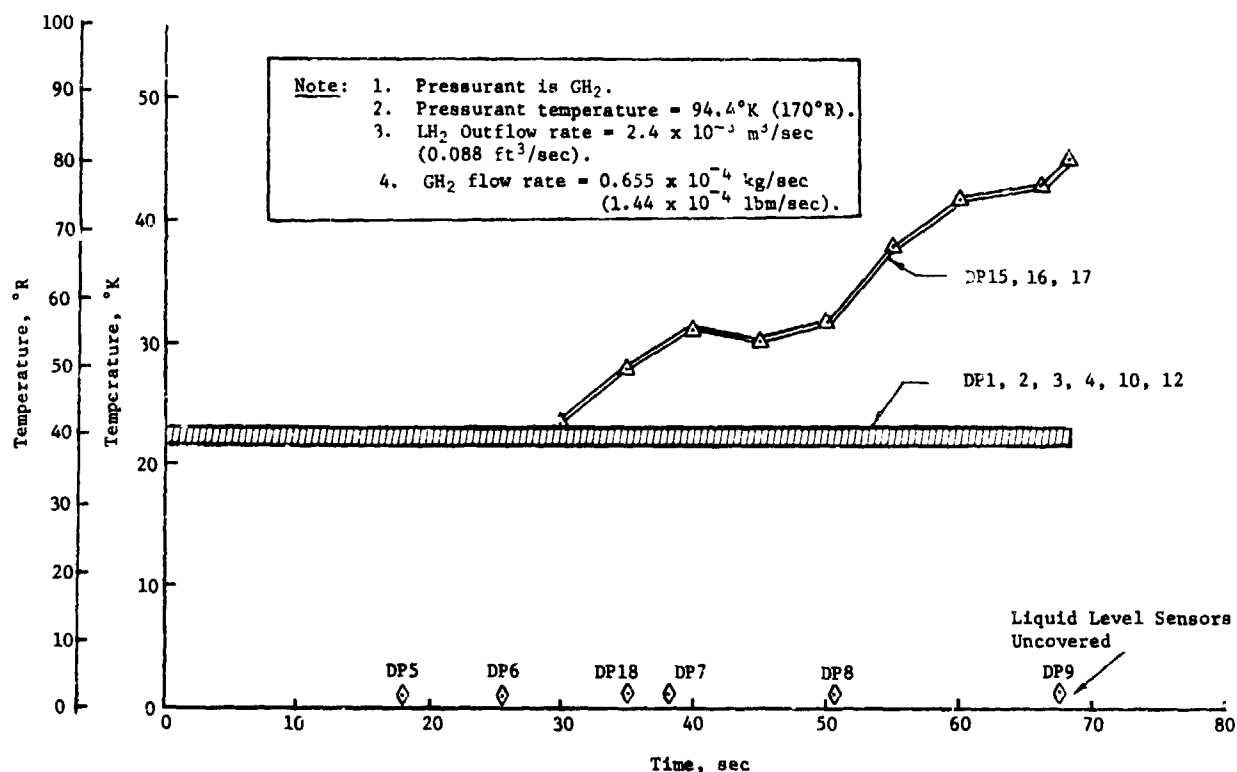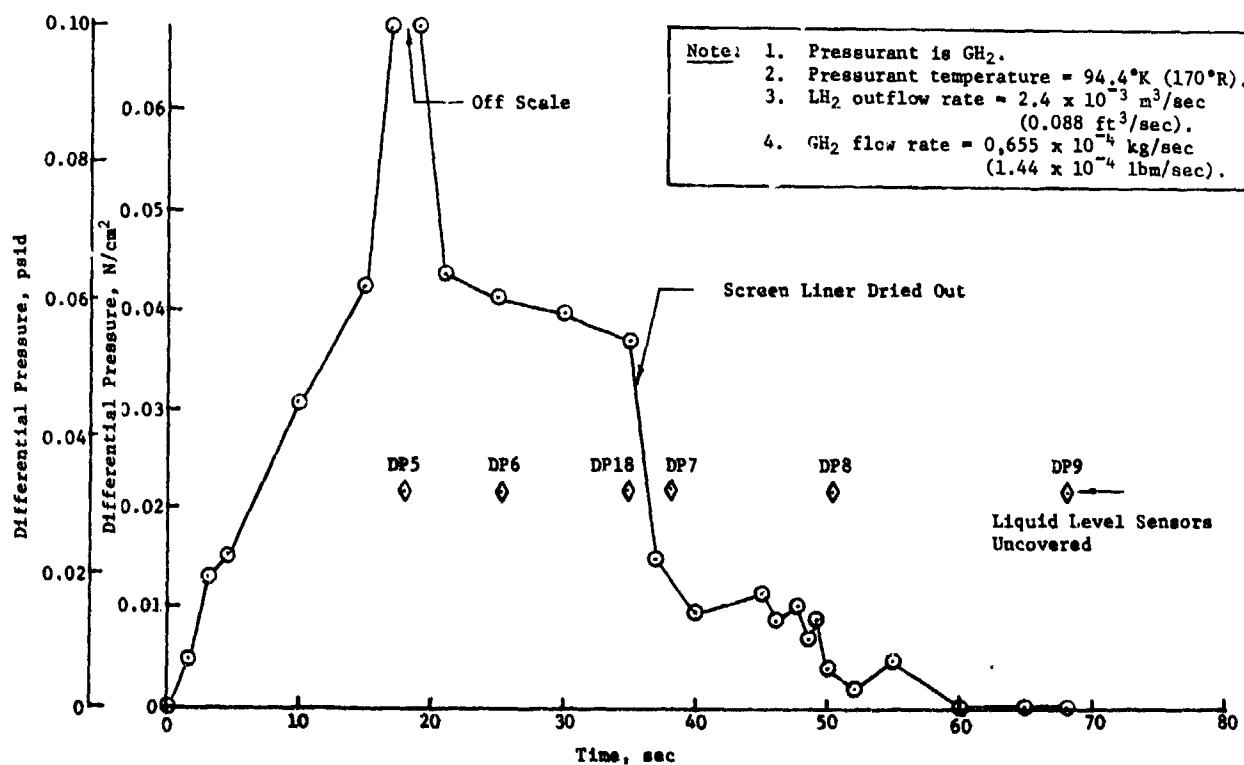
Test 4 and those of the first three tests is related to the
amount of liquid remaining in the outer annulus. In the first
three tests, as previously mentioned, there was a small amount of
liquid remaining in the outer annulus that could not be expelled.
This amount of liquid cooled the pressurant gas as it entered
through the submerged diffuser. In Test 4, the residual liquid
in the outer annulus was depleted due to the high pressurant inflow
rate. This was verified by sensor DP18 indicating gas after ap-
proximately 35 sec. Without this residual liquid to cool the
pressurant, the three ullage temperatures increased as shown in
Fig. III-26.

In the first four tests, the communication screen liner performed
generally as expected. Figures III-18, III-21, III-24, and
III-27 all show $\Delta P_{s\ell}$ increasing to its maximum value, which was
greater than 0.069 N/cm^2 (0.1 psi), and then decreasing to zero,
indicating screen liner dryout. In all four tests, the times
at which the peak $\Delta P_{s\ell}$ occurred was consistent with the times
that DP5 indicated gas. During all of these tests, screen liner
dryout was observed and was most evident in Test 4 after sensor
DP18 was uncovered (Fig. III-27).

The effect of increasing the pressurant entering temperature is
not significant as shown by the results of Test 5 in Fig. III-28
thru III-30. Both the fluid temperature histories and the $\Delta P_{s\ell}$
history are similar to the results of Test 2. The most apparent
reason for the lack of any noticeable difference is the cooling
of the pressurant by the residual liquid in the outer annulus.
Without this residual liquid, there would have, in all probability,
been a significant increase in fluid temperatures between Test
2 and Test 5.

A comparison between the results of Tests 6 through 8 and the
results from Tests 1, 2 and 5 does not show a significant dif-
ference in hydrogen and helium pressurization. The results of
the helium pressurization tests are presented in Figs. III-31
through III-39 for Tests 6 through 8. The fluid temperatures
in the helium pressurization tests were approximately the same
as those in the hydrogen pressurization tests. The only noiticeable
differences between the two pressurants appears in the $\Delta P_{s\ell}$
histories. For the GHe pressurant tests, the maximum $\Delta P_{s\ell}$ is
less than that of the GH$_2$ tests and $\Delta P_{s\ell}$ also goes to zero much
faster with GHe than it does with GH$_2$. Both of these effects

III-48

Fig. III-28 Pressurization and Outflow Test Results, LH₂ Tank Pressure History, Test 5

Fig. III-29 Pressurization and Outflow Test Results, LH₂ Tank Temperature Histories, Test 5

III-49

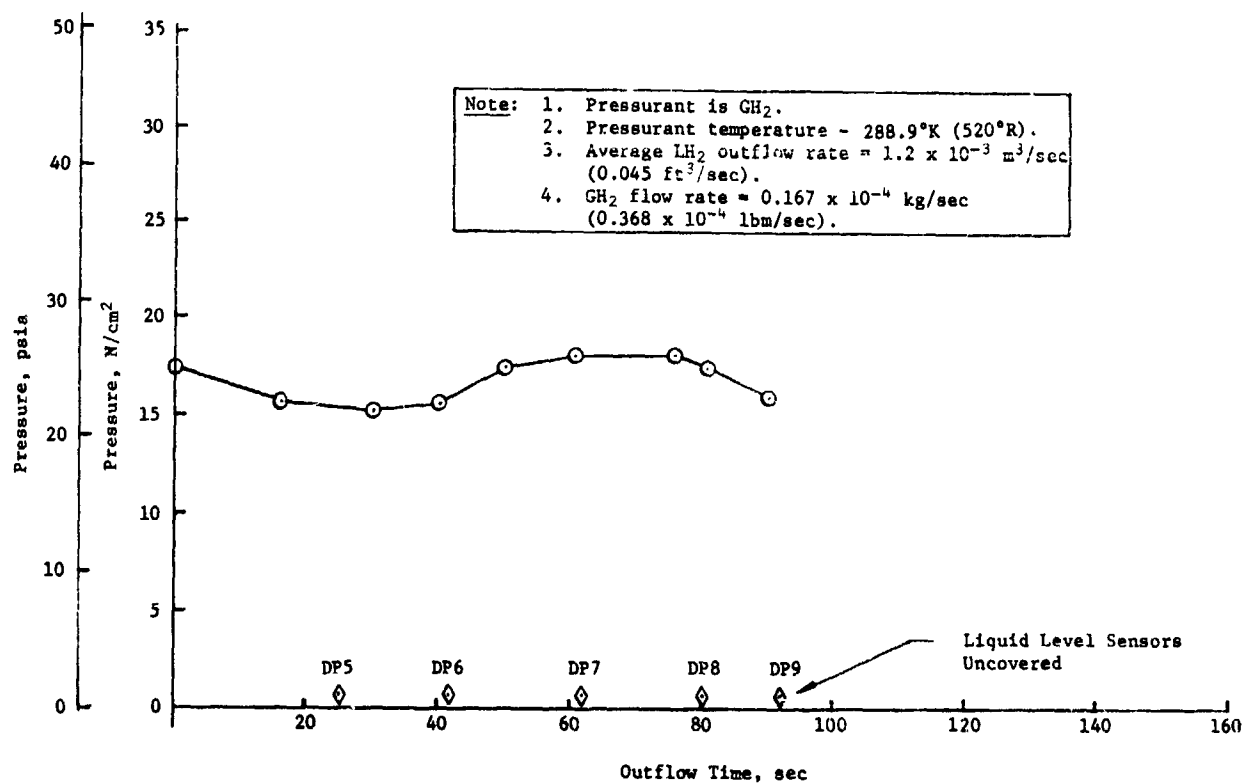Fig. III-30 Pressurization and Outflow Test Results, Vapor Annulus-Bulk Region Pressure Differential Test 5

Fig. III-31 Pressurization and Outflow Test Results, LH₂ Tank Pressure History, Test 6

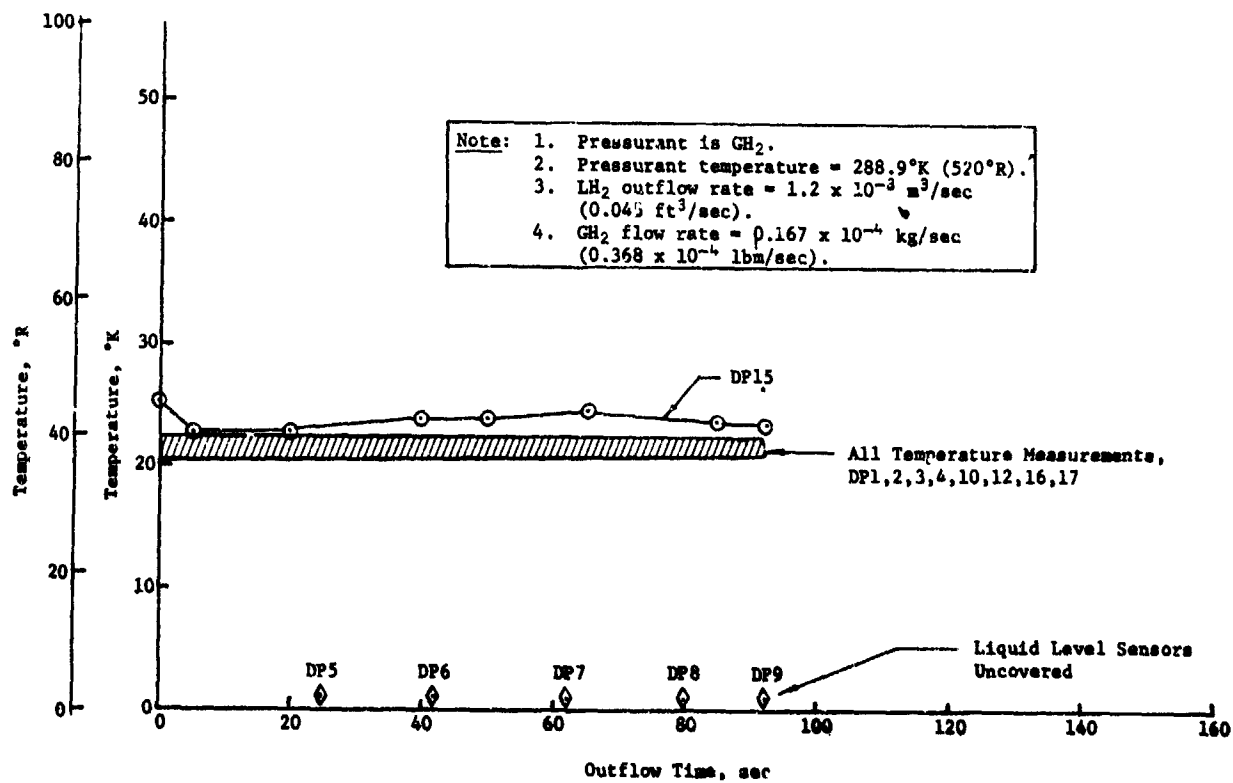Fig. III-32 Pressurization and Outflow Test Results, LH₂ Tank Temperature Histories, Test 6

Fig. III-33 Pressurization and Outflow Test Results Vapor Annulus-Bulk Region Pressure Differential, Test 6

III-51

Fig. III-34 Pressurization and Outflow Test Results, LH₂ Tank Pressure History, Test 7

Fig. III-35 Pressurization and Outflow Results, LH₂ Tank Temperature Histories, Test 7
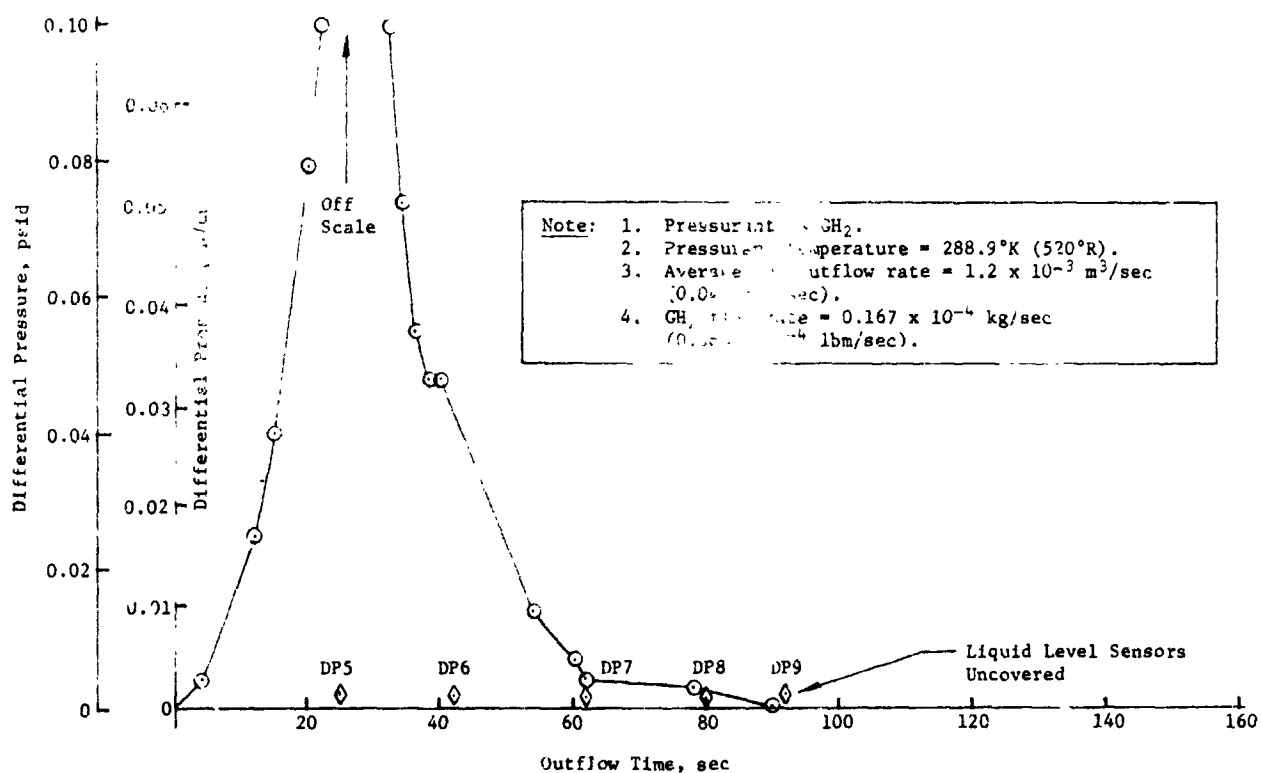
III-52

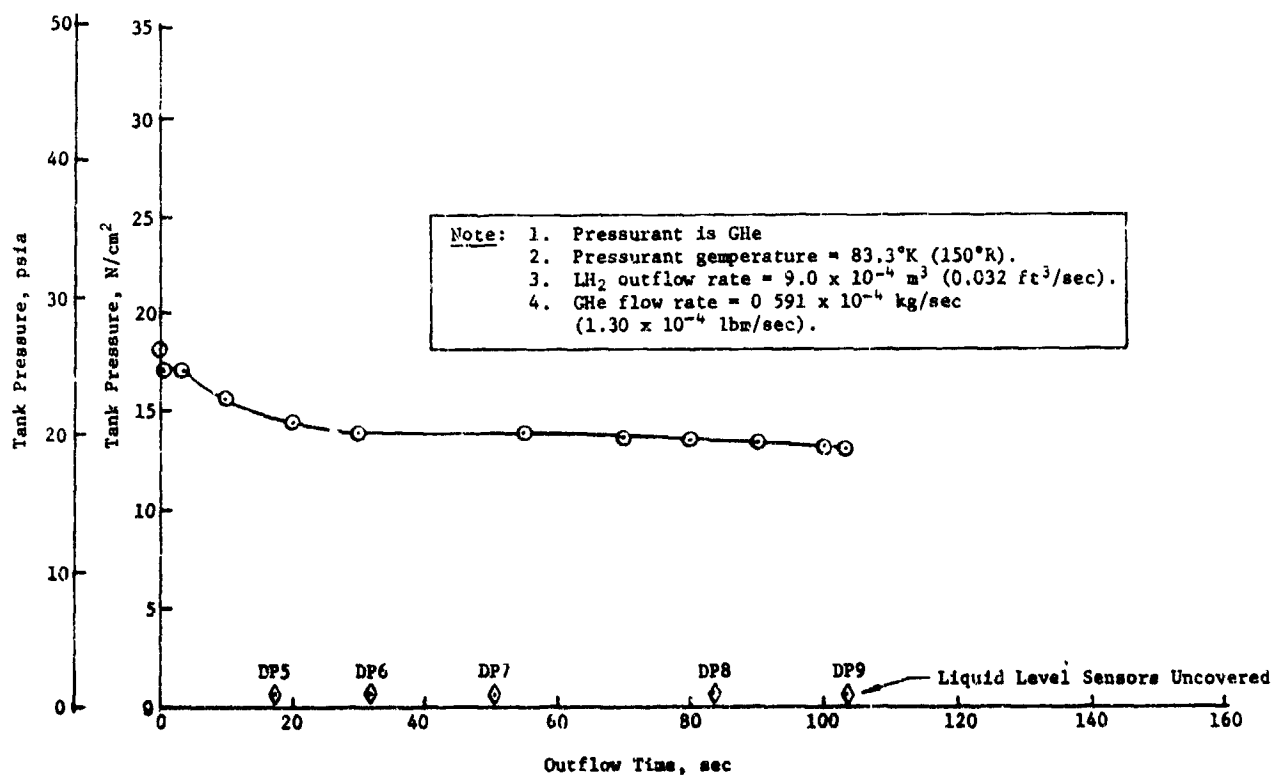Fig. III-36 Pressurization and Outflow Test Results, Vapor Annulus-Bulk Region Pressure Differential, Test 7

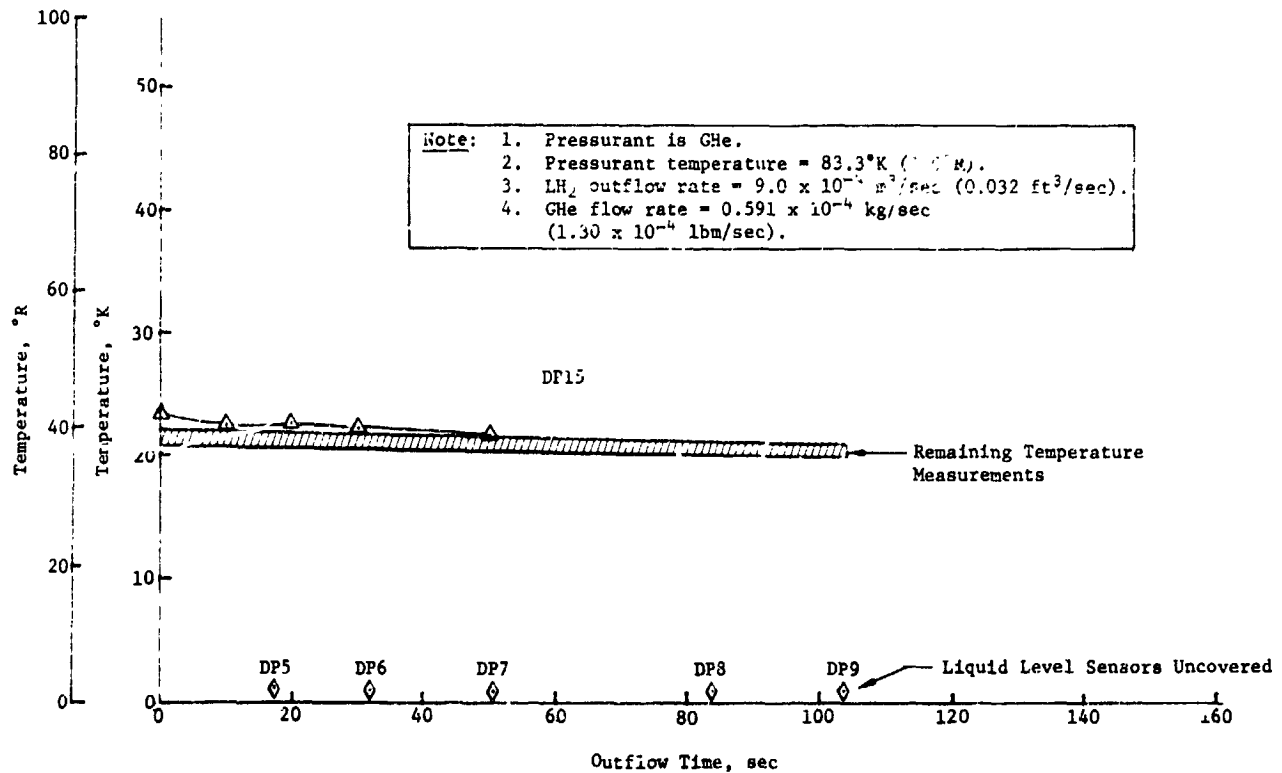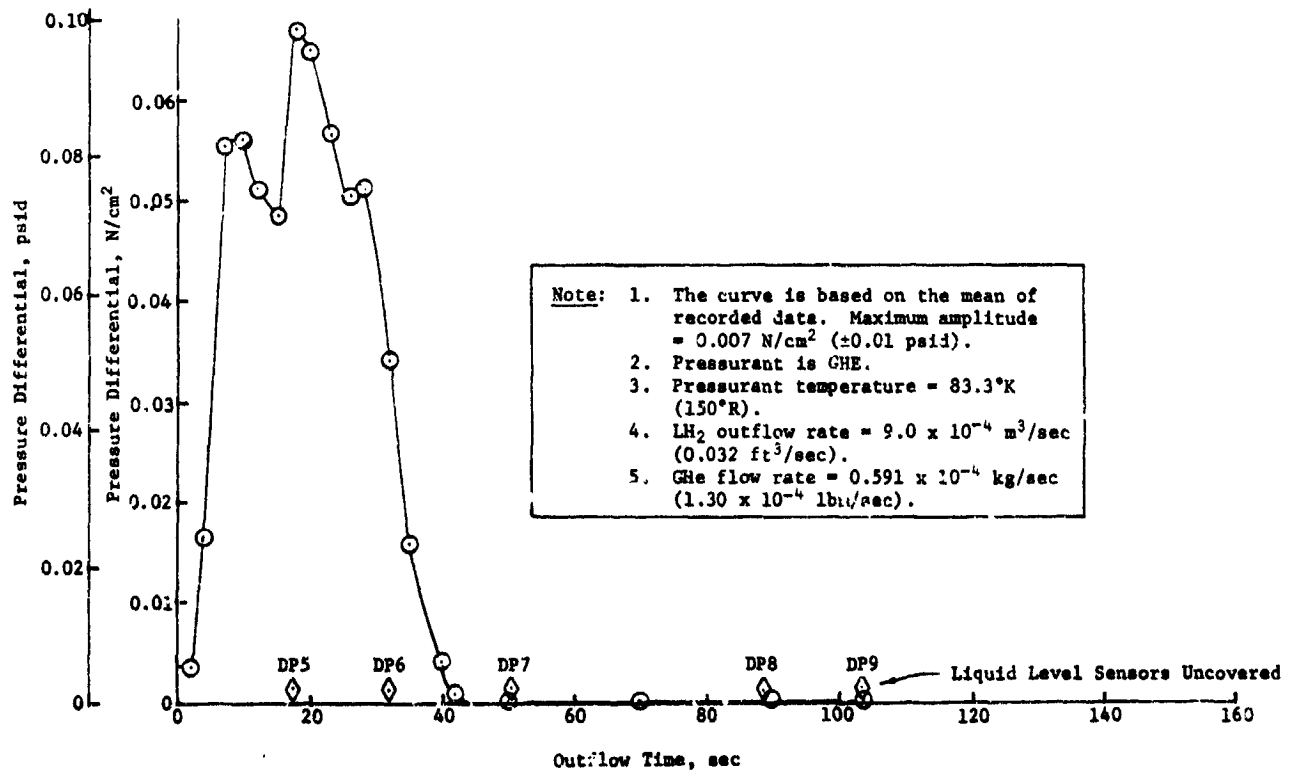Fig. III-37 Pressurization and Outflow Test Results, LH₂ Tank Pressure History, Test 8

III-53

Fig. III-38 Pressurization and Outflow Test Results, LH₂ Tank Temperature Histories, Test 8

Note:
1. The curve is based on the mean of recorded data.
   Maximum amplitude = ±0.007 N/cm² (±0.01 psid).
2. Pressurant is GHe.
3. Pressurant Temperature = 278°K (500°R).
4. LH₂ Outflow Rate = 1.1 x 10⁻³ m³/sec (0.04 ft³/sec).
5. GHe Flow Rate = 0.344 x 10⁻⁴ kg/sec
   (0.757 x 10⁻⁴ lbm/sec).

Fig. III-39 Pressurization and Outflow Test Results, Vapor Annulus-Bulk Region Pressure Differential, Test 8

indicate that the screen liner dries more readily with GHe than with GH$_2$. Evidently the reduction of the hydrogen partial pressure by GHe increases the vaporization of liquid from the screens, and dries out the screens more readily than GH$_2$. This phenomenon was also observed during the acceptance tests using methanol and GH$_2$ pressurant.

As previously mentioned, Test 9 was the only test where breakdown of the liquid flow channel screens was observed. The results of Test 9 are presented in Figs III-40 and III-41. During Test 9 at approximately 110 sec after start of expulsion, DP13 began to indicate minor breakdown of the screen flow channels. Finally at about 122 sec, the breakdown was classified as major and the run was terminated at about 130 sec. However, during this test approximately 97% of the liquid available for expulsion was drained from the tank. This is particularly significant because the pressurant entering the tank directly impinged on the screens. The pressurant entered the tank through a 0.635-cm (1/4-in.) line that was designed to sense tank pressure rather than to diffuse the pressurant. As a result, the screens dried out prematurely and produced the failure. It should be noted that this provided the most stringent pressurization conditions of all the minus 1 g expulsion tests.

By pressurizing through the top of the tank, the warmest ullage conditions of all the tests were obtained (see Fig. III-41). These temperatures reached values as high as 51°K (92°R) as indicated by sensor DP15. It is significant that all of the bulk ullage temperatures except DP4 were as much as 30.5°K (55°R) above the liquid temperature during the tests. This warm ullage condition existed throughout the run and demonstrated that the warm ullage does not dry out the screens. Therefore, Test 9 verified the thermal stability of the screens under a most severe pressurization environment. The differential pressure across the screen liner was not recorded during Test 9 because the pressurant gas entered the tank through the line that normally was used to sense $\Delta P_{s\ell}$.

In the final expulsion and pressurization test, Test 10, the effect of multiple expulsion events was investigated. The results of Test 10 are presented in Figs. III-42 through III-44. The temperature histories and $\Delta P_{s\ell}$ history were generally as expected and consistent with those of Tests 2 and 3. In Fig. III-42, the tank pressure following the first expulsion event remained relatively constant. Not until the final simulated coast period
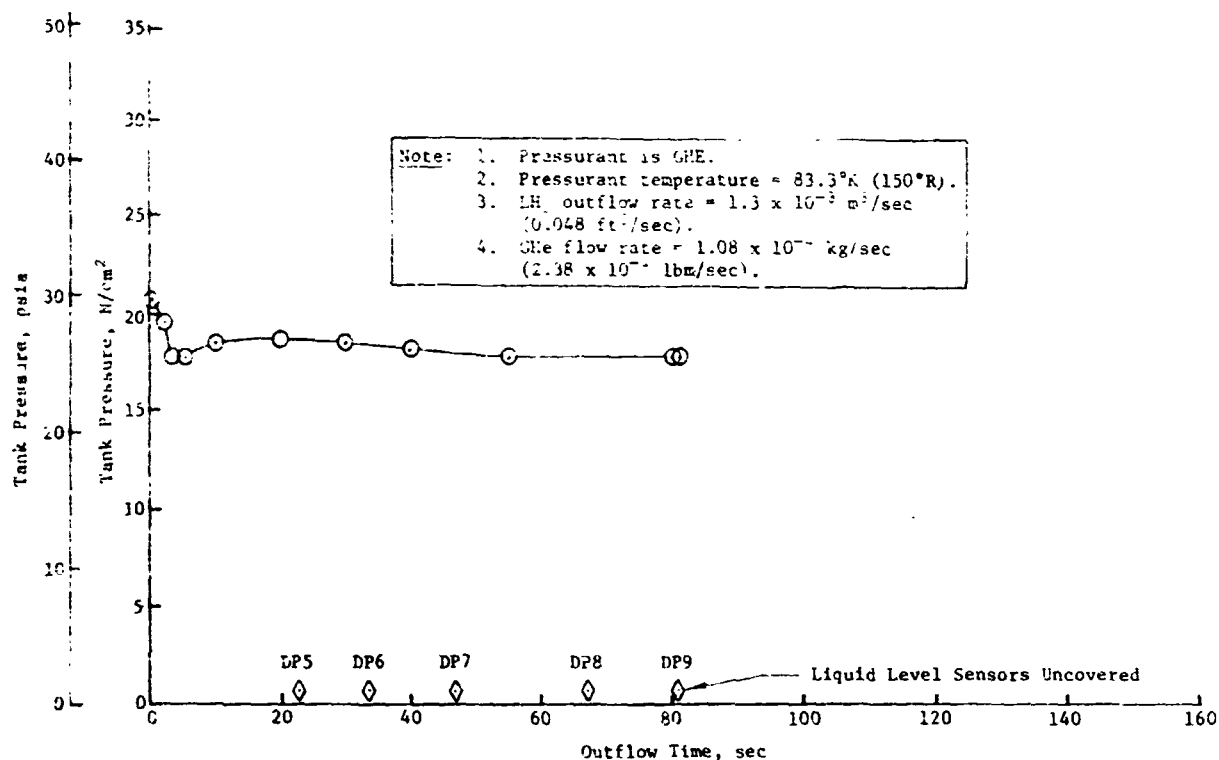
III-55

Fig. III-40 Pressurization and Outflow Test Results, LH₂ Tank Pressure History, Test 9
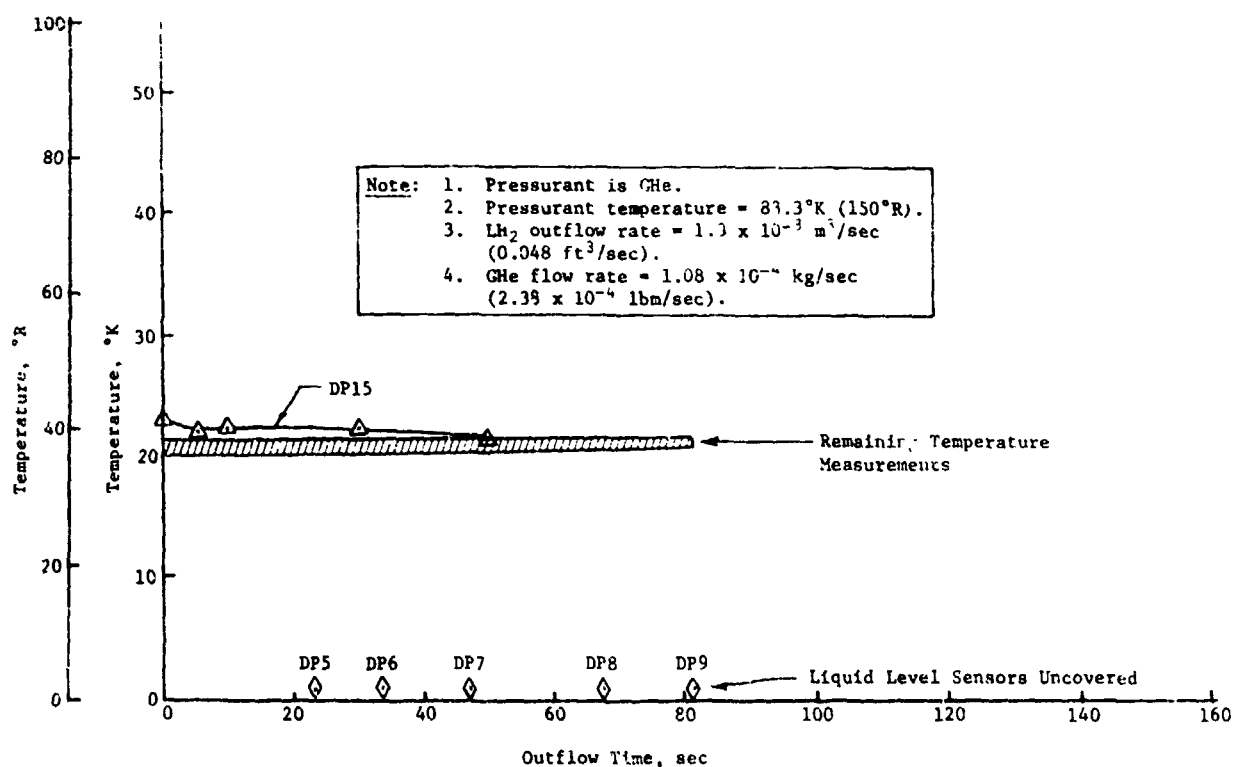

Fig. III-41 Pressurization and Outflow Test Results, LH₂ Tank Temperature Histories, Test 9

III-56

Fig. III-42 Pressurization and Outflow Test Results, LH₂ Tank Pressure History, Test 10

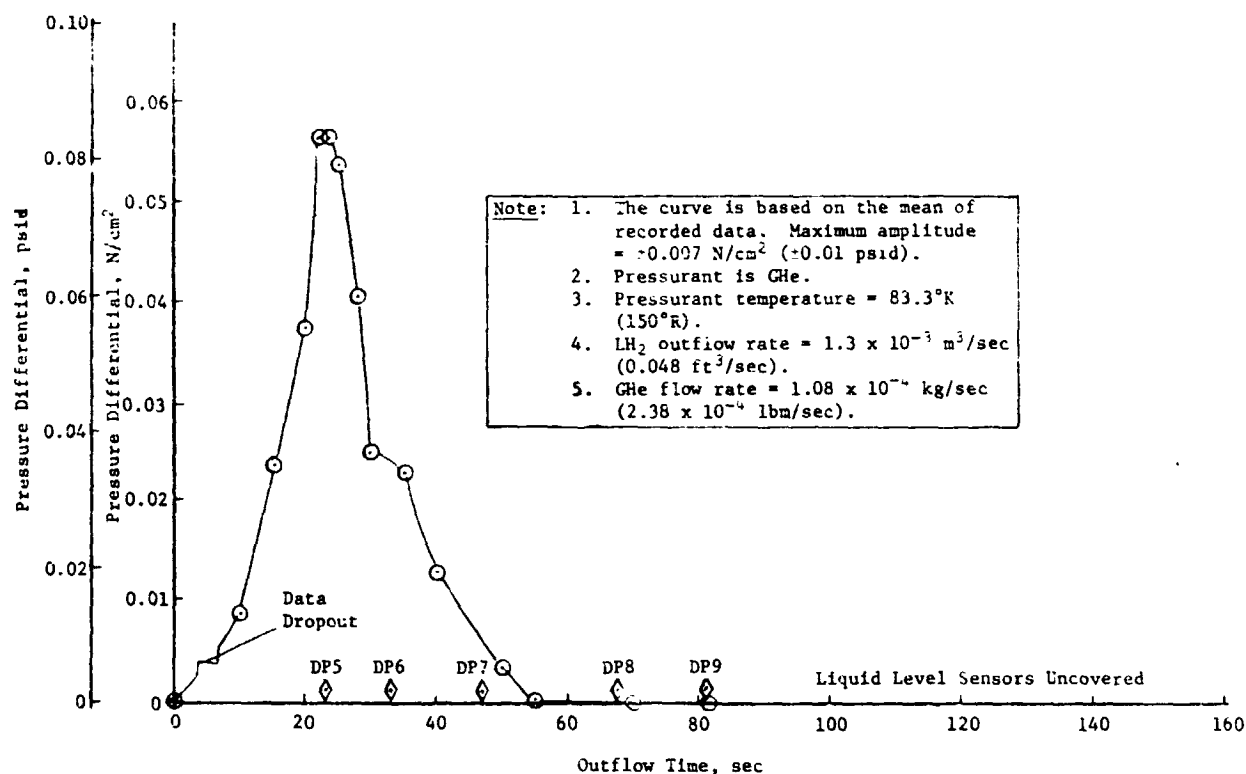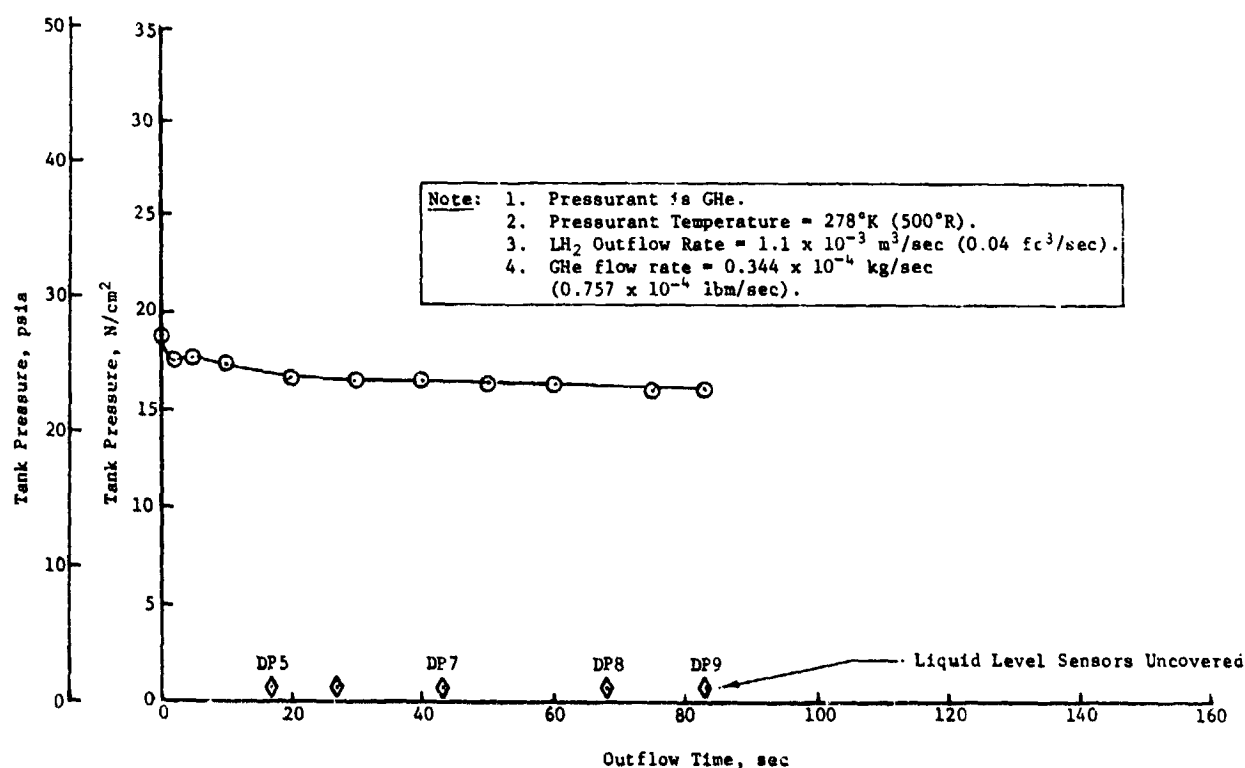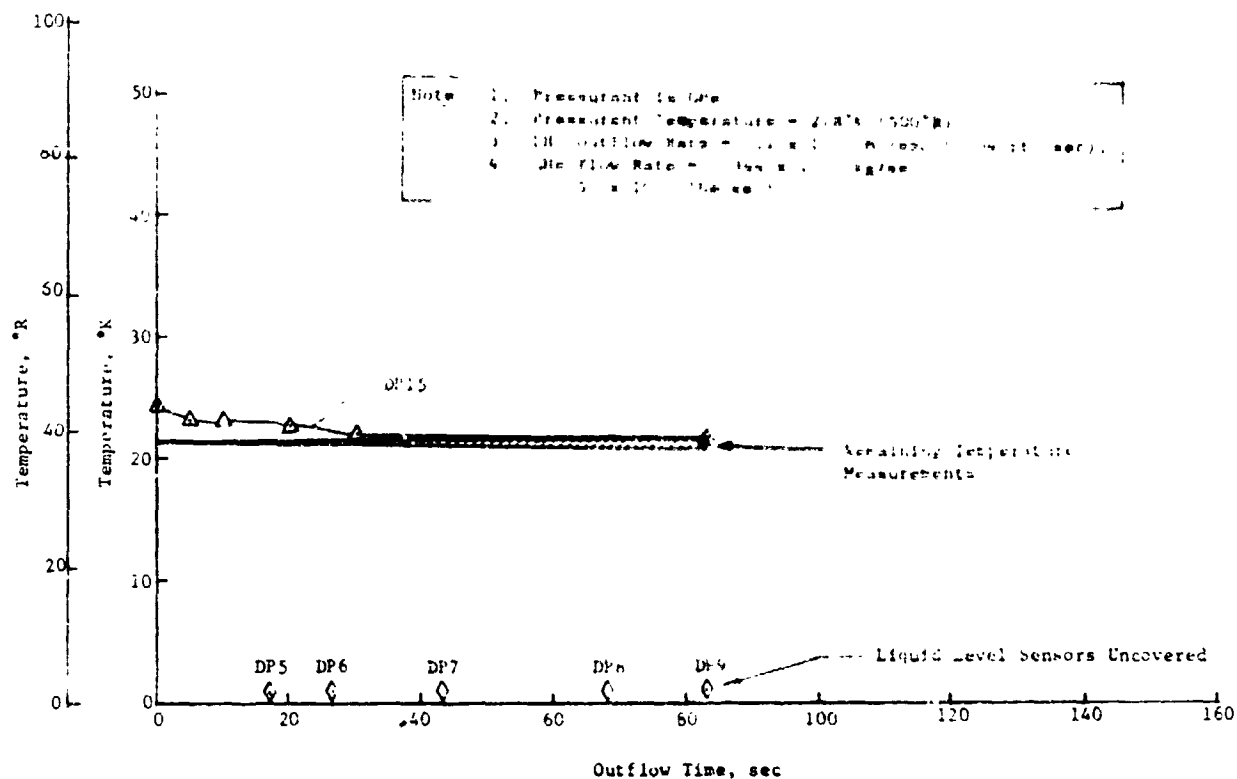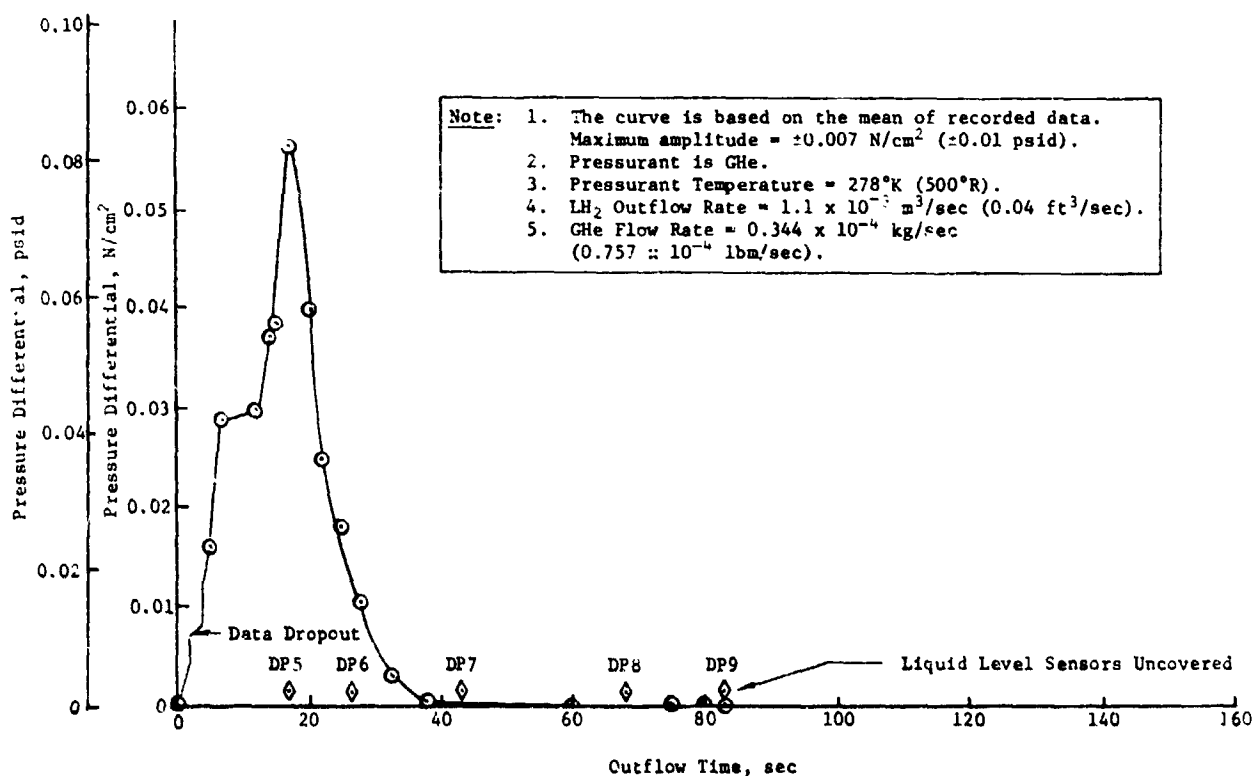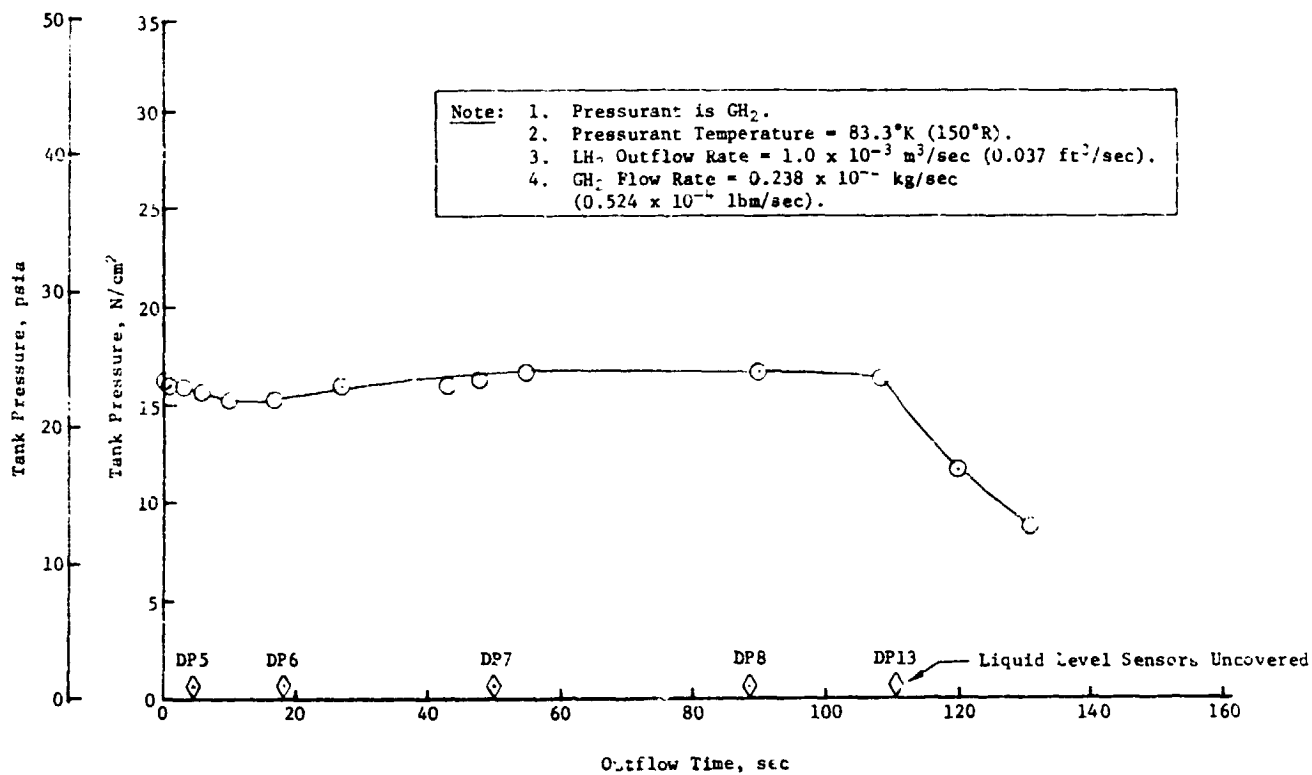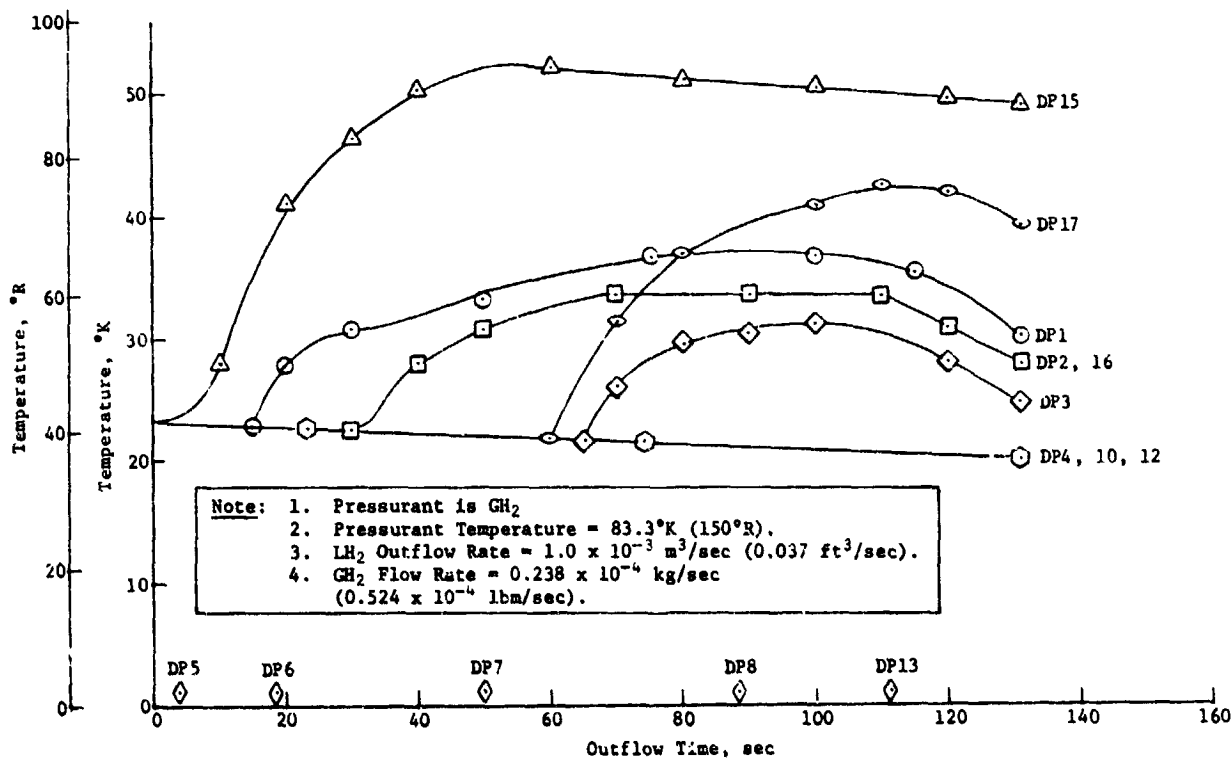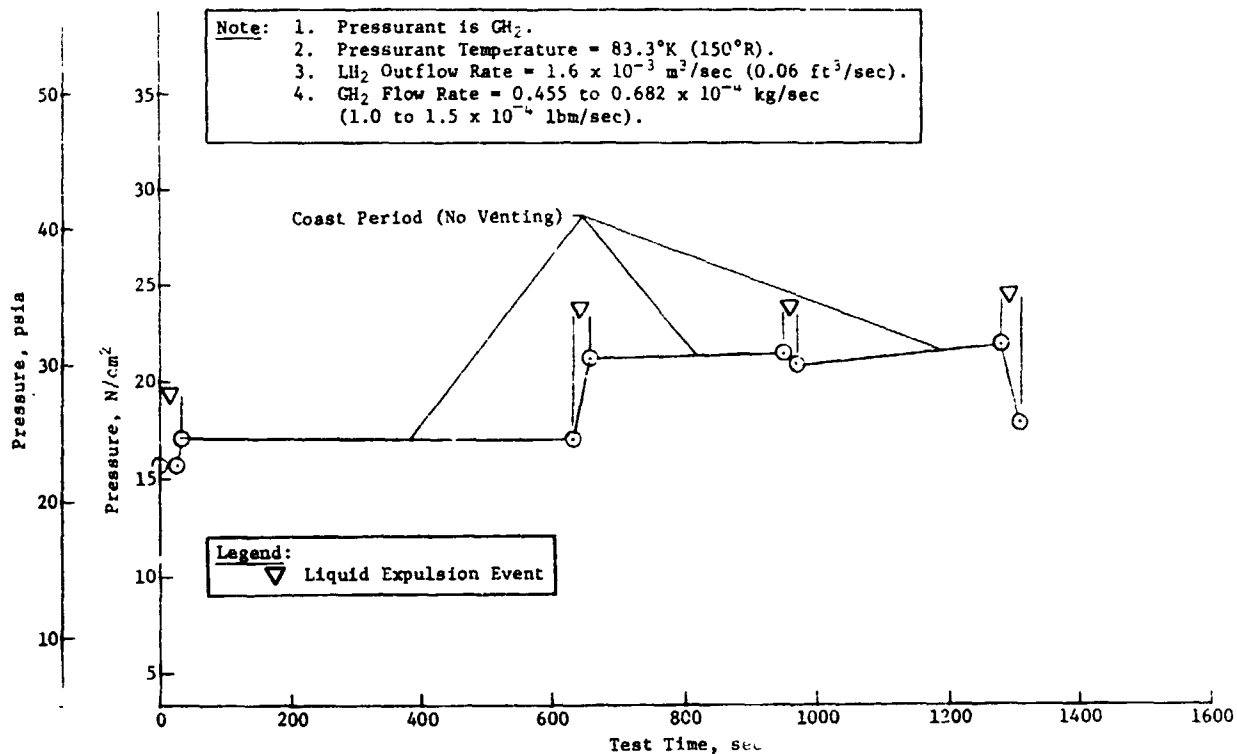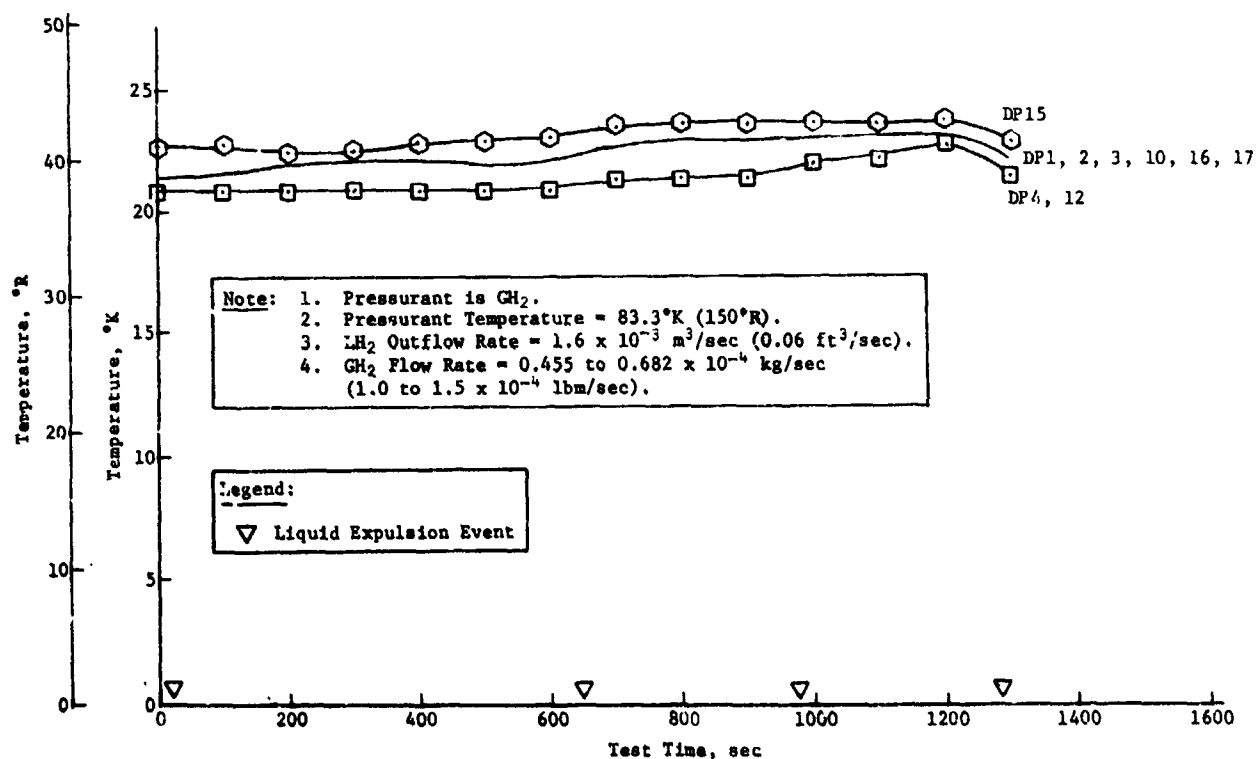Fig. III-43 Pressurization and Outflow Test Results, LH₂ Tank Temperature Histories, Test 10

III-57

was there any noticeable increase in tank pressure during the no-vent coasting periods. After the first expulsion event, the screen liner was able to remain wet until just before the start of the second expulsion event. As shown in Fig. III-44, $\Delta P_{s\ell}$ remains relatively constant at approximately 0.022 N/cm^2 (0.032 psi) for about 600 sec and then drops to zero. The sharp peaks in $\Delta P_{s\ell}$ during the next three expulsion periods indicate that the liner was partially wet.

These tests verified the inability of the screen liner/channel to wick liquid and maintain a wet liner. The results were expected because this design problem was uncovered during the initial acceptance tests.

4.   Vent Test Results

As discussed in the test plan, the vent tests were to be conducted in conjunction with the minus 1-g expulsion and pressurization tests. This was attempted, but it soon became evident that the conditions required to demonstrate the DSL vent system could not be obtained.

A detailed discussion of the DSL vent system characteristics is presented in Chapter II of Volume I. The system relies on an increase in the pressure differential between the outer annulus and bulk region, $\Delta P_{s\ell}$. The vent system controls tank pressure by controlling $\Delta P_{s\ell}$ within the specified limits. The communication screen liner must remain wet during vent periods.

During vent system operation it is expected that the outer annulus vapor temperature will be warmer than the bulk ullage. This is because the heat entering the tank increases the outer annulus temperature and pressure, while the bulk ullage is thermally isolated by cooling due to liquid vaporization at the outer liner. The expected thermal stratification in low-g is in a radial direction while that in normal 1g is in a vertical direction. The low-g thermal stratification should favor the DSL system as discussed in Chapter II of Volume II. One of the primary objectives of these tests was, therefore, to demonstrate the DSL vent system and determine the effect of a normal 1-g environment on system operation.

Note:
1. Pressurant is GH_2.
2. Pressurant Temperature = 83.3°K (150°R).
3. LH_2 Outflow Rate = 1.6 x 10^{-3} m^3/sec (0.06 ft^3/sec).
4. GH_2 Flow Rage = 0.455 to 0.682 kg/sec
   (1.0 to 1.5 x 10^{-4} lbm/sec).

Coast Period (No Venting)

Legend:
▽ Liquid Expulsion Event

Differential Pressure, psid

Differential Pressure, N/cm^2

Test Time, sec
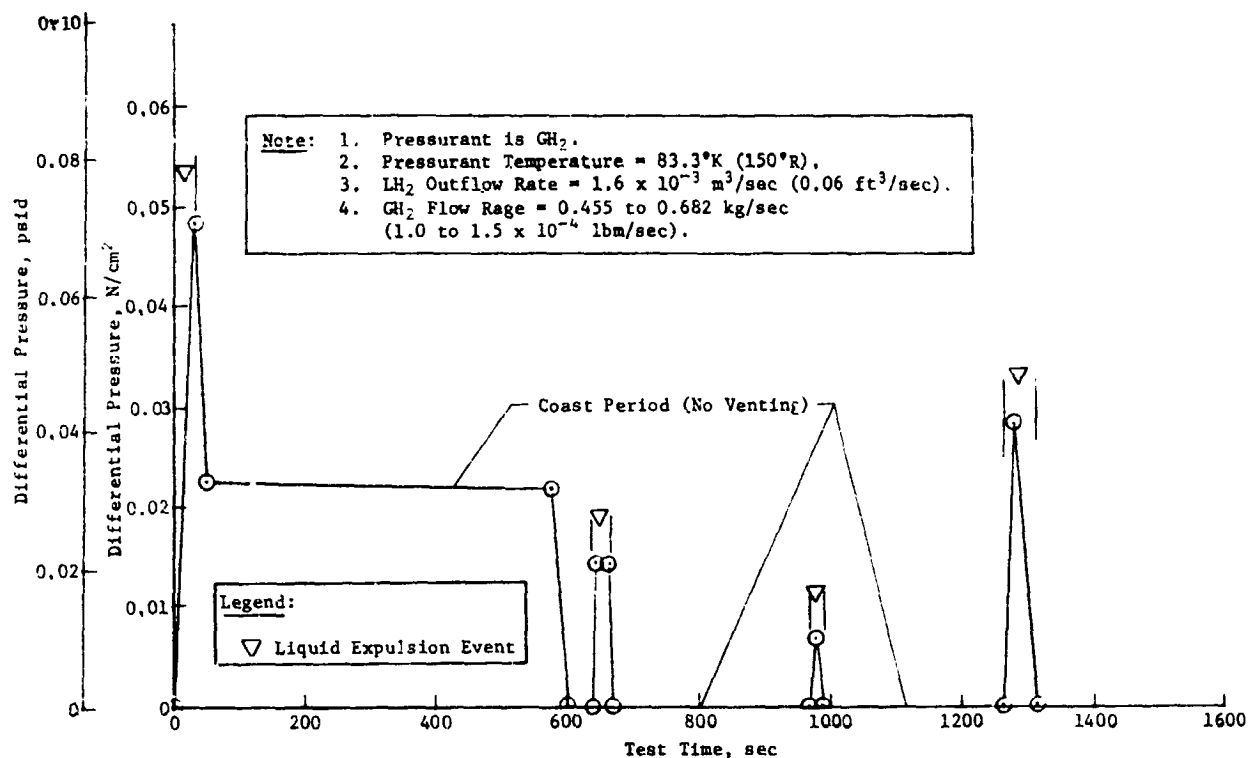
Fig. III-44 Pressurization and Outflow Test Results, Vapor Annulus-Bulk Region Pressure Differential, Test 10

Note:
1. Pressurant is GH_2.
2. Vent Cycle Frequency = 10 sec.
3. Ullage Volume = 35%.

Tank Pressure, psia

Tank Pressure, N/cm^2

Venting
Initiated

Venting
Terminated

Venting
Initiated

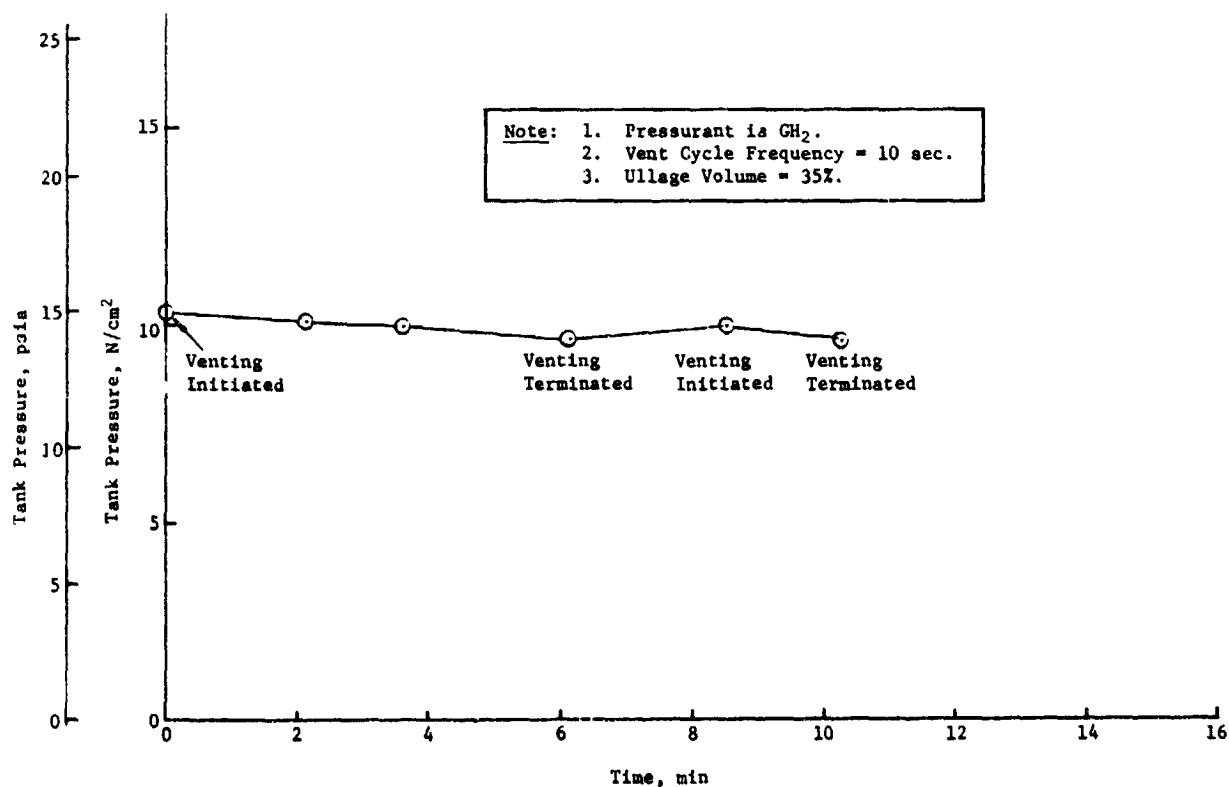Venting
Terminated

Time, min

Fig. III-45 Vent Test Results, LH_2 Bulk Ullage Pressure History

Results of the venting tests are presented in Fig. III-45 through III-47. Although other tests were attempted, this particular test illustrates the conditions required to accomplish venting using the DSL vent system. Several attempts were made to use the test procedure described in the previous subsection. The procedure called for venting to be initiated after expelling all liquid from the outer annulus and about 20% of the bulk liquid. Venting was to be attempted through the bottom pressurization and vent line. After several attempts, the results that were consistently obtained by monitoring $\Delta P_{s\ell}$ and fluid temperatures were:

1) without venting, $\Delta P_{s\ell}$ gradually decreased, as shown in Fig. III-44, until it reached zero;

2) venting of the outer annulus increased the trend described in 1);

3) fluid temperatures in the bulk region increased instead of remaining constant;

4) the temperature (DP17) in the bottom of the outer annulus normally was between 2.8 to 5.5°K (5 to 10°R) colder than DP15 at the top of the tank.

It was concluded that since $\Delta P_{s\ell}$ was a positive value, the screen liner was wet. However, the bulk pressure was increasing at a faster rate than the outer annulus pressure. This was verified by the gradual decrease in $\Delta P_{s\ell}$ and the increase in bulk ullage temperatures. This implies that some of the heat entering the tank was being transferred into the bulk region. Because the top outer annulus temperature (DP15) was the warmest temperature recorded, it became obvious that heat from outer annulus gas was being transferred into the bulk ullage. Also, venting from the bottom of the tank did not eliminate this stratification.

To reduce the 1-g stratification in the outer annulus, it became necessary to vent from the top of the tank. The system was modified to vent through the same 0.635-cm (1/4 in.) diameter line that was used to pressurize the tank in Test 9. Therefore, for the venting part of the tests, the $\Delta P_{s\ell}$ and the automatic vent control system could not be used. Consequently, venting was accomplished manually by activating the vent solenoid valve (SV1 in Fig. III-15).
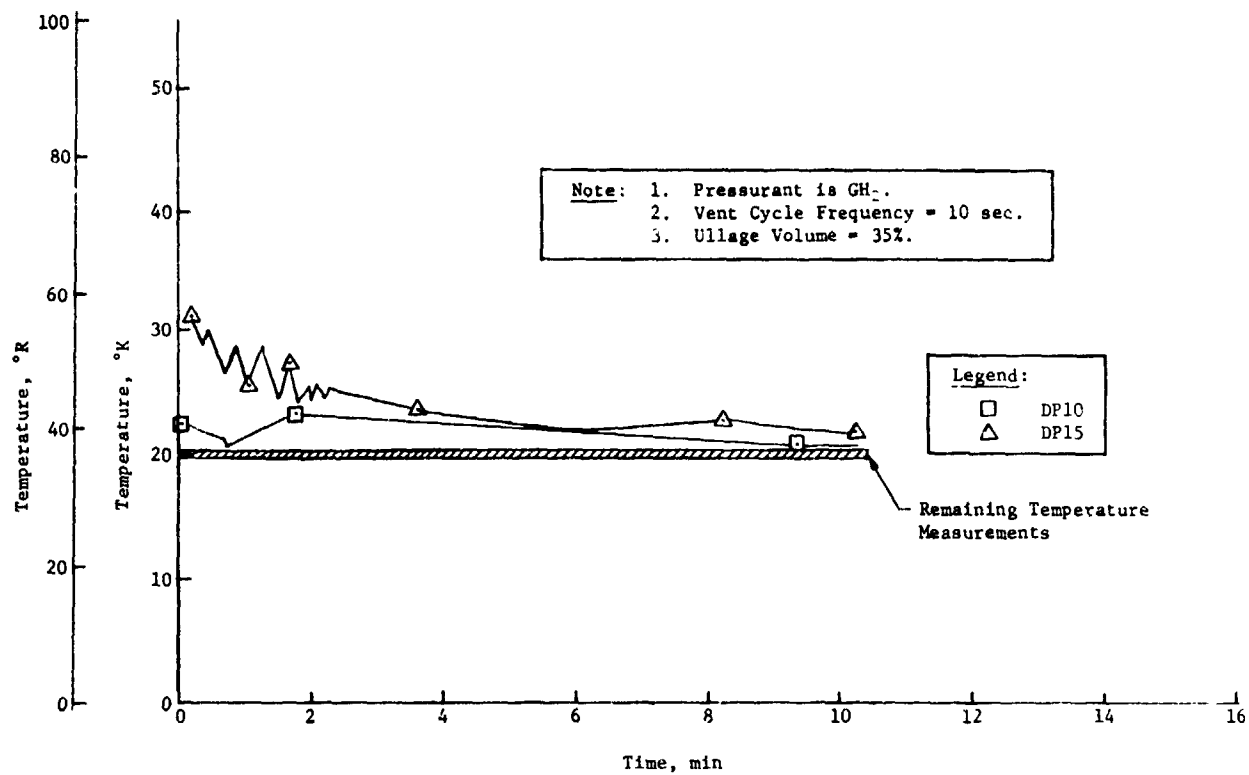
III-60

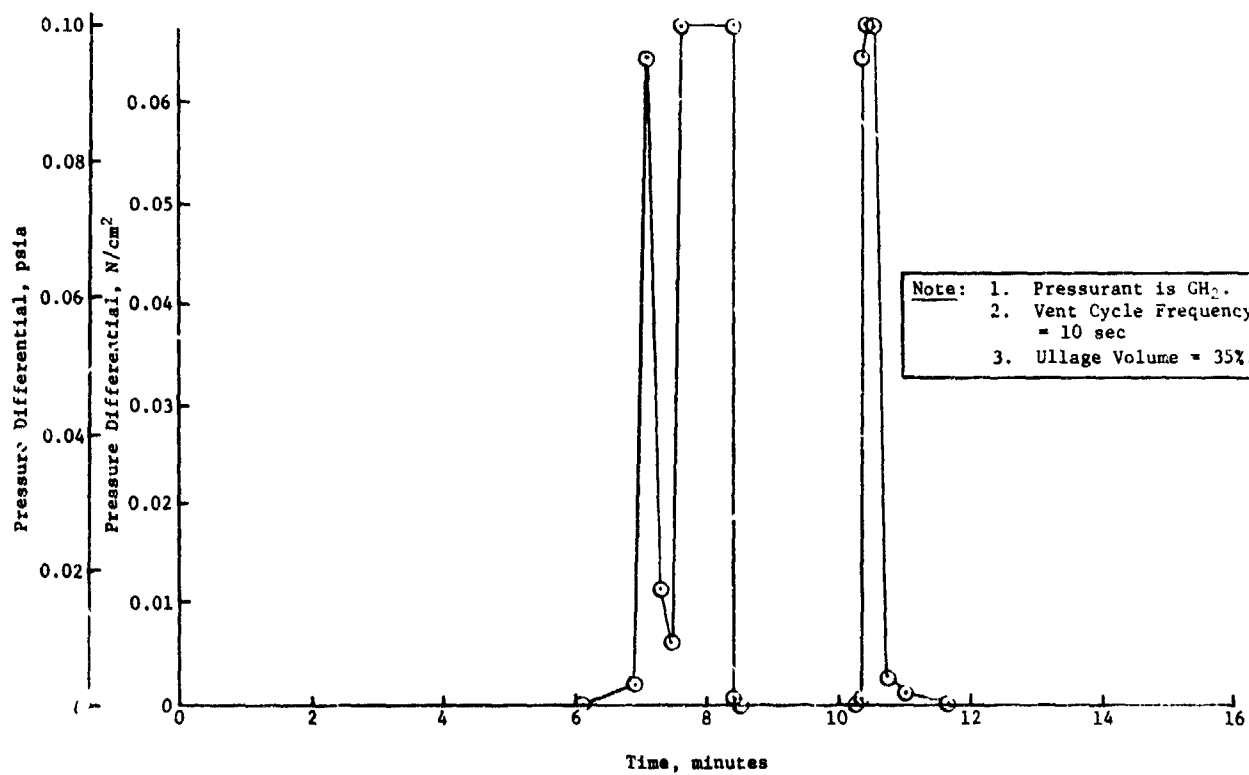Fig. III-46   Vent Test Results, LH_2 Tank Temperature Histories

Fig. III-47   Vent Test Results, Vapor Annulus-Bulk Region Pressure Differential, $\Delta P_{s\ell}$

The first vent period lasted approximately 6 minutes. This was followed by a 2.5-minute hold period. The final vent period was approximately 2 minutes, followed by another brief hold that was slightly less than 2 minutes.

The results of this test are presented in Figs. III-45 through III-47. Figure III-45 is the bulk ullage pressure history and shows when venting was initiated and terminated. It also shows that the bulk ullage pressure decreased slightly during both the first and final vent periods. A slight increase in pressure is also noted during the first hold period.

The temperature histories (Fig. III-46) illustrate the reduction in stratification that resulted from venting at the top rather than the bottom of the tank. Initially, the top temperature (DP15) was approximately 11°K (20°R) greater than the liquid temperature. During the 6-minute vent period, this temperature differential decreased significantly to approximately 3.1°K (5.5°R). A slight temperature increase at DP15 was noted during the first hold period while the remaining temperatures decreased, as shown by DP10, or remained constant. These results were repeated in the final vent and hold periods.

The clearest demonstration of communication screen liner performance is shown in Fig. III-47. Due to the problem discussed previously, the first $\Delta P_{s\ell}$ measurement does not start until the end of the first 6-minute vent period. With the tank in a no-vent (hold) condition, $\Delta P_{s\ell}$ increases to approximately the bubble point of the screen and then gas from the outer annulus breaks through the wet screen liner and into the bulk ullage. The outer annulus pressure drops, as does $\Delta P_{s\ell}$, until the screen liner is resealed by wicking. The cycle is repeated again before initiating the second vent period and also following the final vent period.

The test successfully simulated the conditions necessary to demonstrate the DSL vent system. During normal operation the outer annulus would have been vented, automatically controlling $\Delta P_{s\ell}$ within a specified band. This test did demonstrate, in a limited way, the operation of the cryogenic DSL and also the limitations of testing the DSL in a normal 1-g environment.

III-62

G.   CONCLUSIONS

A representative, subscale model of the preferred DSL designs
(presented in Volume II Chapter III was designed, fabricated,
assembled, and tested. Fabrication, assembly, and inspection
techniques for these cryogenic systems were developed.

Comprehensive testing of the 63.5-cm (25 in.) diameter model
verified several operational and functional characteristics of
the DSL. Tests were successful in demonstrating the fill capa-
bilities of the system with both LN_2 and LH_2. The preferred
fill method established for LH_2 was to subcool the LH_2 in the
dewar and then fill the tank at a relatively slow rate.

The minus 1-g expulsion and pressurization tests verified the
DSL's ability to outflow gas-free liquid using either GH_2 or GHe
as pressurants. The hydrodynamic and thermal stability of the
liquid flow channels was demonstrated under several operating
conditions. Under the severe pressurization conditions imposed
by pressurant impinging directly on the screens, the DSL was still
able to outflow 97% of the expellable liquid.

Operational characteristics of the communication screen were demon-
strated during both expulsion/pressurization and venting. Due to
the 1-g stratification effects, the DSL venting system could not
be adequately verified. However, an automatic vent control system
capable of providing the fine differential pressure control required
for LH_2 was designed, fabricated, and checkout out.

The limitations of the normal 1-g test environment emphasize the
need for additional testing in a low-g Earth orbital environment.

IV.   CAPILLARY SCREEN FABRICATION TECHNOLOGY

Martin Marietta is conducting several continuing IRAD tasks on capillary screen technology. One of the tasks, entitled *Capillary Screen Fabrication Technology*, concerns the development of manufacturing methods for fine-mesh screen systems for all types of propellant management systems. This task is intended to provide technical support and procedures for the fabrication and assembly of full-scale capillary screen devices. During CY 1972 and CY 1973 a number of specific objectives were established, many of which have been met. These objectives were as follows:

1) Evaluate various candidate screen forming and joining methods using simple subassemblies.

2) Fabricate test specimens using the most promising methods established under 1 above, and conduct bubble-point tests.

3) Design and fabricate a 178-cm (70-in.) diameter spherical capillary screen liner using basic resistance seam welding techniques established under previous programs.

4) Design and fabricate a single liquid flow channel for the 178-cm (70-in.) liner. Addition of the channel to the liner provides the DSL configuration that would be used with space-storable propellants. Fabrication of the channel would use the techniques developed under 1 and 2 above.

5) Conduct bubble-point testing of the 178-cm (70-in.) diameter liner to establish inspection techniques for a fully-assembled DSL system.

In addition to the primary objectives listed above, two secondary objectives were to be met if time and money permitted. These objectives were:

1) Review the manufacturing, cleaning, and inspection state-of-the-art for devices using a capillary screen, and

2) Conduct collapse tests on a spherical screen liner to determine deformation under external pressure and pressure retention degradation, as indicated by bubble-point measurement changes.

A.   EVALUATION OF FORMING AND JOINING METHODS

Considerable effort has been devoted to investigating joining
techniques other than the resistance seam welding method used
in the past. A number of screen-to-sheet and screen-to-screen
samples were fabricated and tested. Testing has primarily con-
sisted of thermal shock and bubble-point measurement since these
are the basic structural and performance criteria. The joining
methods used were soft soldering and metal flame spray, both of
which proved at least partially acceptable.

Forming investigations were conducted in an attempt to produce
screen sections with compound curvature (i.e., spherical sec-
tions). Again, the objective was to minimize bubble-point de-
gradation after forming. Two methods of forming screen hemi-
spheres were tried without success. One method was spin form-
ing; the other was a screen pleating technique. The forming and
joining investigations are summarized in the following sections.

1.   Metal Flame Spray

With the metal spray overlay process, high-velocity molten metal
particles are sprayed on the overlapping surfaces of two sheets
of metal. The gun used for this process melts the metal supplied
to it in wire form and propels the molten metal at high velocity
using pressurized gas. Three types of metal overlay were tried:
copper, Monel, and aluminum. These were sprayed to join stain-
less steel screen to stainless steel structure, stainless steel
screen to aluminum structure, aluminum screen to stainless struc-
ture, and aluminum screen to aluminum structure. After the
screens were spot-welded to the test frames, an application of
bond material was sprayed over the mating surface, followed by a
layer of metal spray.

During bubble-point tests of these samples, tiny leaks were
noticed at the borderline of the overlay and screen. This was
attributed to burning the screen during bond application. This
problem was corrected by operating the spray gun at a different
angle and increasing the width of the metal overlay by approxi-
mately 0.158 cm (1/16 in.) after the bond coat was sprayed.

2.   Soft Solder Method

This method involved using soft solder to join fine-mesh screen
to a metal sheet. Two types of solder were used: Eutectic 157
(96% tin, 4% silver) and Eutectic 1909 (composition unknown).

Eutectic 157 was used to join stainless steel screen to a stain-
less steel structure. The test specimen had excellent bonding
characteristics and was successfully bubble-point tested to a
value approximately equal to that of the as-received screen.
The specimen was found to be flexible even in liquid nitrogen,
and a subsequent visual inspection revealed no cracks or distor-
tions. One disadvantage of this particular solder is its in-
compatibility with liquid oxygen.

Eutectic 1909 was used to join aluminum screen to an aluminum
structure and stainless steel screen to an aluminum structure.
This compound proved unsuccessful. Bonding the screen to the
structure was not possible since the solder attached the aluminum
sheet, producing numerous small cracks.

3.   Forming

Previous forming investigations have been directed toward the
feasibility of fabricating spherical screen devices from a single
sheet of screen material. The major design consideration was
that the screen bubble point be maintained throughout the form-
ing procedure.

Spin forming a single sheet of screen material into a sphere was
attempted with little success. In this process, a sheet of
200x1400-mesh aluminum screen was sandwiched between two sheets
of soft aluminum and spin-formed on a lathe by forcing it over
a dome using standard spinning techniques. The method failed
due to distortion and folding of the screen material, which
caused gross degradation of the bubble point.

A second forming technique involved pleating a screen sheet to
form a full hemisphere from a single sheet of screen. The screen
was formed from the apex of the hemisphere to the equator, with
pleats that increased in depth toward the equator. Forming tools
were built and an attempt was made to form a hemisphere.

Two problems were encountered. First, unless the screen was
actually deformed (i.e., unless the wires were yielded) during
the process, the pleats would not be permanently set; and sec-
ond, double-curvature deformation of the mesh occurred along the
pleats, resulting in bubble-point degradation. Additional work
planned in this area is discussed later in this chapter.

B.   177.8-cm (70-in.) DSL SCREEN LINER

The objectives of this design/fabrication task were to demon-
strate that sufficient data exist to design a full-scale, air-
borne capillary system and to show that such a design is con-
sistent with the fabrication, testing, and handling techniques
that either exist or can be readily developed. The term "full
scale" refers to a system large enough to represent an airborne
propellant tank with a volume of at least 2.83 m' (100 ft^3).

1.   Design

The capillary liner was designed to be installed inside a spheri-
cal tank, since this shape is not only the most common but also
the most challenging to design. Experience has shown that fine-
mesh screen is not easily formed into compound curvature without
degrading its retention capability. Furthermore, the structure
required to support the screen can more easily be formed with-
out elaborate tooling if a compound curvature is avoided.

Bench model tests and analyses (see Chapter II) verified that a
polysphere formed from thin, structural shells was a promising
concept for spherical capillary liners. Such a concept is illus-
trated in Fig. IV-1.

Polyspheres are formed by joining a number of simply-curved gore
sections so that a section through the equator is a polygon,
whereas a section through the poles is a circle. Parameters
such as tank diameter and expulsion efficiency determine the op-
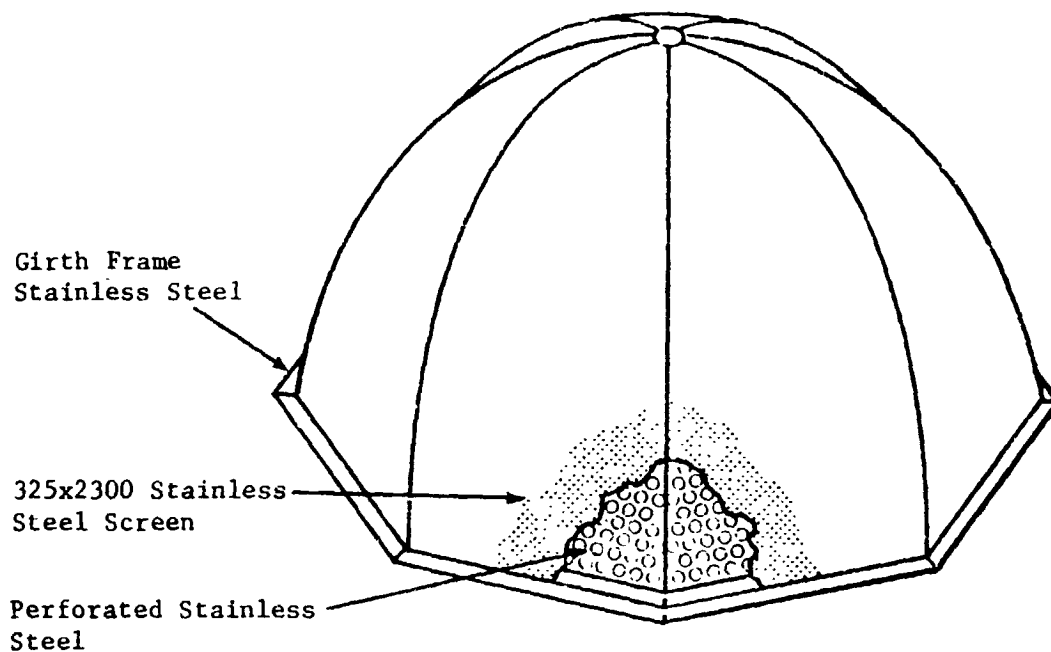timum number of gore panels to be used for a given design.

Girth Frame
Stainless Steel

325x2300 Stainless
Steel Screen

Perforated Stainless
Steel

Fig. IV-1   Octosphere Cap Filling Screen Structure

An additional variable in polysphere design is the eccentricity
of a polar section. As stated above, a section through the poles
will be circular; however, this can be accomplished in two ways.
One way is for the section to bisect a gore panel; the other way
is for the section to pass through the seam between gore panels.
The circular-seam method was chosen since the constant curvature
allowed it to be more readily welded by automatic means and since
it could be made to conform more closely to the curvature of the
tank wall.

The 25.4-cm (10-in.) bench models described in Chapter II (see
Fig. II-62) were formed by cutting the gore sections from flat
sheets of perforated stainless steel plate 0.038 and 0.063 cm
(0.015 and 0.025-in.) thick. Adjacent sections were fusion-welded.
This fabrication technique presented no significant problems ex-
cept for screen attachment: since the entire surface was perfo-
rated, screen could not be resistance-welded to the structure;
instead, a screen cap would have to be formed separately, slipped
over the polysphere, and welded to a nonperforated girth band.
Such an approach was considered impractical for a full-scale
article and was not pursued further.

The 177.8-cm (70-in.) diameter dodecasphere was designed to be fabricated from gore panels that were pattern-perforated (i.e., perforations existed only in specific areas). A margin completely around the periphery was not perforated. This margin provided not only a continuous edge for welding the sections together, but also a solid band for welding the screen. An additional advantage of this assembly technique was the capability of bubble-point testing each gore panel/screen subassembly before welding it to another part.

The panels for this model were 0.064-cm (0.025-in.) thick type 304 stainless steel that was pattern perforated with 0.64-cm (0.25-in.) holes on 1.11-cm (0.438-in.) centers. Perforated areas were covered with 250x1370-mesh Dutch twill stainless steel screen by resistance welding.

The dodecasphere could have been designed for 12 pole-to-pole sections, but each section would have been nearly 2.74 m (9 ft) long, presenting an awkward assembly problem. The actual gore panels ran from pole down to the equator (girth) and, consequently, were small enough to be handled easily.

This design provided for the three discrete volumes required for a cryogenic propellant management system: a bulk region, a vapor annulus, and liquid flow channels (Fig. IV-2). In most systems there are usually a number of flow channels running from pole to pole along the centerline of each gore section, but to minimize cost and complexity without compromising the task objectives, only one flow channel was fabricated. A simple rib along the centerline of the remaining 11 gores provided the required structural stiffness in the absence of these flow channels.

The flow channel was designed for a constant cross-sectional area and was 20.2 cm (7.95 in.) wide (tangentially) by 3.42 cm (1.35 in.) deep (radially) at the equator. These dimensions varied uniformly to become 5.25 and 8.50 cm (2.07 and 3.35 in.), respectively, at a point 10.28 cm (4.05 in.) from the polar axis. This provided a dodecagon-shaped opening at each pole to accommodate an outflow manifold. Each opening was 20.57 cm (8.10 in.) across the flats.

The inward-facing and outward-facing surfaces of the flow channel were perforated in much the same manner as the gore panels and were covered with 325x2300 Dutch-twill stainless steel screen. Using finer mesh screen for the flow channel provided the higher pressure retention capability required for system operation.
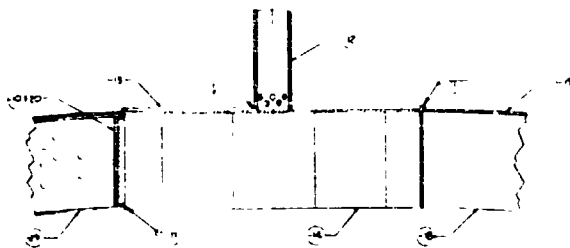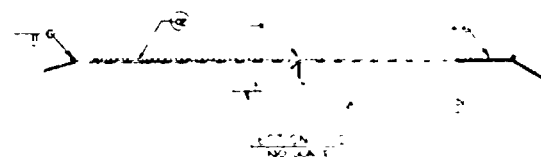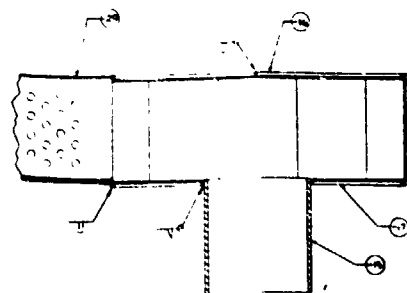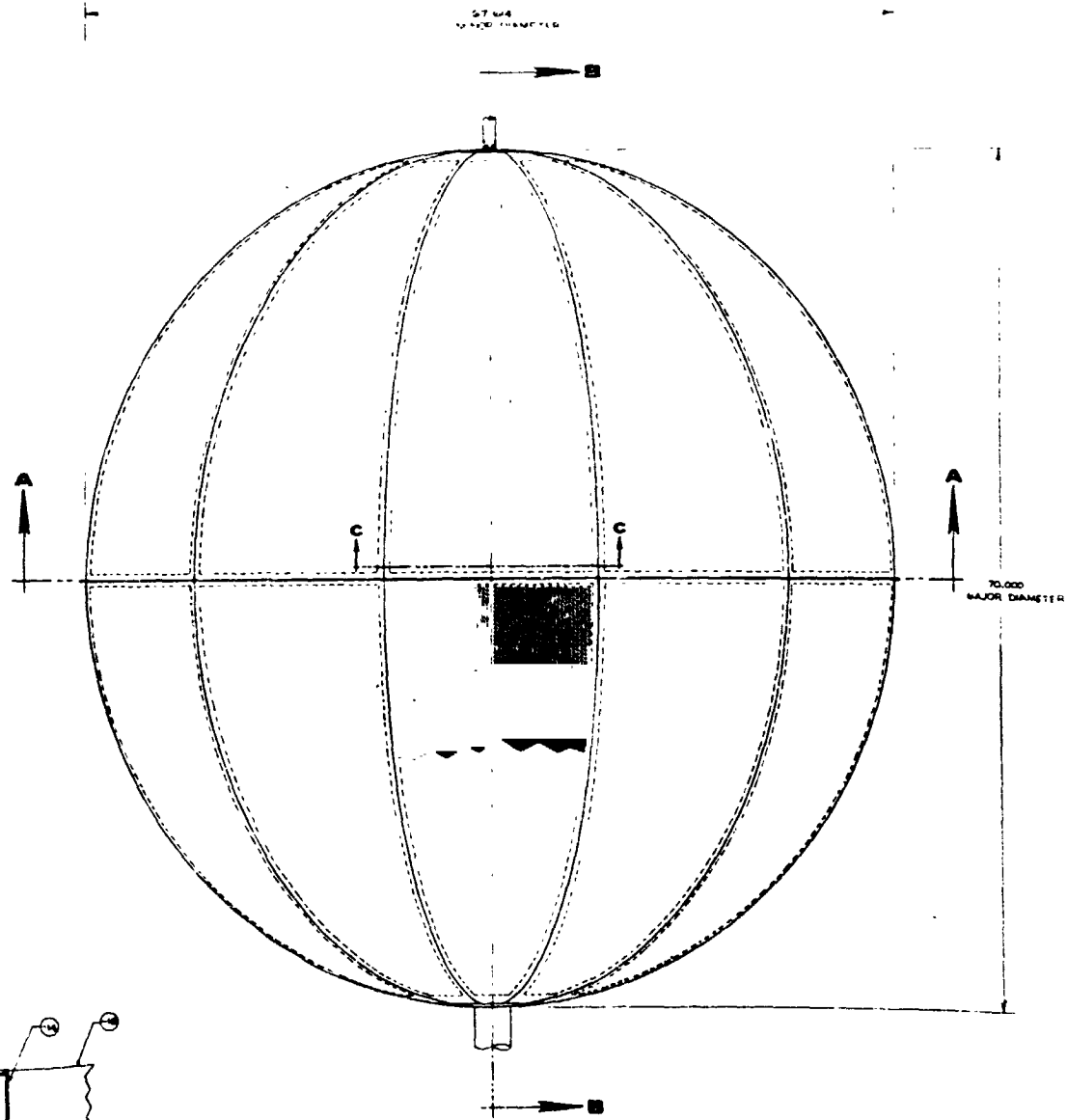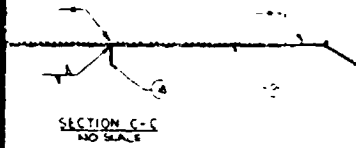
IV-6

DETAIL N
NO SCALE

N

SECTION B-B

M
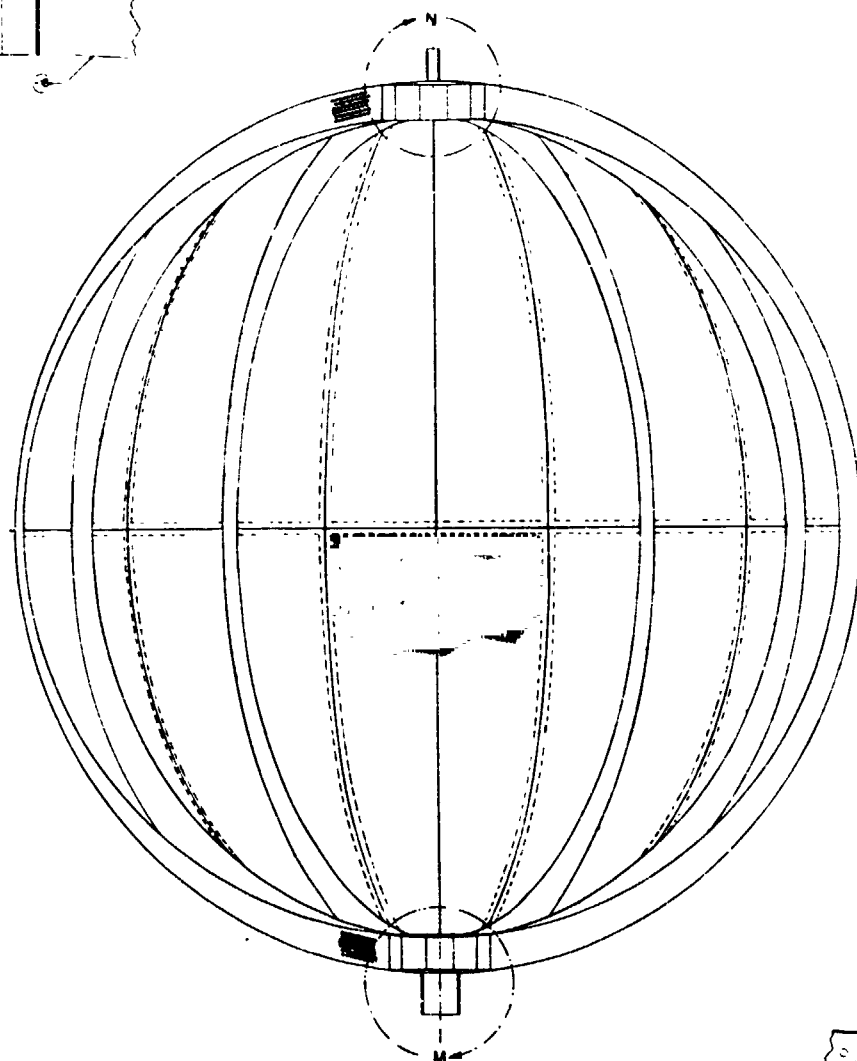
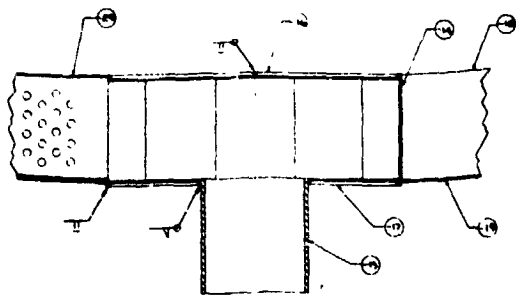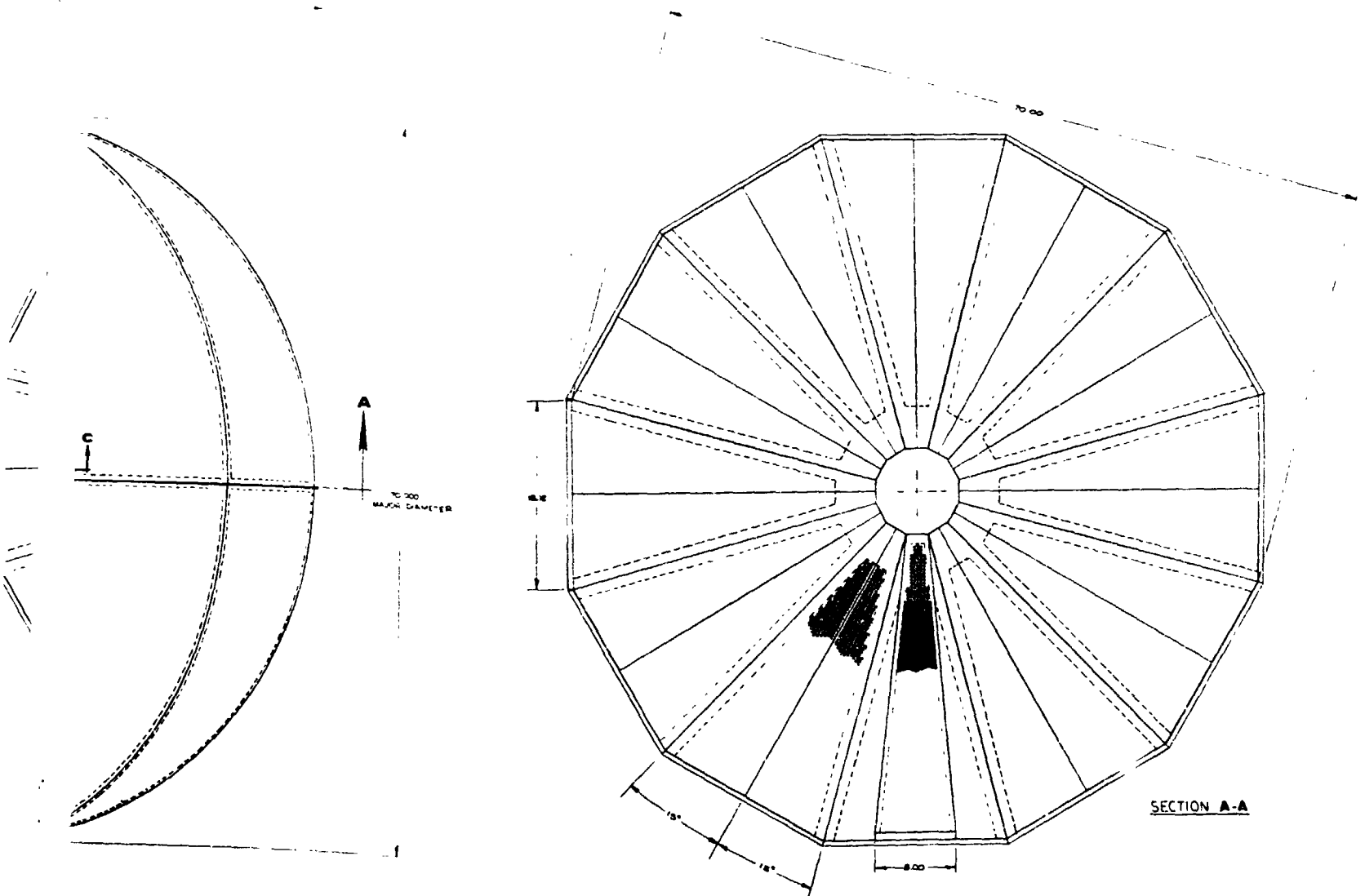DETAIL M
NO SCALE

Figure IV-2 LO$_2$ Acquisition/Expulsion System and Tank Assembly

IV-7 and IV-8

The side panels of the flow channel were not perforated except for 7.62 by 7.62-cm (3 by 3-in.) areas near each end. These areas were covered with 325x2300 mesh screen, fastened by perimeter resistance welding, and permitted the expulsion of all bulk liquid under low-g conditions, regardless of tank/liquid orientation.

2. Fabrication

Two full-scale sample panels of the liner (Fig. IV-3) were built and used to develop an assembly procedure compatible with the size of the capillary liner. The 250x1370-mesh stainless steel screen was permanently attached to the 24-gage 304L stainless steel per-forated plate using a resistance seam-welding technique developed under previous programs. Some difficulty was experienced during the initial attempts due to bunching up of the screen material under the welding wheel. Tacking the screen at 1.27-cm ($\frac{1}{2}$-in.) in-tervals prior to welding the seam solved this problem. A success-ful resistance-welded gore panel is shown in Fig. IV-4.

After the screen was welded to the perforated plate, this subas-sembly, called a gore section, was bubble-point tested to verify that the resistance welding did not degrade the screen's bubble point. Figure IV-5 shows the gore section in the bubble test fixture. A layer of methanol approximately 0.64 cm ($\frac{1}{4}$ in.) deep was placed on top of the gore section while pressurizing the underside with gaseous nitrogen. A manometer was used to indi-cate the pressure at which bubbles formed on top of the screen. The bubble-point value of the sample gore section was within the specified limits for the mesh used.

After the bubble-point tests, the panels were formed to the con-tour necessary to fabricate the hemi-dodesopheres. Figure IV-6 shows two methods considered for welding the gore panels together: butt welding, and forming a lip around the edge of the panels.

Attempts at butt welding were not successful: gaps formed be-tween the panels as the weld progressed. Even pretacking the panels at intervals along the weld did not eliminate the problem, and this approach was dropped.

The samples welded using the second method were successful. This method involved forming a 0.64-cm ($\frac{1}{4}$-in.) lip around the perimeter of the gore section. Figure IV-7 shows the lip and also shows how the gores were mated prior to welding. Figure IV-8 shows the spe-cial tooling designed to form the lip around the gore section.
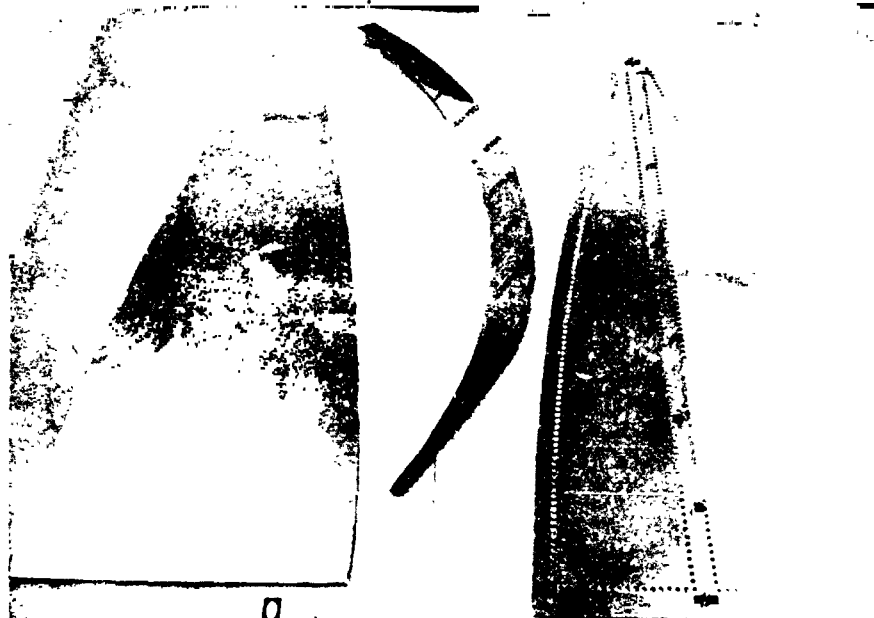
Fig. IV-3 Trial Gore Panels

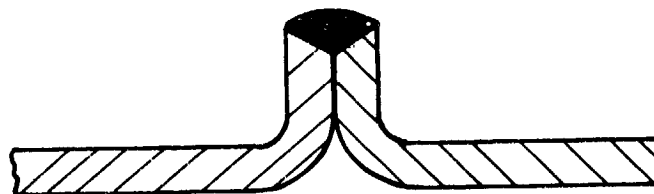*Fig. IV-4 Completed Trial Gore Panel*

IV-10

Fig. IV-5 Gore Panel in Bubble-Point Fixture

Butt Weld

Edge Weld

Fig. IV-6 Gore Panel Weld Joints

IV-11

Fig. IV-7 Gore Panels Prior to Welding

IV-12

Fig. IV-8 Lip Forming Operation

Once the welding problems for the gore section were resolved, a special welding fixture was designed. Figure IV-9 shows two sample gore sections after being welded in the fixture.

The completed gore sections were inspected and fabrication and assembly began on the capillary liner. The perforated plates were trimmed prior to being resistance welded to the fine mesh screen. Figure IV-10 shows the perforated plates as received from the supplier (center), prior to being trimmed (right), and after trimming (left).

The procedure for welding the gore sections together was slightly changed to add tack welding of the sections at approximately 5.08-cm (2-in.) intervals along the edge of the seam. The gore sections were welded in pairs before final assembly to eliminate the need for a sophisticated final assembly fixture. Figure IV-11 shows the final assembly fixture with some of the gore sections in place. Figure IV-12 shows one of the hemispheres after final assembly.

Each of the two hemi-dodecaspheres was bubble-point tested after assembly. The test setup is shown in Fig. IV-13. Each hemisphere was attached to a baseplate using a center tension member and clamps around the lip of the equator; a rubber gasket was used between the hemisphere lip and the baseplate. The entire assembly was placed in a shallow collection pan and methanol spray (from a perforated container above) was used to wet the external surface of the hemisphere. The bubble point was measured by pressurizing the hemisphere with gaseous nitrogen. Screen breakdown was evidenced by bubbles on the external surface of the screen. A bubble point of 50.8 cm (20 in.) of H_2O was used as the acceptance criterion for the hemispheres.

The channel assembly (Fig. IV-14) completed using side channels of stainless steel sheet. The perforated plate was attached by fusion welding, and the screen was attached using the flame spray technique described earlier.

A bubble-point test of the assembled channel indicated that there were numerous leaks at the flame-sprayed plate/screen interface. A sample of the sprayed surface was polished and examined under magnification (Fig. IV-15), and numerous small cracks were noted. Rather than repeat the flame spray, the cracks were repaired using the soft solder techniques discussed previously. These problems revealed the need for additional work and improvement of the flame spray joining method. Plans for future work in this area are presented in the next section.
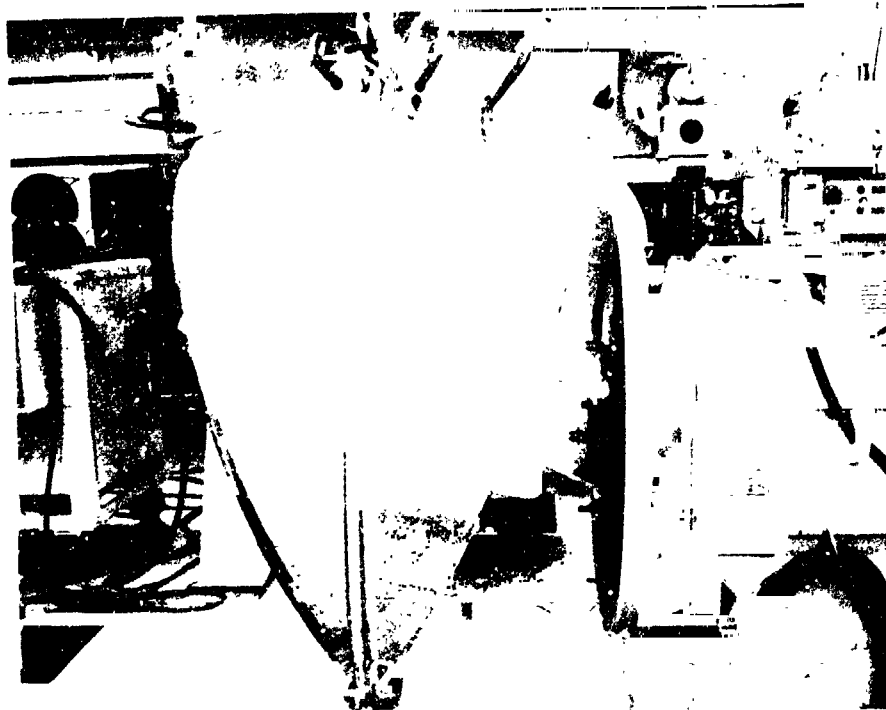
IV-14

Fig. IV-9 Gore Sections on Welding Fixture
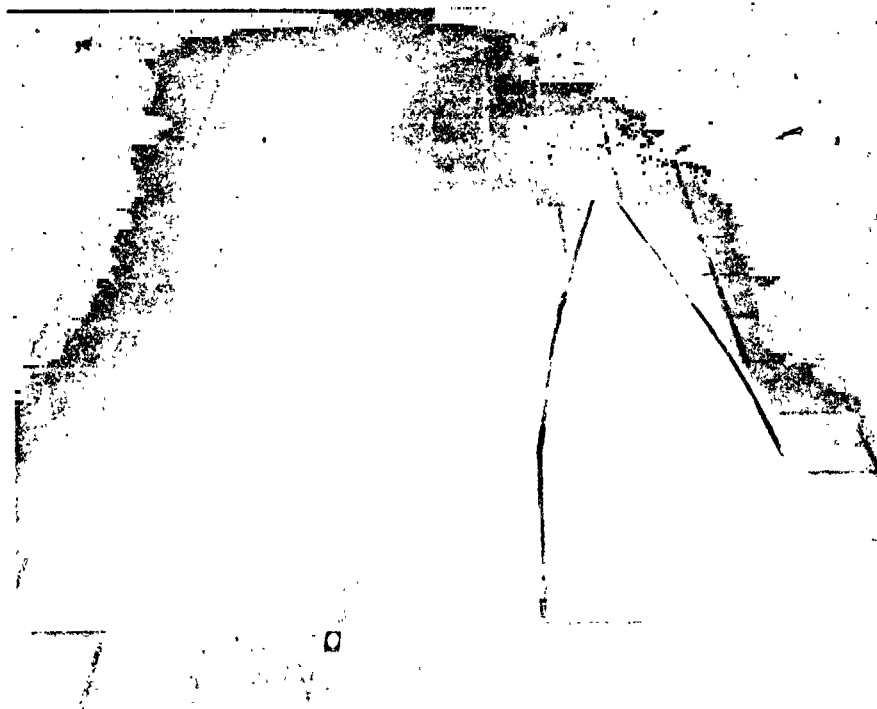
Fig. IV-10 Perforated Plate before and after Trimming

IV-15

Fig. IV-11 Final Assembly Weld Fixture

Fig. IV-12 Completed Hemisphere
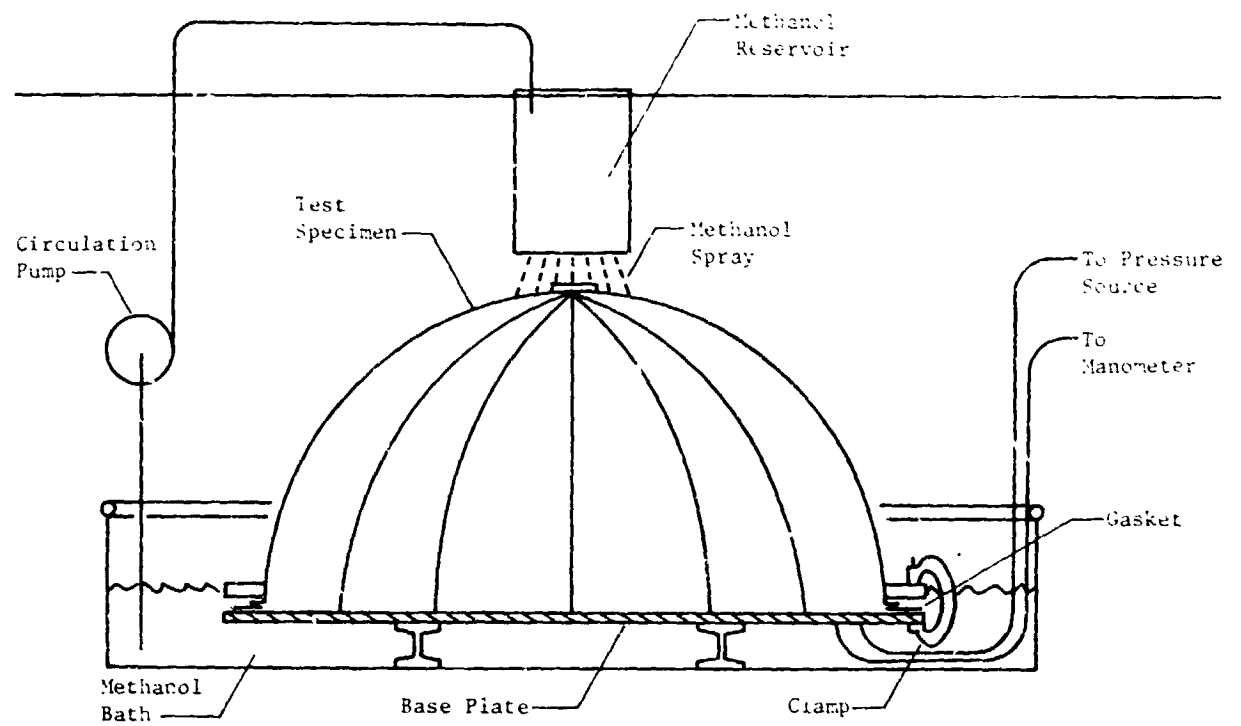
Fig. IV-13 Hemisphere Bubble-Point Test Schematic

Fig. IV-14 Flow Channel Assembly
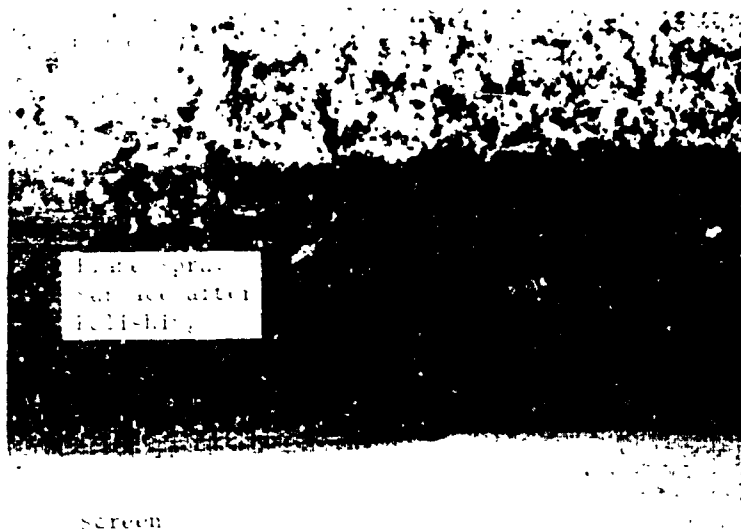
Fig. IV-15 Flame Spray Surface (Magnified), Showing Cracks

C.   FUTURE PLANS

The work accomplished under this IRAD program is considered to be a major contribution toward maintaining Martin Marietta's expertise in the design and fabrication of capillary propellant management systems. Our future plans for this continuing program involve three areas: (1) the 177.8-cm (70-in.) DSL screen liner; (2) screen forming and joining; and (3) the capillary screen design and fabrication manual.

1.   177.8-cm (70-in.) DSL Screen Liner

During the remainder of CY 1973 the assembly of the hemi-dodeca-spheres and the flow channel will be completed. After these tasks, a series of bubble point tests will be conducted and the techniques for DSL liner inspection will be finalized. Figure IV-16 shows the liner before installing the flow channel and making the final closure welds.

IV-18
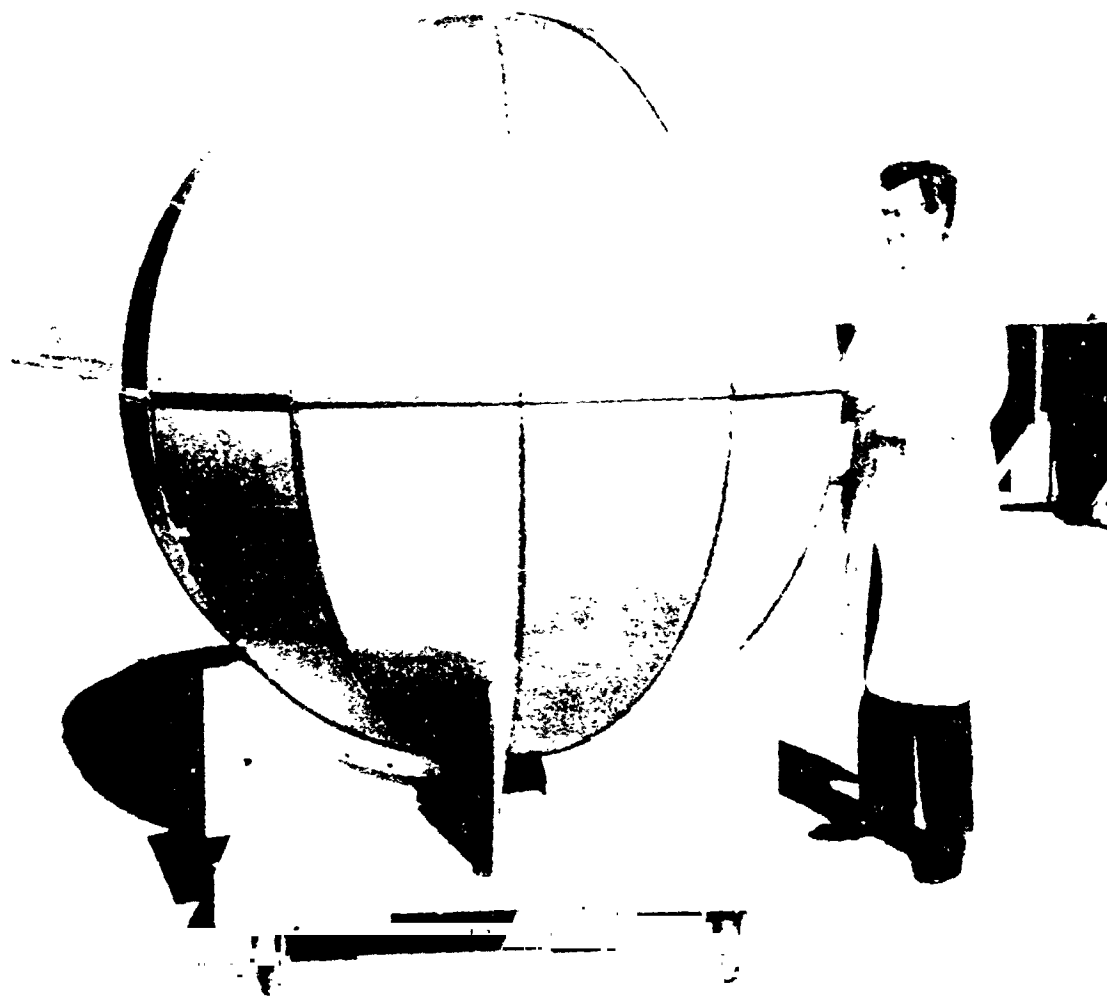
Fig. IV-16   Completed Screen Liner and Channel Assembly

The screen liner and flow channel assembly will be installed in
a spherical tank during CY 1974 and additional tests will be con-
ducted. These tests will include partial outflows and bubble-
point inspections. Leaks will be created in the liner and in-
spection techniques will be used to detect such leaks. To ac-
complish the bubble-point inspections, a device that will spray
methanol on all the screen surfaces will be designed, built, and
installed in the tank through an access port.

2. Screen Forming and Joining

During the second half of CY 1973 we expect to acquire several specialized tools that will allow continued development of capillary screen forming and joining techniques. These tools include a micromesh screen pleating machine, a specialized resistance spot and seam welder, and a large-screen bubble-point test fixture.

Our experience with fine mesh titanium screen has been limited to work with small samples. We will acquire larger titanium samples in the finest mesh sizes available to complete some basic investigations. These investigations will include determining mechanical properties such as tensile strength, yield strength, and elongation. The forming investigations will involve multi-step low-stress procedures unless the mechanical properties studies indicate another approach should be used. Brazing of titanium will be investigated using brazing alloys that are compatible with anticipated propellants. Resistance seam welding of titanium is not expected to be a problem; however, this will require the establishment of welding parameters for the material.

We will continue efforts to improve the techniques for fabricating stainless steel and aluminum assemblies. This will include additional work on the flame spray joining technique. Although resistance seam welding has proved to be an excellent method for joining screen to plate, both sides of the assembly must be accessible to the welder. The metal flame spray technique would allow joining with access to only one side of an assembly, such as the external surface of a sphere.

3. Capillary Screen Design and Fabrication Manual

During the past 2 years, this task has established and experimentally verified several design and fabrication methods and guidelines. These methods and guidelines are numerous and apply to various types of capillary screen devices. Under this task all of this information will be compiled and published as a design and fabrication manual. This document will provide design and fabrication recommendations for screen forming and joining, depending on the choice of material and configuration required.

IV-20

D.   CONCLUSIONS

A full-scale stainless steel capillary liner can be fabricated
using existing techniques. It should be noted, however, that ad-
ditional work is needed to refine and improve the forming and
joining methods used.

Adequate bubble-point inspection techniques for subassemblies such
as hemispheres and individual channels were developed. Further
work must be undertaken on total liner inspection techniques and
liner-in-tank inspection techniques.

Seam welding is currently the best screen-to-sheet joining method
available for like materials. The metal flame spray technique
will require further deve.opment but could be the answer for weld-
.ing to unlike material joints; i.e., aluminum screen to stainless
steel sheet.

V. CRYOGENIC SINGLE-LINER FEEDLINE MODEL

The basic screen feedline concept, described in Volume II, Chapter II, was demonstrated with noncryogens in the 102-cm (40-in.) plexiglass model described in Chapter II of this volume. The cryogenic application of the feedline concept was studied under a Martin Marietta Research Authorization (RA) Task 48631.

A. OBJECTIVES

The major objectives of this study were:

1) to conduct a detailed analysis of the cryogenic feedline concept to determine critical operating parameters;

2) to produce a detailed model design;

3) to develop fabrication techniques;

4) to test a subscale model feedline.

The purpose of the test program was to demonstrate the feedline's capability to maintain a gas-free liquid core at the outlet under both static and flowing conditions. The test program was divided into three phases. The first phase consisted of establishing and maintaining a gas annulus around the liquid core at various levels of heat input.

The second test phase was to demonstrate the flow capability of the feedline. At low flow rates, the liquid/gas interface remains stable. As flow rate increases, frictional pressure losses will continue to increase until the pressure diffenential at the downstream end of the feedline exceeds the bubble point of the screen liner. This is an undesirable condition because vapor ingestion will result. Proper design of capillary feedlines requires accurate prediction of frictional losses as a function of flow rate (velocity). These tests were designed to determine an empirical relationship for friction factors as a function of flow rate (Reynolds number) for the capillary feedline. These data are considered valuable when designing capillary feedlines.

A third set of tests was designed to simulate a mission duty cycle application of the feedline. A typical test included intermittent flow at various flow rates, and simulated coast periods with the vapor annulus established and maintained.

Concurrent with these test phases, data were taken to define the time required to first obtain liquid flow from an initially "dry" feedline.

B.   TEST MODEL DESIGN

The cryogenic feedline test article is shown schematically in Fig. V-1. Figure V-2 shows the detailed design drawing of the feedline model. The 3.66-m (12-ft) screen test section was enclosed in a 5-m (16-ft) long vacuum jacket. The test model was fitted with Pyrex windows to allow monitoring of liquid quality downstream from the test section. A 5.1 cm (2-in.) dia tube was welded into the top of the vacuum jacket near its midpoint to permit connection of a diffusion pump. A hot-filament ionization gage was mounted at a penetration cut into the jacket near the outlet end. All other penetrations were through the inlet and outlet flanges.

Fig. V-1 Feedline Test Article Schematic

SECTION B-B

LI8-6002567
264 ----- 1
LEVEL SENSOR

LAB-60025
O.D. X .020
TYPE 904

196 1/8

144

3.75

LAB-6002555
LAB-6002562
LAB-6002564
LAB-6001

T.O16 W
1 SST
LAB-6002568
LAB-6002539
O.D. X .020 W
TY 321 SST
O.D. X .020 W
TY 904 SST
1000-008 AZ-
BELLOWS

LAB-6002563

SECTION A-A

O.D. X .035 H
TYPE 904 SST

6002561
560

.032 NEOPRENE
GASKET
.032 TEFLON GASKET
45° (TYP)
PYREX WINDOW
LAB-6002556
(3 REQ'D)
LAB-6002557
(3 REQ'D)

SECTION C-C

A
B
A

FOLDOUT FRAME

LAB-60025   ∅ O.D. ±.020W
             TYPE 304 SST

½-28UNF X ⅞ LG
HEX HD CAPSCREW
18-8 SST (8 REQ'D)

LAB-6002552

2-240 O-RING
(NEOPRENE)

LAB-6002551

CUT-A-B ADAPTER
(2 REQ'D)

∅ O.D. ±.035 W X 7⅞ TY 304 SST
(2 PLACES)

LAB-6002560

1000-0081A2
BELLOWS

LAB-6002554

∅ O.D. ±.035 W
TYPE 304 SST

LAB-0201643

LAB-0201640

4.375

8.75

10.125 (APPROX.)
ADJUST THIS DIM TO ALIGN
FOR TOLERANCE ACCUMULATION

W GASKET

PYREX WINDOW

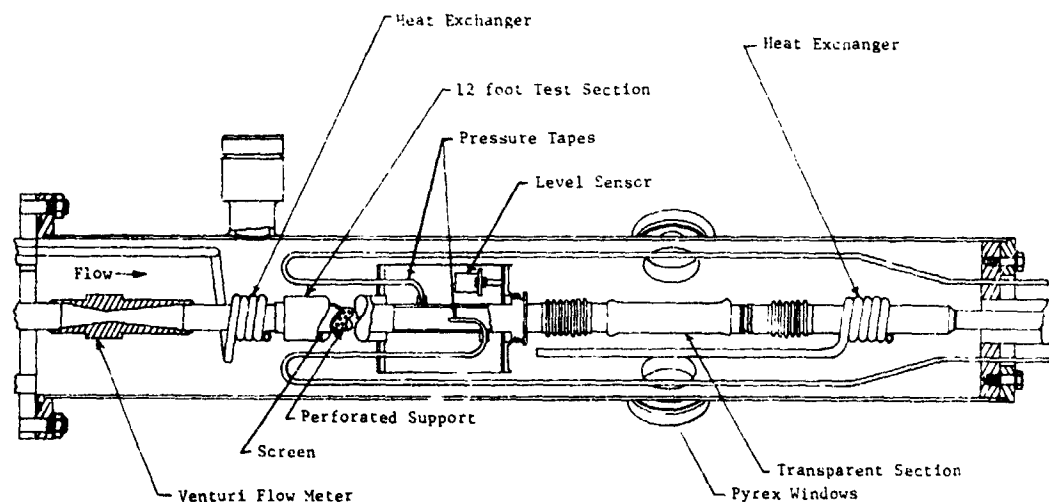LAB-6002556
(2 REQ'D)

AB-6002557
(2 REQ'D)

Fig. V-2 Feedline Test Article Detail Design

V-3 and V-4

The test sections consisted of a 3.2 cm (1.25-in.) dia stainless steel tube with a 1.9 cm (0.75-in.) dia screen core. The screen was replaced by solid tube in the enlarged section that forms the downstream end of the gas annulus. The solid tube simplified attachment of the instrumentation. The enlargement provided both the volume required for liquid level sensors and a convenient location for vent and instrumentation line penetrations.

Downstream from this enlarged section, a sightglass (transparent section) provided a view of the gas collector device. This device was a screen cylinder through which the core liquid must flow. A metal cone on its upstream side minimized flow disturbance. The gas collector allowed visual monitoring of liquid quality in the liquid core, because the gas would not tend to flow across the screen.

During static operation, the gas collector operates with the feedline inclined about 2 deg above the inlet. This creates a buoyant force on gas in the liquid core, bringing the gas to the collector. While the gas volume was small, observation of the liquid vapor interface gave an indication of the amount of gas.

With liquid flowing through the line, gas is carried by the flow to the collector and restrained at the wetted screen. Gas will continue to collect, reducing the flow area and increasing the flow pressure drop across the collector screen, until it equals the bubble point of the screen. Any additional gas will pass through the screen. Because the collector device is made from a coarser mesh than the screen liner, the gas collector is always the preferred path for liquid flow. A sufficiently high flow rate will purge all gas from the collector. This flow is estimated at more than twice the flow necessary to cause screen breakdown in the test section.

Heat exchanger coils were installed near each end of the test article. These were intended to condition the incoming liquid during flow and reduce heat leak from the ends. This heat leak could add heat to the liquid core where it is not protected by the gas annulus. The initial design fed liquid through the coils in series.

Eight platinum resistance thermometers were attached to the test article. These sensors, which are accurate to approximately 0.05°K (0.1°R), were calibrated for a range of 74.5 to 91.2°K (134 to 164°R) so that both gas and liquid temperatures could be accurately measured. The sensors were located on the screen at

the inlet and outlet; on the tube wall across from the screen sensors; at the top and bottom of the liner within the expanded section (where the liner is a solid tube); and on top of the heat exchanger coils at each end of the test article.

Pressure can be monitored from taps at five points in the system: two taps for a venturi flowmeter, two for a pitot-type flowmeter at the expanded section, and one on the gas annulus vent. These pressure taps are attached to external pressure transducers to record pressure readings from the flowmeters, liquid pressure both upstream and downstream, gas annulus pressure, and differential pressures at the inlet and outlet of the screen section. These differential pressure readings correspond to the pressure drop across the screen.

Flow rate was measured by a Ramapo (vane deflection type) flowmeter located at the outlet of the test article. The venturi and pitot flowmeters were installed primarily for the proposed testing with hydrogen, but could also be used (by comparison to each other) to assist in the detection of gas ingestion.

Two liquid level sensors were located in the expanded section to monitor the gas annulus condition. One was mounted in the upper section, with the other at the centerline of the expanded section.

C.   FABRICATION AND ASSEMBLY

The test article was designed to be assembled as two subassemblies. The internal assembly feeds all flow and instrumentation lines through the inlet and the outlet (reverse flange). This internal assembly slips inside the vacuum jacket tube. All the tube penetrations were welded, with the exception of the O-ring seals on the end flanges.

Inlet and outlet flow is connected with bayonet fittings to extend insulation of flow by a vacuum jacket.

The 3.66-m (12-ft) long screen liner for the test section was fabricated in 61-cm (24-in.) sections. Each section was cut to size and rolled over a mandrel with string. With intermittent tack welds in place, the strings were removed and a longitudinal resistance weld was made. The section furthest downstream is shown in Fig. V-3. Each screen tube was then removed from the mandrel and its bubble point verified in methanol. The spots of solder repaired occasional burnthroughs caused in welding.
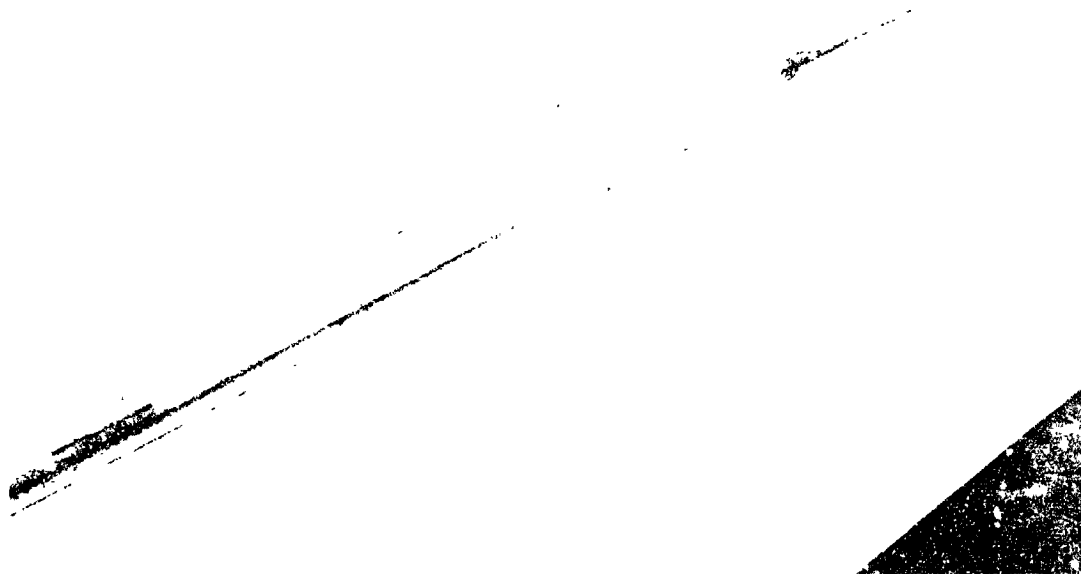
V-6

Fig. V-3 Section of Screen Liner

Acceptable screen tubes were placed over rolled perforated plate
tubes welded to solid end sections. A collar (shown in Fig. V-4)
was then slipped over the screen and tube so that the screen pro-
trudes 0.32-cm (1/8-in.) or less. A fusion weld over this pro-
trusion sealed the screen section. The end tubes of adjacent
screen sections could then be welded to form the full length
screen liner. Figures V-3 and V-4 also show the liquid core
penetrations for downstream pressure taps.

The 8.9-cm (3.5-in.) long sightglass was shrink-fitted over 1.9-
cm (0.75-in.) dia Kovar tubes. The metal and Pyrex were bonded
with epoxy. The gas collector itself was of soldered construc-
tion, as described above. The completed gas collector device is
shown in Fig. V-5. This assembly was mounted between expansion
bellows to avoid excessive stress on the glass due to metal
shrinkage at cryogenic temperatures.

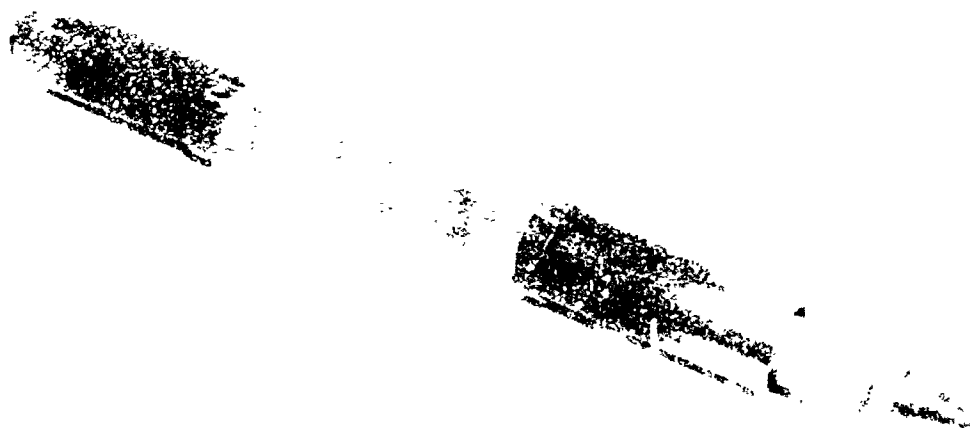Fig. V-4 Detail of Screen Weld

Fig. V-5 Gas Collector Assembly

The assembled screen section was inserted into the 3.2-cm (1.25-in.) dia stainless steel tube and welded to the enlarged section. Figure V-6 shows this assembly from the downstream end. Also pictured (at left), is the 10-cm (4-in.) dia stainless steel (Schedule 5S) tube used to form the vacuum jacket.
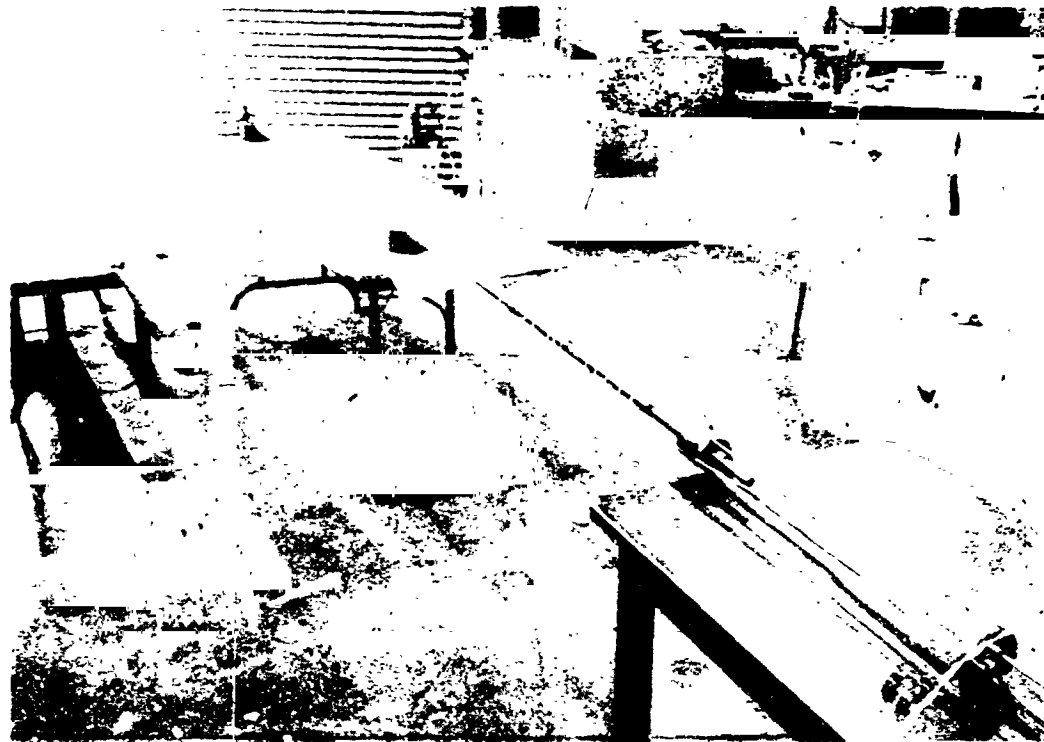

Fig. V-6   Assembled Test Section

The assembled sightglass and enlarged section are shown in Fig. V-7 and V-8. Some of the coils of the heat exchanger are shown without insulation. The aluminized Mylar tape over the enlarged section serves as a radiation shield.

The partially insulated inlet end is shown in Fig. V-9. This flange mates with the vacuum jacket for the O-ring seal.
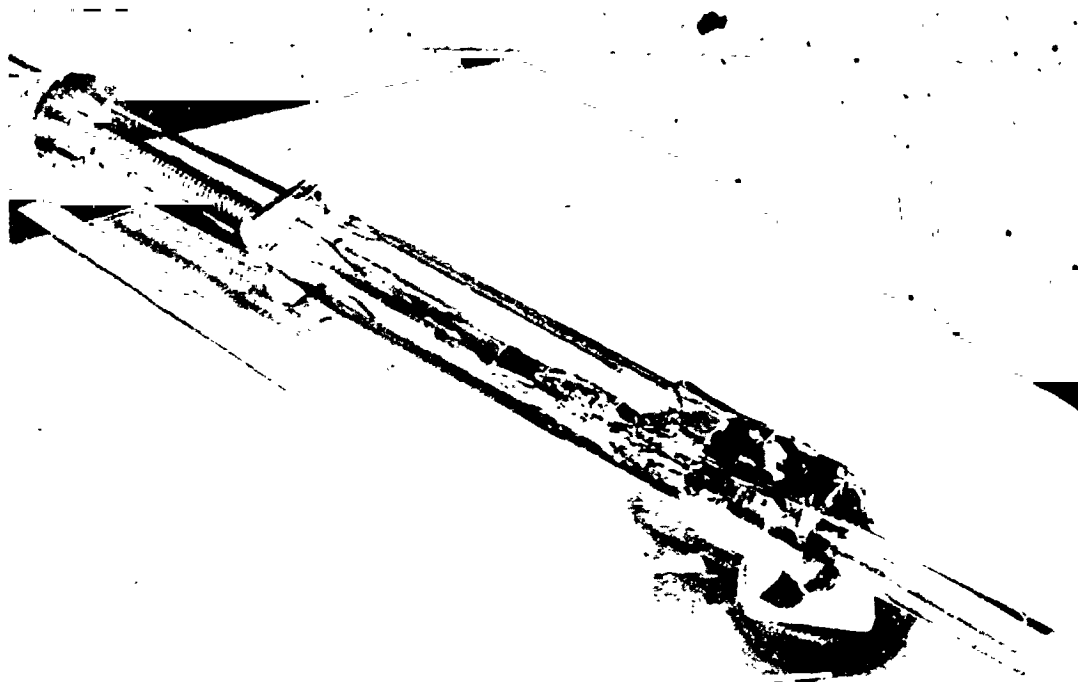
Fig. V-7 Enlarged Section Assembly
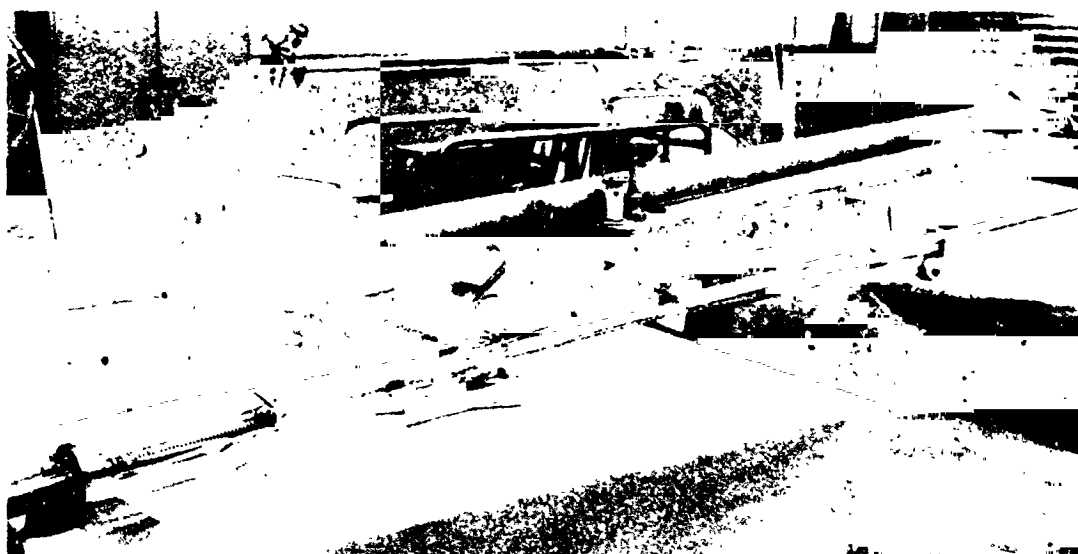
Fig. V-8 Partially Insulated Test Section

V-10

Fig. V-9   Inlet End Flange

The multilayer insulation for the end portions was made of Mylar
sheet aluminized on both sides, wrapped in strips, and separated
by nylon net.   Ten to twenty layers were used, depending on the
clearance available between the hardware and the vacuum jacket.
The test section was insulated with Mylar sheet pre-sandwiched
on rayon net as shown in Fig. V-10.

Fig. V-10   Test Section Insulation

D.   TEST PLAN

The test article and related equipment are shown schematically
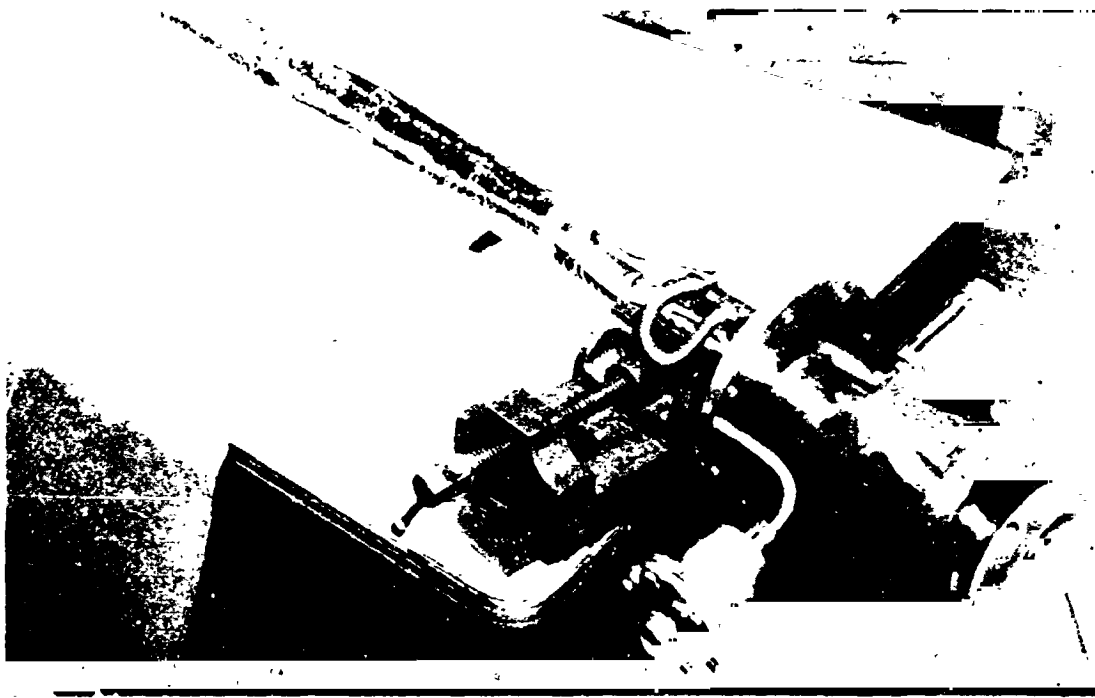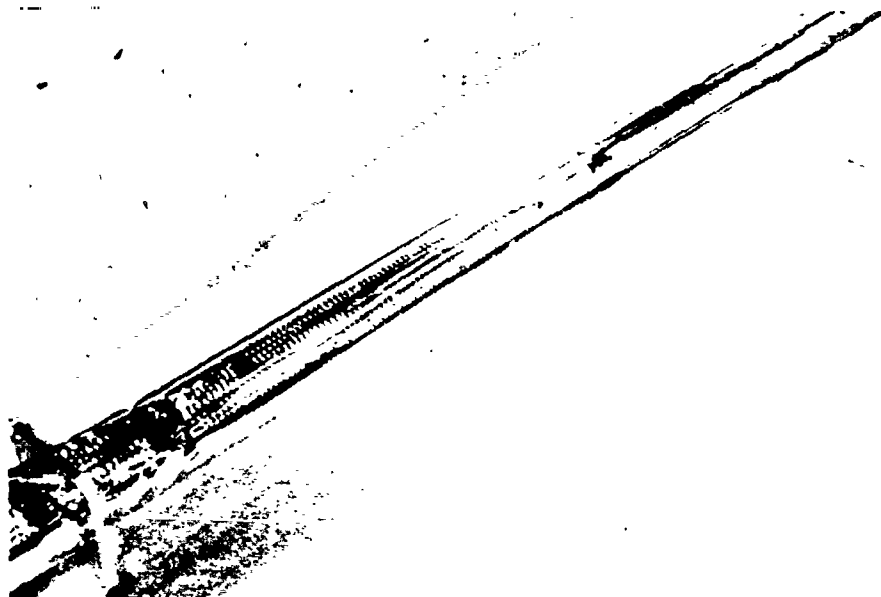in Fig. V-11. A 2.26-cu m (600-gal) supply dewar, used to fill
the supply tank, was excluded from the system for each test run.
The supply tank could be closed to self-pressurize, or could be
pressurized from a GN_2 source. It was equipped with liquid level
sensors at 20%, 50%, and 80% liquid capacity.

Liquid nitrogen testing of the feedline model will consist of
three phases. Phase 1 will demonstrate and investigate the feed-
line operation during static conditions. That is, a liquid core
surrounded by a vapor annulus will be established and maintained
for a period of approximately 1 hr. Phase 2 will examine flow
characteristics of the article as a function of pressure. Phase
3 will demonstrate operation under a mission timeline set of con-
ditions, to include coast periods, outflows at various flow rates,
and reestablishment of the liquid/vapor interface following break-
down of the screen by vapor ingestion to the core and/or flooding
of the outer annulus.

V-12

Fig. V-11 Feedline Flow Schematic

V-13

The static testing phase should consist of three primary tests. During each test the vapor annulus will be established and maintained by continuous venting. The tests will differ, primarily, in the vacuum level maintained in the vacuum jacket. Increasing the vacuum jacket pressure (accomplished by throttling the vacuum pump port) will increase the convective contribution of the radial heat leak. The magnitude of this increase will be measured by the steady-state vent rate. The relationship between the two can be used as a reference during future testing.

Other data to be collected will include liquid temperatures at the various positions, liquid pressure, and differential pressures at each end of the test section, as well as the time required to obtain the all-vapor condition in the annulus. A valuable result of this testing phase will be familiarity with the vent valve. Differential pressure across the screen liner is critical in the flow tests as the frictional effect increases the pressure differential at upstream and downstream locations.

Initial conditions for the first flow tests will be the same as for the static tests. Venting of the outer annulus will be terminated as the exit valve is opened.

The exit valve would be opened in stepwise fashion allowing steady conditions to be recorded until a maximum flow rate is observed. This maximum flow rate will be determined either by a fully open valve (at lower tank pressure) or by gas ingestion occurring when frictional pressure drop in the line becomes equal to the screen bubble point. Design estimates indicate that this flow rate is 16.1 l/min (3.8 gal/min) or 0.2 kg/sec (0.43 lb/sec).

In this test, the differential pressure between the outer annulus and the liquid core will be recorded at the inlet and outlet ends to determine if it can remain between zero and a value less than the screen bubble point. The first four tests will vary supply tank pressure from 2.1 N/cm^2 (3.0 psig) to 6.9 N/cm^2 (10 psig). This should permit correlation of Reynolds number to pressure drop in a screen tube and define flow rate maxima for further testing. Quality of the liquid outflowed will be noted throughout testing.

Further flow tests will establish similar characteristics of a feedline where the outer annulus is intentionally filled with liquid. The final phase of testing should simulate a typical mission timeline.

E.   TEST RESULTS

The cryogenic feedline test article was designed and fabricated
for testing. Checkout tests of the system were completed. By
pressurizing the supply tank with gaseous nitrogen, liquid could
be delivered to the test article effectively subcooled for fill-
ing the test section. With the exit valve opened, it was possible
to flow 100% liquid to clear the gas collector. The subcooled
liquid was in a nonequilibrium state, and liquid temperatures
rose to saturation in approximately 20 sec. For a period of about
20 min, we could initiate flow, clear the gas collector, and
resume flow of 100% liquid.

As flow rate was decreased, a point was reached at which a gas
pocket formed, held by flow to the downstream end of the gas col-
lector. The gas pocket grew only if the flow rate was decreased.
At zero flow rate the growth of these vapor pockets eventually
pushed all liquid from the sightglass.

This verified that the test article could be used to transfer 100%
liquid cryogen; nevertheless, model verification could only be
complete when it was possible to hold liquid in the screen core
with the outlet fully closed.

The test results showed that heat input from the ends, particu-
larly the downstream end, was too high relative to the radial
heat leak. Effort was, therefore, concentrated on improving the
performance of the heat exchangers. A tee was installed immedi-
ately upstream of the inlet end coil so that the respective coils
were fed in parallel from the source line. This, it was hoped,
would deliver cooler liquid downstream. Although this did ap-
parently improve performance, results were still unsatisfactory.

The system was subsequently rearranged to supply the heat ex-
changer system directly from the large dewar, from the supply
tank, and finally from a separate source. Although each modifi-
cation apparently improved performance in the test section,
temperatures measured at the coils remained higher than core
(saturated) temperatures.

Attempts to introduce subcooling into the system included introduction of a helium injection system. The helium, fed in at the heat exchanger system inlet, caused evaporation of LN_2 in the gas pockets and thus effected cooling.

Best results were obtained using a separate source located at the outlet end of the test article and flowing through the inlet end coil into a catch tank equipped with a vacuum pump. This allowed the option of flowing in series through the inlet end coil or bypassing that coil completely. In both cases, the downstream (source) end had a steady-state temperature, 2.8 to 4°K (5 to 7°R) warmer than the liquid core. The downstream end was 2 to 3°K (3.7 to 5.5°R) warmer than the core when fed in series, but fell to the core temperature when it was bypassed. The obvious conclusion was that the heat exchangers as installed were not capable of intercepting sufficient end heat leak.

The strip chart recordings of the venturi and pitot-tube flowmeters showed surges on the order of 0.35 N/cm^2 (0.5 psid). This was a full-scale deflection on the pitot system, and both were electrically disconnected. Such surges are caused by flash boiling at the liquid/vapor interface within the pressure sensing tubes.

The test system is being modified to eliminate these problems. The test section will be mounted in a portion of the existing vacuum jacket, which is a minimum amount longer than the 3.66-m (12-ft) test section. Beyond the vacuum jacket, the extended liquid core line passes through liquid nitrogen reservoirs. These will be kept at ambient pressure while the test section is at 3.5 to 10.4 N/cm^2 (5 to 15 psig). This should eliminate the thermal short circuit to the liquid core. The downstream reservoir will also contain the exit valve.

The venturi and pitot flowmeters will be eliminated since the model is not intended for hydrogen testing, and the liquid pressure taps will be fitted with an orifice to damp out pressure surges.

F.   CONCLUSIONS

During the cryogenic single-liner feedline study, design and anal-
ysis of a subscale test article were completed. Fabrication tech-
nology and procedures for full-size application were developed and
verified.

The final objective of the study, the test program, has been ini-
tiated. The test article was filled with liquid nitrogen and
used to flow 100% liquid from a saturated source. Although the
test program has indicated the feasibility of liquid transfer,
the basic static mode operation has not been demonstrated.

Problems encountered during testing were apparently caused by
test hardware difficulties. The basic screen liner section is,
therefore, being incorporated into a simpler test configuration.
Fabrication of the modified test article has been initiated and
continues on schedule. Resumption of the test program is ex-
pected during July 1973, with test program completion expected
well before the end of the year.

VI. CONCLUSIONS AND RECOMMENDATIONS

The ground test program conducted to verify the passive cryogenic storage designs was part of the cryogenic study phase of the contract. The test program was successful and results verify the DSL designs, as described in Chapters III, IV, and V of Volume II.

The operational performance was demonstrated, in part, and data supporting the design features of the capillary screen systems were obtained from the test program. A variety of models were tested in a low-g environment using the KC-135 aircraft, and under plus and minus 1-g in Martin Marietta's engineering laboratories.

The 1-g testing of the 63.5-cm (25-in.) dia DSL tank was particularly significant. Tests were conducted using liquid hydrogen and liquid nitrogen as test fluids. The gas-free liquid expulsion characteristics of the DSL system were verified by expelling LH_2 under -1g. The expulsions were successfully accomplished, and the screen liner and liquid supply channels were stable, as predicted, using both GH_2 and GHe as pressurants at temperatures of 89°K (160°R) to 278°K (500°R). The tests also successfully demonstrated that the single screen liner provided the predicted passive communication between the outer annulus and the bulk region of the DSL tank. Loading was successfully accomplished using both LH_2 and LN_2. A system capable of satisfying the narrow vent band for the DSL, as dictated by the 1-g condition, was built and successfully demonstrated for LH_2 during bench tests. Thermal stratification, however, prevented the desired demonstration of the liquid-free vapor venting performance using the concept and control system under -1g test conditions.

Results of direct benefit to the program were also obtained from two Martin Marietta IRAD programs. One program demonstrated that a large screen liner system 178 cm (70 in.) in diameter can be successfully fabricated using existing techniques. Remote inspection of the large screen tank using standard bubble-point techniques was successfully demonstrated in early 1973. The second IRAD program also demonstrated that a cryogenic DSL feedline can be fabricated using existing methods. The performance of the feedline under static and dynamic conditions is being evaluated using LN_2 as the test liquid. Both programs will continue during 1973.

In addition to the two IRAD programs, we recommend that the next
step required to complete the verification of the DSL concept is
to conduct the orbital test program as proposed and outlined in
Volume IV. The orbital test bed provides the long-term, low-g
environment needed to demonstrate vapor venting and can be used
to demonstrate gas-free liquid expulsion and bulk liquid control.

VII. REFERENCES

I-1. T. R. Barksdale and H. L. Paynter: _Design, Fabrication, and Testing of Surface Propellant Tank with Internal Drape._ MCR-68-11. Martin Marietta Corporation, Denver, Colorado, March 1968. (Contract NAS8-20837)

I-2. H. L. Paynter, et al.: _Experimental Investigation of Capillary Propellant Control Devices for Low-Gravity Environments, Volume I - Summary Report._ MCR-69-585. Martin Marietta Corporation, Denver, Colorado, June 1970. (Contract NAS8-21259)

I-4. D. L. Blazer, et al.: _Advanced Propellant Management System for Spacecraft Propulsion Systems. Phase I - Survey Study and Evaluation._ MCR-69-87. February 1969. _Phase II - Detail Design._ MCR-69-436. September 1969. Martin Marietta Corporation, Denver, Colorado. (Contract NAS9-8939).

II-1. H. C. Hewitt and J. D. Parker: "Bubble Growth and Collapse in Liquid Nitrogen." _Transactions of the ASME Journal of Heat Transfer_, Vol 90, Series C, February 1968, pp 22-26.

II-2. L. W. Florschuetz and B. T. Chao: "On the Mechanics of Vapor Bubble Collapse." _Transactions of the ASME Journal of Heat Transfer_, Vol 87, Series C, May 1965, pp 209-220.

II-3. _Investigation of Space-Storable Propellant Acquisition Devices, Vol II - Final Report._ MCR-70-171. Martin Marietta Corporation, Denver, Colorado, December 1970, p III-3. (Contract No. NAS7-754)

II-4. _Study and Design of a Cryogenic Propellant Acquisition System. Third Quarterly Progress Report._ MDC G2940. April 15, 1972, pp 72-78.

II-5. J. C. Armour and J. N. Cannon: "Fluid Flow Through Woven Screens." _AIChE Journal_, Volume 14, No. 3, May 1968, pp 415-420.

II-6. _Low-gravity Propellant Control Using Capillary Devices in Large-Scale Cryogenic Vehicles, Phase II - Final Report._ GDC-DDB70-006. General Dynamics/Convair Division, San Diego, California, August 1970. (Contract NAS8-21465)

II-7. K. R. Chun: "Some Experiments on Screen Wick Dry-Out Limits." *Transactions of the ASME Journal of Heat Transfer*, February 1972, pp 46-51.

II-8. *Study and Design of a Cryogenic Propellant Acquisition System, Final Quarterly Progress Report*. MDAC Report MDC G3695. McDonnell Douglas Astronautics Corporation, Huntington Beach, California, July 15, 1972, pp 116-129.

II-9. *Experimental Investigation of Capillary Propellant Control Devices for Low Gravity Environments, Volume II - Final Report*. Martin Marietta Corporation, Denver, Colorado, June 1970, p III-20. (Contract NAS8-21259)